“Be yourself, everyone else is already taken.”

Oscar Wilde (1854-1900)


Ghent University

Faculty of Pharmaceutical Sciences

DEVELOPMENT AND VALIDATION OF PROCESS ANALYTICAL METHODS FOR A CONTINUOUS PHARMACEUTICAL MANUFACTURING PROCESS OF TABLETS BASED ON WET GRANULATION

Margot FONTEYNE

Master in Drug Development

Thesis submitted to obtain the degree of Doctor in Pharmaceutical Sciences

2014

Promoter: **Prof. Dr. T. De Beer**

Laboratory of Pharmaceutical Process Analytical Technology

Co-promoter: **Prof. Dr. J.P. Remon**

Laboratory of Pharmaceutical Technology

Ghent, July 3 2014

The author	The promoter	The co-promoter
Pharm. Margot Fonteyne	Prof. Dr. Thomas De Beer	Prof. Dr. Jean Paul Remon

This ship disembarked as early as 2008, setting sail to Copenhagen as its first destination. It was Thomas De Beer who convinced me of the excellent learning possibilities up in the north. Dr. Holger Grohganz and Prof. Jukka Rantanen determined the first sea route and helped me navigating during this maiden voyage.

Once anchored back in Ghent, it was again Prof. Thomas De Beer who invited me to continue the journey. I am very grateful for this chance, his most valued help during my travel and the endless amount of great opportunities offered. Furthermore, I thank Prof. Jean Paul Remon and Prof. Chris Vervaet for their technical support throughout the years.

During the past four years, seven young scientists stepped aboard. They all had their own talents and their contribution to this work is highly appreciated. Carmen (Madrid), Delphine (Ghent), Sandra (Porto), Niko (Kuopio), Henrika (Turku), Sofie (Ghent) and Ana (Porto): Gracias, Dank je, Obrigado, Kiitos, Tack for your enthusiasm!

Furthermore, several great researchers hopped on and off the ship for a discussion or collaboration: Prof. Damián Córdoba Díaz (Madrid), Prof. Niklas Sandler (Turku), Prof. Vincent Bulone (Stockholm), Prof. Jarkko Ketolainen (Kuopio), Prof. Krist Gernaey (Copenhagen), Prof. Ingmar Nopens (Ghent), Séverine Mortier (Ghent), Dr. Clare Strachan (Helsinki), Maunu Toiviainen (Kuopio), Andrew Fussell (Twente), Sara Fraser (Dunedin), Björn Peters (Kuopio), Søren Vinter Søgaard (Copenhagen), Julen Arruabarrena Gamboa (Barcelona), Jacques De Beer (Brussels), Mario Hellings, Tom Van den Kerkhof (Beerse), Rut Besseling, Ad Gerich, Wim Oostra (Oss), Fernanda Onofre (Brussels), Ilija Ilić (Ljubljana), Qi Zhou (Stockholm) and Kaisa Naelapää (Copenhagen). Thank you!

Two very important crew members may not be forgotten: Jurgen and Liesbeth, thank you for the countless discussions, practical help, reading of papers and much, much more!

Kris, Tomas, Dirk, Tessa and Alain, thanks for the support from the dockyard!

In 2011, this vessel navigated to the southern hemisphere to continue the research work. Prof. Thomas Rades, thank you for accepting me in your group for these six months. I am grateful to the FWO for financial support. Furthermore, a big thanks to all people who helped me in Dunedin, both research- and otherwise: my office mates, the School of Pharmacy staff and York Zoo'ers.

During long travels away from home, nothing is as important as a good atmosphere aboard. Two shipmates were there from the start. Anneleen, you have set an example for us, it was an honour to follow your wake. Lien, thank you for your friendship and endless support. To my fellow PAT'ers: our galley-time was always great, and yes we dó laugh till our midriffs hurt! Wim and Valerie, thanks for the many fun hours we've spend at both the North and the South side! Everybody on the third deck has been very helpful, this has been highly appreciated.

Luckily, during its journey, this boat could beach on several isles. I could say 'isles of rest', but for sure they were not ☺. Bloso-chaps and -gals, Vormers, thanks for clearing my head every once in a while. This was as important as the real journey!

Of course, when sailing back into the harbour, it is great to have people waiting on the quayside. To my parents, grandmothers, brothers, nieces, parents-in-law, family and friends: thank you for the trust and support!

Benji, Kilo Alfa Uniform.

Margot, Basel 2014

TABLE OF CONTENTS

LIST OF ABBREVIATIONS

API	active pharmaceutical ingredient
BEST	bootstrap error-adjusted single-sample technique
BET	Brunauer-Emmett-Teller
CARS	coherent anti-Stokes Raman scattering
CLS	classical least squares
COST	changing one seperate variable at a time
CQA	critical quality attribute
DIA	dynamic imaging analysis
DoE	design of experiments
DPMO	defects per million opportunities
ECM	exchangable compression module
EMA	European medicines agency
FBRM	focused beam reflectance measurement
FDA	Food and Drug Administration
H	Hausner ratio
HPC	hydroxypropyl cellulose
HPLC	high performance liquid chromatography
HPMC	hydroxypropylmethylcellulose
ICH	International Conference on Harmonisation
ISO	international standards organization
KF	Karl Fischer
LHP	LightHouseProbe^{TM}
LIF	light induced fluorescence
MBSD	moving block standard deviation
MCC	microcrystalline cellulose
MCR	multiple curve resolution
MLR	multiple linear regression
NAS	net analyte signal
NCO	non-contact optic

NIR	near infrared
OPO	optical parametric oscillator
PAT	process analytical technology
PC	principal component
PCA	principal component analysis
PCH	product control hopper
PCR	principal component regression
PLS	partial least squares
PSD	particle size distribution
PVP	polyvinylpyrrolidone
QbD	quality by design
RH	relative humidity
RMSEC	root mean square error of calibration
RMSECV	root mean square error of cross validation
RMSEP	root mean square error of prediction
rpm	rotations per minute
RS	resonance sensing
RSD	residual standard deviation
SEC	standard error of calibration
SEM	scanning electron microscopy
SEP	standard error of prediction
SFSTP	La societé Française des sciences et techniques pharmaceutique
SFV	spatial filter velocimetry
SIMCA	soft independent modeling of class analogies
SNV	standard normale variate
SSA	specific surface area
TA	anhydrous theophylline
TH	theophylline monohydrate
TS	tensile strength
UV	univariate

UV-VIS	Ultraviolet-visible
WBC	water binding capacity
XRD	X-ray diffraction

CHAPTER 1

INTRODUCTION AND OBJECTIVES

"Perplexity is the beginning of knowledge."

Kahlil Gibran (1883-1931)

CHAPTER 1

INTRODUCTION AND OBJECTIVES

Pharmaceutical manufacturers of conventional solid dosage forms (i.e. capsules, tablets) are interested to switch from batch processing towards continuous processing [1]. Continuous processing is a method to manufacture, produce or process materials without interruption, hence making the most amount of product in the least amount of space and time. It is characterized by (i) an integration of all unit operations and (ii) the "one in, one out" principle. Starting materials are continuously fed into the process, whilst end products are continuously removed at the same speed [2]. Furthermore, during the last decade, several companies have developed full from-powder-to-tablet production lines [2]. It is obvious that for continuous processing real-time quality control is indispensable. Therefore, the need to invest in process analytical technology (PAT) is strengthened.

The adoption of continuous manufacturing of solid dosage forms brings several advantages, but also challenges (Table 1.1). The advantages have their impact in three fields: advantages regarding (i) product development and quality, (ii) costs and (iii) ecological footprint. Continuous production equipment does not imply scale-up issues, since the size of the production lot is defined by the factor 'time'. Therefore, the same equipment size can be used for development and pilot studies, clinical trials and full commercial production. Since the time-intensive scale-up experiments are hence annulled, the development time can decrease significantly and the product can be launched faster to the market. It is important to mention that, especially now with scarcely filled pipelines, a shorter development time implies a longer monopoly for the company prior to the product patent's expiration. This is of course a major economic advantage. An economical comparison between batch and continuous pharmaceutical production has been performed by Schaber et al. [3]. The capital investment of a continuous plant is lower since the equipment is smaller and intermediate products do not need to be stored and transferred. Therefore, less floor space is required. In addition, the operating expenses decrease, because less operators are required for both

processing, transferring and storage. The evaluation and assurance of product quality will no longer occur via off-line testing, which implies a significant cost reduction as well. Furthermore, the production of tablets in a continuous way will be more sustainable than via batch production, since the footprint reduces significantly [4].

Table 1.1. Advantages and challenges for the adoption of continuous processing in the pharmaceutical industry.

Advantages	Challenges
No scale-up issues	Regulatory uncertainty
Ease of automation	Less flexible regarding successive process steps
Production of desired product amount	Need for fast steady state
Better product quality assurance	Need for robust processes
Shorter product development time	No obvious batch definition
Shorter time-to-market	Production changes for already licensed products
Just-in-time production	New mind-set needed for quality assurance (based on continuous in-process measurements)
Reduced capital investment	
Reduction of labor costs	
No transferring of intermediate products	
No storing of intermediate products	
Less floor space required	
Less energy consumption	
Less waste	

One fair comment is that continuous manufacturing processes allow less flexibility. It is true that batch processes are very flexible. An almost infinite amount of different process steps can be virtually chained, whereas a continuous physically chained process is what is it. However, recent advances have been made in the development of readily 'plug and play' continuous equipment, which allows flexible changes between direct compression and wet and dry granulation [5]. Continuous processes need to be robust for changes in raw material product quality and need to reach a fast steady state to avoid wastage of product. The "batch"-concept is deep-seated within the pharmaceutical industry and small batches

minimize financial losses in case a product needs to be recalled. A continuous process asks for a different tracking method, for example by means of time stamps. Nevertheless, the biggest burden for the pharmaceutical industry to adopt continuous manufacturing seems to be the regulatory issues. If changes are made in the production of an already licensed product, these changes will have to be re-evaluated by the authorities. When a new production line needs to be evaluated and the product registration must be renewed, it is the right time to switch from batch to continuous processing. A continuously produced pharmaceutical has already been licensed, namely nimesulide-tablets (Severin® by Chinion) are licensed and available on the Mexican market.

Batch processes have mostly relied on off-line analysis for quality evaluation of intermediate and end products (i.e. Quality by Inspection). Continuous processes on the other hand should be evaluated *in real-time* by means of at-line, on-line and in-line measurements as it is described in the PAT guidance for industry, launched by the FDA [6]. Furthermore, in their "Pharmaceutical Development" guideline, the ICH defines the Real Time Release Testing principle: the quality of both intermediate and final products needs to be evaluated and ensured based on *process data* [7]. These data can then be used for the construction of feedback and feedforward control loops. This means that when a process is fully understood and the quality of the end product can be assured at any time, a product can be released directly to the market after production.

These two guidances [6, 7] have defined the direction of this research thesis. PAT is defined as *"a system for designing, analyzing, and controlling manufacturing through timely measurements of critical quality attributes of raw and in-process materials and processes, with the goal of ensuring final product quality."* In this work, a continuous from-powder-to-tablet production line (ConsiGma™ 25) has been investigated in depth and both the critical quality attributes (CQA's) of raw materials (**Part I**) as of in-process materials, end products and processes have been studied (**Part II**).

In **Chapter 2**, the continuous granulation equipment, used for all research experiments discussed in this thesis, is extensively described. **Chapter 3** provides an overview of the published literature, which discusses the application of PAT tools in continuous

pharmaceutical processes. The focus is on opportunities and challenges regarding the in-line use of the different applied PAT tools.

Part I focuses on the critical quality attributes , performance attributes and processability of different raw materials. As it is stated in the PAT guidance, not all physical and mechanical attributes of raw materials are fully understood. This intrinsic, undetected variability of the starting materials might influence both their processability and the quality of the end product. The ICH Q8 guideline mentions that the physicochemical properties of the drug substance, used in a formulation, should be identified and discussed. In **Chapter 4,** the use of different grades of anhydrous theophylline for continuous wet granulation and tableting is evaluated. Seven different grades of theophylline were taken into account. They differed in several CQA's but the particle size of the starting material was the main variation. The granulation process parameters were kept constant to examine the differences in the end product quality caused by the variability of the raw materials properties only. Lactose monohydrate (67.5%) and polyvinylpyrrolidone (PVP, 2.5%) were used together with the anhydrous theophylline as a model formulation. The formulations containing the different grades of theophylline were granulated and the granules were tableted afterwards. The characteristics of granules and tablets were determined and analyzed by means of principal component analysis (PCA).

Whereas in **Chapter 4**, the variability of the different grades of theophylline was documented by the supplier, **Chapter 5** discusses the effect of *undetected* raw material variability. Indeed, the PAT guidance states that even if the raw materials are conform the pharmacopoeial specifications, there can still be an undetected property, which hinders an adequate production process. The ICH Q8 guideline stresses that next to the properties of the active pharmaceutical ingredient (API), the influence of the excipients on the drug product performance an/or manufacturability should be taken into account as well. Therefore, in **Chapter 5** a case-study is presented, which discusses the influence of undetected variability of microcrystalline cellulose (MCC). During a blind study, the different samples of MCC were granulated together with lactose and starch and the resulting granules were evaluated in order to identify the difference between the six samples. The obtained granules differed in size distribution, due to varying water binding capacity of the MCC

batches. This different water binding capacity was caused by a changing degree of crystallinity. Afterwards, an experimental design was conducted in order to evaluate and compare the effect of both product variability and process variability upon the granule size distribution. This model was used in order to calculate the necessary process parameters to obtain a preset granule size distribution regardingless of the type of MCC used. To end with, different binder types were evaluated to investigate if the difference in water binding capacity was still present when using a binder.

In **Part II**, the measurements of both the CQA's of in-process materials and end products as well as measurements of process parameters itself are discussed.

The quality by design (QbD) principle is defined as *"a systematic approach to development that begins with predefined objectives and emphasizes product and process understanding and process control, based on sound science and quality risk management"* (ICH Q8). The motto is "*quality cannot be tested into products; it should be built-in or should be by design"*. Therefore, the identification of material attributes and process parameters that can have an effect on product CQA's via experimentation is mandatory. In **Chapter 4 and 5**, a typical bimodal size distribution of the granules produced via twin screw granulation was identified. In **Chapter 6**, extra understanding regarding the binder distribution within the granules was gained, in order to evaluate if an inhomogeneous spread of binder is causing this bimodal size distribution. The intra-granular distribution of PVP was evaluated by means of hyperspectral coherent anti-Stokes Raman scattering (CARS) microscopy.

In **Chapter 7**, timely measurements of wet granules are presented. The strengths and weaknesses of Raman and NIR spectroscopy and a particle size distribution analyzer for the real-time monitoring of critical process parameters during the continuous wet granulation of an anhydrous theophylline – lactose blend are discussed. The solid state characteristics and particle size of the granules were analyzed in real-time and the critical process parameters influencing these granule characteristics were identified. The effect of the temperature of the granulator barrel, the amount of granulation liquid, the powder feed rate and the screw speed was evaluated by means of an experimental design.

Chapter 8 focuses on the continuous fluid bed dryer. Conventionally, the end point of fluid bed drying is either time-defined or derived from indirect parameters (i.e. humidity of the outlet air and product temperature). The PAT guidance suggests to improve the efficiency of pharmaceutical processes by reducing production cycle times through the use of on-, in- and/or at-line measurements instead of these time-definitions. In **Chapter 8**, the classic indirect methods are compared to both in-line moisture and solid state determination by means of PAT tools (Raman and NIR spectroscopy) and a mass balance approach. A PLS, NIR-based moisture determination model was constructed and six test-experiments were conducted afterwards. The product was monitored in-line with both NIR and Raman spectroscopy during drying. In **Chapter 9**, a thorough validation of an in-line NIR based moisture determination model by means of the accuracy profile approach is presented. The β-expectation tolerance interval (expressing 95 out of 100 future in-line moisture assessments) for the residual moisture content assessment at the end of the continuous drying process, was evaluated.

In **Chapter 10**, the QbD principle is applied on granules when leaving the fluid bed dryer. The two evaluated CQA's were the residual moisture content and the solid state of the active pharmaceutical ingredient (API), theophylline. The different size fractions of the dried granules obtained during various experiments (fines, yield and oversized granules) were compared separately in order to investigate if differences in solid state of theophylline and/or moisture content occur between the different granule size fractions.

In the PAT guidance several possible steps for *process control* are listed. In **Chapter 11**, this approach is applied with regards to dry granules. The evaluated CQA's are residual moisture content, solid state of the API and flowability of the granules. The granules were monitored at-line by means of three complementary PAT tools (NIR and Raman spectroscopy as well as photometric imaging). Then, a mathematical relationship between the product QA's and the at-line measurements was developed in order to predict the products' QA's by means of the data obtained via PAT tools.

In **Chapter 12**, the in-line blending capacity of the twin screw granulator of the ConsiGma™ 25 unit is investigated. Furthermore, the feasibility of in-line NIR spectroscopy (SentroPAT,

Sentronic GmbH, Dresden, Germany) for evaluating the blend uniformity of powders after the granulator was tested. Anhydrous theophylline was used as a tracer molecule and was blended with lactose monohydrate. Theophylline and lactose were both fed from a different feeder into the twin screw granulator barrel. The blend homogeneity was evaluated by means of the moving F-test.

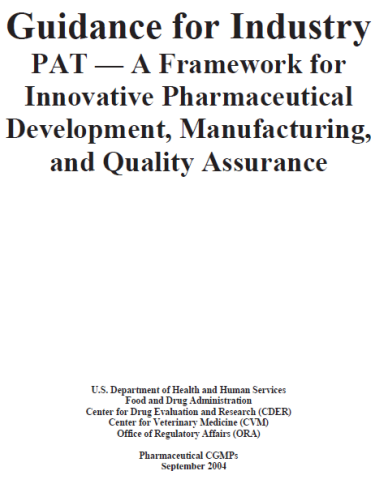

Guidance for Industry

PAT — A Framework for Innovative Pharmaceutical Development, Manufacturing, and Quality Assurance

U.S. Department of Health and Human Services
Food and Drug Administration
Center for Drug Evaluation and Research (CDER)
Center for Veterinary Medicine (CVM)
Office of Regulatory Affairs (ORA)

Pharmaceutical CGMPs
September 2004

INTERNATIONAL CONFERENCE ON HARMONISATION OF TECHNICAL REQUIREMENTS FOR REGISTRATION OF PHARMACEUTICALS FOR HUMAN USE

ICH HARMONISED TRIPARTITE GUIDELINE

PHARMACEUTICAL DEVELOPMENT
Q8(R2)

Current *Step 4* version
dated August 2009

This Guideline has been developed by the appropriate ICH Expert Working Group and has been subject to consultation by the regulatory parties, in accordance with the ICH Process. At Step 4 of the Process the final draft is recommended for adoption to the regulatory bodies of the European Union, Japan and USA.

REFERENCES

[1] K. Plumb, Continuous Processing in the pharmaceutical industry - Changing the Mind Set, Chemical Engineering Research and Design, 83 (2005) 730-738.

[2] C. Vervaet, J. Vercruysse, J. Remon, T. De Beer, Continuous Processing of Pharmaceuticals, in: Encyclopedia of Pharmaceutical Science and Technology, Fourth Edition, Taylor and Francis, New York, 2013, pp. 644-655.

[3] S.D. Schaber, D.I. Gerogiogis, R. Ramachandran, J.M.B. Evans, P.I. Barton, B.L. Trout, Economic analysis of integrated continuous and batch pharmaceutical manufacturing: a case study, Industrial & Engineering Chemistry Research, 50 (2011) 10083-10092.

[4] W. De Soete, J. Dewulf, P. Cappuyns, G. Van der Vorst, B. Heirman, W. Aelterman, K. Schoeters, H. Van Langenhove, Exergetic sustainability assessment of batch *versus* continuous wet granulation based pharmaceutical tablet manufacturing: a cohesive analysis at three different levels, Green Chemistry, 15 (2013) 3039-3048.

[5] P. Hurter, T. Hayden, D. Nadig, D. Emiabata-Smith, A. Paone, Implementing continuous manufacturing to streamline and accelerate drug development, AAPS Newsmagazine, (2013) 15-19.

[6] FDA-Adminstration, Guidance for Industry - PAT - A Framework for Innovative Pharmaceutical Development, Manufacturing, and Quality Assurance, in, 2004.

[7] International Conference on Harmonisation of Technical Requirements for Registration of Pharmaceuticals for Human Use. Pharmaceutical Development Q8, in, 2009.

CHAPTER 2

ConsiGma™ 25

"I am turned into sort of machine
for observing facts
and grinding out conclusions."

Charles Darwin (1809-1882)

CHAPTER 2

ConsiGma™ 25

All granulation experiments described in this thesis are conducted on the ConsiGma™ 25 (Figure 2.1), a product of GEA Pharma Systems, Collette™, situated in Wommelgem, Belgium. In this chapter, the set-up of the system as installed at Ghent University is described in detail. The ConsiGma™ 25 consists of four parts: the powder feeding system, the twin screw granulator, the segmented fluid bed dryer and the granule conditioning unit. Afterwards, the Modul™ P rotary tablet press and a ConsiGma™ coater can be coupled to the system. One asset of the system is that numerous univariate process parameters (e.g., temperatures, pressures, humidity etc.) and conditions are continuously monitored and logged every second.

2.1. POWDER FEEDING SYSTEM

Powder feeding happens via a twin screw loss-in-weight feeder (KT20, K-tron, Niederlenz, Switzerland). Mixtures of powders need to be pre-blended prior to loading them into the hopper of the feeder. At the start of each new production cycle a feed factor calibration needs to be performed. During 40 seconds, the motor of the powder dosing unit will turn at a speed of 200 rpm. The weight loss during these 40 seconds is determined and from this information the feed factor is calculated. The feed factor is then used to calculate the necessary speed of the powder dosing motor to obtain a preset powder feed rate. The powder is fed into the first segment of the granulator barrel after passing a rotational bridge breaker. During powder feeding the mass flow (kg/h), speed of the powder dosing motor (rpm) and the total weight of the powder dosing unit (kg) are continuously monitored. Furthermore, the average feed factor is continuously calculated and saved as well. There is a possibility to add a second feeder, which feeds the powder in a second inlet in the granulator barrel. The distance between the two powder feed ports is approx. 13.5 cm.

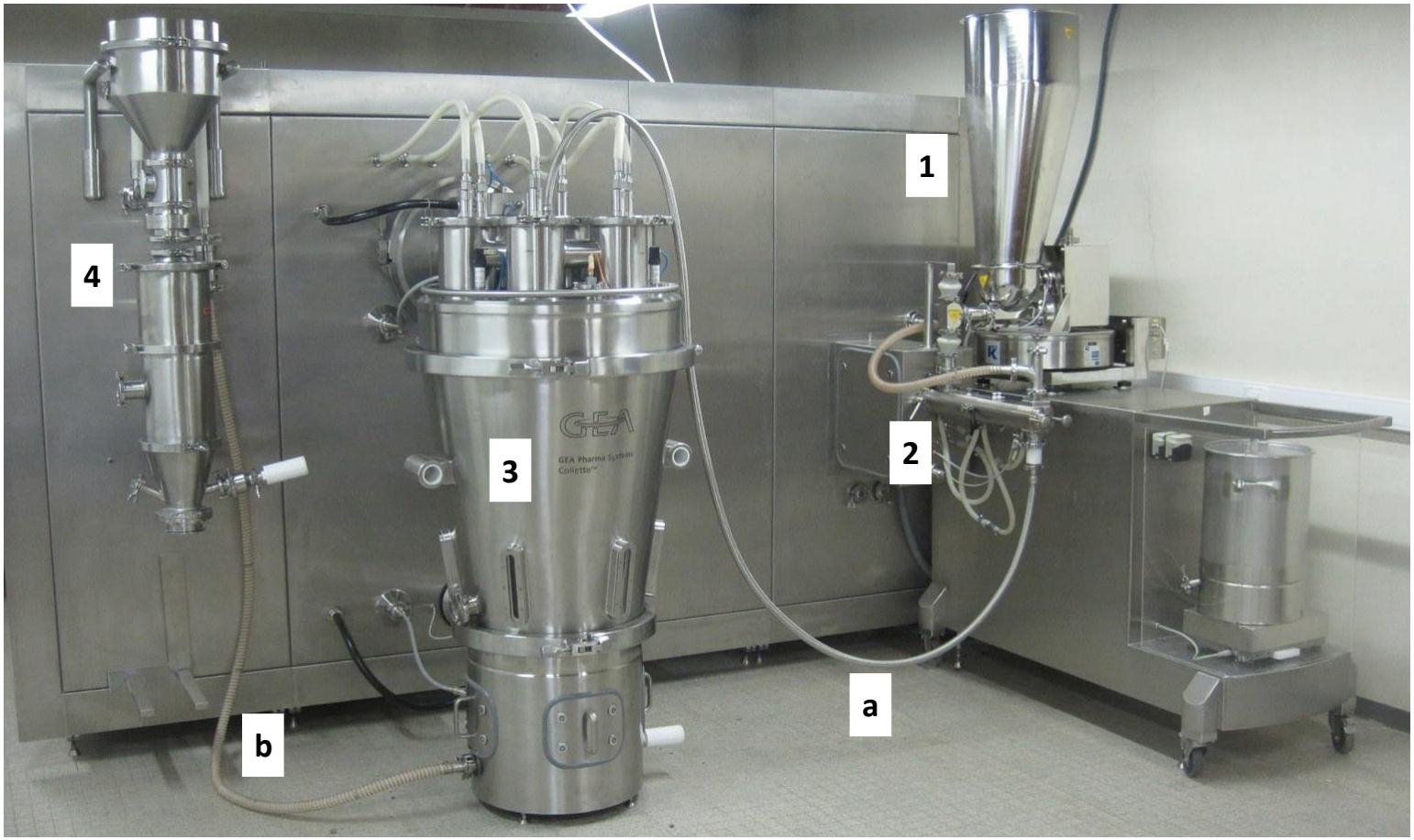

Figure 2.1. Set-up of the ConsiGma™ 25 at Ghent University with (1) powder feeding system, (2) twin screw granulator, (3) six-segmented fluid bed dryer and (4) granule conditioning unit. The two transfer lines are indicated with (a) and (b).

2.2. TWIN SCREW GRANULATOR

The granulator (Figure 2.2) comprises a segmented barrel equipped with two co-rotating screws. The granulator barrel consists of three parts: (i) a feed segment with two powder feed ports, (ii) a work segment, where granulation liquid is added to the system and (iii) a discharge element, via which the granules are transported to the fluid bed dryer. The temperature of the barrel wall is controlled by means of water, which is cooled or heated in a temperature control unit. Unfortunately, the temperature of the barrel wall (i.e. 'jacket temperature) can only be pre-set. The water in the temperature control unit will be cooled or heated to that pre-set jacket temperature. Although the actual temperature of the granulator barrel is monitored, no feedback system towards the temperature control unit is implemented.

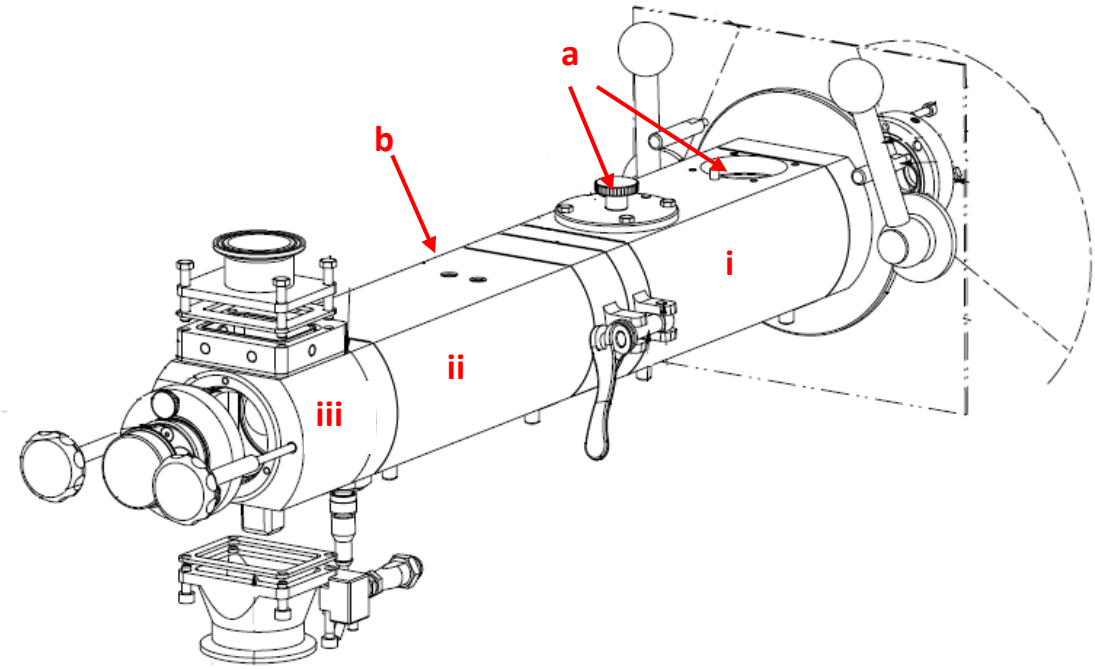

Figure 2.2. Granulator barrel consists of three parts: (i) feed segment, (ii) work segment and (iii) discharge element. With: (a) two powder feeder ports, (b) liquid addition ports.

The granulation liquid needs to be fed manually in the granulation liquid tank. From this tank, the granulation liquid is transported to the granulator via two tubes by means of two peristaltic pumps. The two tubes end in two injection nozzles which are mounted in the work segment of the granulator (Figure 2.2, b) and feed the granulation liquid into the barrel. The liquid addition is also monitored by means of loss-in-weight. For the calibration of the liquid feeding system, two liquid pump speeds need to be pre-set. During one minute, the pump will turn at speed 1 and the weight loss is determined, the same happens for speed 2. From this information, a calibration curve is derived and the needed speed for a pre-set liquid addition (g/min) is calculated and evaluated at the calibration stage.

The screws (Figure 2.3) have a length-to-diameter ratio of 25:1 and consist of a shaft, which can be filled with screw elements ad libitum. Next to conveying elements, kneading elements can be added to the screws. The formulator can change the screw configuration by changing the amount of kneading zones, the amount of kneading elements in one kneading zone and the staggering angle between two kneading elements (30°, 60°, 90°).

The wet granules are pneumatically transferred from the discharge element to the fluid bed dryer via a transfer line (Figure 2.1, a).

Figure 2.3. Twin screws.

2.3. SEGMENTED FLUID BED DRYER

The fluid bed dryer (Figure 2.4) consists of six identical drying cells (Figure 2.5). Wet granules are loaded in the fluid bed dryer via the wet granule inlet tube. At the start of the process, wet granules are loaded in cell one, during a preset filling time. After this filling time, the wet granule inlet tube rotates towards the second cell to continue the transfer of the continuously produced granules in cell two. Granules will dry in their respective cell during a set drying time. This implicates that there exists a difference in drying time between the first and last loaded granule in each cell. After a set drying time period the granules are subsequently guided from the drying segment through a rotational outlet valve. They are pneumatically transported via transfer line b (Figure 2.1) to the granule conditioning unit. The repeated cycle of filling, drying and discharging in each cell makes continuous drying possible.

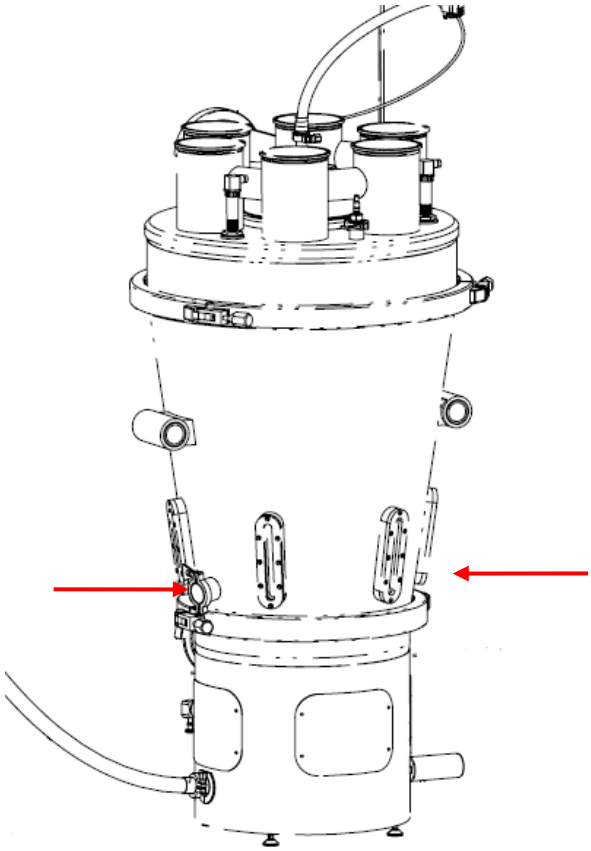

Figure 2.4. Six cell segmented fluid bed dryer, the PAT interfacing places are indicated.

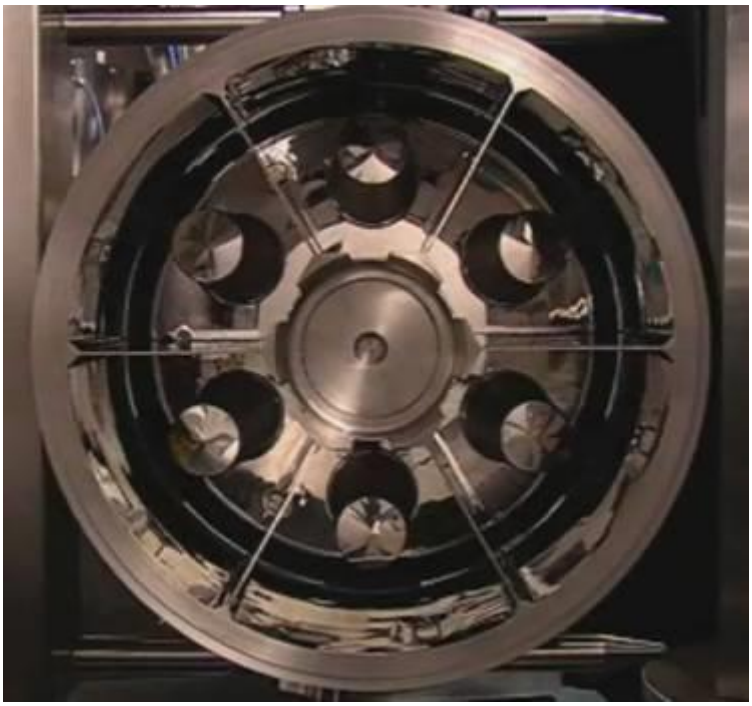

Figure 2.5. Six cell segmented fluid bed dryer.

The dryer air distribution plate, found in the bottom of the fluid bed dryer is characterized by a unique pattern of openings in the plate. The openings are each directed in another direction, resulting in a “flowing wave” pattern of the powder instead of a spouted bed pattern.

Both the temperature of the drying air (°C) and the applied air flow (m^3/h) need to be set. The humidity of the drying air (% RH) cannot be controlled but is monitored both at the inlet and the outlet of the dryer via one sensor. Hence this sensor is monitoring the humidity of the air as a result of the six drying cells. Each cell individually is equipped with a temperature sensor, which measures the product temperature (°C). The fluid bed dryer is equipped with two PAT interfacing places, namely in cell two and cell five (Figure 2.4).

2.4. GRANULE CONDITIONING UNIT

The dry granules are consecutively transferred per cell to a product evaluation unit (Figure 2.6), where they are collected in a product control hopper (PCH). The dry granules are gradually fed to the mill in via a metering valve. A Quadro Comil U10 mill is used, which is equipped with a conical mill screen with a companioning impeller. A mill screen with round holes is used in this set-up. Two screen hole diameters are available, namely 1397 µm and 1575 µm. After milling, the milled product is collected in a milled product buffer reservoir. When all the product from one cell is milled, the outlet valve of the reservoir will be opened. A PAT interfacing station is provided under the PCH above the metering valve. Beneath the outlet valve of the reservoir a blender can be added.

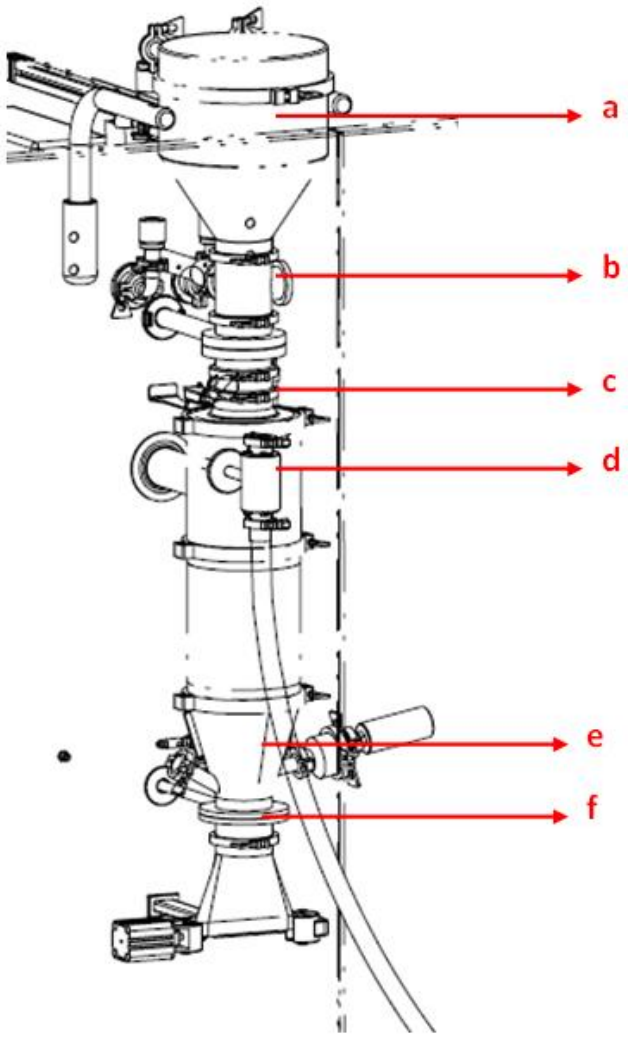

Figure 2.6. Granule conditioning unit with (a) Product Control Hopper, (b) PAT interfacing station, (c) metering valve, (d) mill, (e) milled product buffer reservoir and (f) outlet valve.

2.5. TABLET PRESS AND COATER

Although the dry granules are transferred to the conditioning unit per cell, granules from different cells can be combined again in the hopper of the tableting press. A rotary tablet press (Modul™ P, of GEA Pharma Systems, Courtoy™, Halle, Belgium, Figure 2.7) can be connected for tablet compression. The Modul™ P is a high speed 10-station rotary tablet press, with some typical characteristics: (i) the exchangeable compression module (ECM) concept is applied on this press. The ECM is fully contained and can be removed for cleaning. This means that only the ECM needs cleaning, and not the whole press. (ii) The press can be equipped with two different kinds of tooling (B and D) on the same die table and (iii) the equipment is capable of constant density tableting. Besides conventional compression to constant thickness, the Modul™ P also has the ability to apply compression to a constant compression force on pre- as well as on main compression, thanks to an air compensator system. The press can be used with a speed of 5 rpm, as well as 100 rpm and is therefore suitable for both R&D experiments as industrial scale production. Recently, a ConsiGma™ coater has also been developed. A twin drum coater system (Figure 2.7) can be attached to the ConsiGma™ line for continuous coating and has a capacity up to 30 kg/h.

Figure 2.7. Modul P™ tablet press and twin drum coater.

CHAPTER 3

STATE OF THE ART

"Study the past, if you would divine the future."

Confucius (551-479 BC)

CHAPTER 3

STATE OF THE ART

3.1. INTRODUCTION

This chapter aims at summarizing the status of the implementation and suitability of PAT tools for *continuous* pharmaceutical manufacturing processes of solid dosage forms, focusing on opportunities and shortcomings. In fact, several processing steps, currently used in batch manufacturing are continuous as such: (i) feeding, (ii) continuous milling, (iii) roller compaction, which is a dry granulation technique, (iv) direct compression, where the blend of the API and excipients is directly compressed into tablets and (v) spray-drying, in which a liquid is atomized into drops and then dried in a hot air flow, are examples of classical continuous processes (Figure 3.1).

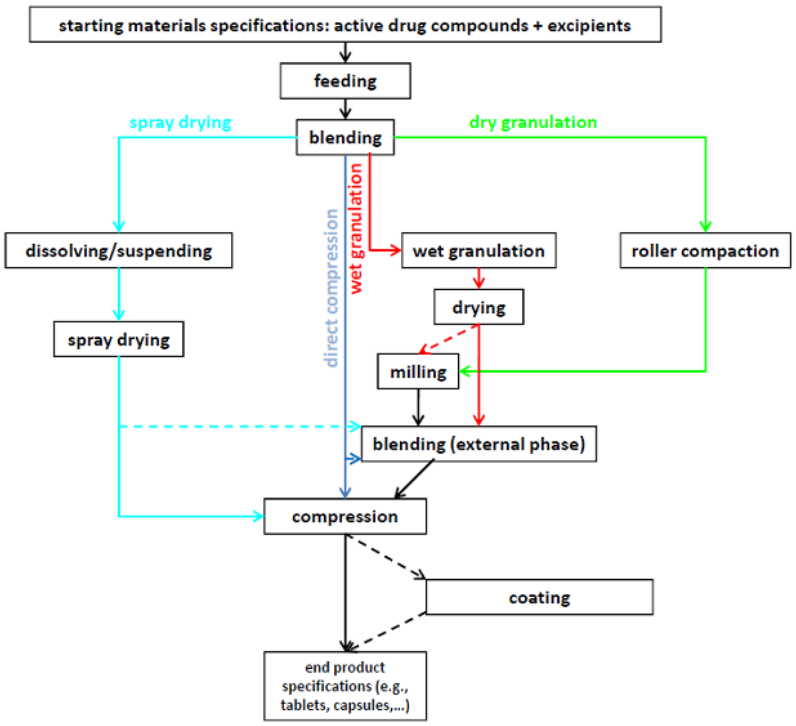

Figure 3.1. Most used industrial processes for the production of pharmaceutical solid dosage forms.

3.2. CONTINUOUS MATERIAL TRANSFER

At certain timepoints during pharmaceutical processes the homogeneity (segregation) of powder streams needs to be evaluated. The in-line measurement of powder streams is challenging, for several reasons: (i) fouling of the measurement probe frequently occurs, (ii) it is not always easy to define the actual sample size (e.g., the sampling volume of powder measured during the collection of a spectrum) and (iii) the location of the probe should be investigated since the probe should not block nor influence the powder stream. At the same time it should be implemented such that the actual moving powder stream is measured, and not, for example, only powder which is sticking to the hopper wall (i.e. when channeling occurs). Benedetti et al. [1] developed a specially designed, non-contact sampling interfacing device with sapphire glass to quantitatively evaluate the API concentration in a flowing powder stream by means of Near Infrared (NIR) spectroscopy. Spectra collection happened through the sapphire window and no fouling of the window has been reported. A partial least squares (PLS)-calibration model was built, using manually blended samples, which were measured in a static way. These samples were not fully homogeneous, and so, not representative for the actual powder stream, which was homogenously blended on an industrial scale. The authors solved this problem by averaging ten calibration spectra of each manually produced calibration blend and then obtained a good PLS model. Another concern was the fact that statically collected measurements are not influenced by any interference of air diffusion, powder packing differences or flow velocity. The spectral variation did not seem to be affected by the flow rate, whereas differences in compaction level and particle flow discontinuity could be removed by data pretreatment. The real-time measured API concentration showed a large standard deviation (around 6%), but this was overcome by averaging the model-predicted API concentration over one unit dose of product.

3.3. CONTINUOUS BLENDING

Till now, two techniques have been presented for the monitoring of continuous blending, namely NIR and Light Induced Fluorescence (LIF). In 2010, Vanarase et al. [2] constructed an NIR PLS model to determine the API concentration of flowing powder in-line. The spectra were collected from blends, passing under the NIR probe head on a chute at the outlet of a continuous blender. The calibration model was constructed using spectra of flowing powders. In a second paper [3], measurements were again conducted with the help of a chute, but this time a multi-point NIR system, equipped with 5 probes was mounted above the chute. Multi-point systems have several advantages such as instrument or process failure diagnostics (by comparison of the spectra collected by different probes). Furthermore, one spectrometer can be used to monitor a whole continuous production process. In this study, the correlation between in-line (NIR) and off-line (UV) measurements was determined as well as the analytical method error of the respective methods, which was negligible for both techniques. A PLS-calibration model was constructed with spectra of static samples. One PLS model was constructed, based on the spectra collected by the five different probes. The model consisted of five latent variables, which was due to the fact that the use of different probes increased the complexity of the spectra. Another way to overcome this, would have been the construction of five separate models, one for each probe. In this paper the calculations of the amount of spectra that need to be averaged in order to be comparable to one unit dose, are also explained extensively. Whereas Vanarase et al. prepared the calibration samples with a separate batch blender, Martínez et al. [4] produced the calibration samples for the construction of a PLS model directly with the continuous blender, which was equipped with two feeders. A PLS model for API-quantification was constructed and the influence of changing process parameters was evaluated. When the powder flow rate was decreased, the predicted API concentration decreased with 20% as well, whereas the HPLC reference method showed that the blend was within spec. The authors suggest that a lower interaction between incident light and powder particles might cause this underestimation. On the other hand, the absolute prediction of the target concentration was not influenced by changing the rotation speed of the blender. Moreover, a decreasing rotation speed led to less fluctuations in the predictions

of the API concentration and the residual standard deviation (RSD). This is because at lower rotation speeds the sample is presented more adequately to the NIR probe and the mixtures are more uniformly blended at lower rotations speeds. The authors also applied principal component analysis (PCA) on the spectra of runs with different process parameters. The PCA classified the spectra according to stirring rate (PC1) and powder flow rate (PC2), indicating that NIR is sensitive to powder flow and powder density. The according loadings of the principal components were reported to be complicated to interpret. Furthermore, the in-line collected spectra were used to determine the start-up, steady-state and shutdown phase of the continuous blending process. Calculations were performed via PCA, the RSD and Moving Block Standard Deviation (MBSD), but no method was superior to another for the determination of the end of the start-up phase.

An extensive study on the performance of both a continuous ZigZag® blender and a double helical ribbon blender has been conducted by Pernenkil [5]. Tests were not only performed by in-line NIR spectroscopy, but Light Induced Fluorescence was used as well. In [6], Volker Kehlenbeck summarizes parts of his PhD dissertation [7], in which in-line concentration determination of continuously blended mixtures by means of NIR was published. Furthermore, a device that can be mounted on a probe head and cleans the probe tip by means of compressed air during processing was presented.

Although Raman spectroscopy has proven its usefulness to monitor blend homogeneity in batch processes [8, 9], to our best knowledge, no applications of Raman spectroscopy in continuous blending have been presented so far.

3.4. SPRAY DRYING

Particle size distribution is a critical quality attribute (CQA) of spray-dried material and therefore the size of the microspheres was monitored by a laser diffraction system [10]. The performance of the system was compared when used in-line, at-line and off-line. In-line measurements were performed in between the spray dryer and the cyclone, whereas the at-line measurements were conducted after the product had left the process stream. Off-line analysis was performed both by laser-diffraction and light microscopy. Both during the in- and at-line measurements a purge air flow was a necessity in order to prevent adherence of particles to the lenses of the measurement system. Furthermore, extra purged air was used for a better dispersion of the particles during the at-line measurements. The four different measurements did not lead to the same results: the median particle size was found to be higher when the measurements were conducted in-line. The results from the at-line and off-line laser diffraction were similar, but still higher than the median particle size values obtained via light microscopy. This phenomenon was caused by the abundance of a dispersion stage during in-line measurements, resulting in the measurement of more agglomerates instead of discrete particles. On the other hand, an in-line system measures product changes in real-time, providing information regarding intermittent process upsets, length of the start-up phase, etc. Unfortunately, the in-line system seemed to be insensitive to small changes in particle size. Furthermore, the at-line set-up has the advantage that lenses can be cleaned without the need to stop the production process. Moreover, the same measurement equipment can be used after different processes, which allows a greater flexibility and reduces the costs. Even though the at-line analysis method is destructive, it was still preferred by the authors.

3.5. ROLLER COMPACTION

The first monitoring technique applied on roller compaction is acoustic emission, where the signal produced by compressed powder is recorded with a microphone and then transformed to a frequency spectrum [11-13]. Changes in acoustic emission bands could be noticed with various compression forces and when capping occurred. The in-line monitoring of roller compaction has also been studied by a research group at Purdue University (US), which has performed several studies with NIR spectroscopy on roller compacted ribbons. The CQA's of roller compacted granules are the granule characteristics (moisture content, relative density, tensile strength, particle size distribution, …) and the content uniformity. To monitor these CQA's, a series of three studies has been presented [14-16], in which NIR spectra from the mid-point of the ribbons as they exited the rolls were, collected in-line. In a first study, samples were produced under different process conditions and measured off-line to construct predictive models. These models, constructed with off-line data, were then used to monitor the continuously produced ribbons in real-time. When ribbons were produced with higher compression forces, an increase in absorbance could be notified. Then, a model for the prediction of the mechanical strength of the ribbons, based on the slope of the best-fit line through the spectra was constructed (calculated by regression analysis). The model could also be used to predict the particle size distribution of the compacts after milling [14]. In a second study [15], PLS models were constructed in order to predict the moisture content, relative density, tensile strength and Young's modulus of the ribbons. Although the off-line constructed model showed good agreements between the spectra and the values from reference methods, the model could not be transferred to an in-line setting. Large differences between the values obtained by means of reference techniques and the predictions from the PLS model could be notified. This was due to the fact that the NIR-spectra, used for the construction of the PLS model were collected after 24h of storage. The different degrees of elastic recovery between fresh and stored ribbons caused the discrepancy, according to the authors. Therefore, in their next study [16] the off-line spectra for model-construction were collected from the ribbons directly after their production. Again, an NIR based PLS model for the prediction of relative density, moisture content, tensile strength and Young's modulus was constructed. In this study, an API was added to

the ribbons as well, so the PLS model also predicted for API concentration. This time, good agreements between the values predicted by the NIR method and values obtained via reference methods were found. Nevertheless, whereas the scatter on the predicted moisture content and API concentration values was low, large scatter was found for the predictions of the other three characteristics. The authors explained that this is due to the phenomenon of powder by-pass during roller compaction. This is a small amount of powder, which is not compacted, and hence creates dust clouds. These powder clouds are also measured by the NIR probe, and whereas the moisture content and API-concentration in the powder cloud is similar to that of the ribbon, this is not the case for relative density, tensile strength and Young's modulus. Consequently, extra scatter is caused for the latter properties. These studies also learned that it is important to conduct the calibration experiments in similar circumstances as the circumstances the model will be applied in afterwards. Later, predictive models for granule and ribbon properties were constructed, taking not only the NIR spectral slope into account, but also including the raw material properties, operating parameters and the roll gap [17].

The fact that dust and the rather low detection sensitivity might lead to inconsistent collection of in-line NIR spectra was also recognized by Feng et al. [18]. They determined the sources of variability in in-line collected NIR spectra during roller compaction (i.e. motion of the rolls) and designed a new in-line control kit. By using this kit, the above mentioned dust clouds reduced, hence the light stray effects decreased as well. Furthermore, the position and movement of the ribbons was strictly controlled after compaction, which reduced the fluctuations in light stray even more. Less relaxation and deformation of the ribbons occurred, causing less disturbances in the NIR signal as well.

In 2012, a study, monitoring ribbon density in real-time by means of NIR, aimed at implementing NIR spectroscopy to monitor physical changes in the ribbons, which are caused by variation in the operating conditions [19]. Not only pure spectral changes (baseline shifts) were evaluated for monitoring, but also PCA (qualitative analysis) and PLS (quantitative analysis) were used. The authors reported that PCA was the most suitable and less time-consuming method for density measurements.

NIR spectroscopy has also been compared to microwave resonance sensing for the in-line monitoring of density and moisture content of roller-compacts [20]. PLS models were constructed and in both cases microwave resonance proved to be more accurate than NIR. Root mean square errors were double as high for NIR compared to microwave resonance models. Both techniques have different penetration depths: where the penetration depth of NIR is a few millimeters, microwave resonance sensors penetrate several centimeters in the material, hence the microwave signal is transmitted through the whole ribbon. Since there is a direct relation between microwave sensor measurements and the presented mass in the measurement field, an accurate model for the determination of ribbon density could be obtained. Furthermore, there is a high contrast between the dielectric properties of water and most excipients, leading to the fact that microwave resonance is very sensitive to water. Hence, microwave resonance models are more accurate than NIR-models for moisture determination as well. In addition, no chemometrical calculations are necessary to derive the relevant information out of microwave resonance data. On the other hand, microwave resonance does not provide chemical information of the sample, as does NIR.

A research group in Singapore has performed similar work on *ribbed* flakes produced by means of roller compaction. Different PLS models, based on off-line NIR spectra were constructed for the prediction of API concentration, tensile strength, Young's modulus and relative density [21]. Calibration spectra were collected both in a static and a dynamic way (with a conveyor belt). The advantage of dynamic spectra collection is that a larger sample size is measured. The performance of the models was superior when using the spectra which were collected (i) dynamically and (ii) at the underside of the conveyor belt. A good correlation between the predicted and reference value was observed for all characteristics. The variation of the predicted tensile strength, Young's modulus and relative density was higher than the variation of the API concentration. This was again attributed to the fact that samples were stored during three days prior to off-line investigation and were subject to relaxation and temperature effects. The researchers corrected for the powder by-pass dust cloud by vacuuming out the dust particles, hence preventing the probe from fouling. In a second study [22] the optimal probe lens diameter and distance to the sample were determined.

3.6. TWIN SCREW GRANULATION

Critical quality attributes of wet granules are: solid state of the API and excipients, granule size distribution, shape of the granules, flowability and moisture content.

The influence of process parameters upon the solid state of theophylline (anhydrous or monohydrate) after twin screw granulation has been monitored with NIR and Raman spectroscopy [23]. Both spectroscopic techniques, with the help of multivariate data-analysis, were capable of detecting even small non-expected solid state changes. Solid state differentiation was more definite in the Raman spectra compared to the NIR spectra. As spectra were collected in a static way, more investigations on probe implementation in wet granulation would be advantageous. In the same study the granule size distribution of the wet granules was investigated in a dynamic way, by means of a Spatial Filter Velocimetry probe (Parsum®). Although it was equipped with an air-cleaning system, fouling of the probe remained a problem. The effect of formulation and process parameters upon granule size distribution has also been measured dynamically with a high-speed imaging camera (Eyecon™). This is a photometric stereo imaging technique equipped with LEDs in three colors and provides not only information regarding particle size, but also shape and surface information can be obtained, although not discussed in this study [24]. The size determination measurements do not need prior calibration and the technique is completely non-invasive. An adequate sample presentation is challenging since non-spherical particles will always be presented at their largest particle dimension when they are measured on a chute. Therefore a free-falling stream was used. Furthermore, when the field of view is overfilled, this interferes with an adequate granule size measurement calculation. Therefore, it is important that fine and coarse particles are separated during sample presentation. Fouling might be a problem when working with small powders. The distance of the samples to the lens needs to be constant and adopted to the focus distance of the system. In this study *d10* values and particle count were preferred for process monitoring over *d50* and *d90* values. The camera showed to be sensitive to changes in granule size and count when the liquid:solid ratio was changed.

An extensive study on the mixing behavior of powder and granulation liquid has been conducted by visualizing the granules at-line on a conveyer belt at the outlet of the granulator with NIR chemical imaging [25]. Different formulation and process parameters were investigated and the link between moisture uniformity and granule size distribution was evaluated. Moisture maps, which visualize the distribution of water in the granules on the conveyor belt, showed periodical fluctuations in moisture content. Improvement in moisture uniformity was noted when higher moisture contents and twin screws with more kneading zones were used. Since the granules have to be transported to the camera via a transport belt, this method is not applicable in-line.

Twin screw granulation is also used as the wet granulation technique in a full continuous from-powder-to-tablet production line, which has been recently developed (ConsiGma™ 25 system). Chablani et al. [26] mounted an NIR probe in the conditioning unit (Figure 2.6 (b)), which is situated just after the fluid bed dryer, hence evaluating the dried granules. Two PLS models were constructed where the NIR spectra were regressed against the moisture content of the granules determined via Karl Fischer titration and Loss on Drying respectively. Karl Fischer titration showed to result in the superior model. Only a small range (0.43 to 1.06 % w/w, measured with KF) of moisture contents was evaluated. After the fluid bed granulator, a continuous mill is installed and the particle size distribution of milled granules has been evaluated by focused beam reflectance measurement (FBRM) [27]. Fonteyne et al. [28] performed a Design of Experiments were the temperature of the granulator barrel, the powder feed rate and the temperature of the drying air in the fluid bed dryer were varied. The obtained granules were then evaluated at-line by means of Raman and NIR-spectroscopy and a photometric imaging technique (Flashsizer3D). The spectroscopic techniques gave insight in the changing solid state of the API when different process parameters were applied, whereas the Flashsizer determined the granule size distribution and roughness of the granules. This complementary physical and chemical information was then used to predict the CQA's of the granules, namely moisture content, bulk and tapped density and flowability. Three PLS models were successfully constructed. The spectroscopic data had the highest predictive capability for the moisture content whereas the imaging data were mostly correlated with the flowability of the granules. The measurements were

performed at-line since fouling occurred when using the Flashsizer in-line. The development of an interfacing device which prevents the Flashsizer-window from fouling is the next challenge.

The use of classical fluid bed end point detection methods (i.e. humidity of the outlet drying air and product temperature) has been compared to the use of PAT tools (NIR and Raman spectroscopy) and a mass balance model approach [29]. Both the NIR and Raman spectroscopy probe were mounted in the continuous fluid bed dryer and an NIR-based moisture prediction model was constructed. Next to the real-time monitoring of the residual moisture of the granules, the solid state of the API was also successfully monitored. The PAT approach showed to be superior for real-time end point detection to classical end point detection.

3.7. DIRECT COMPRESSION

In 2009, the successful use of NIR spectroscopy in a tablet press for the monitoring of powder segregation has been presented at the EMEA/Efpia QbD application workshop [30]. Measurements were conducted in-line in the feed frame. Karande et al. [31] placed an NIR probe just after the tablet ejection area and constructed a PLS model for the calculation of the concentration of the API and the excipients. This study exposed that it is important to use similar sampling methods and circumstances for the collection of the calibration spectra as well as the in real-time collected process spectra. Therefore, the calibration spectra were also collected in a dynamic way using the tableting machine, equipped with blank discs instead of punches and dies. Furthermore, preprocessing techniques (Standard Normal Variate-correction and derivatives) were used to minimize effects caused by differences between preparation during calibration and production. The in-line NIR monitoring discovered a segregation towards the end of the production process. The concentration of the API in the tablets decreased in the second half of the process. Whereas this was clearly detected by the NIR method, no anomalies could be detected with the classical UV method. Järvinen et al. [32] did not only monitor the individual tablets on the tablet press but also the powder stream coming from a continuous mixer prior to tableting. Both calibration and test run spectra were collected in-line. This study proved that it is possible to perform a 100% identity check (i.e. each individual tablet is monitored). The goodness of the method was confirmed during test runs with differing API content, tableting speed and compaction force. NIR measurements have also been performed in the feed frame of a tablet press [33]. The derivative intensity of the API band was plotted versus time and the influence of mass flow rate, potency ingress and paddle wheel speed upon the method's performance was studied. Both at changing mass flow rate and potency ingress the change in NIR signal could be correlated to the off-line measured tablet potency. When changing the paddle wheel rotation speed though, a faster increase of the NIR signal compared to the tablet potency could be detected. The reason for this discrepancy was not yet understood.

3.8. SUMMARY

EVALUATED CQA	PAT TOOL	INTERFACING	REFERENCE
continuous powder streams			
% API	NIR	through sapphire window	[1]
continuous blending			
% API	NIR	probe above the powder, which flows on a chute	[2]
% API	multipoint NIR	probe above the powder, which flows on a chute	[3]
% API	NIR	probe measuring at the outlet of the continuous blender	[4]
% excipient	NIR	probe measuring at the outlet of the continuous blender	[6]
Spray drying			
particle size distribution	Laser diffraction (Insitec®)	both in-line and at-line	[10]

Roller compaction			
Compression	acoustic emission	microphone 10 cm away from the powder	[11]
Capping	acoustic emission	microphone, isolated from surrounding structures	[12]
Breaking force particle size after milling	NIR	real-time measurements	[14]
relative density moisture content tensile strength Young's modulus	NIR	non-contact measurements, focus on mid-point of the ribbons	[15]
% API relative density moisture content tensile strength Young's modulus	NIR	non-contact measurements, focus on mid-point of the ribbons	[16]

granule tablet tensile strength granule mean particle size ribbon density	NIR	real-time measurements of the unloaded ribbons	[17]
ribbon density	NIR	real-time non-contact measurements, probe head situated above the ribbons	[19]
ribbon density moisture content	NIR & microwave resonance sensing	NIR: non-contact measurements, probe head situated above the ribbons RS: in-line with the produced ribbon	[20]
% API relative density tensile strength Young's modulus	NIR	use of rectangular channel, creating a constant gap between probe head and flakes	[21]

Twin screw granulation

solid state of the API	NIR, Raman	at-line static measurements, using a cuvet	[23]
granule size (d50)	Spatial filter velocimetry	in-line, dynamic measurements under granulator outlet	
granule size (d10, d50, d90)	high speed imaging camera	camera installed above the powder, which flows on a chute	[24]
moisture distribution	NIR imaging	granules were unloaded on a conveyer belt - camera was installed above the belt	[25]
moisture content	NIR	in-line, implemented in the evaluation module after the dryer	[26]
granule size distribution	FBRM	in-line, implemented after the mill	[27]
moisture content flowability of the granules solid state of the API	NIR, Raman and photometric imaging	at-line, static measurements	[28]
residual moisture content solid state of the API	NIR and Raman	in-line, implemented in the fluid bed dryer	[29]

Direct compression

% API	NIR	in-line, adjacent to the tablet ejection area	[31]
% API	NIR	in-line in the tablet press, measuring each individual tablet	[32]
% API	NIR	through a plexi-glass observation window in the feed frame	[33]

3.9. REFERENCES

[1] C. Benedetti, N. Abatzoglou, J.S. Simard, L. McDermott, G. Leonarda, L. Cartilier, Cohesive, multicomponent, dense powder flow characterization by NIR, International Journal of Pharmaceutics, 336 (2007) 292-301.

[2] A.U. Vanarase, M. Alcala, J.I.J. Rozo, F.J. Muzzio, R.J. Romanach, Real-time monitoring of drug concentration in a continuous powder mixing process using NIR spectroscopy, Chemical Engineering Science, 65 (2010) 5728-5733.

[3] A.U. Vanarase, M. Jarvinen, J. Paaso, F.J. Muzzio, Development of a methodology to estimate error in the on-line measurements of blend uniformity in a continuous powder mixing process, Powder Technology, 241 (2013) 263-271.

[4] L. Martinez, A. Peinado, L. Liesum, G. Betz, Use of near-infrared spectroscopy to quantify drug content on a continuous blending process: Influence of mass flow and rotation speed variations, European Journal of Pharmaceutics and Biopharmaceutics, 84 (2013) 606-615.

[5] L. Pernenkil, Continuous blending of dry pharmaceutical powders, in: Department of Chemical Engineering, Massachusetts Institute of Technology, 2008.

[6] V. Kehlenbeck, Use of near infrared spectroscopy for in- and off-line performance determination of continuous and batch powder mixers: opportunities & challenges, Procedia Food Science, 1 (2011) 2015-2022.

[7] V. Kehlenbeck, Continuous dynamic mixing of cohesive powders in: Lehrstuhl für Maschinen- und Apparatekunde, Technische Universität München, München, 2006.

[8] G.J. Vergote, T.R.M. De Beer, C. Vervaet, J.P. Remon, W.R.G. Baeyens, N. Diericx, F. Verpoort, In-line monitoring of a pharmaceutical blending process using FT-Raman spectroscopy, European Journal of Pharmaceutical Sciences, 21 (2004) 479-485.

[9] T.R.M. De Beer, C. Bodson, B. Dejaegher, B. Walczak, P. Vercruysse, A. Burggraeve, A. Lemos, L. Delattre, Y.V. Heyden, J.P. Remon, C. Vervaete, W.R.G. Baeyens, Raman spectroscopy as a process analytical technology (PAT) tool for the in-line monitoring and understanding of a powder blending process, Journal of Pharmaceutical and Biomedical Analysis, 48 (2008) 772-779.

[10] L.W. Chan, L.H. Tan, P.W.S. Heng, Process Analytical Technology: Application to Particle Sizing in Spray Drying, AAPS PharmsciTech, 9 (2008) 259-266.

[11] A. Hakanen, E. Laine, H. Jalonen, K. Linsaari, J. Jokinen, ACOUSTIC-EMISSION DURING POWDER COMPACTION AND ITS FREQUENCY SPECTRAL-ANALYSIS, Drug Dev. Ind. Pharm., 19 (1993) 2539-2560.

[12] A. Hakanen, E. Laine, ACOUSTIC CHARACTERIZATION OF A MICROCRYSTALLINE CELLULOSE POWDER DURING AND AFTER ITS COMPRESSION, Drug Dev. Ind. Pharm., 21 (1995) 1573-1582.

[13] J. Salonen, K. Salmi, A. Hakanen, E. Laine, K. Linsaari, Monitoring the acoustic activity of a pharmaceutical powder during roller compaction, International Journal of Pharmaceutics, 153 (1997) 257-261.

[14] A. Gupta, G.E. Peck, R.W. Miller, K.R. Morris, Nondestructive measurements of the compact strength and the particle-size distribution after milling of roller compacted powders by near-infrared spectroscopy, J. Pharm. Sci., 93 (2004) 1047-1053.

[15] A. Gupta, G.E. Peck, R.W. Miller, K.R. Morris, Influence of ambient moisture on the compaction behavior of microcrystalline cellulose powder undergoing uni-axial compression and roller-compaction: a comparative study using Near-Infrared spectroscopy, J. Pharm. Sci., 94 (2005) 2301-2313.

[16] A. Gupta, G.E. Peck, R.W. Miller, K.R. Morris, Real-time Near-Infrared monitoring of content uniformity, moisture content, compact density, tensile strength, and Young's modulus of roller compacted powder blends, J. Pharm. Sci., 94 (2005) 1589-1597.

[17] J.L.P. Soh, N. Boersen, M.T. Carvajal, K.R. Morris, G.E. Peck, R. Pinal, Importance of raw material attributes for modeling ribbon and granule properties in roller compaction: multivariate analysis on roll gap and NIR spectral slope as process critical control parameters, Journal of Pharmaceutical Innovation, 2 (2007) 106-124.

[18] T. Feng, F. Wang, R. Pinal, C. Wassgren, M.T. Carvajal, Investigation of the variability of NIR in-line monitoring of roller compaction process by using fast fourier transfrom (FFT) analysis, AAPS PharmSciTech, 9 (2008) 419-424.

[19] D. Acevedo, A. Muliadi, A. Giridhar, J.D. Litster, R.J. Romanach, Evaluation of three approaches for real-time monitoring of roller compaction with Near-Infrared spectroscopy, AAPS PharmSciTech, 13 (2012) 1005-1012.

[20] J. Austin, A. Gupta, R. McDonnell, G.V. Reklaitis, M.T. Harris, The use of Near-Infrared and microwave resonance sensing to monitor a continuous roller compaction process, J. Pharm. Sci., 102 (2013) 1895-1904.

[21] A.K. Samanta, A.D. Karande, K.Y. Ng, P.W.S. Heng, Application of near-infrared spectroscopy in real-time monitoring of product attributes of ribbed roller compacted flakes, AAPS PharmsciTech, 14 (2013) 86-100.

[22] P.V. Quyet, A.K. Samanta, C.V. Liew, L.W. Chan, P.W.S. Heng, A prediction model for monitoring ribbed roller compacted ribbons, J. Pharm. Sci., 102 (2013) 2667-2678.

[23] M. Fonteyne, J. Vercruysse, D.C. Díaz, D. Gildemyn, C. Vervaet, J.P. Remon, T.D. Beer, Real-time assessment of critical quality attributes of a continuous granulation process, Pharmaceutical Development and Technology, 18 (2013) 85-97.

[24] A.S. El Hagrasy, P. Cruise, I. Jones, J.D. Litster, In-line size monitoring of a twin-screw granulation process using high-speed imaging, Journal of Pharmaceutical Innovation, 8 (2013) 90-98.

[25] J. Vercruysse, M.M. Toiviainen, M. Fonteyne, N. Helkimo, J. Ketolainen, M. Juuti, U. Delaet, I. Van Assche, J.P. Remon, C. Vervaet, T. De Beer, Visualization and understanding of the granulation liquid mixing and distribution during continuous twin screw granulation using NIR chemical imaging, European Journal of Pharmaceutics and Biopharmaceutics, in press.

[26] L. Chablani, T.M. K, M. Amit, R. Patrick, S.W. C, Inline Real-Time Near-Infrared Granule Moisture Measurements of a Continuous Granulation-Drying-Milling Process, AAPS PharmsciTech, 12 (2011) 1050-1055.

[27] V. Kumar, M.K. Taylor, A. Mehrota, W.C. Stagner, Real-time particle size analysis using focused beam reflectance measurement as a process analytical technology tool for a continuous granulation-drying-milling process, AAPS Pharmscitech, 14 (2013) 523-530.

[28] M. Fonteyne, S. Soares, J. Vercruysse, E. Peeters, A. Burggraeve, C. Vervaet, J.P. Remon, N. Sandler, T. De Beer, Prediction of quality attributes of continuously produced granules using complementary pat tools, European Journal of Pharmaceutics and Biopharmaceutics, 82 (2012) 429-436.

[29] M. Fonteyne, D. Gildemyn, E. Peeters, S. Mortier, J. Vercruysse, K.V. Gernaey, C. Vervaet, J.P. Remon, I. Nopens, T. De Beer, Moisture and drug solid state monitoring during

a continuous drying process using empirical and mass balance models, European Journal of Pharmaceutics and Biopharmaceutics, (2014).

[30] M. Diller, J. Kerridge, Feedback EMEA/Industry Discussion Eli Lilly & Co Ltd Case study: Use of in-line near-infrared spectroscopy to monitor segregation of a pharmaceutical powder blend in a tablet press, in: EMEA/Efpia QbD Application Workshop, London, 2009.

[31] A.D. Karande, P.W.S. Heng, C.V. Liew, In-line quantification of micronized drug and excipients in tablets by near infrared (NIR) spectroscopy: Real time monitoring of tableting process, International Journal of Pharmaceutics, 396 (2010) 63-74.

[32] K. Jarvinen, W. Hoehe, M. Jarvinen, S. Poutiainen, M. Juuti, S. Borchert, In-line monitoring of the drug content of powder mixtures and tablets by near-infrared spectroscopy during the continuous direct compression tableting process, European Journal of Pharmaceutical Sciences, 48 (2013) 680-688.

[33] H.W. Ward, D.O. Blackwood, M. Polizzi, H. Clarke, Monitoring blend potency in a tablet press feed frame using near infrared spectroscopy, Journal of Pharmaceutical and Biomedical Analysis, 80 (2013) 18-23.

PART I

CHAPTER 4

INFLUENCE OF RAW MATERIAL PROPERTIES UPON CRITICAL QUALITY ATTRIBUTES OF CONTINUOUSLY PRODUCED GRANULES AND TABLETS

"Education is not the filling of a pail, but the lighting of a fire."

Original source unknown

Fonteyne M., Wickström H., Peeters E., Vercruysse J., Ehlers H., Peters B., Remon J.P., Vervaet C., Ketolainen J., Sandler N., Rantanen J., Naelapää K., De Beer T. (2014). Influence of raw material properties upon critical quality attributes of continuously produced granules and tablets, European Journal of Pharmaceutics and Biopharmaceutics, 87, 252-263.

ABSTRACT

Continuous manufacturing gains more and more interest within the pharmaceutical industry. The International Conference of Harmonisation (ICH) states in its Q8 'Pharmaceutical Development' guideline that the manufacturer of pharmaceuticals should have an enhanced knowledge of the product performance over a range of raw material attributes, manufacturing process options and process parameters. This fits further into the Process Analytical Technology (PAT) and Quality by Design (QbD) framework. The present study evaluates the effect of variation in critical raw material properties on the critical quality attributes of granules and tablets, produced by a continuous from-powder-to-tablet wet granulation line. The granulation process parameters were kept constant to examine the differences in the end product quality caused by the variability of the raw materials properties only. Theophylline-Lactose-PVP (30-67.5-2.5%) was used as model formulation. Seven different grades of theophylline were granulated. Afterwards, the obtained granules were tableted. Both the characteristics of granules and tablets were determined. The results show that differences in raw material properties both affect their processability and several critical quality attributes of the resulting granules and tablets.

CHAPTER 4

INFLUENCE OF RAW MATERIAL PROPERTIES UPON CRITICAL QUALITY ATTRIBUTES OF CONTINUOUSLY PRODUCED GRANULES AND TABLETS

4.1. INTRODUCTION

Currently the interest has arisen in the pharmaceutical industry to shift its manufacturing principles from traditional batch production towards continuous production [1, 2]. Continuous manufacturing has several advantages including minimal scale-up issues, reduction in cycle time, less product variability and lower production costs, faster product release, increased flexibility and efficiency, and improvement of product quality. These advantages result for example in a shorter “time-to-market” and lower operating costs. Continuous production allows “just-in-time” production and will minimize the stock, according to LEAN principles. Furthermore, a continuous production line requires less floor space and fewer operators. Hence, once implemented, a continuous manufacturing line will imply a significant cost reduction. Whereas continuous production is well implemented in chemical and food industry, it is still in its infancy when it comes to the pharmaceutical industry. The most common pharmaceutical solid dosage form is the tablet. Tableting often involves a granulation step. Recently, advances in pharmaceutical continuous granulation and tableting have been reported [3-11].

The introduction of continuous manufacturing comes with a major concern: “How to assure a persistent quality of the pharmaceutical products?” The classical off-line quality control analysis methods, which are used in traditional batch production, are not directly suitable

for continuous production. This situation has been greatly improved after the FDA launched its idea of Process Analytical Technology. The PAT guidance [12] states that *"quality cannot be tested into products; it should be built-in or should be by design".* This strengthens the need for an enhanced process knowledge, which is a critical element in the ICH Q8 guideline [13]. This guideline on "Pharmaceutical Development" encourages manufacturers to understand systematically and mechanistically the relationship between critical material attributes and drug products' critical quality attributes (CQA's). Unlike for batch production, where a batch which does not meet the specifications can be rejected, this is not the case for continuous production, where all starting materials introduced into the line will be processed. Therefore, it is relevant to understand the characteristics of the raw materials and their influence on the processability and end product quality.

The influence of raw materials in roller compaction, a continuous dry granulation method, has been investigated by several research groups. The potential impact of starting material properties and processability together with end product specifications and their respective characterization methods has been listed by Hlinak et al. [14]. Mixtures of microcrystalline cellulose (MCC) and lactose, both with varying particle sizes were blended with magnesium stearate and roller compacted by Kushner et al. The particle size of the excipients had a significant influence on the particle size of the granules: larger starting material particles resulted in larger granules. The granulation parameters were kept constant [15]. Different types of lactose were roller compacted by using different combinations of the roller compactor settings (air pressure, roll speed, vertical screw speed and horizontal screw speed) after which the granule friability was evaluated [16]. Soh et al. [17] also roller compacted three different grades of MCC, three grades of lactose and their blends. They used a multivariate data analysis approach in order to construct a model to predict ribbon and granule characteristics. The model consisted of the roller compactor parameters together with the characteristics of the starting materials. Herting and Kleinebudde used theophylline as a model drug [18]. Binary mixtures of MCC and anhydrous theophylline, which differed in particle size, were roller compacted and compressed into tablets. Three different kinds of MCC and anhydrous theophylline with two different particle sizes were evaluated. The tensile strength of both direct compressed tablets and tablets made after

roller compaction increased with lower particle size of the starting powders. Hadzovic et al. [19, 20] used the same API and excipients. Roller compaction, direct compression and tableting after roller compaction were performed on two different grades of anhydrous theophylline (powder and fine powder) and theophylline monohydrate and their blends with MCC. They focused on tensile strength [19] and compressibility [20]. The compressibility of the two anhydrous theophylline powders was higher than of the granules, and the compressibility of theophylline monohydrate increased after roller compaction. The influence of raw material properties of mannitol and dicalcium phosphate on roller compaction and subsequent tableting was investigated by Souihi et al [21], who applied a QbD approach. A study on a twin screw granulator has been conducted as well [22]. Mixtures of lactose, MCC, HPMC and croscarmellose sodium were granulated, while the primary particle size of lactose was varied. The granulator performed robust when changing starting materials, however starting material with a smaller particle size resulted in smaller granules. A similar study was performed by the same researchers, using the Eyecon™ camera [23]. Granules with a different porosity were obtained when the grade of lactose was changed. Haware et al. [24] made tablets by means of direct compression, using nine different types of lactose, differing in particle size, in combination with 1% of magnesium stearate. They found differences in powder compression properties and tensile strength of the tablets, but a clear relationship with the particle size of the starting materials could not be determined. They further managed to predict the tensile strength of the tablets successfully by means of partial least squares models (PLS-1) with the type of lactose and two compression parameters as input. Similar work was done by the same research group, comparing five different grades of MCC. The MCCs differed in particle size distribution and brand [25]. For MCC, they did not find an impact on the compression response (value of plastic deformation) but could correlate the tensile strength to the particle size of the raw materials. Smaller starting material led to stronger tablets. To date, limited studies regarding raw material variability on continuous wet granulation have been published.

It is clear that inherent, undetected variability of the raw materials may be manifested in the final product properties. Furthermore, processing difficulties can arise, which can result in a failure of the aimed end product specifications.

Mevik et al. [26] described a process as follows:

Equation 4.1.

$$y = f(x) + \varepsilon$$

where:

y= vector of one or more response variables;

x= vector of model variables;

f= vector-valued function, which is unknown and needs to be estimated by means of data

ε= error term

In the case of continuous granulation and tableting *y* might for example be the granules' particle size distribution or the tensile strength of the tablets. The model variables *x* are factors that influence the quality of the end product. Examples for *x* are process settings, environmental factors and the starting materials' quality characteristics. The **aim** of this study was to evaluate the influence of the model variables upon *y* in a continuous wet granulation process. Process settings were held constant; hence the focus was only on the variability of the raw materials. This project aims at examining and understanding the effects of the physical variability (e.g. particle size distribution, density, etc.) of raw material properties on the critical quality attributes of continuously produced granules and tablets. Furthermore the influence of varying raw material properties on processability was investigated.

4.2. MATERIALS AND METHODS

4.2.1. Materials

Seven different grades of anhydrous theophylline were compared. One was purchased from Farma-Quimica sur SL (Malaga, Spain). Additionally, theophylline anhydrous powder, fine powder, 200, 200M, 325M and micronized powder (all donated by BASF, Ludwigshafen, Germany) were used. The 200 grade is referred to as 200_ in order to make a clear distinction with 200M. Thirty percent of theophylline was blended with 67.5% (w/w) of lactose monohydrate 200M (Caldic, Hemiksem, Belgium). Polyvinylpyrrolidone (Kollidon®30, BASF, Ludwigshafen, Germany) was used in a 2.5% (w/w) concentration as a binder. Demineralized water was used as granulation liquid.

4.2.2. Production of granules and tablets

All granules were produced using the ConsiGma™ 25 unit (GEA Pharma Systems, Collette, Wommelgem, Belgium). For this study only the granulator with a standard screw configuration was used [10]. The temperature of the cooling water around the granulator barrel was held constant at 25°C and the pre-blended formulations were fed at a rate of 25 kg/h, with a liquid addition rate of 45 g/min. The screw speed was held constant at 950 rpm. The granules produced during the first minute were discarded. After one minute approximately 3 kg of granules was collected on trays and oven dried at 40°C during 24h. The dried granules were then tableted as such with the Modul™ P tablet press equipped with an overfill cam of 12 mm (GEA Pharma Systems, Courtoy, Halle, Belgium). Ten flat faced bevel edged punches with a diameter of 13 mm were used as tooling. Two sets of tablets were produced from each batch: “sub-ideal” and “ideal” tablets. Sub-ideal tablets were produced in order to enlarge the differences in critical tablet characteristics of the seven different tablets. The sub-ideal samples were tableted with a 6.75 mm distance between the punches. For the ideal tablets, a distance between punches of 6.25 mm was used. The resulting average compression forces are listed in Table 4.1. The machine produced 250 tablets per minute and tablets were collected after 20 seconds.

Table 4.1. Average compression force (kN) applied on the different granule loads during tableting. 6.25 mm (ideal) and 6.75 mm (sub-ideal) are the two applied distances between the punches

		Ideal	stdev	Sub-ideal	stdev
Spain	*Large*	18.46	3.02	6.20	0.69
Powder	*Large*	16.12	2.68	5.23	0.65
200_	*Small*	23.09	3.50	8.66	1.05
Micronized	*Small*	24.52	2.93	9.54	0.81
Fine		19.71	2.60	7.03	0.77
200M		17.71	2.76	8.20	1.47
325M		19.78	2.98	8.03	1.15

4.2.3. Flowability of powders and granules

The flowability of the raw materials was measured using the RST-XS Schulze ring shear tester (Schulze Schüttgutmesstechnik, Wolfenbüttel, Germany). For the powders, the applied normal load at preshear was 2000 Pa, afterwards shear-stresses of 400, 1000, 1600 and again 400 Pa were applied. The ff_c, which is the ratio of consolidation stress to unconfined yield strength, was used to evaluate the flowability. Measurements were done in triplicate. For the granules, the applied normal load at pre-shear was 1000 Pa, with shear-stresses of 250, 525, 800 and again 250 Pa.

Furthermore, the flowability (flow rate (mg/s)) of the samples was studied using a FlowPro instrument (iPAT Ltd, Turku, Finland) under controlled conditions (24±1°C, 50±2% RH). The funnel of the instrument was cleaned with dried pressurized air prior to each measurement. All the samples were measured five times (n=5). Both the value obtained from the Schulze ring shear tester and the FlowPro were taken into account for further analysis.

4.2.4. Particle size analysis of powders

The particle size distribution of the powders was measured by means of laser diffraction. The wet dispersion method using the 300 RF lens (Malvern Instruments, Malvern, UK) was applied. Powder samples were dispersed in Miglyol 812 (triglyceride saturated medium), (Fagron, Capelle aan den Ijssel, The Netherlands) with 0.2% Tween 80 (Polysorbate 80), (BUFA, Ijsselstein, The Netherlands). Measurements were performed in triplicate. The smallest sieve fraction of the granules (0-150 µm) was measured separately following the same procedure.

4.2.5. Specific Surface Area of powders

Nitrogen adsorption measurements at 77K were performed on the samples using TriStar 3000 gas sorption apparatus (Micromeritics Inc., Norcross, USA). The specific surface area of the powder samples was determined from the adsorption isotherm using the Brunauer-Emmett-Teller (BET) –theory.

4.2.6. True density of powders and granules

The true density (ρ) of both powders and granules was determined by means of Helium-pycnometry (Accupyc 1330 Pycnometer, Micrometrics, Norcross, USA). A total of ten runs and ten purges was performed per experiment. A purge fill pressure of 19.5 psig was used.

4.2.7. Visualization of granules

The particle shape of the granules was visualized with an RSZ research stereomicroscope (Olympus Optical Co. LTD, Tokyo, Japan) equipped with a digital camera (Camedia, C-3030 Zoom, Olympus, Tokyo, Japan). A cold light source (Highlight 2100, Olympus, Germany) and a ring light guide (LG-R66, Olympus, Germany) were used to obtain top illumination of the granules against a dark surface.

4.2.8. Particle size analysis of granules

Sieve analysis was performed using a Retsch VE 1000 sieve shaker (Haan, Germany), with a series of 8 sieves (150, 250, 500, 710, 1000, 1400, 2000 and 3150 µm). An amount of 100 grams of granules was sieved during 10 minutes with an amplitude of 2 mm. The amount of

granules retained on each sieve was determined and collected. All seven granule grades were measured in triplicate.

4.2.9. Bulk and tapped density of powders and granules

The bulk and tapped density of the pure theophylline powders, seven premixes and seven different granule grades were determined according to the European Pharmacopeia 7.0. Approximately 60 mL of material was poured into a 100 mL graduated cylinder. The granule weight and exact volume were used to calculate the bulk density. Each sample was tapped 1250 times using an automatic tapping instrument (J. Engelsmann AG, Ludwigshafen am Rhein, Germany) and the volume reading was then used to determine the tapped density. All density measurements were performed in triplicate and the average density was calculated.

4.2.10. Raman spectroscopy

A RamanRxn1 spectrometer (Kaiser Optical Systems, Ann Arbor, Michigan) equipped with an air-cooled CCD detector (back-illuminated deep depletion design) was used. The laser wavelength was the 785 nm line from a 785 nm Invictus NIR diode laser. All spectra were recorded with a resolution of 4 cm^{-1}. An exposure time of 10 seconds for the granules and 5 seconds for the tablets was applied, using a laser power of 400 mW. Spectra were taken from all sieve fractions (except of the granules >3150 µm). Four spectra were taken from each sieve fraction. Measurements were performed with a Raman non-contact probe and the granules were presented to the probe in a quartz cuvette. Spectra were centered and SNV-corrected with the Simca P+ 12.1 software (Umetrics, Umeå, Sweden).

4.2.11. Friability of tablets

The friability of tablets was investigated with a friabilator (PTF E Pharma Test, Hainburg, Germany). A large drum, developed for the measurement of tablets was used. Ten tablets were dedusted and weighed prior to and after four minutes rotation at a speed of 25 rpm. The friability was calculated as ((starting weight-weight after test)/starting weight)*100.

4.2.12. Porosity of tablets

The porosity of all tablets was calculated after investigation with the RSZ research stereomicroscope (Reickert, 96/0226, Vienna, Austrich). From each batch, ten tablets with a known weight were investigated; five dimensions were evaluated as shown in Figure 4.1. The volume of the tablet was calculated according to Eq. 4.2. Weight divided by the volume of the tablet resulted in the apparent density (ρ_{app}). With the true density of the granules (ρ) determined by helium pycnometry, the porosity of the tablets (ε) could be calculated according to Eq. 4.3.

Equation 4.2.

$$V = \left[\left(\pi \cdot \left[\frac{A}{2}\right]^2 \cdot B\right) + 2.\left(\frac{1}{3}.\pi.C.\left(\left[\frac{D}{2}\right]^2 + \left[\frac{E}{2}\right]^2 + \frac{D}{2}.\frac{E}{2}\right)\right)\right]$$

Equation 4.3.

$$\varepsilon = \frac{(1 - \rho_{app})}{\rho} .100$$

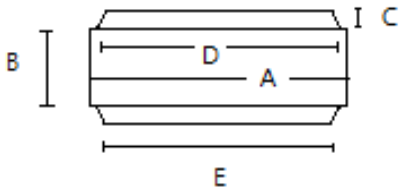

Figure 4.1. Five determined dimensions (A-E) for the volume determination of tablets.

Secondly, tablets made with Powder, 325M and Micronized granules were evaluated with a high resolution Micro-X-ray computed tomography device, SkyScan1172 (Bruker-MicroCT, Kontich, Belgium). Both the ideal and sub-ideal tablets were investigated, using a resolution of 4.6 µm. An X-ray source of 40 kV (250 µA) and a rotation step of 0.4° were used. To reconstruct cross-sectional images of the tablets NRecon® software (Bruker-MicroCT, Kontich, Belgium) was applied. The cylindrical part in the middle of the tablet was taken into account and in order to obtain an equal amount of data for multiple samples, 750 slides of this cylindrical part of the tablet were taken into account and analyzed. Analysis was done with the CTAn-software (Bruker-MicroCT, Kontich, Belgium).

4.2.13. Tensile strength

Tablets (n=20) were evaluated with the Sotax HT 10 (Basel, Switzerland) directly after tableting. Hardness, thickness, diameter of the tablets and their weight were determined. With these obtained data, the tensile strength (TS) was calculated according to the equation described by Fell and Newton [27].

Equation 4.4.

$$TS = \frac{2F}{\pi\, d\, t}$$

where:

F= hardness of the tablet (N);
d= tablet diameter (mm) and
t= tablet thickness (mm)

4.2.14. Disintegration of tablets

The disintegration time of both the ideal and sub-ideal tablets (n=2x6) was evaluated with the PTZ-E Pharma Test (Hainburg, Germany) as described in the European Pharmacopoeia. The temperature of the distilled water was kept at 37°C. The disintegration time was determined as the time when no visible particles were left in the mesh wire.

4.2.15. Dissolution of the tablets

Dissolution tests were performed on both the ideal and the sub-ideal tablets (n=3) in 900 mL demineralized water, using the paddle method (VK 7000&7010, Vankel, Cary, NC, USA). The temperature of the dissolution medium was set at 37.5°C, with a paddle speed of 100 rpm. 5 mL samples were taken after 5, 10, 15, 20, 30, 45, 60, 75, 90 and 120 minutes after starting the dissolution. The theophylline concentration was determined with a UV-VIS spectrophotometer at 272 nm, using an UV-1650PC double-beam spectrophotometer (Shimadzu Benelux, Antwerp, Belgium). By means of a standard calibration line, the concentration of theophylline at these time points was calculated and a dissolution profile was derived.

4.2.16. Multivariate Data Analysis

All data obtained from the analysis on powders, granules and tablets were summarized using Principal Component Analysis with the Simca P+ 12.0.1 software (Umetrics AB, Umeå, Sweden). Data were UV-scaled prior to analysis.

4.3. RESULTS AND DISCUSSION

4.3.1. Powder characteristics

An overview of raw material properties is given in Table 4.2. Regarding the particle size, it is clear that Powder and Spain consist of the largest particles, whereas 200_, Fine and Micronized are characterised by very low *d10* values. Three main groups can be distinguished: Powder and Spain as the raw materials having the largest particle size (i.e. the large powders), 200_ and Micronized as the raw materials with the smallest particle size (i.e. the small powders) and 200M and 325M are an intermediate group. Regarding particle size, Fine can be situated in the middle of the small and intermediate group, because it has a *d10* below 1 µm, but its *d50* is comparable with the *d50*s of 200M and 325M. The span is the smallest for the powders with the highest d50 values (Spain, Powder and 325M), whereas the powders with the lowest d50 values (200_, Fine and Micronized) have high span values. 200M is intermediate regarding span. When evaluating the density of the powders, the large powders (Powder and Spain) have both a high bulk and tapped density. The small powders, 200_, Fine and Micronized are more 'fluffy' powders with a low bulk density. The density stays low when tapping the powders; especially Micronized and 200_ (small) are very voluminous powders. Again, 200M and 325M can be labeled intermediate regarding density. The flowability of the seven theophylline powders was tested in two ways: with the Schulze Ring Shear Tester (ff_c) and with the FlowPro (mg/s). From both techniques it is clear that the large powders have the best flowability. No ff_c value, other than 0, could be obtained for 200_ and Fine, since these powders had a low flowability, this 0 value was used to characterize the flowability. Regarding the specific surface area (SSA), the SSA decreases when the particle size increases. This means that the large powders (Powder and Spain) have the lowest specific surface area and the small powders (200_ and Micronized) have the highest specific surface area. Evaluating the Helium-pycnometer results, the large powders are characterized by a slightly lower true density value, compared to the other five powders.

Table 4.2. Characteristics of the raw materials, all are mean values.

		d10 **µm**	***d50*** **µm**	***d90*** **µm**	**Span**	**Bulk density g/ml**	**Tapped density g/ml**	ff_c	**Flow Rate mg/s**	**Surface Area m^2/g**	**True density g/cm^3**
Powder	*Large*	4.16	40.12	93.47	2.2	0.49	0.62	3.3	7.1	0.36	1.464
Spain	*Large*	7.46	66.41	140.70	2.0	0.50	0.59	3.4	5.5	0.39	1.463
200_	*Small*	0.533	9.72	34.55	3.5	0.28	0.32	0.0	2.0	1.23	1.494
Micronized	*Small*	0.516	8.44	29.81	3.5	0.30	0.34	1.1	2.8	1.36	1.490
Fine		0.923	15.56	57.84	3.7	0.31	0.37	0.0	1.2	0.77	1.487
200 M		2.46	17.34	74.89	2.6	0.38	0.45	1.2	1.4	0.51	1.488
325 M		2.05	21.47	48.55	2.2	0.38	0.43	1.4	2.6	0.68	1.491
Lactose		2.71	23.46	88.80	3.7	0.57	0.68	2.6	/	0.55	/

4.3.2. Granule characteristics

4.3.2.1. Granule size distribution

Figure 4.2 shows the granule size distribution of the seven granulation experiments. A bi-modal granule size distribution is observed for all experiments. This phenomenon has been reported earlier [22, 28-30]. A similar amount of in-spec granules (=within the 150-1400 µm size range) was obtained for all granulation experiments, varying between 57.4% and 62%. Hence, the yield is similar for all experiments. Granules either consist of in-spec granules and a large amount of fines (<150 µm) or they contain of in-spec granules and a large amount of oversized granules (>1400 µm). The large powders (Powder and Spain) result in high amounts of oversized granules and low amounts of fines. 325M shows the same trend, but to a lesser extent. The granules produced with Micronized powder result in a lot of fines (16.2%) and a low amount of oversized granules. The granule size distribution is thus directly correlated with the particle size of the starting theophylline. Smaller starting material results in more fines as also reported by El Hagrasy et al. [22]. The granule size distribution of the smallest sieve fraction (0-150 µm) was investigated separately by means of laser diffraction.

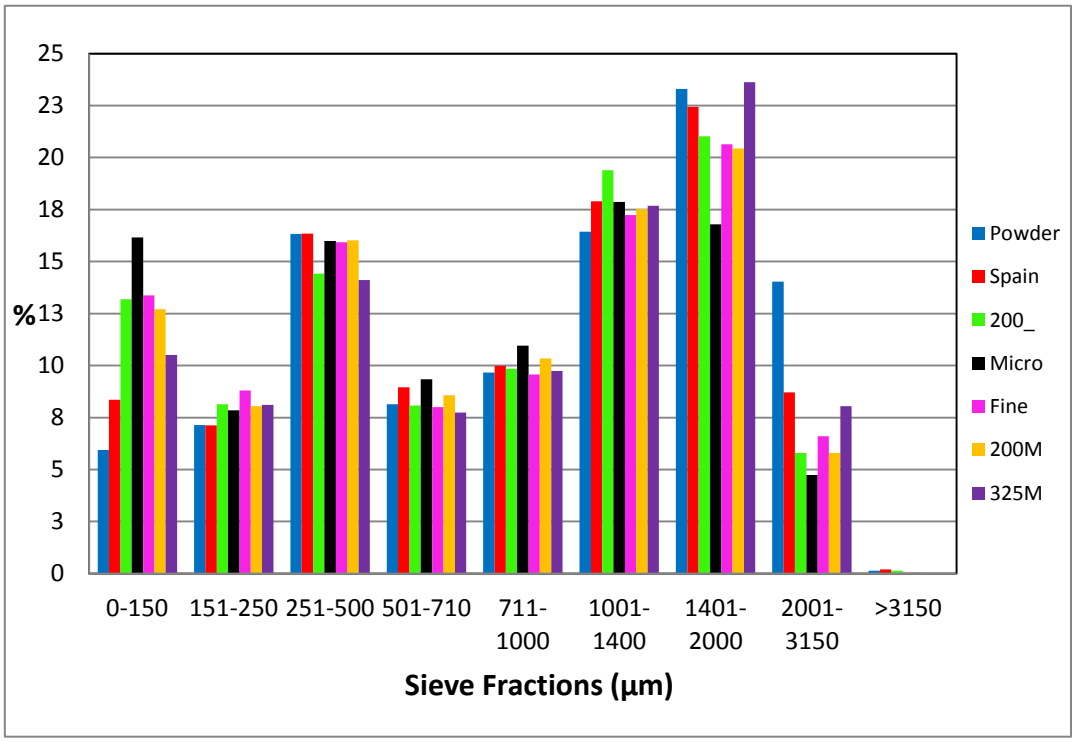

Figure 4.2. Granule size distribution of the seven granule samples.

Figure 4.3 shows the granule size distribution plots of both the pure raw material powders and the smallest sieve fraction of granulated material, a small (Micronized) and a large (Spain) powder are plotted as examples. A clear increase in particle size can be distinguished, indicating that the smallest sieve fraction contains small granules above 10 microns. However, results show a small fraction between 0.1 µm and 1 µm as well, suggesting the presence of a small amount of ungranulated powder.

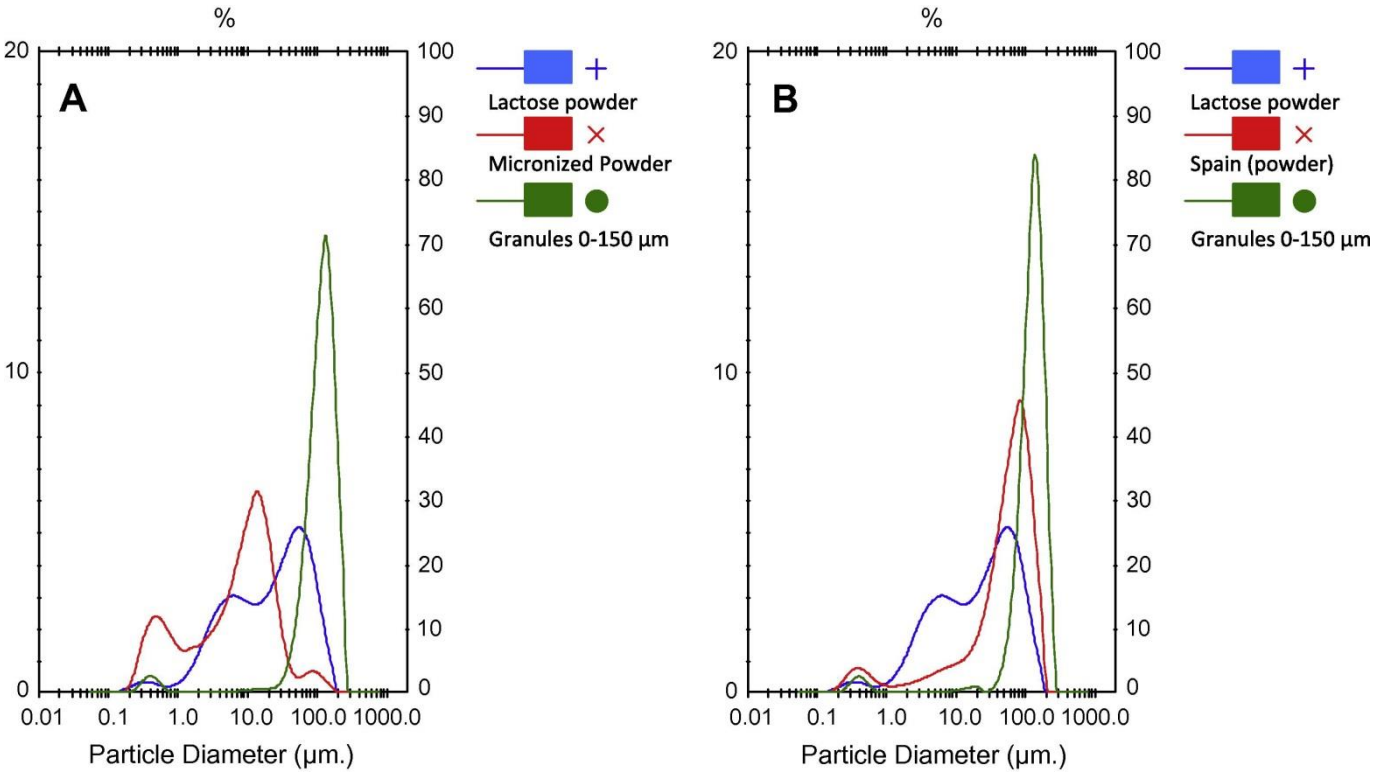

Figure 4.3. Particle size distribution in volume % of pure lactose, pure theophylline and the granules of the 0-150 µm fraction. A. Micronized – B. Spain.

4.3.2.2. Density of granules

The bulk and tapped density of the powder blends (premixes) and the granules are plotted in Figure 4.4. The bulk and tapped density of the premixes made with the large powders is higher than the bulk and tapped density of their respective granules. The same can be said for the tapped density of 200M and 325M, but their bulk densities are the same for premixes as for granules. The small powders are characterized by lower bulk and tapped densities for

the premixes than for the granules. The granules produced with Fine powder have a higher bulk density and a lower tapped density than the powder premix they are produced of. Podczeck and Lee-Amies [31] obtained a similar conclusion: no tapped volume reduction could be achieved by granulation of powders with high tapped densities. For the presented example, the threshold value for twin screw granulation with the presented model formulation is 0.55 g/mL for the tapped premix, which means only when the density of the tapped premix is below 0.55 g/mL a volume reduction could be achieved by granulation (when comparing tapped granules to tapped powder). When comparing bulk powders and granules the threshold value is 0.5 g/mL. Only when the bulk premix has a density of 0.5 g/mL or higher, a significant decrease in bulk density when comparing premix to granules will be obtained.

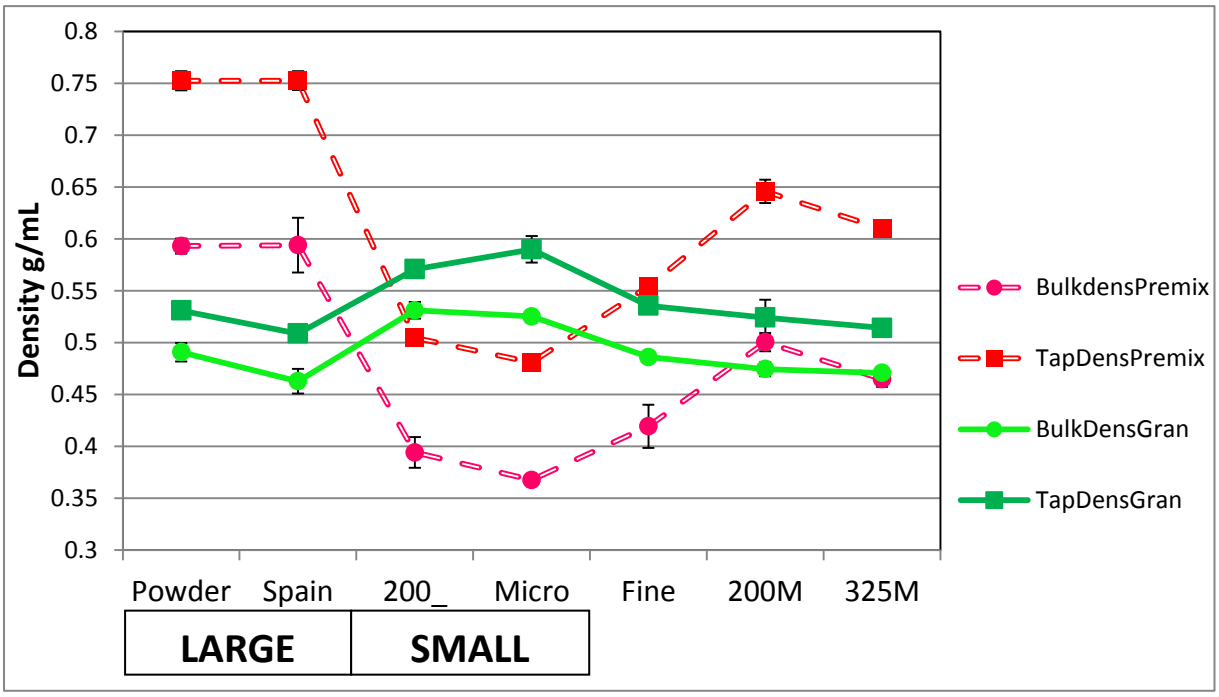

Figure 4.4. Bulk and tapped density of premixes and granules.

4.3.2.3. Flowability of granules

The flow properties of pharmaceutical powders and granules are usually characterized with multiple test methods in order to get adequate aspects of product flow [32]. The angle of repose apparatus, equipped with a 100 mL funnel seemed to be unsuitable for flowability measurements of these seven granule grades. Only granules made with small powders (200_, Fine and Micronized) could pass the 100 mL funnel without blocking, the other grades contained too large granules. The Schulze ring shear tester had difficulties to reach a steady state after preshear for Spain, Powder and especially for 200M. Evaluating the ring shear results, the seven different granule grades showed no significant differences regarding flowability. All had values higher than 7, and can therefore be characterized as easy or free flowing: Micronized, 200_, Fine and 325M were easy flowing, whereas 200M, Spain and Powder were determined to be free flowing granules.

4.3.2.4. True density of granules

The true density was 1.52 g/cm³ for all seven grades of granules.

4.3.2.5. Granule shape

Granules produced via wet twin screw granulation tend to be more needle-shaped than granules which are, for example, produced by fluid bed granulation [29]. The smaller sieve fractions contained more spherical granules whereas the larger sieve fractions contained more oblong shaped granules (Figure 4.5). No clear differences regarding shape could be identified between the seven different granule grades.

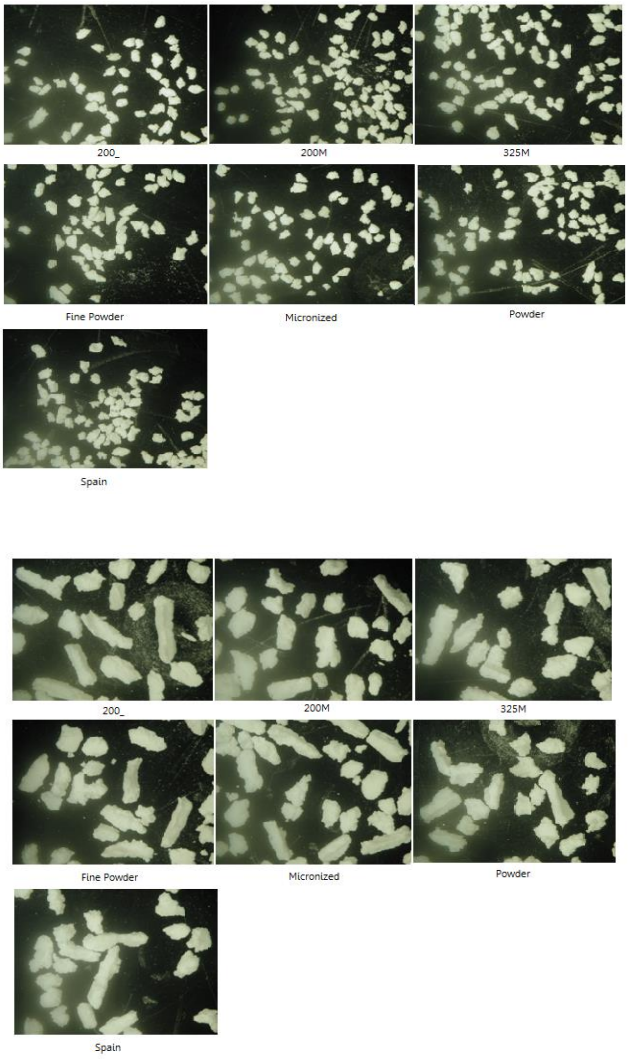

Figure 4.5. Pictures of two sieve fractions of the seven granule loads: 500-710 µm (up) and 1000-1400 µm (below).

4.3.2.6. Dosage of theophylline in the different granule size fractions

Raman spectra were collected and investigated in order to determine the solid state of theophylline after oven drying. All granules showed to contain anhydrous theophylline after drying.

Principal Component Analysis (PCA) was applied on all SNV-corrected Raman spectra of the different sieve fractions, resulting in three principal components. Figure 4.6 shows the PC 2 (14.6%) vs. PC 3 (4.4%) scores plot. First of all, granules produced with the Spanish theophylline are clustered together (dots), in the negative part along the PC 2 and the PC 3

axis, whereas the other granule grades are randomly scattered. Spain is the only powder obtained from a different supplier (not BASF): therefore, a small difference in i.e. color, minor impurities, etc. might explain this clustering. Furthermore, along the PC 2-axis, spectra are clustered according to particle size. The smaller granules are clustered in the negative part of PC 2, whereas the larger granules are clustered in the positive part of the PC 2 axis. To explain this clustering the loading of the second PC should be interpreted (Figure 4.7). The maxima of this loadings plot are peaks typical for anhydrous theophylline [10], whereas the minima are peaks that can be attributed to lactose monohydrate [33]. This can indicate that the smaller granules (<500 µm) contain more lactose monohydrate, whereas the larger granules (>710 µm) contain more theophylline. This corresponds to earlier findings from Vromans et al. [34] and van den Dries et al. [35]. They only found more API in larger granules when the particle size of the drug was smaller than the particle size of the diluent particles. In this case, theophylline is more abundant in all larger granule fractions. So even though the particle size of Powder and Spain is larger than the particle size of lactose, still more theophylline could be found in the larger granules.

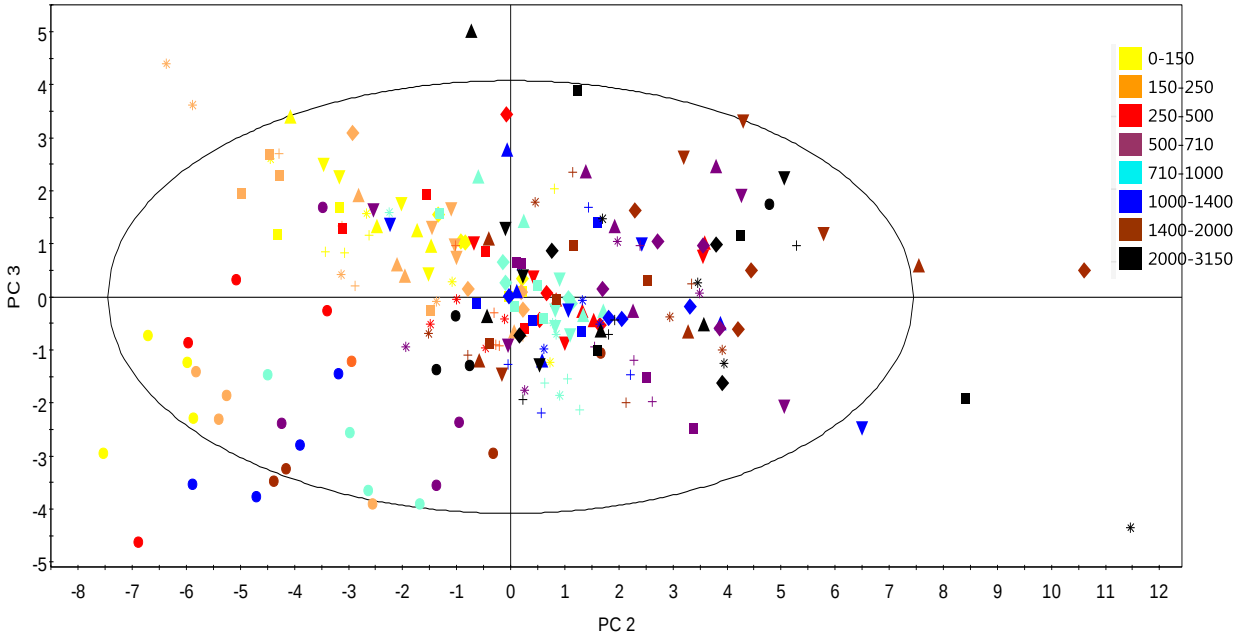

Figure 4.6. PC 2 vs PC 3 scores plot. Raman spectra are colored after sieve fraction with Powder (squares), Spain (dots), 200_(triangles), Fine (stars), Micronized (diamonds), 200M (crosses), 325 M (inverted triangles).

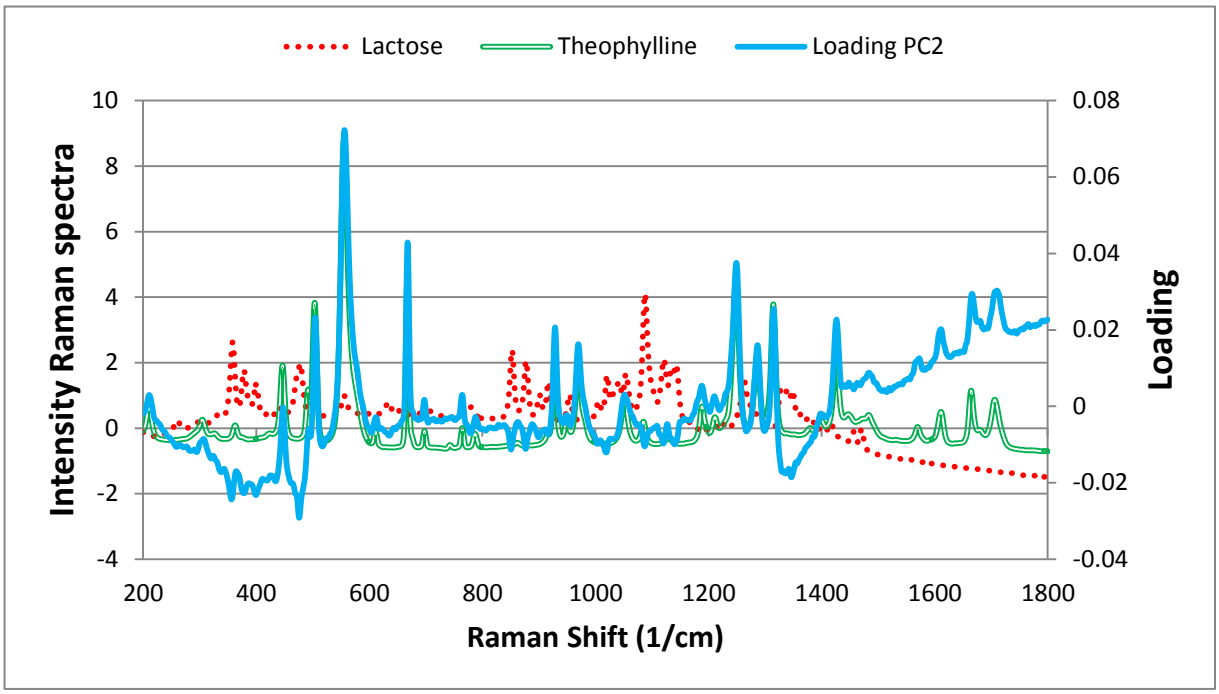

Figure 4.7. Pure spectrum of lactose monohydrate (red dots), pure spectrum of anhydrous theophylline (green double line) and the loadings plot of the second PC (full blue line).

4.3.3. Tablet characteristics

4.3.3.1. Tablet appearance

The ideal tablets (compressed with a distance between the punches of 6.25 mm) were shiny, flat and showed no capping. Capping could only be observed for the sub-ideal tablets (compressed with a 6.75 mm distance between the punches). The surface of the sub-ideal tablets was rougher.

4.3.3.2. Porosity of tablets

Investigating the porosity, determined with the stereomicroscope, the sub-ideal tablets are characterized by a higher porosity than the ideal tablets (Table 4.3).

Table 4.3. Porosity (determined with the microscope and XRMCT), friability and disintegration time of ideal and sub-ideal tablets.

Ideal					
		Porosity (%) (microscope)	**Porosity (%) (XRMCT)**	**Friability(%)**	**Disintegration time (min)**
Powder	*Large*	14.90	5.16	0.097	30
Spain	*Large*	11.24		0.058	31
200_	*Small*	11.49		0.119	37
Micronized	*Small*	10.00	2.00	0.164	35
Fine		11.89		0.131	37
200M		12.14		0.078	27
325M		11.90	4.17	0.120	30

Sub-ideal					
		Porosity (%) (microscope)	**Porosity (%) (XRMCT)**	**Friability (%)**	**Disintegration time (min)**
Powder	*Large*	23.97	17.95	0.702	20
Spain	*Large*	21.22		0.528	22
200_	*Small*	20.20		0.137	30
Micronized	*Small*	17.43	6.44	0.188	25
Fine		22.54		0.414	25
200M		21.52		0.312	19
325M		21.45	16.43	0.323	27

When a higher compression force is applied, the porosity of the tablets diminishes [36]. Furthermore it can be stated that the tablets made of granules produced with micronized theophylline have the lowest porosity. These granules contained the most fines and lower granule sizes resulting in tablets with finer pore structures [37]. From these values, three grades of tablets were selected to be investigated with X-ray micro-computed tomography, namely Powder, with the highest porosity, Micronized with the lowest porosity and 325M as an intermediate. Although the absolute values for the porosity of Powder, 325M and Micronized tablets, obtained by means of X-ray tomography differ from the values obtained by means of the microscope due to the different measurement techniques, the relative differences between the three tablets are the same. Again the Micronized tablets show clearly a lower porosity.

4.3.3.3. Friability of tablets

The European Pharmacopoeia [38] states that tablets should not lose more than 1% of their starting weight during a friability test. All tablets meet this specification (Figure 4.8). From the graph it can be stated that a higher compression force will result in a lower friability [39]. For the granule grades, which contain a low amount of oversized granules (produced with the small powders; 200_ and Micronized), an increased compression force does not result in a significant decrease in friability, whereas for the other tablets, a significant decrease in friability can be noted. When compressing small granules, not much extra surface for the formation of new bonds becomes available, whereas compressing larger granules results in an increase in binding surface.

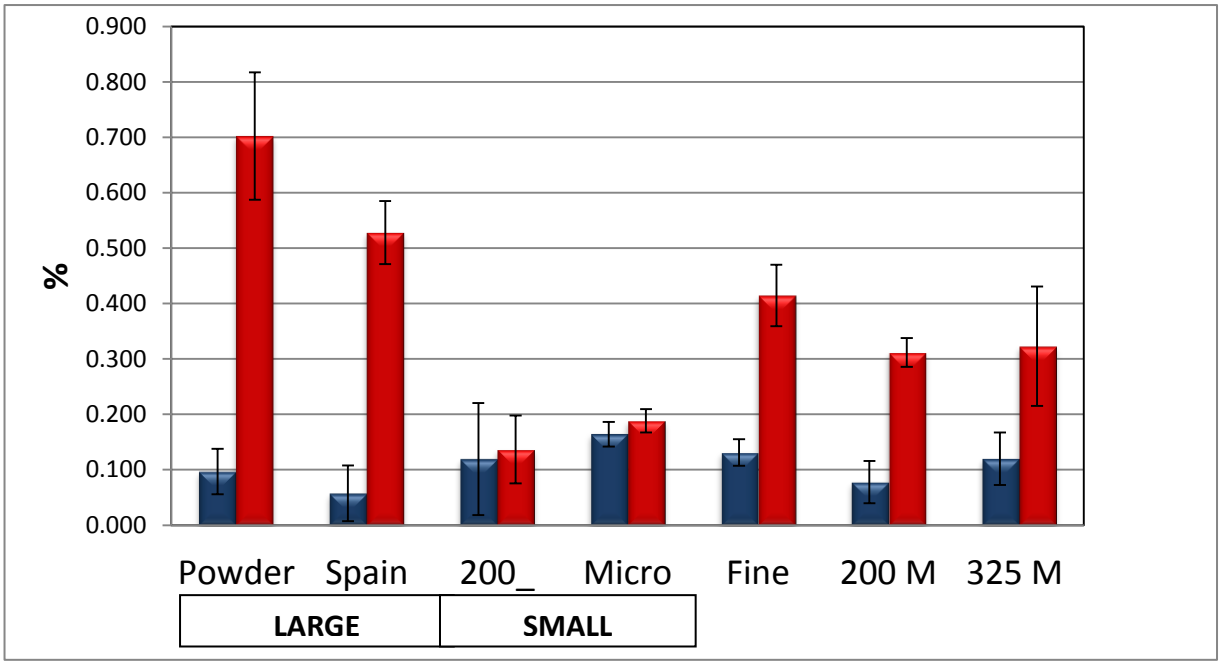

Figure 4.8. Friability of ideal (blue) and sub-ideal (red) tablets.

4.3.3.4. Hardness and tensile strength of tablets

The higher the compression force, the higher the tensile strength will be (Figure 4.9 and Table 4.1) [19, 40]. For both the ideal and sub-ideal tablets, the tableting of smaller granules (Micronized, 200_, Fine) results in stronger tablets. It has been reported that the tableting of smaller powders particles for direct compression results in stronger tablets [15, 24, 25]. Likewise, the tableting of smaller granules results in stronger tablets [37]. A clear correlation between the porosity of the tablets and their tensile strength can be observed (Figure 4.10).

This is because a finer pore structure will result in stronger tablets. The stronger tablets are thus the result of both a higher applied compression force and smaller starting granules.

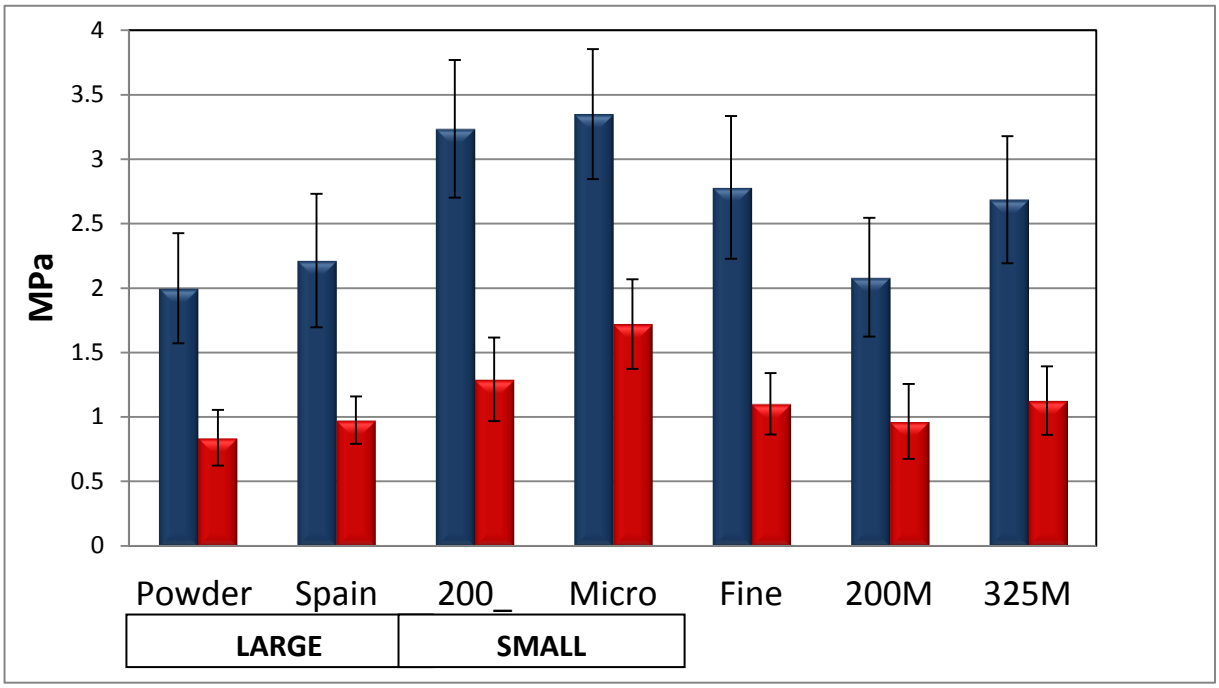

Figure 4.9. Tensile strength of ideal (blue) and sub-ideal (red) tablets.

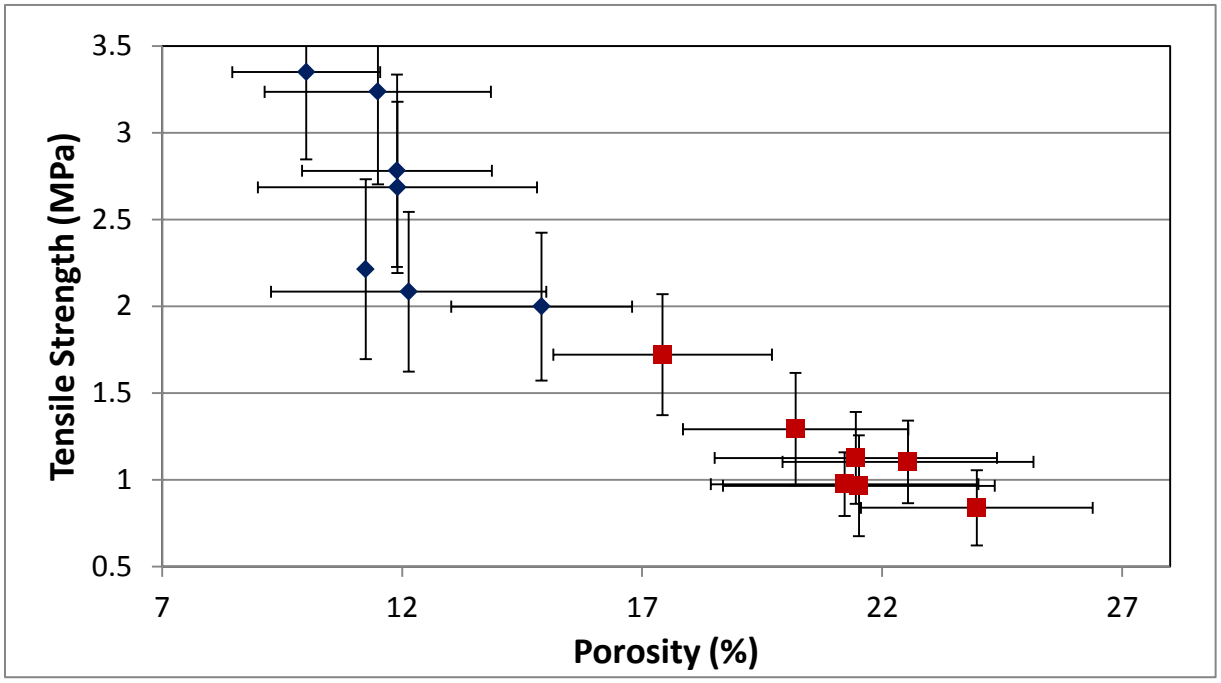

Figure 4.10. Tensile strength as function of porosity of tablets, ideal tablets (blue) and sub-ideal tablets (red).

4.3.3.5. Disintegration and dissolution of tablets

Clearly, the disintegration time (Table 4.3) is longer for the ideal tablets than for the sub-ideal tablets, but for both ideal and sub-ideal tablets the disintegration time is too long (recommended around 15 minutes) [41]. It takes a longer time for less porous and harder tablets to disintegrate. The disintegration time for both the ideal and sub-ideal tablets is the longest for the tablets derived from small powders, namely 200_, Fine and Micronized. This is in accordance with the tensile strength of those tablets, which is higher compared to the other tablets. The dissolution profiles (Figure 4.11) of the seven tablets were compared to each other according to the respective distance between the punches. Drug release was complete after 60 min for the sub-ideal tablets whereas it was 75 min for the ideal tablets. The dissolution profiles of the seven different grades of theophylline are comparable, but two grades are peculiar, both as ideal and sub-ideal tablets. 200M shows a faster release, whereas 200_ shows a slower release. This is in accordance with the disintegration times for both the ideal and sub-ideal tablets.

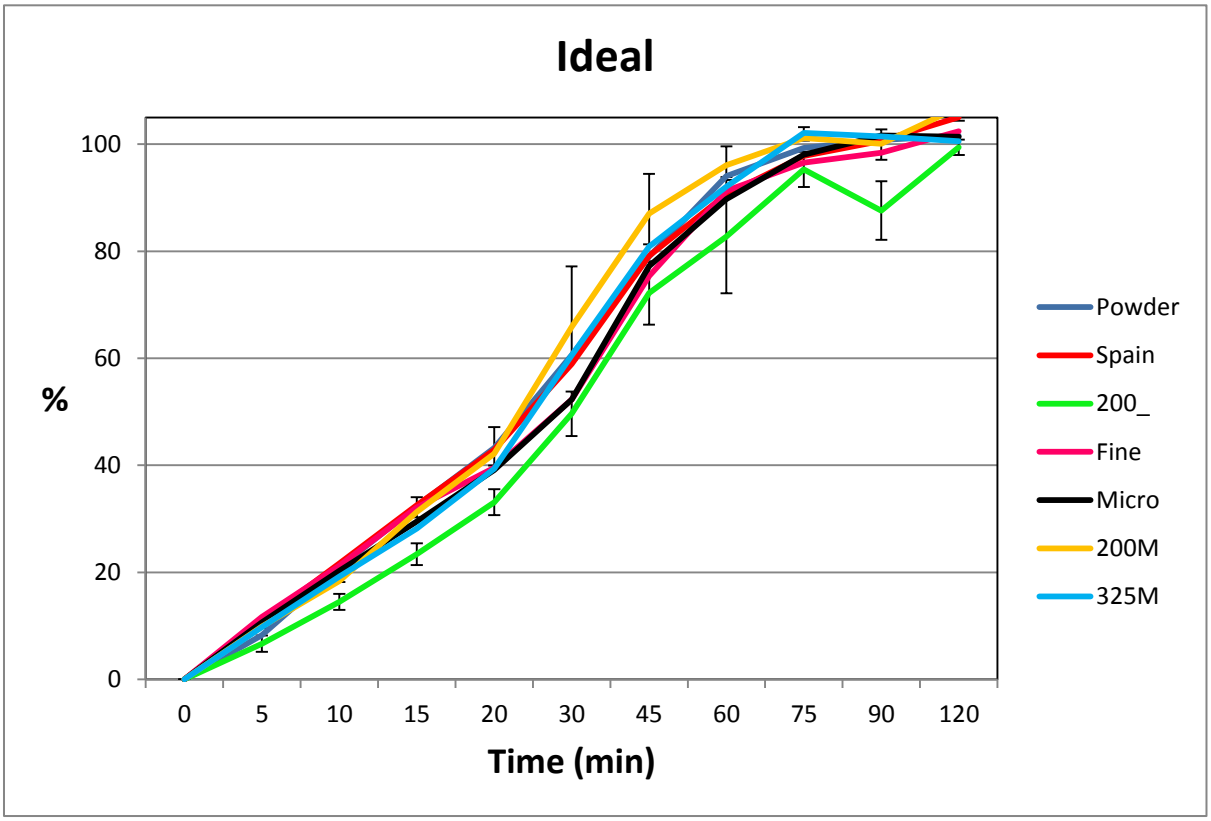

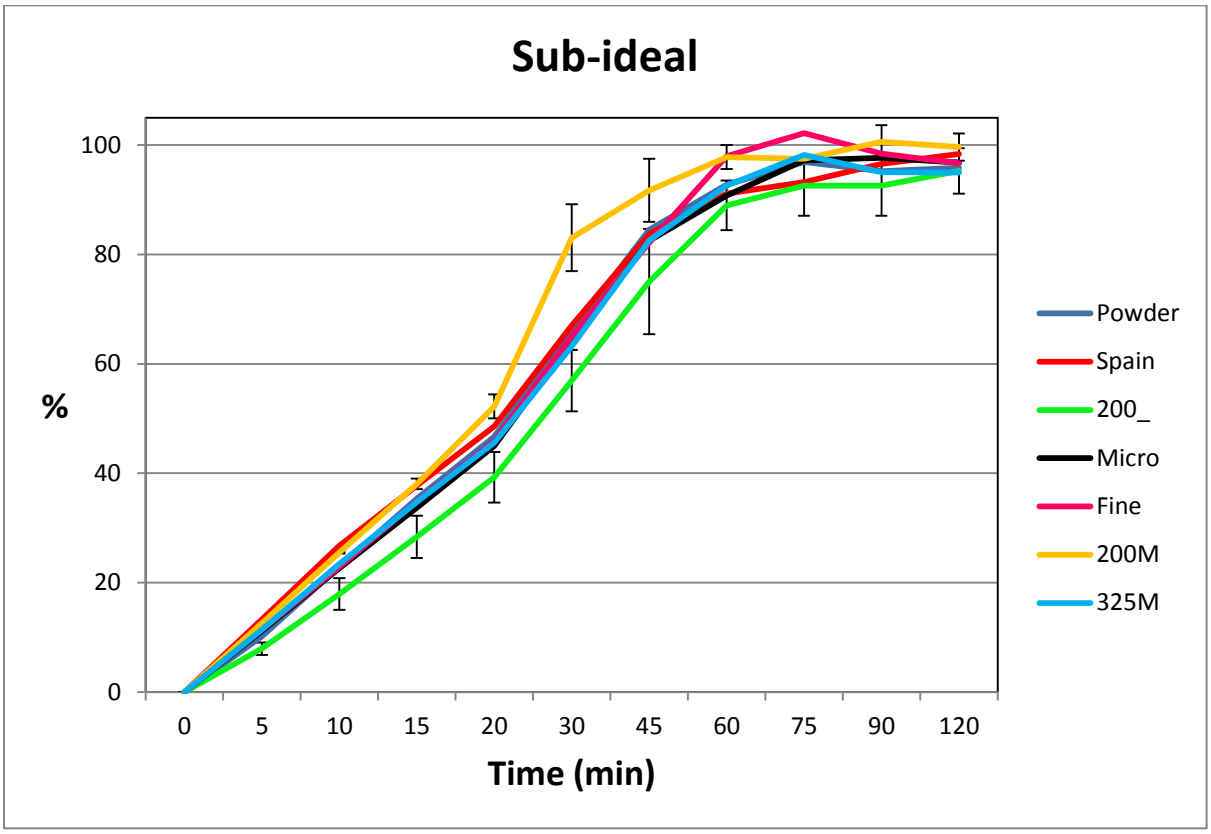

Figure 4.11. Dissolution profiles of the seven ideal and sub-ideal tablets.

4.3.4. Processability

Both during granulation and tableting some powders showed to be less processable than others. First of all, during granulation, with all powders, except for the large powders, the injectors of the granulation liquid tubes were pushed upward out of the barrel. The different theophyllines differ highly regarding density (Table 4.2.). Although theophylline is only used in a concentration of 30 % of the total mixture, this difference has a significant influence on the density of the premixes (Figure 4.4). Since powder feeding occurs in a loss-in-weight manner, the volume added for the small powders will be significantly higher than for the large powders. That extra volume will expand in the barrel, hence pushing the injectors out of the granulator barrel.

On the other hand, the runs granulated with the large powders seem to have higher torque values during granulation (Figure 4.12). The influence of formulation parameters on the torque is very little investigated when it comes to pharmaceutical twin screw granulation. Interesting research in the biomass industry has been performed by Dai and Grace [42] who

investigated the torque of a screw during the transport of woody biomasses. They state that larger particles, more irregular shapes, rougher particle surfaces and larger bulk densities of the materials will result in higher torque values. Similarly, Spain and Powder will result in higher torque values, not only because of the larger density and particle size of their starting materials, but also because of the larger granules, formed at the end of the screws. Although the granulator barrel, used in our study was surrounded by water kept at 25°C, the product temperature increased with a similar rate as the increasing torque (Figure 4.13). The large powders heated clearly faster and to higher temperatures than the other mixtures.

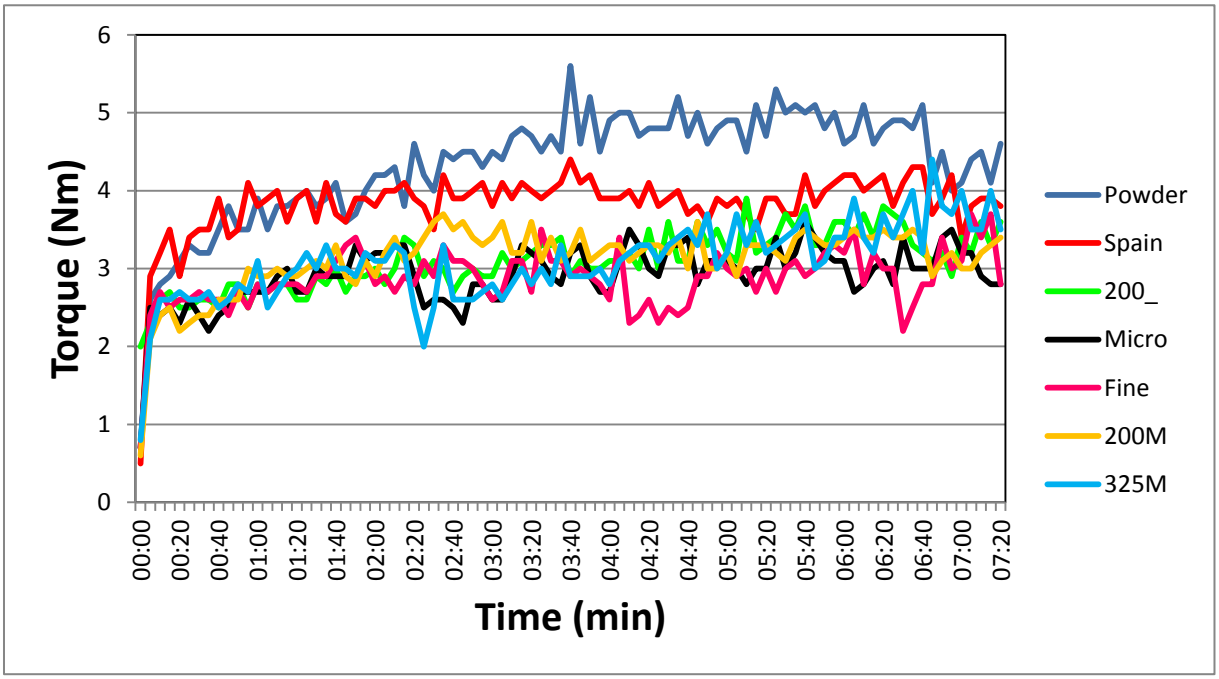

Figure 4.12. Inline torque measurements during the seven granulation experiments.

The compression force applied on the granules is automatically logged on the Modul™ P and listed in Table 4.1. A direct correlation between particle size of the granules and compression force can be identified: more fines (<150 µm) and less oversized granules will result in higher compression forces.

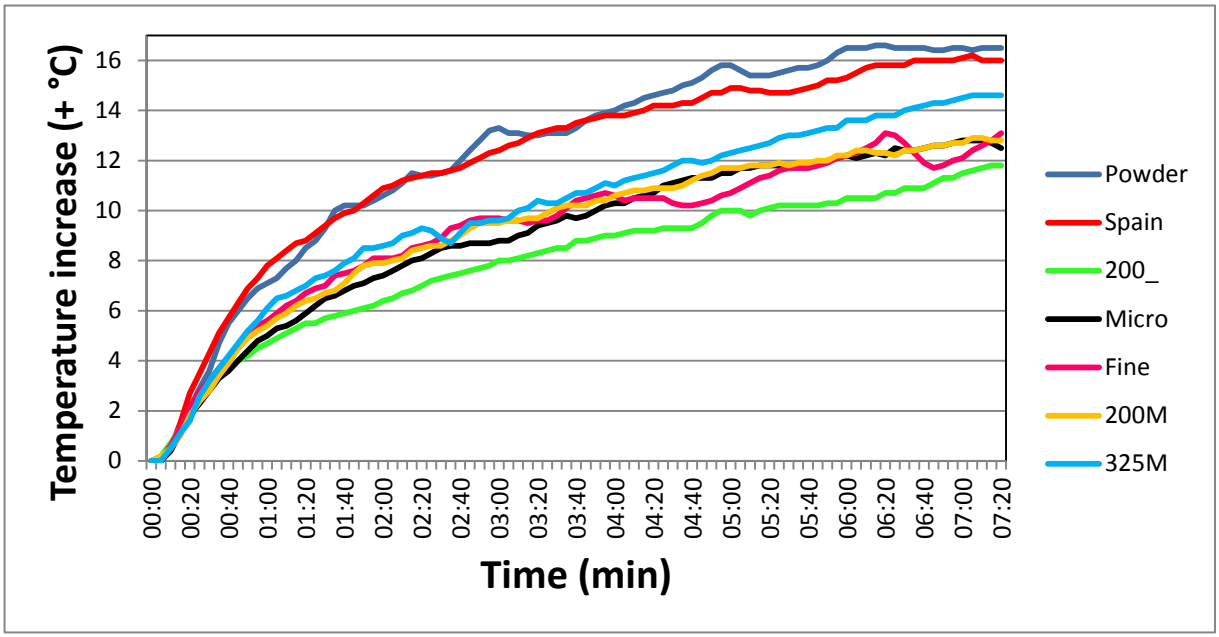

Figure 4.13. Temperature increase during the seven granulation experiments.

During tableting, problems were encountered during two runs, since the tablet press stopped because of lower punch blocking. This happened when the granules made with the small powders, 200_ and Micronized, were tabletted, using a distance between the punches of 6.25 mm, in order to obtain the "ideal" tablets. As stated earlier (Figure 4.3), the smallest sieve fraction (0-150 µm) consists not only of small granules, but also of a small amount of remaining powder. The Micronized and 200_ powders have the smallest particle size. Small remains of these powders can get in the space between the lower punch tip and die wall and will hence potentially block the punch (Figure 4.14).

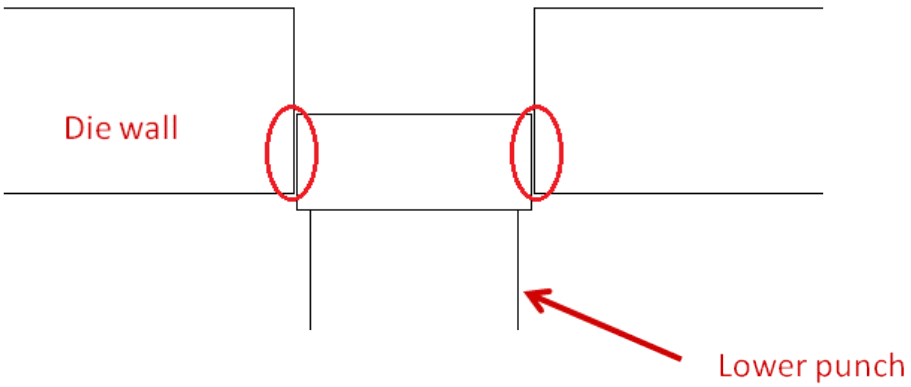

Figure 4.14. Lower punch blocking.

4.3.5. Principal Component Analysis: Summary

In order to investigate the relations between all examined variables in a single context, multivariate data-analysis was applied on all observations. Principal Component Analysis (PCA) allows a fast and explicatory overview of a vast and diverse dataset. Seven variables were investigated, the observations regarding pure powder, granules and tablets were considered as the observations of one variable. This resulted in an X-matrix, constructed of seven rows and 41 columns. PCA was applied, resulting in two PCs, each explaining 62.54 % and 11.66 % of the variation, respectively. The PC 1 versus PC 2 loadings bi-plot (Figure 4.15) shows three clusters along the PC 1-axis. Spain and Powder are grouped together, Fine, 200M and 325M form a cluster and 200_ is grouped with Micronized. When grades are clustered together, they have similar powder, granule and tablet characteristics. The further the grades are plotted away from each other, the more dissimilar they are. These three groups are in accordance all higher discussed results.

A bi-plot overviews the observations as well as their correlations and anti-correlations with the variables, which results in a clear overview. Spain and Powder (i.e. the large powders) are characterized by high particle sizes and low span as raw materials, with high bulk and tapped density values and a good flowability. This results in high torque values, together with a high absolute and a high increase in barrel temperature. Granules are large (>1400 µm) and the sub-ideal tablets produced with Powder and Spain granules are the most friable of all sub-ideal tablets. Micronized and 200_ (i.e. the small powders) are the most dissimilar from Powder and Spain. They are characterized by small starting materials and high span, with low flowability and density. These powders have a high specific surface area. After granulation, the granule grades contain a high amount of fines and have both high bulk and tapped density values. Micronized and 200_ granules require a higher compression force to be tableted. Tablets are heavy, tick and strong, they are characterized by a low porosity. The ideal tablets made with Micronized and 200_ granules are more friable than the others. The tablets produced with 200_ and Fine granules are characterized by their high disintegration times. The 200M tablets are remarkable because of their fast dissolution behavior, whereas 200_ is plotted on the opposite site of the concentration loadings, which means 200_ knows

a slow dissolution. The scores value for the first principal component of 325M is 0, indicating the 325M powder, granules and tablets are the most 'average' of the seven grades.

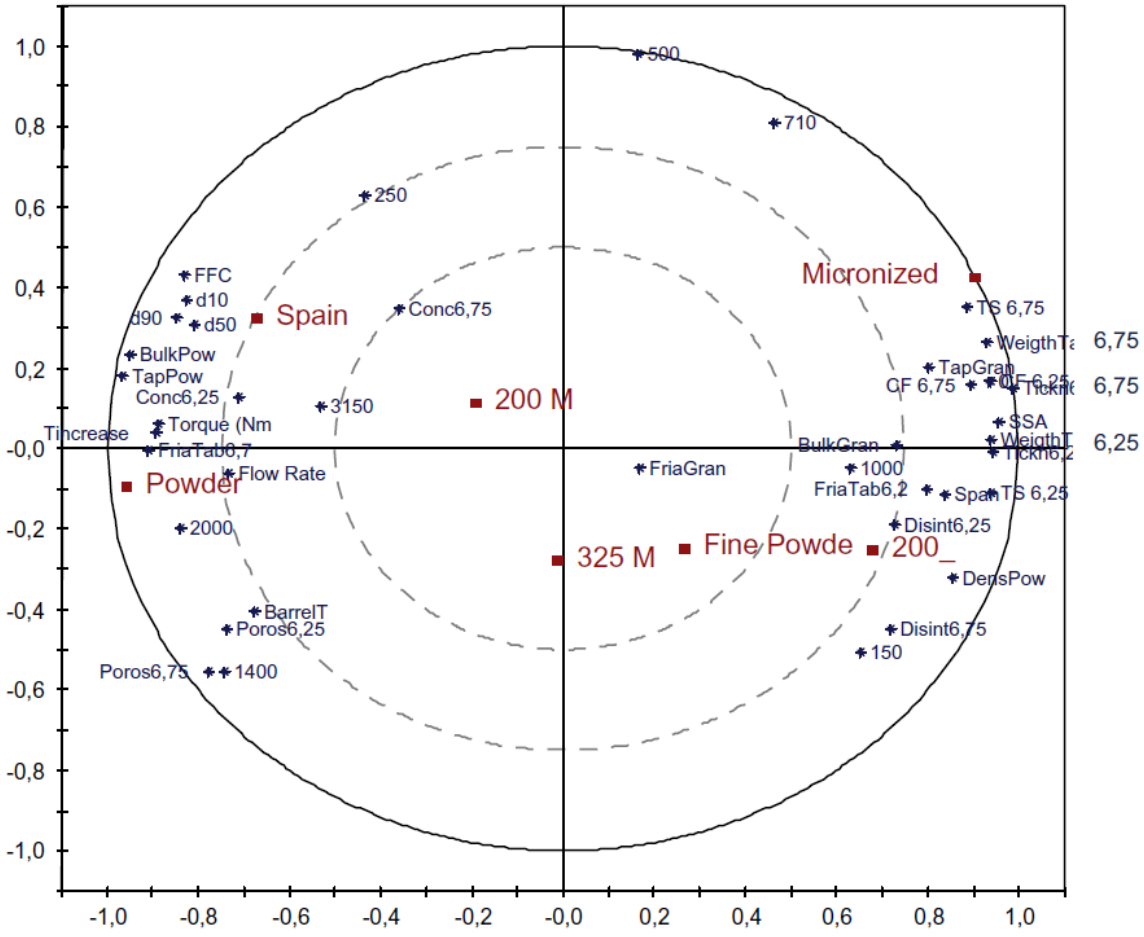

Figure 4.15. PC 1 versus PC 2 bi-plot.

Variables

Powder

Spain

200_

Fine

Micronized

200M

325M

Observations

Powders

d10

d50

d90

Span as obtained after laser diffraction measurements on the powders

FFC	Flowability value as obtained with the Schulze ring shear tester
Flowrate	Flowability value as obtained with the FlowPro
SSA	Specific Surface Area
BulkPow	Bulk density of the theophylline powder
TapPow	Tapped density of the theophylline powder
DensPow	True density of the theophylline powder

Processability

Torque	average torque of the screws during granulation
BarrelT	average temperature of the granulator barrel during granulation
Tincrease	increase in temperature of the granulator barrel

Granules

0	% of granule sieve fraction <150 µm
150	% of granule sieve fraction 150-250 µm
250	% of granule sieve fraction 250-500 µm
500	% of granule sieve fraction 500-710 µm
710	% of granule sieve fraction 710-1000 µm
1000	% of granule sieve fraction 1000-1400 µm
1400	% of granule sieve fraction 1400-2000 µm
2000	% of granule sieve fraction 2000-3150 µm
3150	% of granule sieve fraction >3150 µm
BulkGran	Bulk density of the granules
TapGran	Tapped density of the granules
FriaGran	Friability of the granules

Tablets

CF 6,25	Average applied compression force - distance between the punches of 6,25 mm
CF 6,75	Average applied compression force - distance between the punches of 6,75 mm
TS 6,25	Tensile strength of the tablets - distance between the punches of 6,25 mm
TS 6,75	Tensile strength of the tablets - distance between the punches of 6,75 mm
Weight 6,25	Weigth of tablets - distance between the punches of 6,25 mm
Weight 6,75	Weigth of tablets - distance between the punches of 6,75 mm
Disint 6,25	Disintegration time of tablets - distance between the punches of 6,25 mm
Disint 6,75	Disintegration time of tablets - distance between the punches of 6,75 mm
FriaTab 6,25	Friability of tablets - distance between the punches of 6,25 mm
FriaTab 6,75	Friability of tablets - distance between the punches of 6,75 mm
Tickn6,25	Tickness of tablets - distance between the punches of 6,25 mm
Tickn6,75	Tickness of tablets - distance between the punches of 6,75 mm
Poros 6,25	Porosity of tablets - distance between the punches of 6,25 mm
Poros 6,75	Porosity of tablets - distance between the punches of 6,75 mm

Conc 6,25	Released fraction of theophylline after 30 min in the dissolution vessel for tablets with a distance between the punches of 6,25 mm
Conc 6,75	Released fraction of theophylline after 30 min in the dissolution vessel for tablets with a distance between the punches of 6,75 mm

4.4. CONCLUSIONS

Variation in starting material properties showed to have a significant influence on both the granule and tablet characteristics and processability of raw material. A better understanding of the effects of raw materials (i.e. their particle size) was gained, which can optimally be used in order to manage the variability in the production process in order to obtain a high-quality end-product at any time. The next step is to identify critical process parameters that could be varied in order to get an end-product with similar properties, when starting from different starting materials.

4.5. REFERENCES

[1] C. Vervaet, J.P. Remon, Continuous granulation in the pharmaceutical industry, Chemical Engineering Science, 60 (2005) 3949-3957.

[2] C. Vervaet, J.P. Remon, Continuous Granulation, in: D.M. Parikh (Ed.) Handbook of Pharmaceutical Granulation Technology, Informa Healthcare, New York, 2009, pp. p. 308-322.

[3] G. Betz, P. Junker-Burgin, H. Leuenberger, Batch and continuous processing in the production of pharmaceutical granules, Pharmaceutical Development and Technology, 8 (2003) 289-297.

[4] H. Leuenberger, New trends in the production of pharmaceutical granules: batch versus continuous processing, European Journal of Pharmaceutics and Biopharmaceutics, 52 (2001) 289-296.

[5] H. Leuenberger, Scale-up in the 4th dimension in the field of granulation and drying or how to avoid classical scale-up, Powder Technology, 130 (2003) 225-230.

[6] H. Leuenberger, New trends in the production of pharmaceutical granules: the classical batch concept and the problem of scale-up, European Journal of Pharmaceutics and Biopharmaceutics, 52 (2001) 279-288.

[7] J. Werani, M. Grunberg, C. Ober, H. Leuenberger, Semicontinuous granulation - the process of choice for the production of pharmaceutical granules?, Powder Technology, 140 (2004) 163-168.

[8] L. Chablani, T.M. K, M. Amit, R. Patrick, S.W. C, Inline Real-Time Near-Infrared Granule Moisture Measurements of a Continuous Granulation-Drying-Milling Process, AAPS PharmsciTech, 12 (2011) 1050-1055.

[9] M. Fonteyne, S. Soares, J. Vercruysse, E. Peeters, A. Burggraeve, C. Vervaet, J.P. Remon, N. Sandler, T. De Beer, Prediction of quality attributes of continuously produced granules using complementary pat tools, European Journal of Pharmaceutics and Biopharmaceutics, 82 (2012) 429-436.

[10] M. Fonteyne, J. Vercruysse, D.C. Díaz, D. Gildemyn, C. Vervaet, J.P. Remon, T.D. Beer, Real-time assessment of critical quality attributes of a continuous granulation process, Pharmaceutical Development and Technology, 18 (2013) 85-97.

[11] J. Vercruysse, D. Córdoba Díaz, E. Peeters, M. Fonteyne, U. Delaet, I. Van Assche, T. De Beer, J.P. Remon, C. Vervaet, Continuous twin screw granulation: Influence of process variables on granule and tablet quality, European Journal of Pharmaceutics and Biopharmaceutics, 82 (2012) 205-211.

[12] FDA-Adminstration, Guidance for Industry - PAT - A Framework for Innovative Pharmaceutical Development, Manufacturing, and Quality Assurance, in, 2004.

[13] International Conference on Harmonisation of Technical Requirements for Registration of Pharmaceuticals for Human Use. Pharmaceutical Development Q8, in, 2009.

[14] A. Hlinak, K. Kuriyan, K. Morris, G. Reklaitis, P. Basu, Understanding critical material properties for solid dosage form design, Journal of Pharmaceutical Innovation, 1 (2006) 12-17.

[15] J. Kushner, B.A. Langdon, J.I. Hiller, G.T. Carlson, Examining the impact of excipient material property variation on drug product quality attributes: A quality-by-design study for a roller compacted, immediate release tablet, J. Pharm. Sci., 100 (2011) 2222-2239.

[16] S. Inghelbrecht, J.P. Remon, The roller compaction of different types of lactose, International Journal of Pharmaceutics, 166 (1998) 135-144.

[17] J.L.P. Soh, F. Wang, N. Boersen, R. Pinal, G.E. Peck, M.T. Carvajal, J. Cheney, H. Valthorsson, J. Pazdan, Utility of multivariate analysis in modeling the effects of raw material properties and operating parameters on granule and ribbon properties prepared in roller compaction, Drug Dev. Ind. Pharm., 34 (2008) 1022-1035.

[18] M.G. Herting, P. Kleinebudde, Roll compaction/dry granulation: Effect of raw material particle size on granule and tablet properties, International Journal of Pharmaceutics, 338 (2007) 110-118.

[19] E. Hadzovic, G. Betz, S. Hadzidedic, S.K. El-Arini, H. Leuenberger, Investigation of compressibility and compactibility parameters of roller compacted Theophylline and its binary mixtures, International Journal of Pharmaceutics, 416 (2011) 97-103.

[20] E. Hadzovic, G. Betz, S. Hadzidedic, S.K. El-Arini, H. Leuenberger, Roller compaction of different pseudopolymorphic forms of Theophylline: Effect on compressibility and tablet properties, International Journal of Pharmaceutics, 396 (2010) 53-62.

[21] N. Souihi, M. Dumarey, H. Wikström, P. Tajarobi, M. Fransson, O. Svensson, M. Josefson, J. Trygg, A quality by design approach to investigate the effect of mannitol and dicalcium

phosphate qualities on roll compaction, International Journal of Pharmaceutics, 447 (2013) 47-61.

[22] A.S. El Hagrasy, J.R. Hennenkamp, M.D. Burke, J.J. Cartwright, J.D. Litster, Twin screw wet granulation: Influence of formulation parameters on granule properties and growth behavior, Powder Technology.

[23] A.S. Hagrasy, P. Cruise, I. Jones, J.D. Litster, In-line Size Monitoring of a Twin Screw Granulation Process Using High-Speed Imaging, Journal of Pharmaceutical Innovation, (2013) 1-9.

[24] R.V. Haware, I. Tho, A. Bauer-Brandl, Multivariate analysis of relationships between material properties, process parameters and tablet tensile strength for α-lactose monohydrates, European Journal of Pharmaceutics and Biopharmaceutics, 73 (2009) 424-431.

[25] R.V. Haware, A. Bauer-Brandl, I. Tho, Comparative evaluation of the powder and compression properties of various grades and brands of microcrystalline cellulose by multivariate methods, Pharmaceutical Development and Technology, 15 (2010) 394-404.

[26] B.H. Mevik, E.M. Faergestad, M.R. Ellekjaer, T. Naes, Using raw material measurements in robust process optimization, Chemometrics and Intelligent Laboratory Systems, 55 (2001) 133-145.

[27] J.T. Fell, J.M. Newton, Determination of tablet strength by the diametral-compression test, J. Pharm. Sci., 59 (1970) 688-691.

[28] R.M. Dhenge, J.J. Cartwright, M.J. Hounslow, A.D. Salman, Twin screw granulation: Steps in granule growth, International Journal of Pharmaceutics, 438 (2012) 20-32.

[29] R.M. Dhenge, R.S. Fyles, J.J. Cartwright, D.G. Doughty, M.J. Hounslow, A.D. Salman, Twin screw wet granulation: Granule properties, Chemical Engineering Journal, 164 (2010) 322-329.

[30] J. Vercruysse, U. Delaet, I. Van Assche, P. Cappuyns, F. Arata, G. Caporicci, T. De Beer, J.P. Remon, C. Vervaet, Stability and repeatability of a continuous twin screw granulation and drying system., European Journal of Pharmaceutical Sciences, early online (2013).

[31] F. Podczeck, G. Lee-Amies, The bulk volume changes of powders by granulation and compression with respect to capsule filling, International Journal of Pharmaceutics, 142 (1996) 97-102.

[32] N. Sandler, D. Wilson, Prediction of Granule Packing and Flow Behavior Based on Particle Size and Shape Analysis, J. Pharm. Sci., 99 (2010) 958-968.

[33] H. Susi, J.S. Ard, LASER-RAMAN SPECTRA OF LACTOSE, Carbohydrate Research, 37 (1974) 351-354.

[34] H. Vromans, H.G.M. Poels-Janssen, H. Egermann, Effects of high-shear granulation on granulate homogeneity, Pharmaceutical Development and Technology, 4 (1999) 297-303.

[35] K. van den Dries, H. Vromans, Relationship between inhomogeneity phenomena and granule growth mechanisms in a high-shear mixer, International Journal of Pharmaceutics, 247 (2002) 167-177.

[36] H. Leuenberger, J.D. Bonny, C.F. Lerk, H. Vromans, Relation between crushing strength and internal specific surface area of lactose compacts, International Journal of Pharmaceutics, 52 (1989) 91-100.

[37] K.A. Riepma, H. Vromans, K. Zuurman, C.F. Lerk, The effect of dry granulation on the consolidation and compaction of crystalline lactose, International Journal of Pharmaceutics, 97 (1993) 29-38.

[38] Friability of uncoated tablets, European Pharmacopoeia, 7.6 (2013) 2.9.7.

[39] S. Mehta, T. De Beer, J.P. Remon, C. Vervaet, Effect of disintegrants on the properties of multiparticulate tablets comprising starch pellets and excipient granules, International Journal of Pharmaceutics, 422 (2012) 310-317.

[40] H. Murakami, T. Yoneyama, K. Nakajima, M. Kobayashi, Correlation between loose density and compactibility of granules prepared by various granulation methods, International Journal of Pharmaceutics, 216 (2001) 159-164.

[41] Tablets Uncoated tablets, European Pharmacopoeia, 7.6 (2013) 01/2013:0478.

[42] J. Dai, J.R. Grace, Biomass granular screw feeding: An experimental investigation, Biomass and Bioenergy, 35 (2011) 942-955

CHAPTER 5

IMPACT OF MICROCRYSTALLINE CELLULOSE MATERIAL ATTRIBUTES: A CASE STUDY ON CONTINUOUS TWIN SCREW GRANULATION

"If we knew what it was we were doing,
it would not be called research, would it?"
Albert Einstein (1879-1955)

ABSTRACT

The International Conference of Harmonisation (ICH) states in its Q8 'Pharmaceutical Development' guideline that the manufacturer of pharmaceuticals should have an enhanced knowledge of the product performance over a range of material attributes, manufacturing process options and process parameters. The present case study evaluates the effect of unspecified variability of raw material properties upon the quality attributes of granules; produced using a continuous from-powder-to-tablet wet granulation line (ConsiGma^{TM} 25). The impact of different material attributes of six samples of Microcrystalline Cellulose (MCC) was investigated. During a blind study the different samples of MCC were used separately and the resulting granules were evaluated in order to identify the differences between the six samples. Variation in size distribution due to varying water binding capacity of the MCC samples was observed. The cause of this different water binding capacity was investigated and was found to be a different degree of crystallinity. Afterwards, an experimental design was conducted in order to evaluate the effect of both product and process variability upon the granule size distribution. This model was used in order to calculate the required process parameters to obtain a preset granule size distribution regardless of the type of MCC used. The difference in water binding capacity and its effect on granular properties was still present when combining the MCC grades with different binders.

CHAPTER 5

IMPACT OF MICROCRYSTALLINE CELLULOSE MATERIAL ATTRIBUTES: A CASE STUDY ON CONTINUOUS TWIN SCREW GRANULATION

5.1. INTRODUCTION

The Q9-guideline [1] of the International Conference on Harmonisation (ICH) proposes a systematic approach for quality risk management. A risk management process consists of a risk assessment step, followed by risk control and risk review and can (should) be applied to all aspects of pharmaceutical quality. One of the important aspects in quality risk management, is the determination and evaluation of possible quality risks associated with variability of the properties of the starting materials. Moreover, in the PAT guidance for industry [2] the FDA states indeed that "*inherent, undetected variability of raw materials may be manifested in the final pharmaceutical product*". Processing difficulties can arise, which result in the failure of a product to meet specifications, even if the raw materials are conform to the pharmacopoeial specifications. Pharmaceutical manufacturing should be robust towards raw material variability. Therefore, the relationship between raw material variability, process and final product should be fundamentally understood. Microcrystalline cellulose (MCC) is a widely used excipient in the pharmaceutical industry. A schematic overview of the production of MCC (Avicel®PH) is given in Figure 5.1. Highly purified cellulose (α-cellulose) is obtained from trees, then depolymerized by means of acid hydrolysis in order to remove the amorphous regions and achieve the desired degree of polymerization. MCC can be purchased from different suppliers in a large variation of grades, which typically differ in particle size or bulk density. Table 5.1 gives a literature overview of research studies in which the effect of the use of various MCC starting materials on the process and end product quality of pharmaceutical products was investigated.

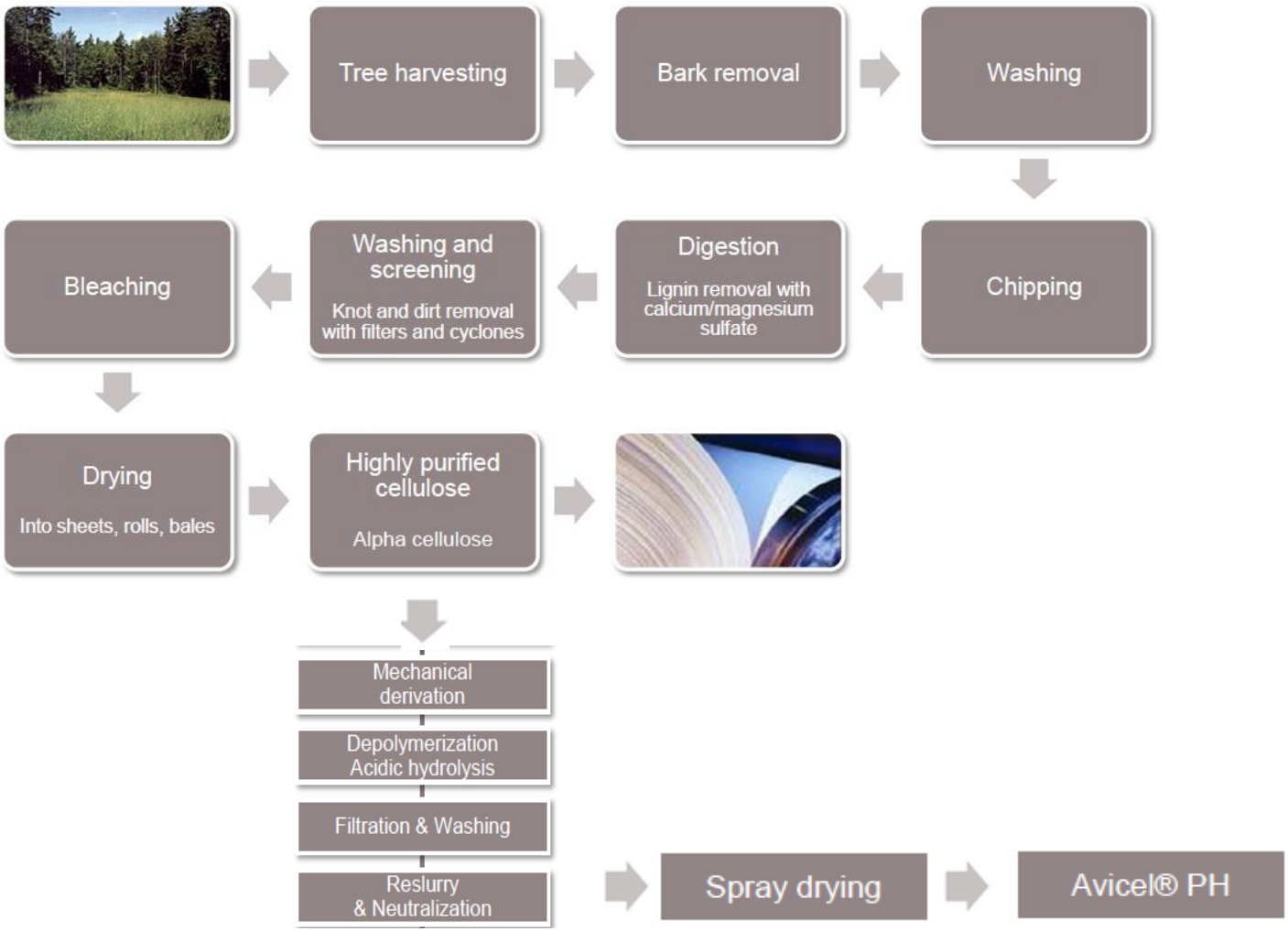

Figure 5.1. Schematic overview of the production of Avicel® PH. Reproduced with permission from FMC Health and Nutrition.

Table 5.1. Overview of research studies on various MCC grades, brands and batches.

Pharmaceutical process	Evaluated MCC differences (number)	Effect on end product or process	Ref.
roller compaction and tableting	brand and grade (3)	particle size MCC↓ => granule size↑ particle size MCC↓ => tensile strength↑	[3]
roller compaction and tableting	brand and grade (13)	full evaluation of the influence of different grades of MCC on the Critical Quality Attributes of ribbons, granules and tablets	[4]
roller compaction and tableting	grades of Emcocel (3)	particle size MCC↓ => tensile strength↑ raw material properties were succesfully included in a predictive model	[5]
roller compaction, granulation and tableting	grades of Avicel (5)	differences in friability and yield of granules differences in tensile strength and friability of tablets	[6]
extrusion/spheronisation	brand and grade (11)	void volume ↓ => less water needed for extr./sfer. better packing => less water needed for extr./sfer.	[7]
extrusion/spheronisation	brand and grade (7)	correlation between degree of polymerization and surface roughness and particle size of the pellets and correlation with the water content of the extrudate	[8]
extrusion/spheronisation	brand and grade (5)	bulk density ↑ => requires less water porosity ↓ => requires less water bulk density ↑ , porosity ↓, water retentive capacity↓ => lower sphericity	[9]
extrusion/spheronisation	grades of Avicel (2)	particle size ↑ => pellet porosity ↓	[10]
extrusion/sferonisation	brands (2)	differences in sensitivity to variation in water addition	[11]
wet massing	brand and grade (3)	different grades of MCC => differing required amount of water for saturation	[12]
wet granulation	Unimac MG 100 and Avicel PH 101	higher torque development for Unimac	[13]
liquisolid tableting	grades of Avicel (3)	differences in dissolution profiles and hardness	[14]

tableting	brand and grade (7)	different grades of MCC => tensile strength differs	[15]
tableting	brands (2)	similar binding properties for Avicel PH 101 and Emcocel	[16]
tableting	grade (4)	degree of polymerization↑ => tensile strength↑	[17]
tableting	brand and grade (5)	particle size ↓ => tensile strength↑	[18]
tableting	grades of Avicel (3)	differences in lubricant sensitivity	[19]
tableting	KG-801 Ceolus and Avicel PH101	use of KG yielded a larger number of rod-shaped particles and a higher compressibility	[20]
tableting	grades of Avicel (2)	differences in tablet properties which diminished when an API was added	[21]
tableting	grades of Avicel (2)	differences in tablet properties	[22]
tableting	grade and brands (6)	lignine concentration ↑ => dissolution rate ↑	[23]
capsule filling	brand and grade (8)	difference in capsule filling performance and disintegration time	[24]
	batches of Avicel PH 102 (7)	batch-to-batch uniformity regarding flow properties	[25]
	grades and batches of Avicel (9)	batch-to-batch differences are comparable to intergrade differences	[26]
wet granulation, fluid bed drying and tableting	brand and batch (3)	batch-to-batch differences are comparable to interbrand differences	[27]
tableting	brand, grade and manufacturer (16)	bulk and tapped density↑ => tensile strength↓	[28]
		turgidity↑ => tensile strength↑	
		degree of polymerization↑ => tensile strength↑	
		molecular weight↑ =>tensile strength↑	
tableting	brand, grade and batch (16)	batch-to-batch variability similar to interproduct variability	[29]
tableting	brand, grade and batch (22)	different batches from the same grade showed different compaction properties	[30]
tableting	brands and batches (15)	batch-to-batch variability was found	[31]

Most studies reported in Table 5.1 were based on the use of different brands and/or grades of MCC, but there are very little analyses available on different samples of MCC of the same brand and grade. The observation of a variable processing behavior or different end product quality of pharmaceuticals arising from different grades or brands of MCC is expected [3-24]. Nevertheless, some authors reported significant batch-to-batch variation even when the same brand and grade were used [25-31]. Landin et al. state that batch-to-batch variation of MCC is caused by the use of different wood pulps as starting materials for the production of MCC [32]. These different wood pulps cause a larger batch-to-batch difference than the used methodology for the MCC production itself. The use of various wood pulps results in a dissimilar degree of crystallinity when comparing batches [33]. It is important to determine the reasons for such variations in crystallinity index between MCC batches, which might be as high as 4%, thereby impacting the properties of the end products [34].

The **aim** of this study was to elucidate the cause and effects of this variability of MCC upon processability and granule properties during continuous twin screw granulation. Earlier investigations showed that variability of MCC caused differences in processes which are characterized by a short interaction time between the powders and water (i.e. pellet size differences in extrusion-spheronization). During twin screw granulation the residence time in the granulator barrel and the contact time between powder and granulation liquid is very short. Six different samples of Avicel® PH 101 were delivered and could be considered as similar from a pharmacopoeial point of view. This chapter reports about the thorough investigation of the raw material characterization of the different samples as well as the properties of the produced granules using these samples. Furthermore, the inherent cause of the observed MCC variability and resulting granule property differences is presented. In addition, solutions to manage these differences are suggested and evaluated. This chapter reports the investigations in chronological order, starting with a blind study on the received samples. Afterwards the effect of MCC variability upon granule properties has been elucidated and the root cause of the obtained differences has been investigated in depth. A comparison between the effect of raw material differences and the modification of process parameters was made, followed by an investigation on the effect of the presence of different binders for twin screw granulation of these MCC samples.

5.2. MATERIALS AND METHODS

5.2.1. Materials

The six samples of Microcrystalline Cellulose (MCC) Avicel® PH101 studied, were donated by FMC Health and Nutrition. For this study, the six samples were labeled X1, X2, X3, X4, X5 and X6. Granules were produced from a preblend consisting of 30% of MCC, 60% lactose monohydrate (Pharmatose 200M, Caldic, Hemiksem, Belgium) and 10 % of unmodified maize starch (Cargill, Ghent, Belgium). Several binders were investigated, namely Hydroxypropylcellulose, HPC (Klucel®, EXF Pharm, Hercules Wilmington, DE, USA), Hydroxypropylmethylcellulose, HPMC (Methocel™E5 Premium, Colorcon, Kent, UK) and polyvinylpyrrolidone, PVP (Kollidon®30 and Kollidon®90, BASF, Ludwigshafen, Germany).

5.2.2. Powder and granule characterization

The six samples of MCC were analyzed without prior knowledge of the powder characteristics. It was only communicated that samples were produced using different wood pulps or combinations of different wood pulps as starting materials. Therefore, an extensive powder characterization study was conducted prior to the granulation experiments.

5.2.2.1. Particle size analysis of powders

The particle size distribution (PSD) of the powders was measured by laser diffraction. The wet dispersion method using the 300 RF lens (Malvern Instruments, Malvern, UK) was applied. Prior to the measurement, powder samples were dispersed in Miglyol 812 (triglyceride saturated medium, Fagron, Capelle aan den Ijssel, The Netherlands) with 0.2% Tween 80 (Polysorbate 80, BUFA, Ijsselstein, The Netherlands). PSD results were reported as d10, d50 and d90 values. Furthermore the span was calculated as a measure of distribution width. Span equals (d90-d10) / d50. Measurements were performed in triplicate.

5.2.2.2. Bulk and tapped density of powders and granules

The bulk and tapped density of powders and granules were determined according to the European Pharmacopeia 7.5. Approximately 60 mL of material was poured into a 100 ml graduated cylinder. The powder/granule weight and exact volume were used to calculate

the bulk density (ρ_b). Each sample was tapped 10 times, followed by 500 and 1250 times using an automatic tapping instrument (J. Engelsmann AG, Ludwigshafen am Rhein, Germany). When the difference between the volume after 500 taps differed more than 1 mL from the volume obtained after 1250 taps, 1250 extra taps were conducted. The volume reading was then used to determine the tapped density (ρ_t). All density measurements were performed in triplicate and the average densities were calculated.

5.2.2.3. Flowability of powders and granules

The Hausner ratio (H) was used as a measure of flowability ($H= \rho_t/ \rho_b$). Secondly, the flowability of the raw materials was measured using a RST-XS Schulze ring shear tester (Schulze Schüttgutmesstechnik, Wolfenbüttel, Germany) equipped with a standard 30 mL shear cell. For the powders, the applied normal load at preshear was 2000 Pa. Afterwards shear-stresses of 400, 1000, 1600 and again 400 Pa were applied. A 70 mL cell was used to measure the flowability of the granules with the ring shear tester. Herewith, a preshear of 1000 Pa was applied, followed by stresses of 250, 525, 850 and 250 Pa. The ff_c, which is the ratio of consolidation stress to unconfined yield strength, was used to evaluate the flowability. Measurements were done in triplicate.

5.2.2.4. True density of powders and granules

The true density (ρ) of the MCC samples and granules was determined by helium pycnometry (Accupyc 1330 Pycnometer, Micrometrics, Norcross, USA). A total of ten runs and ten purges was performed per experiment using a purge fill pressure of 19.5 psig.

5.2.2.5. Particle shape of powders

The shape of the powder particles was evaluated by means of scanning electron microscopy (SEM). The images were recorded on a quanta FEG FEI 200 apparatus (FEI Company, The Netherlands). Samples were put on a silicon wafer and sputtered with a thin layer of palladium/gold prior to visualization.

5.2.2.6. Moisture determination of powders

The moisture content of the starting materials was determined by means of volumetric Karl Fischer titration using a V30 volumetric Karl Fischer titrator (Mettler Toledo, USA). Methanol

(Hydranal, Sigma Aldrich, Germany) was used as medium. The powders were stirred for five minutes prior to titration, and all measurements were done in triplicate.

5.2.2.7. Water sorption of powders

Water sorption measurements were performed using a K-12 tensiometer (Krüss, Germany), equipped with a Krüss Laboratory Desktop v2.0.0.2207. The apparatus was calibrated against double distilled water (γ=72.8 mN/m) using a platinum Wilhelmy plate. The total water sorption of the studied MCC samples was determined using the Washburn method [35], based on liquid penetration into a powder bed (recorded as mass) as a function of time. An alumina capillary (FL12 sample holder, Krüss) with a perforated bottom covered with filter paper was used. About 1.0 to 1.1 g of sample was weighted into the capillary and tapped until constant volume before closing the capillary. Measurements of water sorption were conducted in purified water as medium using a surface detection sensitivity of 0.04 g and a surface detection speed of 6 mm/min. Approximately 100 (2 points/second) of mass versus time data points were recorded during sorption until the maximum mass, which corresponds to the water binding capacity of the studied sample, was achieved (in g water/ g sample). Furthermore water binding capacity (WBC) values (in %) were obtained via FMC Health and Nutrition as such.

5.2.2.8. Degree of crystallinity of powders

X-ray diffraction (XRD) measurements were performed on a Philips X'Pert Pro powder diffractometer (model PW 3040/60). Diffractograms were recorded in the reflection mode in a 2ϑ angular range of 10–40° by steps of ca. 0.02° at room temperature. The Cu Kα radiation (λ = 1.5418 Å) generated at 45 kV and 40 mA was monochromatized using a 20 µm Ni filter. Diffractograms were recorded from rotating specimens using a position sensitive detector. Profile deconvolution was performed with a multiple peak fit tool by using Origin's Peak Analyzer (OriginPro 9, Origin Lab). The fifth-degree polynomial function was used to fit the amorphous background (baseline), and the pseudo-Voigt function was used to express each crystalline reflection [36]. Cellulose crystallinity was determined by calculating the ratio of the separated crystalline peak area to the total reflection area of all signals, including background.

5.2.2.9. Granule size distribution

Sieve analysis was performed using a Retsch VE 1000 sieve shaker (Haan, Germany), with a series of 8 sieves (150, 250, 500, 710, 1000, 1400, 2000 and 3150 µm). Subsamples (100 g) of granules were sieved for 10 minutes with an amplitude of 2 mm. The amount of granules retained on each sieve was determined and collected. All measurements were performed in triplicate.

5.2.2.10. Friability of granules

The granule friability was determined using a friabilator (PTF E Pharma Test, Hainburg, Germany) at a speed of 25 rpm for 10 min, by subjecting 10 g (w_0) of oven-dried granules together with 200 glass beads (mean diameter = 4 mm) to falling shocks. Prior to determination, the granule fraction of less than 250 µm was removed to ensure the same starting conditions. The glass beads were then removed and the weight retained on a 250 µm sieve (w_1) was determined. The friability was calculated as $[(w_0 - w_1)/w_0] * 100$. Measurements were performed in triplicate.

5.2.3. Blind study: effects of MCC variability upon granule properties

Six preblends (MCC:lactose:starch, 30:60:10), each made with one of the six MCC samples, were granulated with two sets of process parameters (experiments A and B). All granulation experiments were conducted on the continuous twin screw granulator of the ConsiGma™ 25 (GEA Pharma systems nv, Wommelgem, Belgium) described earlier [37, 38]. Since the short contact time between water and powders seemed to be important, two experiments were conducted. Experiment A was characterized by the shortest contact time between powder and water, whereas during experiment B the probability of powder and water to interact was higher. For experiment A, a powder feed rate of 25 kg/h and a screw speed of 950 rpm were applied. Experiment B was conducted with a powder feed rate of 10 kg/h and a screw speed of 500 rpm. For both experiments, the temperature of the granulator barrel was held constant at 25°C. Distilled water was used as granulation liquid and the relative amount of liquid added (approx. 41% of total dry mass) was kept constant. This resulted in a granulation liquid addition of 170 g/min for experiment A and 70 g/min for experiment B. The screws consisted of two kneading zones with six elements each with an angle of 60°

between two elements, as described in [37]. Granules were oven-dried at 40°C during 24h prior to further analysis. The 150 µm sieve was not used in the granule size distribution evaluation of the granules from experiment A and B.

5.2.4. Evaluation of process and formulation variables upon granule size distribution

A two-level full-factorial design with five factors was conducted. Four quantitative parameters were varied (MCC water binding capacity, temperature of the barrel, powder feed rate, liquid addition). Furthermore, one qualitative parameter, i.e. the screw configuration, was investigated. Screws with two kneading zones of six elements were used as well as screws equipped with two kneading elements in one kneading zone only. Three center point experiments were performed as well, resulting in a total amount of 35 experiments (2^5 + 3). The screw speed was held constant at 950 rpm. The evaluated response was the granule size distribution. An overview of all performed experiments is presented in Table 5.2.

Table 5.2. Overview of the design factor ranges for the evaluation of process and formulation variables upon granule size distribution.

Factor/Level	-1	0	+1
Water binding capacity (%)	157.5	169.5	181.5
Barrel temperature (°C)	25	32.5	40
Powder feed rate (kg/h)	10	17.5	25
Liquid addition (% on dry mass)	36	42	48
Screw configuration	1x2		2x6

5.2.5. Evaluation of the effect of different binders

A second full-factorial design of experiments was performed with two qualitative and two quantitative factors (Table 5.3) resulting in 35 experiments. The qualitative factors were the type of binder (HPMC, HPC, Kollidon 30 and Kollidon 90) and the method used for adding the binder (either in the dry premix or diluted in the granulation liquid). The quantitative factors evaluated in this design were the water binding capacity and the temperature of the granulator barrel. The granule size distribution was again investigated as a response. For these experiments, the standard screw configuration with 2 kneading zones (each consisting

of 6 kneading elements) was used. Screws rotated with a speed of 950 rpm. The powder premix consisted of 67% lactose, 30% MCC, 3% binder and was fed at 17.5 kg/h, whereas the liquid addition was held constant at 105 g water/minute. A binder concentration of 3% was calculated based on dry mass.

Table 5.3. Overview of the design factors for evaluating the effect of different binders.

Factor/Level	**-1**	**0**	**1**	
Water binding capacity (%)	157,5 X1	169,5 X2	181,5 X3	
Temperature of the barrel (°C)	25	32.5	40	
Qualitative factors:				
Method of binder addition	Dry	Wet		
Type of binder	HPMC	HPC	PVP K30	PVP K 90

5.2.6. Data treatment and analysis

Design analysis was performed using Modde 9.1 (Umetrics, Umeå, Sweden). The granule size distribution values were included as the responses. Since these size distribution responses were correlated, Partial Least Squares (PLS) effects instead of Multiple Linear Regression, MLR) was used to fit the model, allowing the covariance of the responses to be taken into account.

5.3. RESULTS AND DISCUSSION

5.3.1. Powder characterization

The particle size distribution of the six powders was investigated by means of laser diffraction. The experimental d10, d50 and d90 values are presented in Table 5.4.

Table 5.4. Powder characterization: d10, d50, d90 and span with their respective standard deviations, bulk and tapped density, ff_c and moisture content.

	Laser diffraction (µm)							
	d10	**stdev**	**d50**	**stdev**	**d90**	**stdev**	**Span**	**stdev**
X1	14.14	1.40	72.96	1.94	163.82	1.93	2.05	0.06
X2	13.05	2.44	70.39	4.04	149.71	5.08	1.94	0.07
X3	11.76	0.33	70.65	2.24	155.18	3.61	2.03	0.02
X4	12.48	0.77	65.40	1.49	145.38	4.63	2.03	0.04
X5	10.00	0.71	62.26	4.21	160.07	3.01	2.42	0.12
X6	14.15	0.93	75.49	0.41	172.43	0.98	2.10	0.01

	Bulk and tapped density (g/ml)			ff_c	**Moisture content (%)**
	Bulk	**Tapped**	**HR**		
X1	0.33	0.45	1.36	3.9	5.25
X2	0.31	0.43	1.38	4.5	5.07
X3	0.33	0.44	1.34	4.8	5.00
X4	0.32	0.42	1.31	4.7	5.05
X5	0.35	0.44	1.26	4.4	4.82
X6	0.33	0.44	1.33	4.4	4.65

Overall, the six powders can be considered similar regarding particle size distribution. For span, only X5 slightly differs with a higher span value (2.4 +/-0.12). No significant difference was found for the other five samples. The bulk, tapped and true densities are similar for all six powders, with an average bulk density of 0.33 g/mL and an average tapped density of

0.44 g/mL (Table 5.4). The true density was 1.55 g/cm³ for all six MCC samples. The Hausner ratio was derived from the bulk and tapped densities as a measure of flowability. Since a Hausner ratio higher than 1.25 indicates poor flowability, the six samples can be considered as poorly flowing when evaluated by the Hausner ratio. A ring shear tester was also used for the evaluation of the flowability. The ff_c results are similar for the six samples (Table 5.4). Ff_c values from 4 up to 10 indicate that powders are considered to be easy-flowing. The six powders have similar scores regarding flowability, both when evaluating the Hausner ratio and the ff_c values. The moisture content was also comparable for the six powders (Table 5.4). Because the particle shape of powders can also affect their processability, SEM pictures of the six samples of MCC were compared (Figure 5.2). All samples consist of oblong, rough edged particles, with no significant shape differences between the powders. To conclude, no clear differences in evaluated powder properties between the six samples could be observed.

5.3.2. Blind study: MCC variability effects upon granule properties

Since the six MCC samples did not show physical powder property differences, two explorative granulation studies were conducted (experiments A and B) on each of the six MCC samples (twelve granulation runs in total). Experiment A can be considered as a 'high throughput' experiment. The fast screw speed results in a short residence time in the granulation barrel and the high powder feed rate results in a high barrel filling. The combination of the two latter parameters implies that the powder is 'rushed' through the barrel. Experiment B is a 'low throughput experiment' (higher residence time and lower barrel filling degree), with a longer time for the powder to interact with the granulation liquid. The granules were oven-dried and then characterized. The moisture content of the granules was monitored: the samples were analysed directly after granulation and during drying (t=0h, 2h, 22h and 24h). The drying profiles of the different samples were identical (data not shown). The evaluation of the flowability, true density, friability and shape of the granules in experiment A (short residence time and high barrel filling degree), revealed no detectable differences between the six samples.

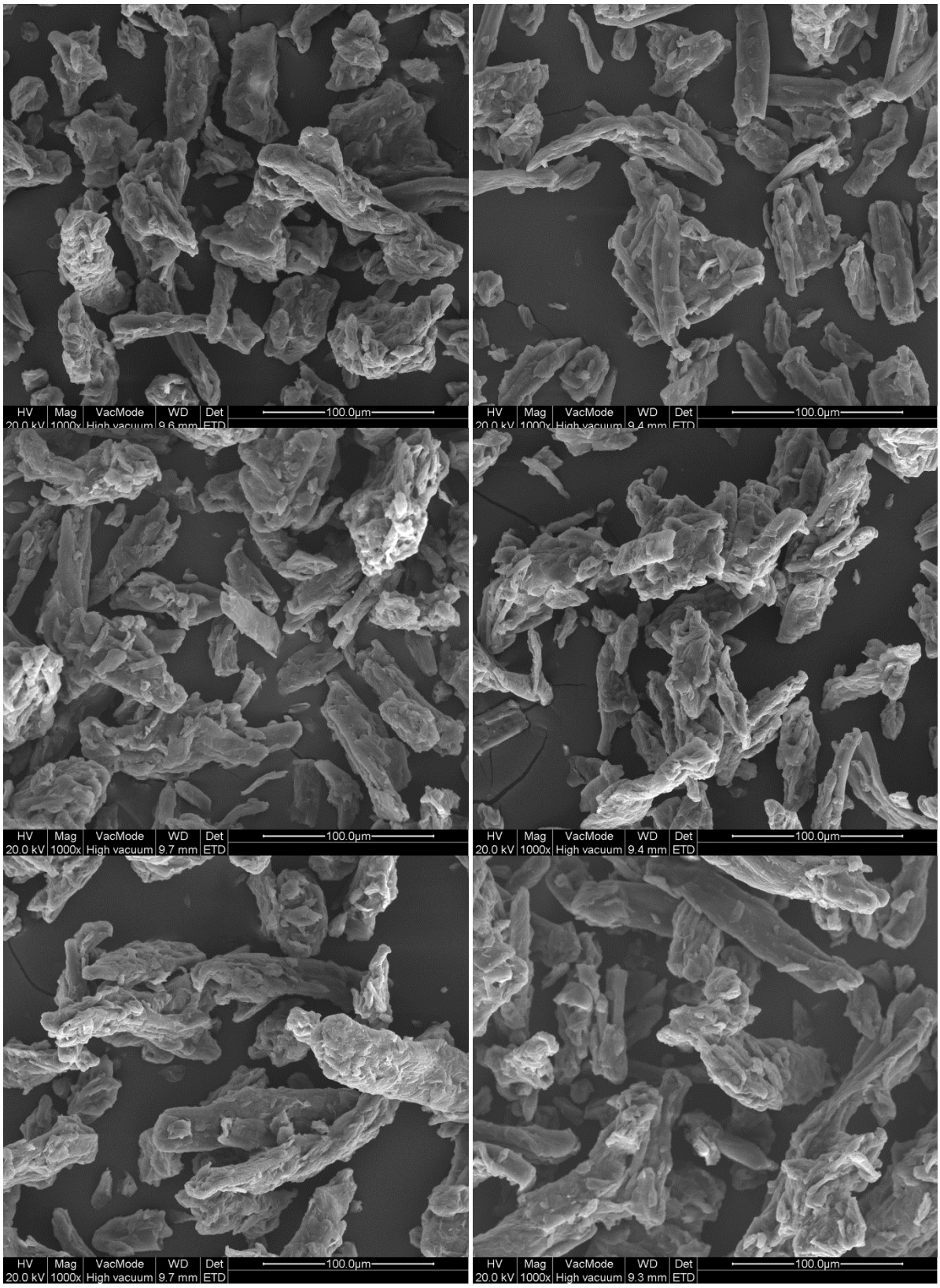

Figure 5.2. SEM pictures of the six different batches of Avicel® PH (top: X1, X2, mid: X3, X4, bottom: X5 and X6).

Figure 5.3 shows the bulk and tapped density of the granules produced in experiment A and B. Similar densities were obtained in both experiments for the different samples. The most interesting quality attribute was the granule size distribution (Figure 5.4). Two groups could be distinguished in experiments A and B: the premixes X2, X4 and X6 yielded high amounts of fines (<250 µm), and a low amount of oversized granules (>1400 µm), whereas premixes X1, X3 and X5 were characterized by more oversized granules and less fines. The yield (250-1400 µm) was constant for all six samples, as reported earlier [39]. When evaluating the results of experiment B, it was seen that when the processed powder and granulation liquid got more time to interact, this resulted in less differences between the samples. It was noteworthy, however, that sample X1 was still characterized by a high proportion of granules in the range 1401-2000 µm, when a low throughput was applied.

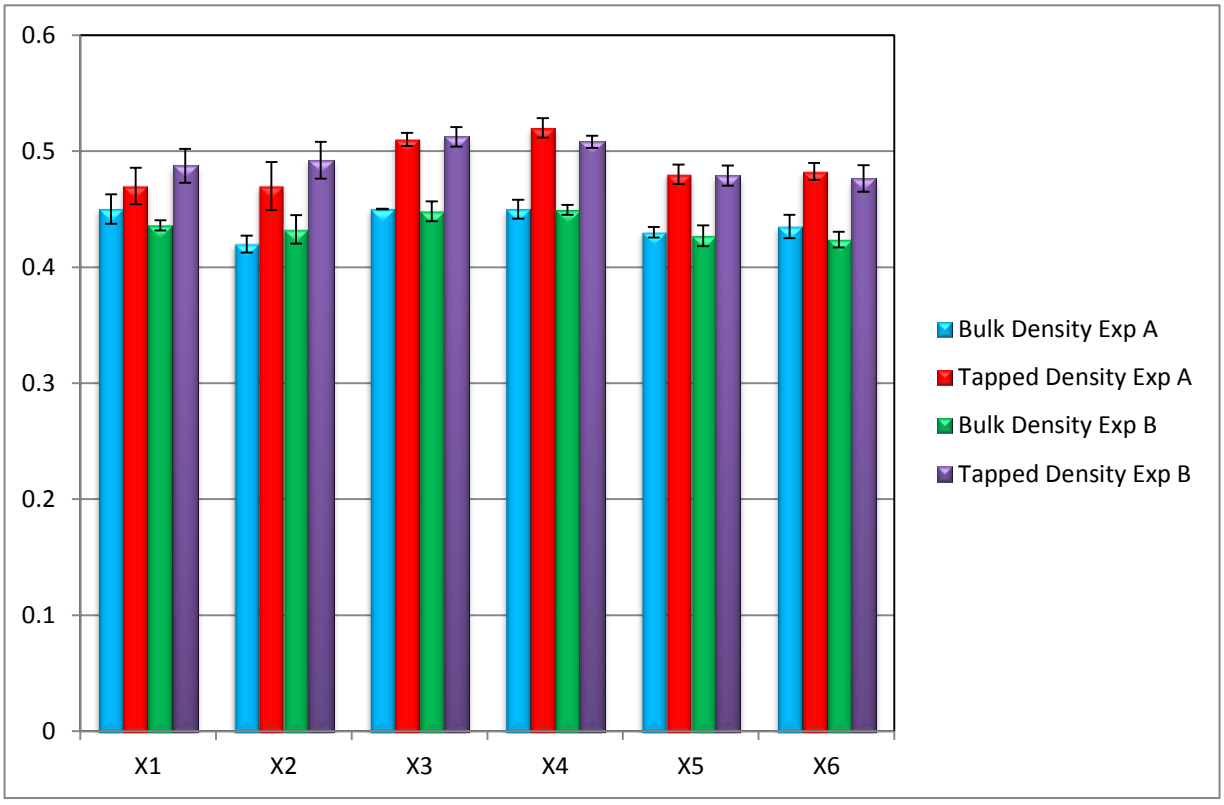

Figure 5.3. Bulk and tapped density of the granules produced during experiment A and experiment B.

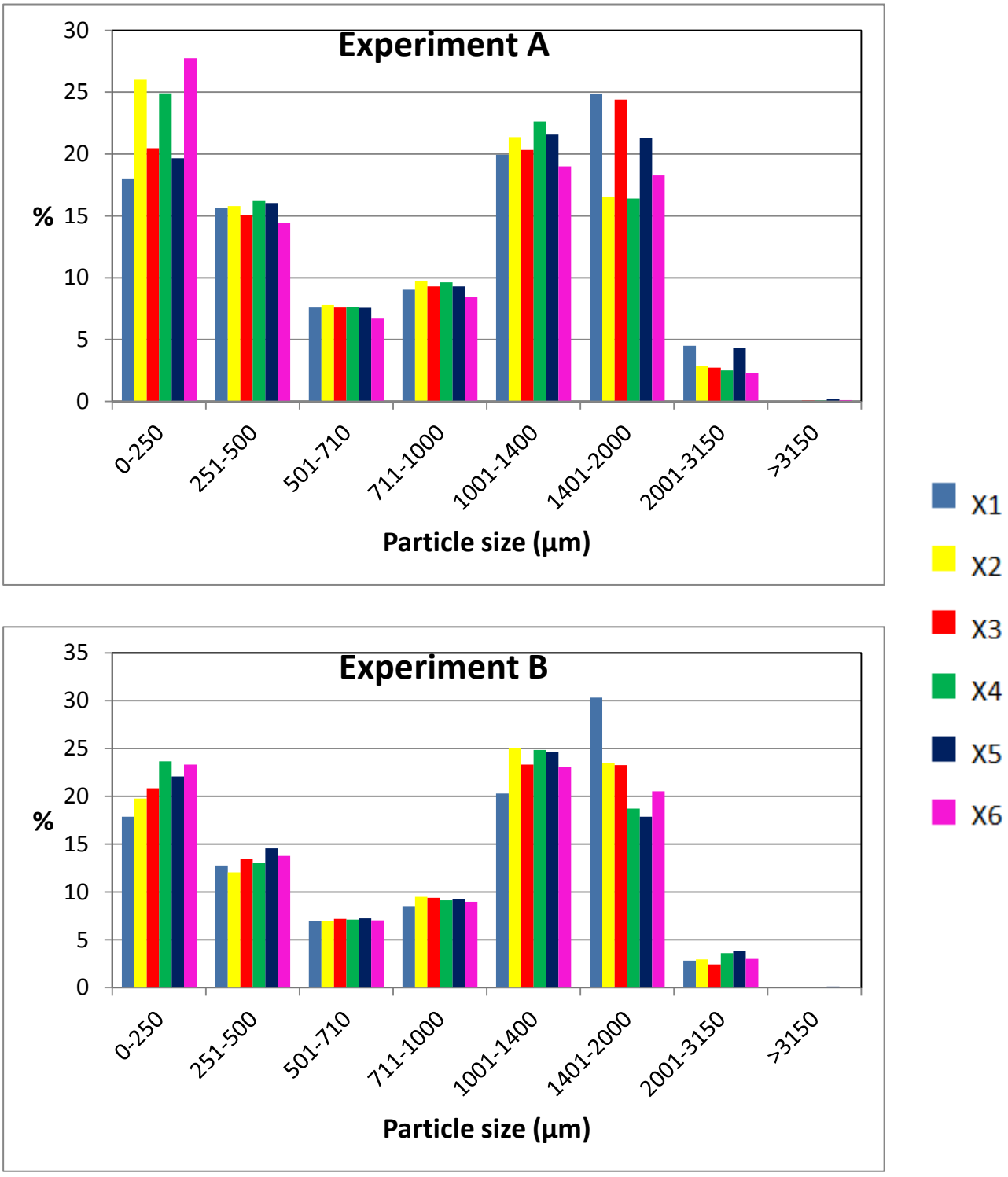

Figure 5.4. Granule size distribution of the oven-dried granules of experiment A and experiment B.

These results clearly show that the granule size distributions were affected by the variability of Avicel® PH101, especially when a high barrel filling degree and short residence time

hindered interaction between the powder and granulation liquid. After communicating these results to the MCC supplier, the authors received more information concerning the water binding capacity (WBC) of the six delivered MCC samples as determined by FMC Health and Nutrition (Figure 5.5). Water binding capacity is not implemented in the specifications defined by the Pharmacopeia. The data in Figure 5.5 clearly show that X1 exhibits the lowest WBC (157.5%), whereas X2 and X4 are characterized by the highest WBC (181.5 and 180.5%, respectively). The lower the WBC of the MCC sample, the less granulation liquid is taken up by the powder during granulation. Hence, more granulation liquid is available for granulation. This explains why X1 consisted of more oversized granules in experiment A and B. Apart from X1, no significant differences in granule size distribution was observed between the MCC samples at low throughput (experiment B). However, the differences in WBC do manifest clearly under high throughput conditions (experiment A). When X2 and X4, with the highest WBC, are granulated, the lowest amounts of oversized granules are obtained and a lot of fines are produced. Although X3 and X6 have a similar WBC, their behavior is different at high throughput: X6 shows a lot of fines and a low amount of oversized, whereas the opposite can be noted for X3.

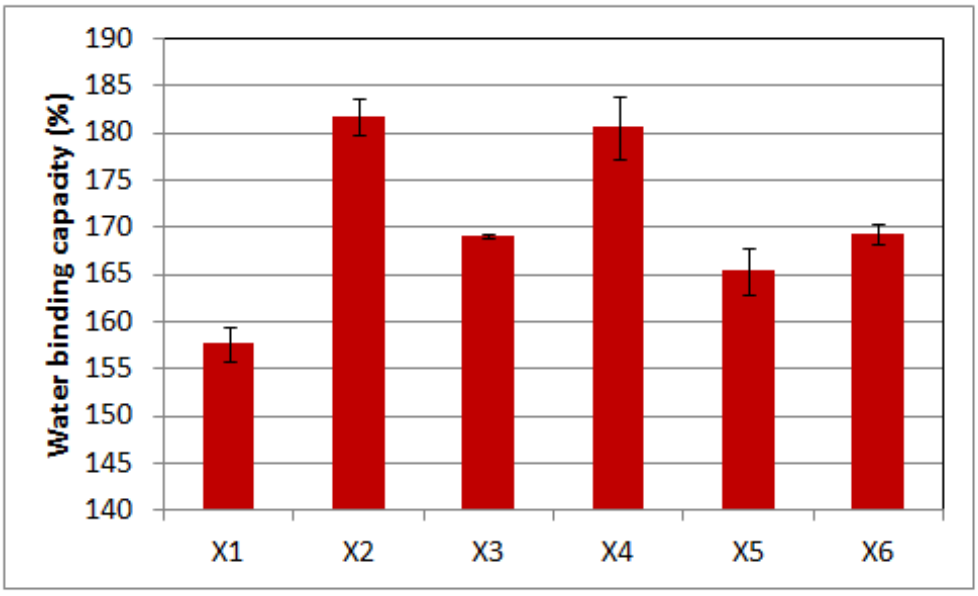

Figure 5.5. Water binding capacity values for the six different batches of Avicel® PH as determined by FMC Health and Nutrition (reproduced with their permission).

5.3.3. Open study: Defining the cause of the differences in water binding capacity

With the extra information regarding WBC, further powder characterization was performed to find the cause of these different water binding capacities. Water sorption measurements were first conducted on the six samples. Figure 5.6 shows the water sorption curves of the six powder samples. It is clear that there is no correlation between the slope of the water sorption curves and the final amount of water absorbed. Also, no explanation for the different behavior of X3 and X6 could be established with respect to their different water sorption behavior. Furthermore, the time span over which all water is absorbed is not correlated to the final amount of water absorbed. Only X1 consisted of a large amount of oversized granules after the low throughput experiment (B). The rate of water sorption is indeed low for X1, hence more water will be available for granulation, even at low throughput. A correlation between the water binding capacity values obtained from FMC Health and Nutrition and the water absorbed per gram sample can be seen (Figure 5.7).

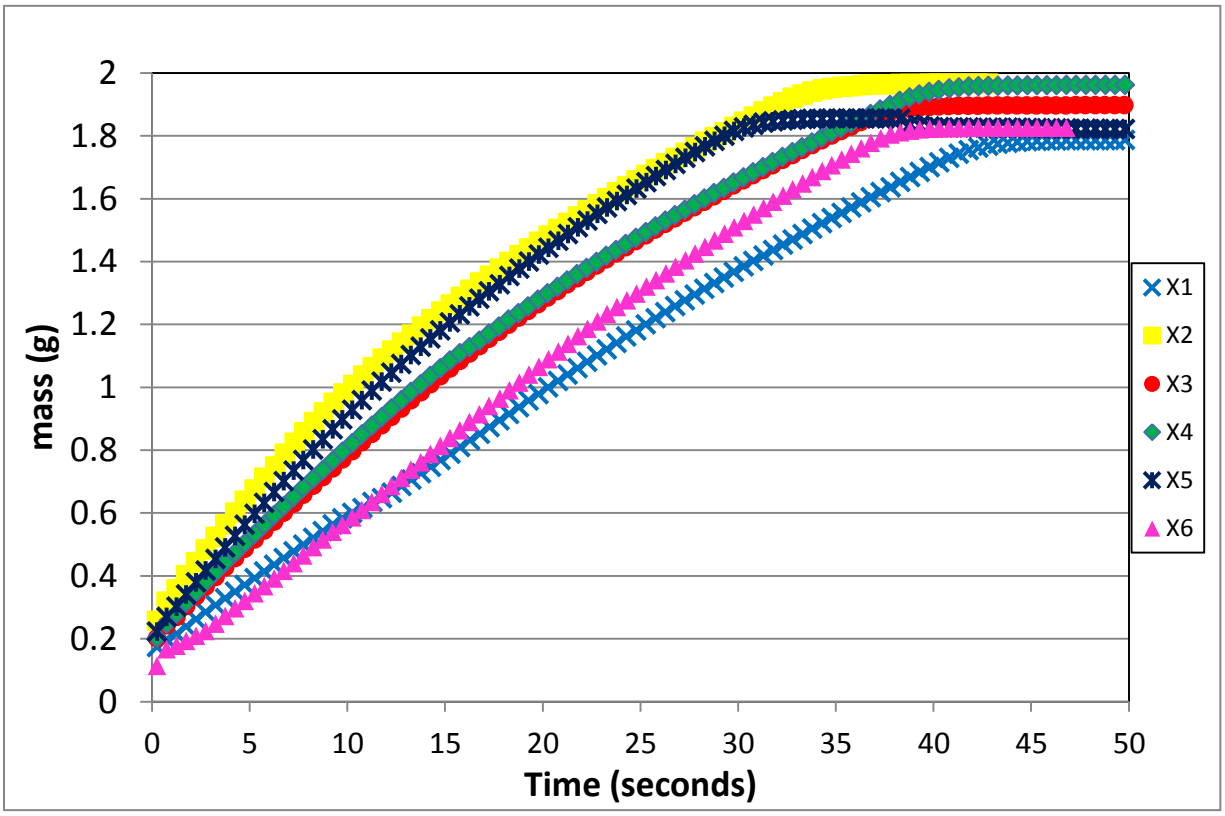

Figure 5.6. Water sorption curves of the six different MCC batches.

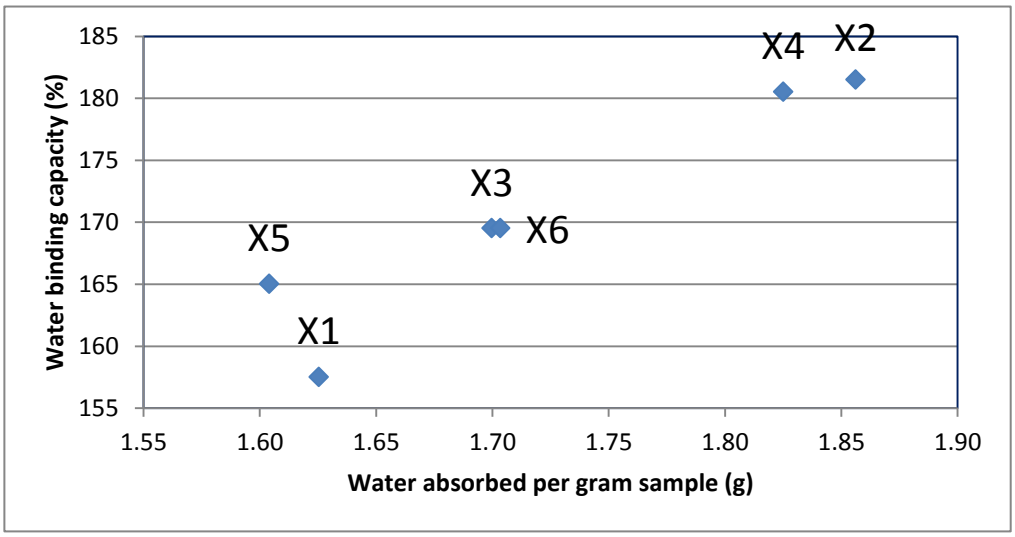

Figure 5.7. Correlation between the water binding capacity values obtained by FMC Health and Nutrition and the water absorbed per gram sample.

A plausible reason for the differences in water binding capacity is the fact that the different MCC samples are produced from different wood pulps. A crystallinity study was performed on the six MCC samples to further investigate the underlying cause of the different WBC values (Table 5.5). Samples X1 and X5 exhibited the highest degree of crystallinity and the lowest water binding capacity. Conversely, sample X4 having the highest water binding capacity showed the lowest degree of crystallinity. The difference in degree of crystallinity between the three remaining samples was too small to observe a correlated variation in water binding capacity. It can nonetheless be concluded that there is a general trend that links the degree of crystallinity with the capacity to bind water, i.e. the higher the degree of crystallinity the lower the water binding capacity. This is an expected correlation as a high degree of crystallinity typically indicates a more organized crystalline core which tends to involve essentially hydrophobic interactions. The interaction with water is essentially taking place with surface-exposed cellulose chains, which exhibit a higher disorder due to higher interactions with water than the chains that are part of the crystalline core of the cellulose structures. In order to confirm the above stated hypothesis, two additional samples were obtained via FMC Health and Nutrition, namely sample A and sample B. These MCC powders are not commercially available and consist of other combinations of pulp mixes. The crystallinity values obtained are all listed in Table 5.5. The degree of crystallinity of samples A

and B was significantly lower than the other six samples. This was expectable, since they are produced from different pulps. The water sorption of samples A and B was measured as well, and was determined to be 2.08 and 2.09 g water/ g MCC respectively. A clear correlation between degree of crystallinity and water sorption capability can be observed (Figure 5.8). It can be concluded that a difference in degree of crystallinity does cause the differences in water binding capacity between the six (eight) evaluated samples.

Table 5.5. Degree of crystallinity of each MCC sample.

	X1	X2	X3	X4	X5	X6	A	B
Crystallinity	71.8%	67.9%	68.2%	66.3%	72.2%	67.8%	61.1%	62.9%
STD	2.0%	1.0%	2.0%	2.0%	3.0%	0.3%		

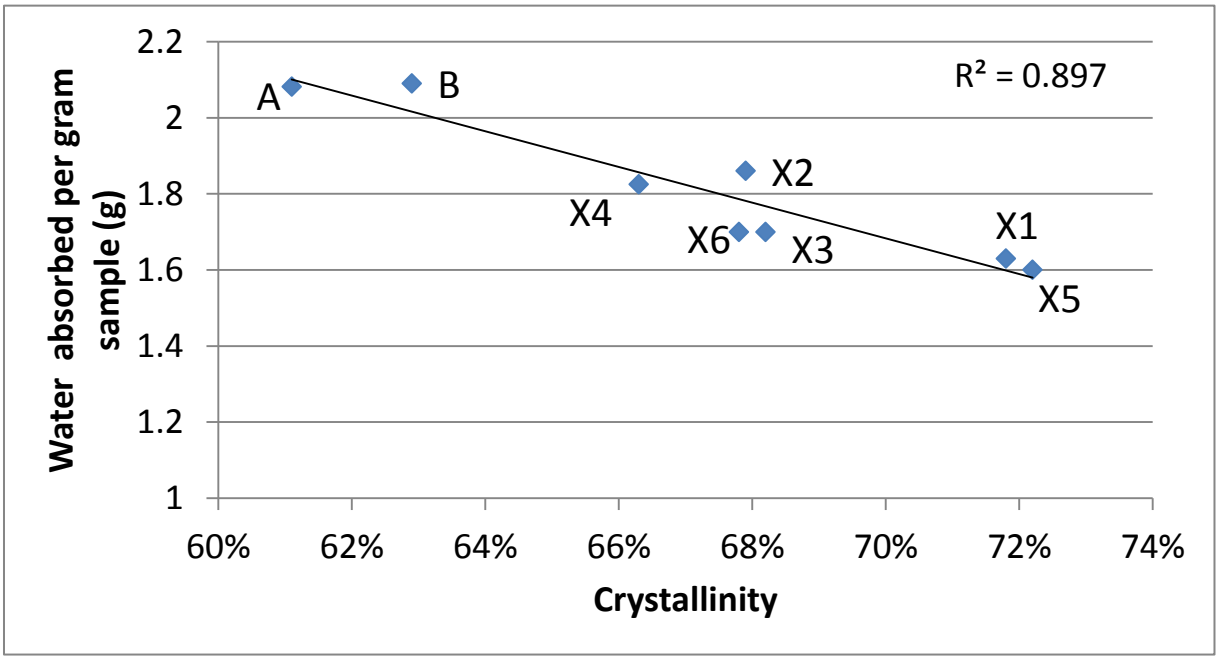

Figure 5.8. Correlation between the crystallinity and the water absorbed per gram sample as determined by means of water tension measurements. The six MCC batches are plotted together with two confirmation samples, A and B.

5.3.4. Evaluation of process and formulation variables upon granule size distribution

To further investigate the effect of WBC upon granule size distribution in combination with the effect of the twin screw granulation process parameters, an experimental design was conducted as presented in Table 5.2. It was preferred to evaluate WBC as a quantitative parameter instead of using the different samples as qualitative parameters. Therefore, the lowest level of the WBC factor corresponded to X1, while the highest level corresponded to X2. The X3 sample was used for the three centerpoint experiments. Furthermore, barrel temperature, powder feed rate and liquid addition were investigated as factors. The screw configuration was added as a qualitative parameter. A kneading zone of two kneading elements (1x2) was compared with two zones of 6 kneading elements divided by a conveying element (2x6). The staggering angle between kneading elements was 60°. The centerpoint experiments were granulated with the 1x2 configuration. As an example, the effects of the factors upon the smallest granule size fraction (0-150 µm) and the largest size fraction (2000-3150 µm) are shown in Figure 5.9. For both responses, the addition of granulation liquid had a clear influence on the granule size fraction. Liquid addition had a negative effect in the case of the smallest granule fraction: the more granulation liquid is added, the less fines are remaining. On the other hand, more granulation liquid results in a larger amount of oversized granules. The WBC has also a significant effect on the granule size fraction. The WBC had a significant effect on the amount of fines. The larger the WBC of MCC, the less water will be available for granulation, resulting in more fines. The negative effect of the WBC on the granule size fraction from 2000-3150 µm can be explained in a similar manner: when the WBC is low, MCC will absorb less water. The remaining water is thus available for granulation, resulting in more oversized granules.

A clear overview of the effects of the different factors on the complete granule size distribution is presented in Figure 5.10. The effect of the water binding capacity is clearly demonstrated for all granule fractions. Next, the effect of liquid addition shows that the addition of more granulation liquid results (expectedly) in larger granules [40, 41]. It was reported earlier [37], that a higher powder feed rate results in a larger d50. However, the effect of the powder feed rate on the granule size distribution seems to be more nuanced. A positive effect is observed on both fines (<250µm) and the 2000-3150 µm fraction.

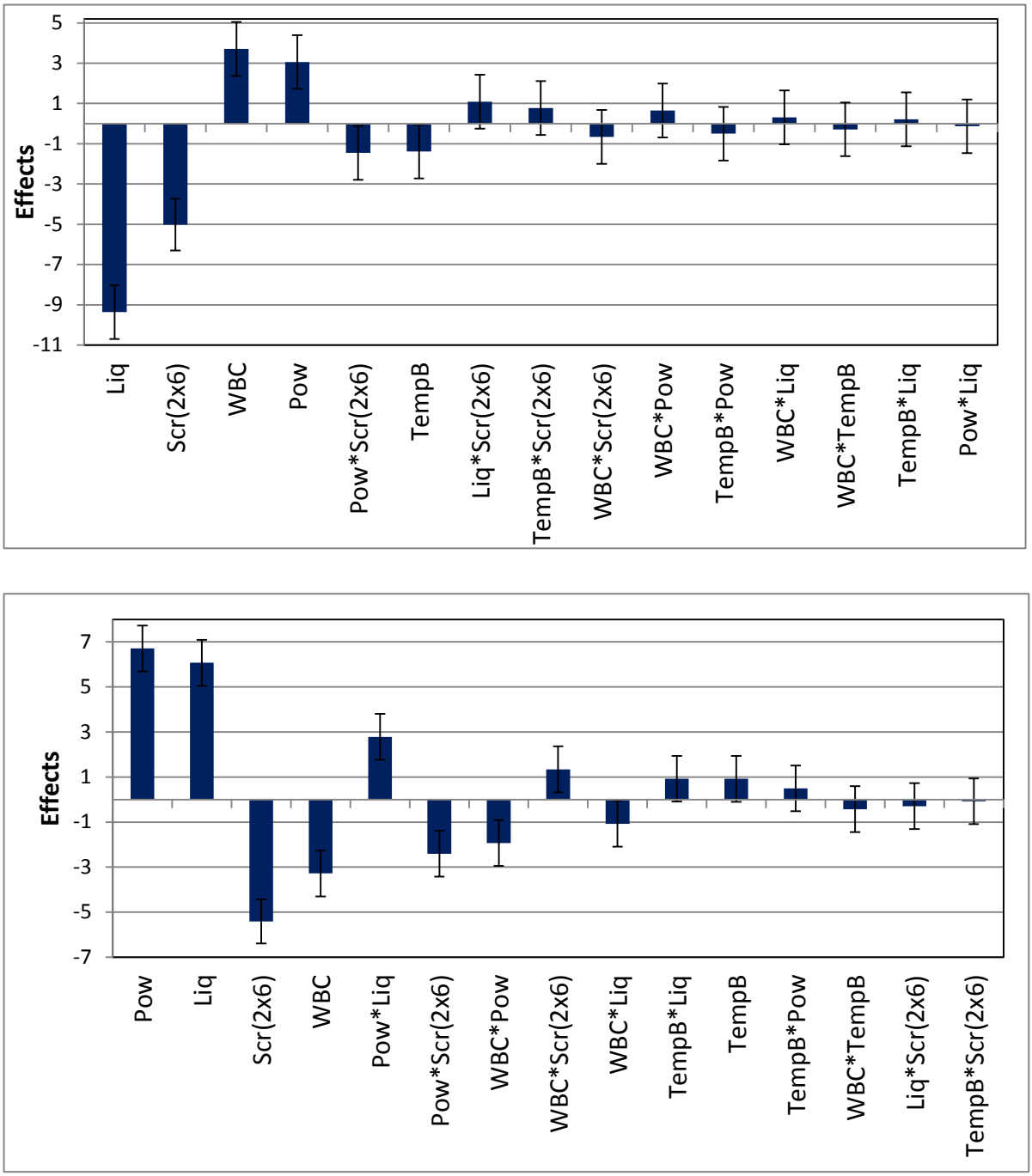

Figure 5.9. Effect plots of size fractions up. 0-150 µm down. 2000-3150 µm.

A high throughput results in a high barrel filling. Consequently, there will be a lower probability for powder to interact with granulation liquid, leading to more fines. On the other hand, the high barrel filling leads to more compaction of the powder in the kneading zones, hence causing more coarse granules. A screw configuration with two kneading zones of six elements results in a large fraction in the range 1000 to 2000 µm. When only two kneading elements are used, a high proportion of fines (<150 µm) is produced, since powder

and liquid are not well mixed. On the other hand, a large amount of granules larger than 2000 µm will be formed as well. This is because no second kneading zone can chop the large granules produced in the first kneading zone. Previous work [37, 42] reported that a higher temperature of the barrel resulted in larger granules. For the current studied formulation, only a significant positive effect of barrel temperature on the 1400-2000 µm fraction and a negative effect on the 0-150 µm fraction could be distinguished.

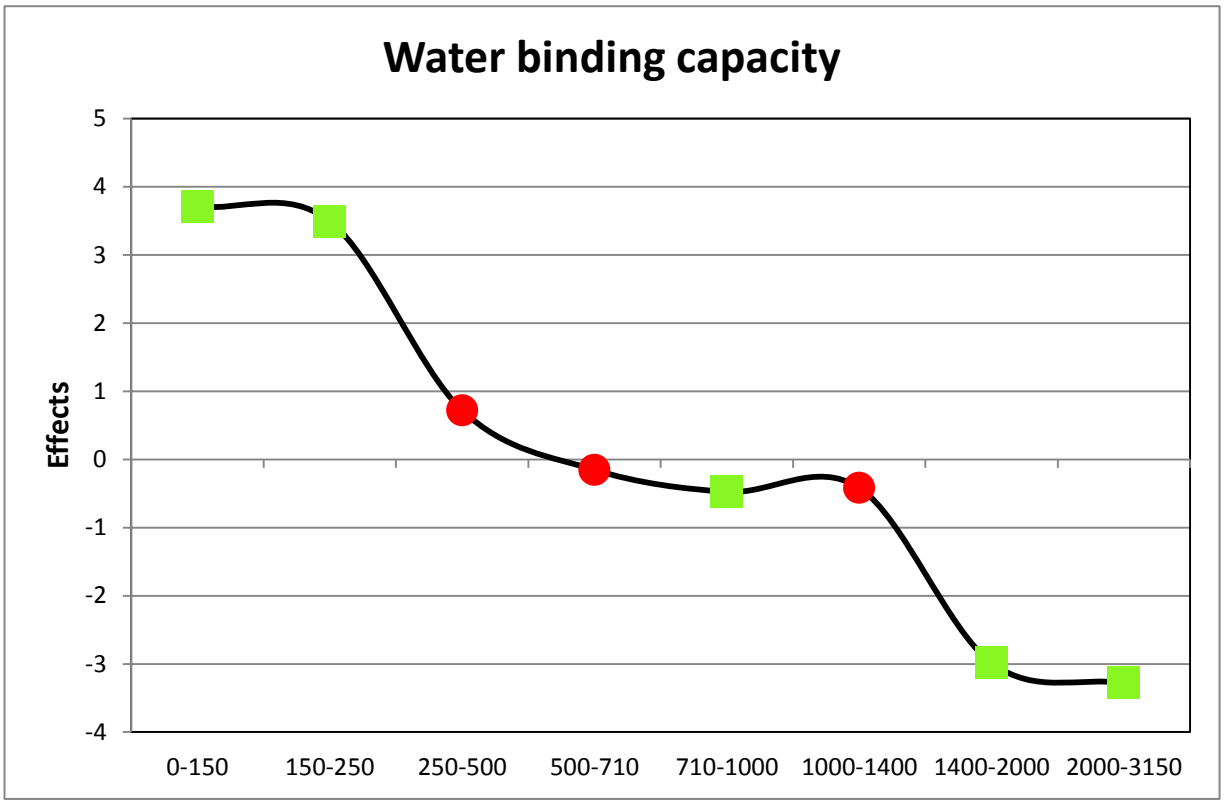

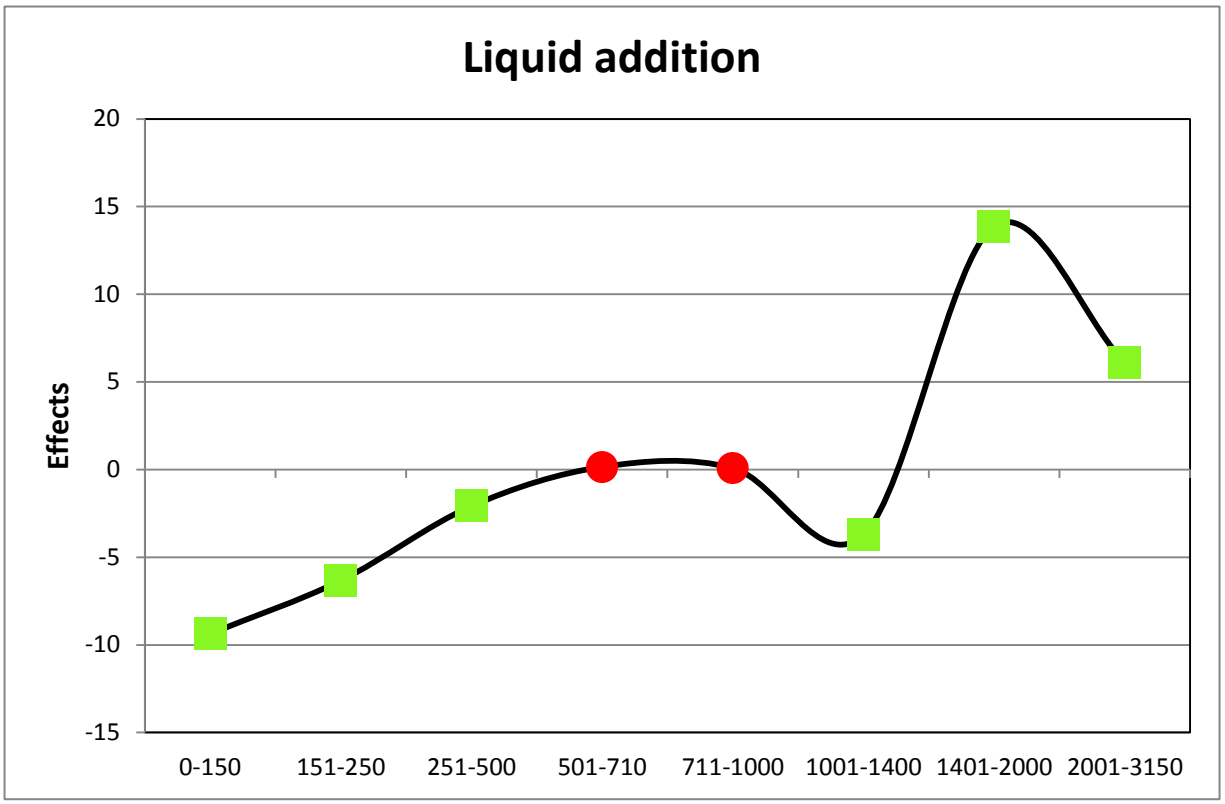
Liquid addition
Effects
20
15
10
5
0
-5
-10
-15
0-150
151-250
251-500
501-710
711-1000
1001-1400
1401-2000
2001-3150

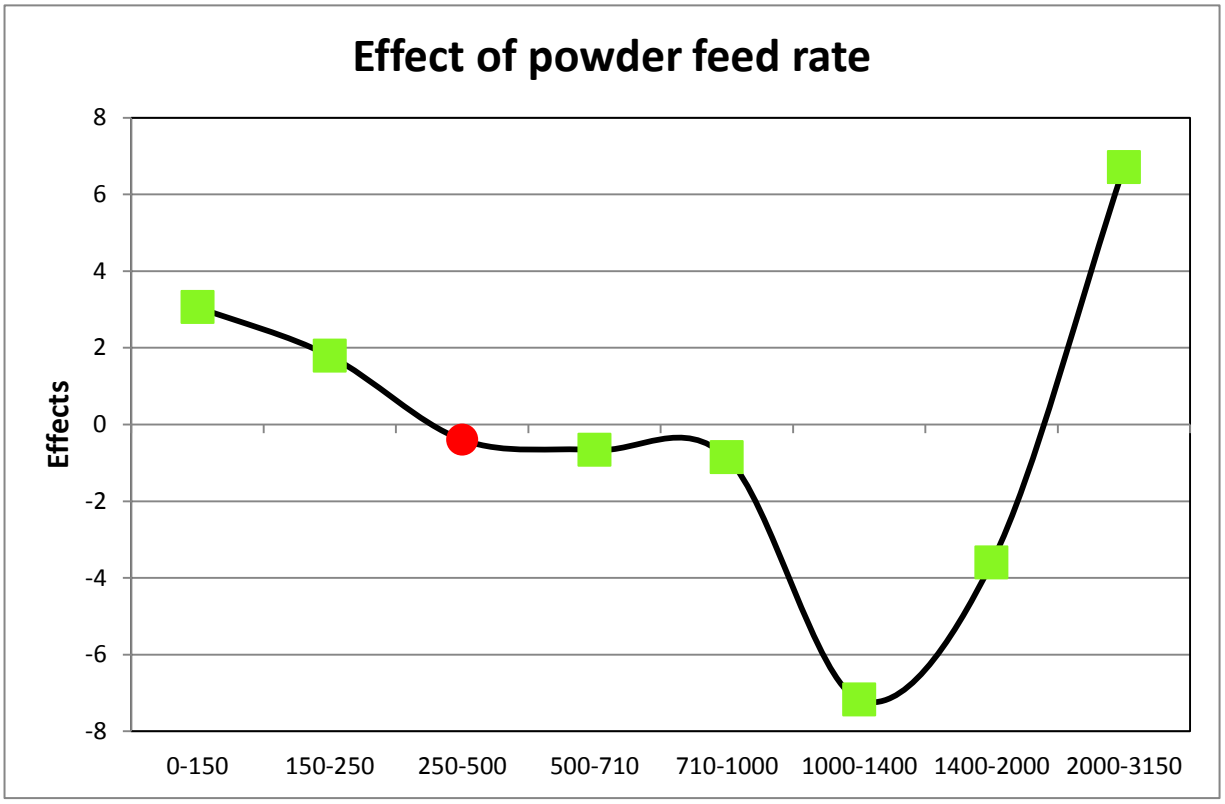
Effect of powder feed rate
Effects
8
6
4
2
0
-2
-4
-6
-8
0-150
150-250
250-500
500-710
710-1000
1000-1400
1400-2000
2000-3150

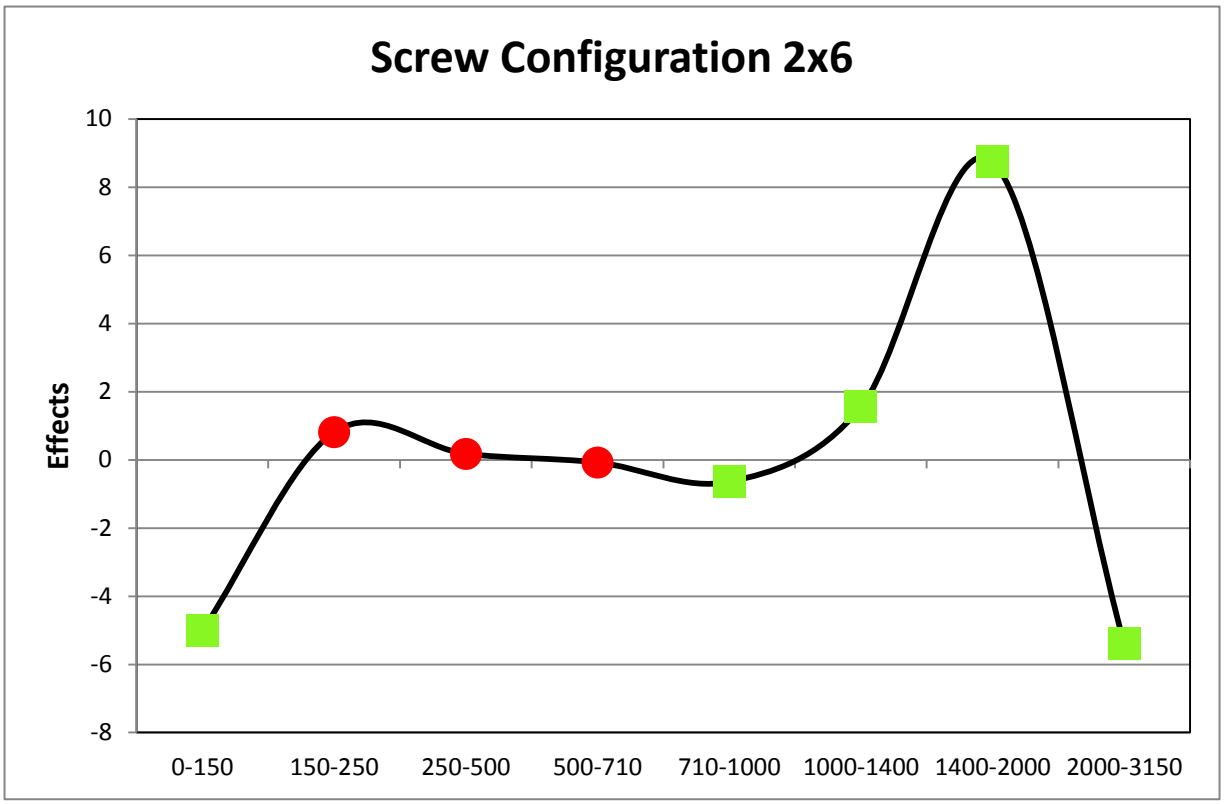

Figure 5.10. Overview of the effects of the different factors upon the granule size distribution (green squares indicate that the effect is significant, red dots indicate that the effect is not significant).

5.3.5. Feed forward steering: managing MCC variability

The data presented and discussed above clearly showed that the WBC has an influence on granule size distribution. Thus, it was investigated whether the process parameters can be adequately adapted to obtain a similar particle size distribution once the WBC of a given MCC sample is known. The DOE-PLS model from the previous section was used to calculate the required process parameter settings to obtain a certain granule size distribution. Therefore the *Optimizer*-function in Modde 9.1 was used, which uses a Nelder-Mead simplex method [43]. This is a heuristic method, which implies that the best possible solution may not always be reached.

For these calculations, the screw configuration was held constant, whereas the temperature of the granulator barrel, the liquid addition and the powder feed rate were flexible parameters. Samples X4, X5 and X6 were considered as 'new samples', hence their respective WBC was introduced into the model as a constant parameter. Two preferred granule size distributions were aimed (fictive example) (Table 5.6): one with a target for a 1400-2000 µm fraction of 20% (high target) and one with a target of 15% (low target).

Table 5.6. Preferred granule size distribution with high and low target (1400-2000 µm).

	High Target (1400-2000µm)			**Low Target (1400-2000 µm)**		
Response Criterion (µm)	Min	Target (%)	Max	Min	Target (%)	Max
0-150	5	10	15	6	11	16
150-250	5	10	15	6	11	16
250-500	10	15	20	11	16	21
500-710	5	10	15	6	11	16
710-1000	5	10	15	6	11	16
1000-1400	18	23	28	15	23	28
1400-2000	15	**20**	25	10	**15**	20
2000-3150	0	2	10	0	2	10
>3150		0	2		0	2

Realistic targets were chosen similar to the granule size distribution information obtained from the 35 experiments of the DoE. The Modde Optimizer allowed calculating the possible combinations of barrel temperature, liquid addition and powder feed rate, which should

lead to these targetted granule size distributions (high and low target). Once the screw configuration and WBC were defined, the set of proposed parameters with the lowest DPMO (Defects Per Million Opportunities) and the lowest Log(D) value was selected. The Log(D) is the normalized distance to target. A Log(D) value lower than 0 indicates that all results are within specification limits or very close, when the Log(D) is -10 all responses are on target. The DPMO expresses the sensitivity, and is a measure of defects outside specifications, based on Monte Carlo simulations. Hence, it gives additional information about how robust the proposed settings perform when disturbances in the factor settings occur. A run is then proposed by the Optimizer: both the predicted granule size distribution and the process parameters to obtain them, are calculated. The calculations performed for sample X6, with a WBC of 169.5 are presented as an example (Figure 5.11). The model-proposed process parameters leading to the aimed granule size distributions, the model-predicted granule size distribution for these optimal process parameters, the Log(D) values and DPMO can be found in Table 5.7. First of all, it can be noted that the predicted granule size fractions do not differ considerably between the high and the low targets. Furthermore, all Log(D) values are below 0 and the DPMO values are low (<5000). After predicting the optimal process conditions that should lead to the targetted granule size distributions, the predictions have been experimentally verified and the actual granule size distribution has been determined by means of sieve shaking. An overview of the observed versus predicted values for all runs can be found in Table 5.8. For all experiments (including experiments performed on X4 and X5), the obtained granules in the size fractions from 500-1400 equalled the predicted size fractions. The fraction between 2000-3150 was also well predicted. On the other hand, more fines than predicted seem to be produced. Only the experiments performed with sample X5 showed good predictions for the fine fraction, or had less fines produced than compared to what was predicted. In the case of X5, the size fraction from 250 to 500 µm was particularly not well predicted. The observed fraction from 1400 to 2000 µm was systematically lower for the predicted fraction. These data suggest that one can (partly) correct for differences in raw material samples by changing the process parameters.

Next page: **Figure 5.11**. Results for granule size distribution. Black dashed line: predicted size fraction, Red line: experimentally obtained size fractions, Blue dots: target values.

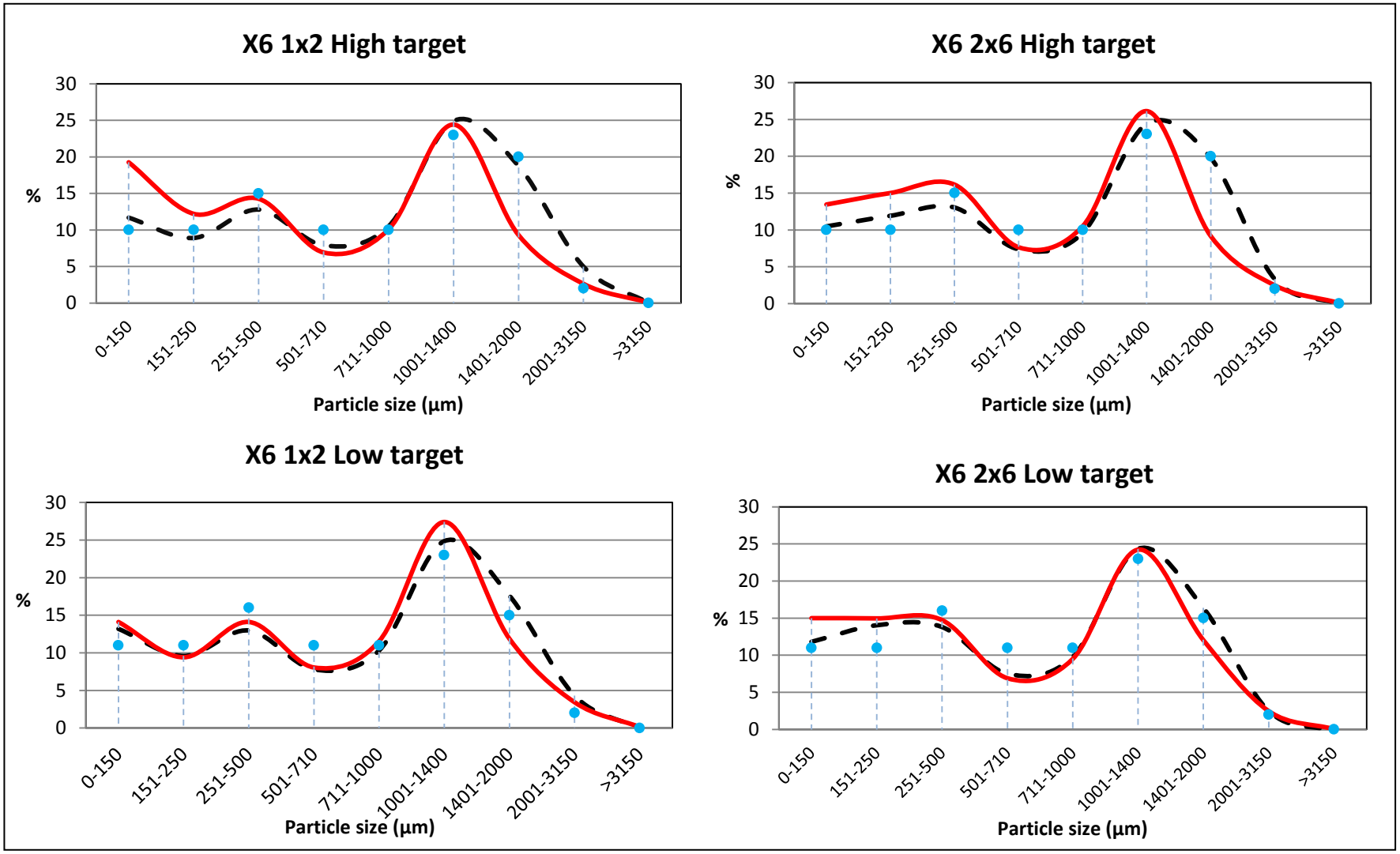
X6 1x2 High target
X6 2x6 High target
X6 1x2 Low target
X6 2x6 Low target
%
Particle size (µm)
0-150
151-250
251-500
501-710
711-1000
1001-1400
1401-2000
2001-3150
>3150
0
5
10
15
20
25
30

Table 5.7. Proposed parameters, predicted granule size distribution, Log (D) values and DPMO values for the calculation regarding X6.

	Screw conf	BarrelT	PFR	Liquid add	0-150	150-250	250-500	500-710	710-1000	1000-1400	1400-2000	2000-3150	>3150	Log(D)	DPMO
High target	1x2	40.00	10.00	40.20	11.69	8.91	12.79	7.90	10.50	24.93	18.77	4.98	0.04	-1.004	1100
	2x6	33.36	19.56	38.76	10.48	11.92	13.04	7.37	9.59	24.39	19.77	3.31	-0.04	-1.1092	0
Low target	1x2	40.00	10.00	38.40	13.19	9.58	12.97	7.79	10.31	24.86	17.61	4.31	-0.06	-0.7606	1050
	2x6	40.00	22.00	36.60	11.81	14.04	13.80	7.52	9.79	24.34	16.38	2.49	-0.18	-0.8452	5000

Table 5.8. Overview of the predicted amount of fines, yield and oversized agglomerates compared to the experimentally obtained amount. For X4, X5 and X6, results for both high and low target using two different screw configurations are presented.

			Fines <250 µm		Yield (250-1400µm)		Oversized >1400µm	
			pred	observed	pred	observed	pred	observed
X4	High	1x2	21.46	26.00	54.80	54.42	24.18	18.71
		2x6	22.54	26.30	52.18	55.03	24.96	18.23
	Low	1x2	24.23	26.18	54.52	58.14	21.75	15.88
		2x6	25.18	33.42	54.67	55.03	19.97	11.14
X5	High	1x2	19.81	17.40	62.20	63.14	24.52	19.46
		2x6	22.15	22.18	54.88	63.34	22.86	14.59
	Low	1x2	21.73	17.31	56.19	65.71	22.64	17.15
		2x6	25.49	25.12	55.44	62.63	19.08	11.95
X6	High	1x2	20.59	31.48	52.07	55.71	23.79	12.01
		2x6	22.40	28.46	54.39	60.42	23.04	11.73
	Low	1x2	22.77	23.51	55.93	61.10	21.85	15.43
		2x6	25.85	29.97	55.45	55.37	18.69	14.53

5.3.6. Evaluation of the effect of different binders

The results presented above describe observations for granules produced with lactose, maize starch and six different samples of MCC, so with filler excipients only. In this section, it was investigated if the difference in water binding capacity still has an effect on the granule size distribution if a binder was added to the formulation. Thus, a second experimental design was performed as presented in Table 5.3. Two quantitative factors were investigated. The water binding capacity was varied again between 157.5 (X1) and 181.5 (X2). Sample X3 was used for the centerpoint experiments. The temperature of the granulator barrel was varied between 25°C and 40°C. Four different binders (hydroxypropylcellulose (HPC), hydroxypropylmethylcellulose (HPMC) and polyvinylpyrollidone (Kollidon®30 and Kollidon®90)) were either added to the dry premix or dissolved in the granulation liquid.

Figure 5.12 represents the coefficient plots for the different binders. The binder type has the largest effect on all granule size distributions. All binder types had a significant influence on the granule size distribution, only HPMC had no significant influence in the range from 500 to 2000 µm. Next to the binder type, both the method of binder addition as well as interactions between binder type and method of binder addition had a significant influence on the granule size distribution. The addition of binder via the granulation liquid had a positive influence on the amount of granules >2000 µm. Furthermore, a significant positive effect of the water binding capacity on the amount of fines can be noted (Figure 5.13). A higher water binding capacity had a positive influence on the amount of granules with a size below 500 µm. Figure 5.13 also shows that the negative effect of the WBC on the granule size fraction between 2000-3150 µm is just not considered to be significant. From these results it can be concluded, that even when using a binder in the formulation, either added via the granulation liquid or via the pre-blend, a difference in water binding capacity between MCC made with different raw materials (wood pulps) still has an influence on the granule size distribution.

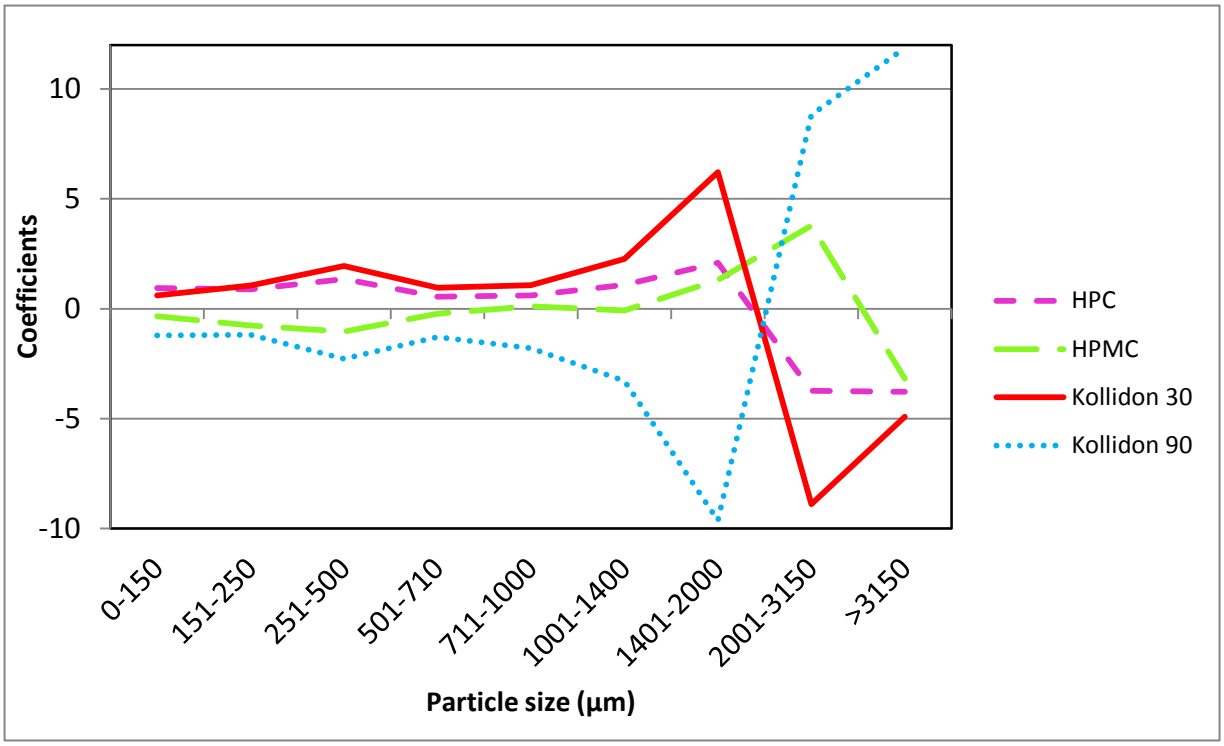

Figure 5.12. Coefficient plots of the four qualitative parameters (four binders, namely HPC, HPMC, Kollidon 30 and Kollidon 90).

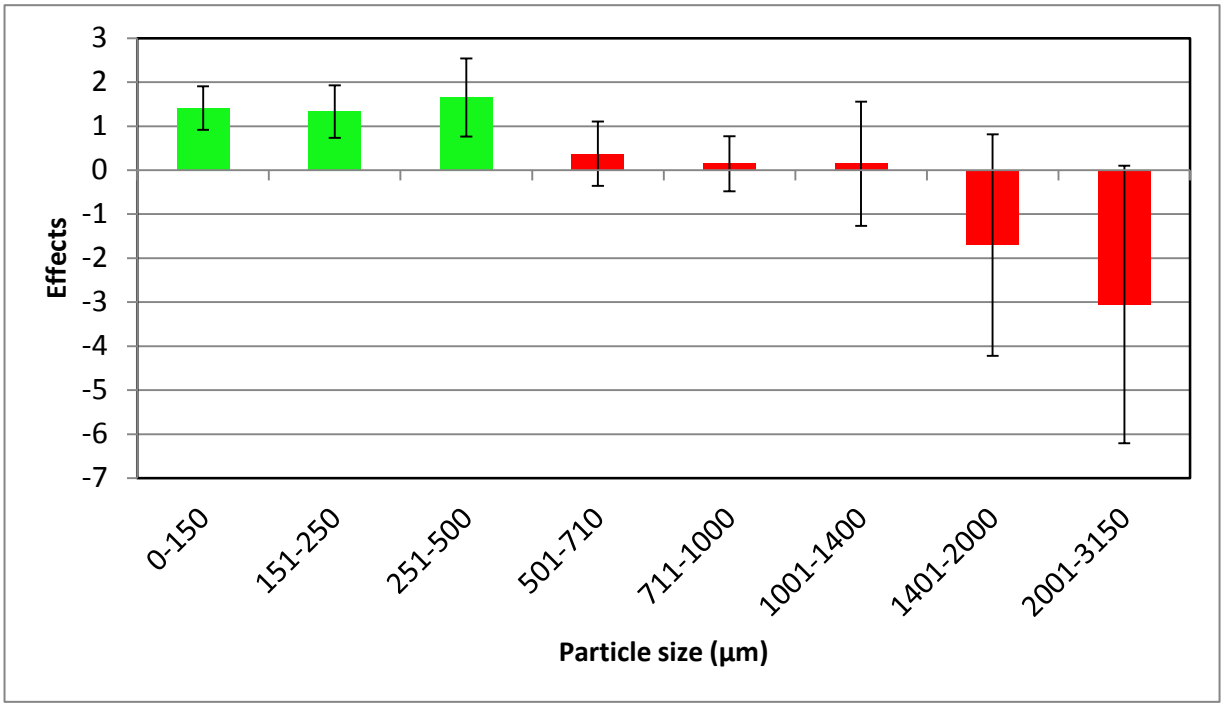

Figure 5.13. Effects of WBC in binderdesign.

5.4. CONCLUSION

This chapter described the variability of microcrystalline cellulose by means of a case study, being continuous wet granulation. The MCC samples differed in water binding capacity, which was related to the raw materials (wood pulps) used for their production. The reason for different water binding capacity between the samples was elucidated and is found to be a different degree of crystallinity of the MCC samples. Using experimental design, the needed adjustments of the granulation process parameters to obtain similar granule size distributions when using different MCC samples could be calculated. Furthermore, it was evaluated if the effect of the difference in water binding capacity could be annulled by adding a binder. However, the water binding capacity was still of influence, indicating that unspecified differences in MCC are important to be detected, evaluated and to be taken into account during processing.

5.5. REFERENCES

[1] International Conference on Harmonisation of Technical Requirements of Registration of Pharmaceuticals for Human Use. Quality Risk Management Q9, in, 2005.

[2] FDA-Adminstration, Guidance for Industry - PAT - A Framework for Innovative Pharmaceutical Development, Manufacturing, and Quality Assurance, in, 2004.

[3] M.G. Herting, P. Kleinebudde, Roll compaction/dry granulation: Effect of raw material particle size on granule and tablet properties, International Journal of Pharmaceutics, 338 (2007) 110-118.

[4] M. Dumarey, H. Wikstrom, M. Fransson, A. Sparen, P. Tajarobi, M. Josefson, J. Trygg, Combining experimental design and orthogonal projections to latent structures to study the influence of microcrystalline cellulose properties on roll compaction, International Journal of Pharmaceutics, 416 (2011) 110-119.

[5] J.L.P. Soh, F. Wang, N. Boersen, R. Pinal, G.E. Peck, M.T. Carvajal, J. Cheney, H. Valthorsson, J. Pazdan, Utility of multivariate analysis in modeling the effects of raw material properties and operating parameters on granule and ribbon properties prepared in roller compaction, Drug Dev. Ind. Pharm., 34 (2008) 1022-1035.

[6] S. Inghelbrecht, J.P. Remon, Roller compaction and tableting of microcrystalline cellulose drug mixtures, International Journal of Pharmaceutics, 161 (1998) 215-224.

[7] P.W.S. Heng, O.M.Y. Koo, A study of the effects of the physical characteristics of microcrystalline cellulose on performance in extrusion spheronization, Pharmaceutical Research, 18 (2001) 480-487.

[8] P. Kleinebudde, M. Jumaa, F. El Saleh, Influence of degree of polymerization on behavior of cellulose during homogenization and extrusion/spheronization, Aaps Pharmsci, 2 (2000) art. no.-21.

[9] O.M.Y. Koo, P.W.S. Heng, The influence of microcrystalline cellulose grade on shape and shape distributions of pellets produced by extrusion-spheronization, Chemical & Pharmaceutical Bulletin, 49 (2001) 1383-1387.

[10] L. Alvarez, A. Concheiro, J.L. Gomez-Amoza, C. Souto, R. Martinez-Pacheco, Effect of micro crystalline cellulose grade and process variables on pellets prepared by extrusion-spheronization, Drug Dev. Ind. Pharm., 28 (2002) 451-456.

[11] M.F.L. Law, P.B. Deasy, J.P. McLaughlins, S. Gabriel, Comparison of two commercial brands of microcrystalline cellulose for extrusion-spheronization, Journal of Microencapsulation, 14 (1997) 713-723.

[12] M.D. Parker, R.C. Rowe, SOURCE VARIATION IN THE WET MASSING (GRANULATION) OF SOME MICROCRYSTALLINE CELLULOSES, Powder Technology, 65 (1991) 273-281.

[13] M.D. Parker, P. York, R.C. Rowe, BINDER-SUBSTRATE INTERACTIONS IN WET GRANULATION .3. THE EFFECT OF EXCIPIENT SOURCE VARIATION, International Journal of Pharmaceutics, 80 (1992) 179-190.

[14] Y. Javadzadeh, H. Shariati, E. Movahhed-Danesh, A. Nokhodchi, Effect of Some Commercial Grades of Microcrystalline Cellulose on Flowability, Compressibility, and Dissolution Profile of Piroxicam Liquisolid Compacts, Drug Dev. Ind. Pharm., 35 (2009) 243-251.

[15] M. Whiteman, R.J. Yarwood, VARIATIONS IN THE PROPERTIES OF MICROCRYSTALLINE CELLULOSE FROM DIFFERENT SOURCES, Powder Technology, 54 (1988) 71-74.

[16] T. Pesonen, P. Paronen, EVALUATION OF A NEW CELLULOSE MATERIAL AS BINDING-AGENT FOR DIRECT COMPRESSION OF TABLETS, Drug Dev. Ind. Pharm., 12 (1986) 2091-2111.

[17] G. Shlieout, K. Arnold, G. Müller, Powder and Mechanical Properties of Microcrystalline Cellulose With Different Degrees of Polymerization, AAPS PharmsciTech, 3 (2002) article 11.

[18] R.V. Haware, A. Bauer-Brandl, I. Tho, Comparative evaluation of the powder and compression properties of various grades and brands of microcrystalline cellulose by multivariate methods, Pharmaceutical Development and Technology, 15 (2010) 394-404.

[19] A. Almaya, A. Aburub, Effect of particle size on compaction of materials with different deformation mechanisms with and without lubricants, Aaps Pharmscitech, 9 (2008) 414-418.

[20] K. Obae, H. Iijima, K. Imada, Morphological effect of microcrystalline cellulose particles on tablet tensile strength, International Journal of Pharmaceutics, 182 (1999) 155-164.

[21] M. Landin, M.J. Vazquez, C. Souto, A. Concheiro, J.L. Gomezamoza, R. Martinezpacheco, COMPARISON OF 2 VARIETIES OF MICROCRYSTALLINE CELLULOSE AS FILLER-BINDERS .1. PREDNISONE TABLETS, Drug Dev. Ind. Pharm., 18 (1992) 355-368.

[22] M. Landin, M.P. Gonzalez, C. Souto, A. Concheiro, J.L. Gomezamoza, R. Martinezpacheco, COMPARISON OF 2 VARIETIES OF MICROCRYSTALLINE CELLULOSE AS

FILLER-BINDERS .2. HYDROCHLOROTHIAZIDE TABLETS, Drug Dev. Ind. Pharm., 19 (1993) 1211-1220.

[23] M. Landin, R. Martinezpacheco, J.L. Gomezamoza, C. Souto, A. Concheiro, R.C. Rowe, INFLUENCE OF MICROCRYSTALLINE CELLULOSE SOURCE AND BATCH VARIATION ON THE TABLETING BEHAVIOR AND STABILITY OF PREDNISONE FORMULATIONS, International Journal of Pharmaceutics, 91 (1993) 143-149.

[24] R. Patel, F. Podczeck, Investigation of the effect of type and source of microcrystalline cellulose on capsule filling, International Journal of Pharmaceutics, 128 (1996) 123-127.

[25] L. Shi, S. Chattoraj, C.C. Sun, Reproducibility of flow properties of microcrystalline cellulose - Avicel PH102, Powder Technology, 212 (2011) 253-257.

[26] J.F. Gamble, W.-S. Chiu, M. Tobyn, Investigation into the impact of sub-populations of agglomerates on the particle size distribution and flow properties of conventional microcrystalline cellulose grades, Pharmaceutical Development and Technology, 16 (2011) 542-548.

[27] J.N. Staniforth, A.R. Baichwal, J.P. Hart, P.W.S. Heng, EFFECT OF ADDITION OF WATER ON THE RHEOLOGICAL AND MECHANICAL-PROPERTIES OF MICROCRYSTALLINE CELLULOSES, International Journal of Pharmaceutics, 41 (1988) 231-236.

[28] Z. Liao, N. Zhang, G. Zhao, J. Zhang, X. Liang, S. Zhong, G. Wang, X. Chen, Multivariate analysis approach for correlations between material properties and tablet tensile strength of microcrystalline cellulose, Pharmazie, 67 (2012) 774-780.

[29] E. DoElker, D. Mordier, H. Iten, P. Humbertdroz, COMPARATIVE TABLETING PROPERTIES OF 16 MICROCRYSTALLINE CELLULOSES, Drug Dev. Ind. Pharm., 13 (1987) 1847-1875.

[30] R.O. Williams, M. Sriwongjanya, M.K. Barron, Compaction properties of microcrystalline cellulose using tableting indices, Drug Dev. Ind. Pharm., 23 (1997) 695-704.

[31] J. Albers, K. Knop, P. Kleinebudde, Brand-to-brand and batch-to-batch uniformity of Microcrystalline Cellulose in Direct Tableting with a Pneumohydraulic Tablet Press, Pharm Ind, 68 (2006) 1420-1428.

[32] M. Landin, R. Martinezpacheco, J.L. Gomezamoza, C. Souto, A. Concheiro, R.C. Rowe, EFFECT OF COUNTRY-OF-ORIGIN ON THE PROPERTIES OF MICROCRYSTALLINE CELLULOSE, International Journal of Pharmaceutics, 91 (1993) 123-131.

[33] M. Landin, R. Martinezpacheco, J.L. Gomezamoza, C. Souto, A. Concheiro, R.C. Rowe, EFFECT OF BATCH VARIATION AND SOURCE OF PULP ON THE PROPERTIES OF MICROCRYSTALLINE CELLULOSE, International Journal of Pharmaceutics, 91 (1993) 133-141.

[34] R.C. Rowe, A.G. McKillop, D. Bray, THE EFFECT OF BATCH AND SOURCE VARIATION ON THE CRYSTALLINITY OF MICROCRYSTALLINE CELLULOSE, International Journal of Pharmaceutics, 101 (1994) 169-172.

[35] E.W. Washburn, Dynamics of capillary flow, Physical Review, 17 (1921) 374-375.

[36] M. Wada, T. Okano, J. Sugiyama, Synchrotron-radiated X-ray and neutron diffraction study of native cellulose, Cellulose, 4 (1997) 221-232.

[37] M. Fonteyne, J. Vercruysse, D.C. Díaz, D. Gildemyn, C. Vervaet, J.P. Remon, T.D. Beer, Real-time assessment of critical quality attributes of a continuous granulation process, Pharmaceutical Development and Technology, 18 (2013) 85-97.

[38] J. Vercruysse, U. Delaet, I. Van Assche, P. Cappuyns, F. Arata, G. Caporicci, T. De Beer, J.P. Remon, C. Vervaet, Stability and repeatability of a continuous twin screw granulation and drying system., European Journal of Pharmaceutics and Biopharmaceutics, 85 (2013) 1031-1038.

[39] M. Fonteyne, H. Wickström, E. Peeters, J. Vercruysse, H. Ehlers, B.-H. Peters, J.P. Remon, C. Vervaet, J. Ketolainen, N. Sandler, J. Rantanen, K. Naelapaa, T. De Beer, Influence of raw material properties upon critical quality attributes of continuously produced granules and tablets, European Journal of Pharmaceutics and Biopharmaceutics, *In press* (2014).

[40] R.M. Dhenge, J.J. Cartwright, M.J. Hounslow, A.D. Salman, Twin screw wet granulation: Effects of properties of granulation liquid, Powder Technology, 229 (2012) 126-136.

[41] A.S. El Hagrasy, J.R. Hennenkamp, M.D. Burke, J.J. Cartwright, J.D. Litster, Twin screw wet granulation: Influence of formulation parameters on granule properties and growth behavior, Powder Technology.

[42] J. Vercruysse, D. Córdoba Díaz, E. Peeters, M. Fonteyne, U. Delaet, I. Van Assche, T. De Beer, J.P. Remon, C. Vervaet, Continuous twin screw granulation: Influence of process variables on granule and tablet quality, European Journal of Pharmaceutics and Biopharmaceutics, 82 (2012) 205-211.

[43] L. Eriksson, E. Johansson, N. Kettaneh-Wold, C. Wikström, W. S, Design of Experiments - Principles and Applications, Umetrics, Umea, 2008.

PART II

CHAPTER 6

DISTRIBUTION OF BINDER IN GRANULES PRODUCED BY MEANS OF TWIN SCREW GRANULATION

Fonteyne M., Fussell A.L., Vercruysse J., Vervaet C., Remon J.P., Strachan C., Rades T., De Beer T. (2014). Distribution of binder in granules produced by means of twin screw granulation, International Journal of Pharmaceutics, 462, 8-10.

ABSTRACT

According to the Quality by Design principle, processes may not remain black-boxes and full process understanding is required. The size distribution of granules produced via twin screw granulation is often found to be bimodal. The aim of this study was to gain a better understanding of binder distribution within granules produced via twin screw granulation in order to investigate if an inhomogeneous spread of binder is causing this bimodal size distribution. Theophylline – lactose – polyvinylpyrrolidone K30 (PVP) (30-67.5-2.5% (w/w)) was used as a model formulation. The intra-granular distribution of PVP was evaluated by means of hyperspectral coherent anti-Stokes Raman scattering (CARS) microscopy. For the evaluated formulation, no PVP rich zones were detected when applying a lateral spatial resolution of 0.5 µm, indicating that PVP is homogenously distributed within the granules.

CHAPTER 6

DISTRIBUTION OF BINDER IN GRANULES PRODUCED BY MEANS OF TWIN SCREW GRANULATION

6.1. INTRODUCTION

Traditionally, the pharmaceutical industry has always relied on batch processing. With changing perspectives from the regulatory bodies (e.g., FDA, EMA) on pharmaceutical manufacturing, it is now possible for companies to switch their production from batch towards continuous production. For wet granulation, a frequently applied intermediate processing step during the production of pharmaceutical solid dosage forms, high shear twin screw granulation, has shown to be a most promising continuous alternative to conventional high shear and fluid bed granulation [1]. Nonetheless, twin screw wet granulation is also known for its typical bimodal granule size distribution [2, 3]. Granule loads mostly tend to contain either a large amount of fines (<250 µm) or a large amount of oversized granules (>1400 µm). Increasing the yield fraction without a milling step remains challenging. In 2010, Crean et al. [4] investigated the intra-granular microstructure of granules produced with lactose and 3% (w/w) of polyvinylpyrrolidone (PVP, both Povidone® K29/32 and K90 were used). X-ray micro-computed tomography, confocal Raman spectroscopy and infrared analysis were applied in order to investigate granules manufactured by means of aqueous high shear granulation (Kenwood CH180 mixer). They suggested the molecular association of PVP with lactose. PVP was found to be inhomogeneously spread within the granules and PVP rich zones with sizes up to 20 µm were reported.

Earlier findings [5] showed indeed a bi-modal size distribution when evaluating granules produced with the twin screw granulator module of the ConsiGma™ 25 (GEA Pharma systems nv, Collette, Wommelgem, Belgium), a fully continuous from powder-to-tablet manufacturing line. A recurring comment on twin screw granulation as an agglomeration

technique is the short residence time of the processed material in the granulator barrel, resulting in a short interaction and mixing time between powder, binder and granulation liquid. The **aim** of this study was to evaluate if the short residence and interaction time between powder and binder results in an inhomogeneous spread of binder, as seen by Crean et al. for batch wise high shear wet granulation. Consequently, the presence of binder rich zones could then be a reason for the bimodal size distribution of the granules. Therefore, the distribution of the binder within granules produced by means of twin screw granulation was investigated using an optical imaging technique.

6.2. MATERIALS AND METHODS

6.2.1. Materials

PVP Kollidon®30 (BASF, Ludwigshafen, Germany) was used as a binder at a concentration of 2.5% (w/w based on dry mass). Anhydrous theophylline (Farma-Quimica sur S.L., Malaga, Spain) was used as a model API in a concentration of 30%, with lactose monohydrate 200M (Caldic, Hemiksem, Belgium) as a filling excipient. PVP was either added to the dry premix or dissolved in the granulation liquid (distilled water) [6, 7]. All granules were produced using the ConsiGma™ 25 production line [8].

6.2.2. Coherent anti-Stokes Raman scattering microscopy

Hyperspectral coherent anti-Stokes Raman scattering (CARS) microscopy was selected for the visualization of PVP in the granules because of its high specificity and fast spectrally and spatially resolved imaging [9]. The CARS microscope used for this study, consisted of an Nd:YVO4 picosecond laser (Coherent, USA) operating at a fundamental wavelength of 1064 nm. This laser was frequency doubled to pump an optical parametric oscillator (OPO) (APE, Germany), which produced two dependently tunable laser beams. The fundamental laser beam was used as Stokes and combined with one of the beams from the OPO, after which they are directed into an inverted microscope (Olympus, FluoView 300, IX71, Japan). The backscattered CARS signal was detected with a photomultiplier tube (Hamamatsu, Japan). No spectral data processing was required to interpret the CARS-data.

6.3. RESULTS AND DISCUSSION

Preliminary tests were conducted in order to evaluate the feasibility of CARS microscopy for the visualization of PVP in granules. Initial hyperspectral images of the individual materials were collected to identify a spectral region to distinguish between the three compounds. The region between 2800 cm^{-1} and 3100 cm^{-1} was selected for further evaluation. A physical mixture (theophylline:lactose:PVP; 1:1:1) was compacted and hyperspectral CARS imaging was conducted collecting backwards scattering light using a 20X/0.55NA objective. Each frame of the hyperspectral image was collected with a 4 cm^{-1} interval for a total of 50 frames. Figure 6.1a shows a hyperspectral image of the surface of the compact, recorded between 2855 cm^{-1} and 2990 cm^{-1}. Three different chemical components can be distinguished, coloured yellow, pink and green. Each of these three components represented approximately a third of the image, as would be expected from the 1:1:1 mixture. Individual spectra were extracted for each coloured zone (Figure 6.1b). These spectra were compared with the spectra of the individual components and represented the theophylline, PVP and lactose zone respectively. It was shown that CARS microscopy can distinguish between PVP, theophylline and lactose when physically mixed and compacted.

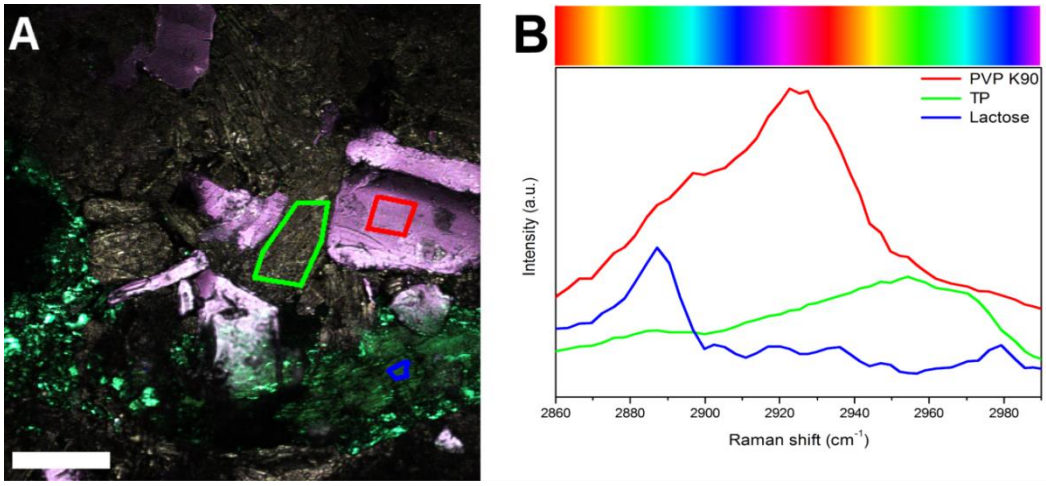

Figure 6.1. a. Hyperspectral image of the surface of a compact consisting of PVP (pink), theophylline (yellow) and lactose (green) (1:1:1), collected in the spectral region of 2885 cm^{-1} to 2990 cm^{-1}. **b.** The spectra extracted from the three marked zones, corresponded to PVP (red), theophylline anhydrate (green) and lactose monohydrate (blue), respectively. Scale bar is 100 µm.

A physical mixture (theophylline:lactose:PVP; 30:67.5:2.5) was compacted and hyperspectral CARS imaging was conducted collecting backwards scattering light using a 20X/0.55NA objective. Each frame of the hyperspectral image was collected with a 4 cm^{-1} interval and a total of 50 frames was collected. Figure 6.2a shows a hyperspectral image of the surface of the compact, recorded between 2855 cm^{-1} and 2990 cm^{-1}. Twenty images (160 µm x 160 µm) of the compact were collected in total. Three different chemical components can be distinguished, coloured blue, orange and yellow. Orange was the most abundant colour, followed by blue and yellow. Individual spectra were extracted for each coloured zone (Figure 6.2b). These spectra were compared with the spectra of the individual components and represented the theophylline (blue), lactose (orange) and PVP (yellow) zone respectively. It was shown that CARS microscopy can distinguish between PVP, theophylline and lactose when physically mixed and compacted. Hence, CARS is a suitable technique for the detection of the PVP binder in continuously produced theophylline-lactose granules.

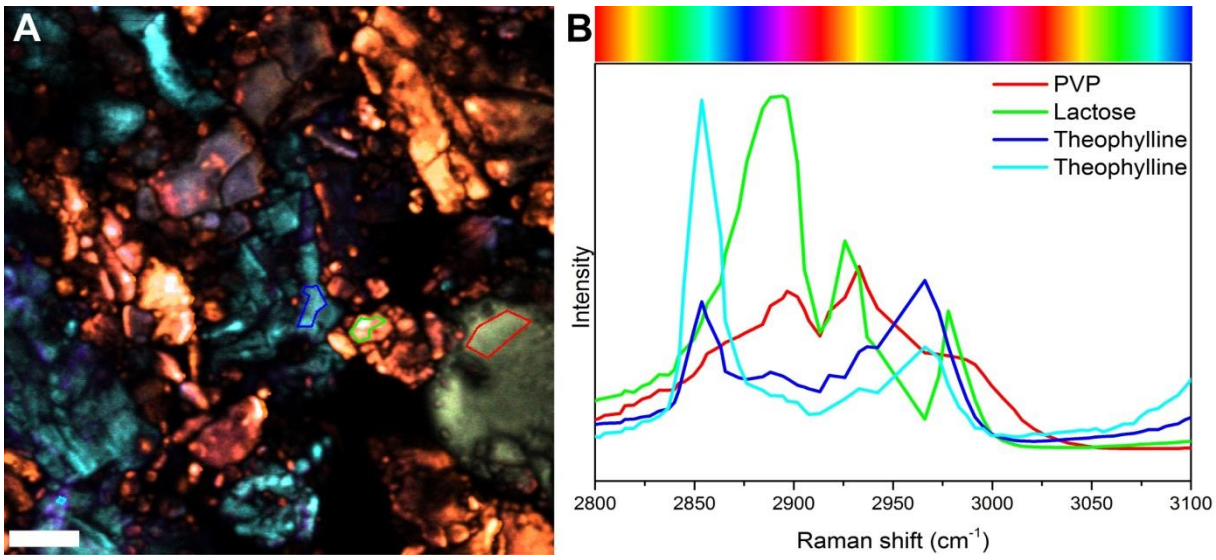

Figure 6.2. a. Hyperspectral image of the surface of a compact consisting of lactose (67.5%), theophylline (30%) and PVP (2.5%), collected in the spectral region of 2800 cm^{-1} to 3100 cm^{-1}. **b.** The spectra extracted from the three marked zones. Scale bar is 20 µm.

For the evaluation of the actual granules, a 60X/1.2NA objective was used, resulting in an axial spatial resolution of 1 µm and a lateral spatial resolution of 0.5 µm. The surface of the granules was evaluated and hyperspectral CARS images were collected from both the

theophylline-lactose-PVP granules and blanks, which only contained PVP and lactose (not shown). Figure 6.3a shows the hyperspectral image taken from the surface of a theophylline-containing granule prepared with PVP added in the dry premix. The same spectral region as for the preliminary experiments was used. Clearly, two components can be determined. The most abundant compound is coloured green, which is representing lactose, whereas purple represents theophylline. From these images collected with a lateral spatial resolution of 0.5 µm, no PVP rich zones could be distinguished, indicating a homogenous spread. Analysis of theophylline-containing granules prepared with PVP dissolved in the granulation liquid (not shown) also identified regions of theophylline and lactose, but no zones of PVP were present. Likewise, when evaluating the lactose-PVP granules (not shown), only lactose was identified.

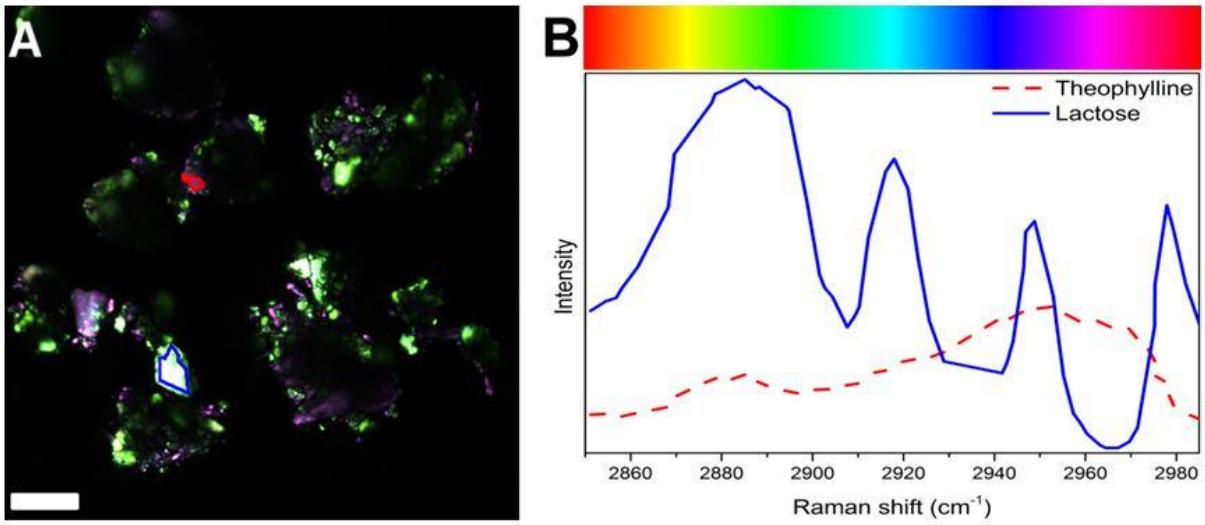

Figure 6.3. a. Hyperspectral image from the surface of a theophylline-lactose-PVP containing granule. PVP was added to the dry premix. **b.** Extracted CARS spectra and hyperspectral image colour map. Scale bar is 20 µm.

Next, the internal granular microstructure was investigated. Granules were sieved, after which granules larger than 1000 µm were sliced lengthwise using a razorblade. Again, hyperspectral scans were collected in the 2800 cm^{-1} to 3100 cm^{-1} spectral region. For each mapping measurement, three different color maps were projected and the map with the highest discriminatory power was chosen for further evaluation. Figure 6.4 shows three examples of the mappings performed on theophylline-containing granules. Again, only two

components could be distinguished. The color covering the largest area of the image represented lactose monohydrate, with theophylline covering the rest of the image. Theophylline and lactose are well mixed and homogenously spread within the granule. Again, no PVP-rich zones were encountered when evaluating the cross-sectional surface of the granules. The hyperspectral images of the blanks resulted in monochrome images in which only lactose could be detected. To sum up: for all the before mentioned experiments, in total 68 images were collected, covering a total area of 13 mm² and no PVP-rich zones could be detected in any of those.

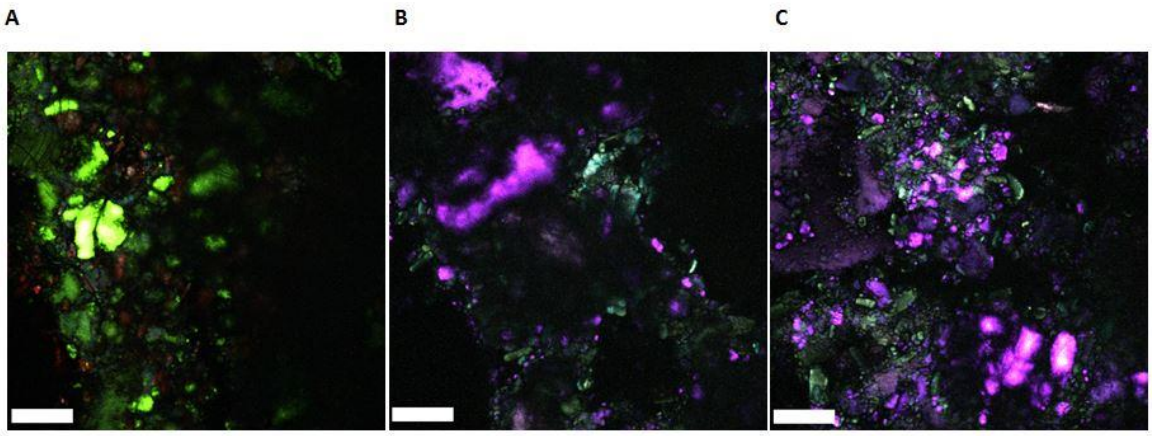

Figure 6.4. Three typical examples of hyperspectral images of cross-cuts of theophylline-lactose-PVP granules. The color map with the highest discriminatory power was selected, resulting in a. theophylline in red and lactose in green, b. theophylline in blue and lactose in pink, and c. theophylline in green and lactose in pink. The scale bars are 20 µm.

6.4. CONCLUSION

In contrast to what has been reported regarding lumps of polyvinylpyrrolidone in granules produced by means of batch high shear aqueous granulation, no PVP-rich zones could be detected in granules manufactured with a twin screw granulator when applying a lateral spatial resolution of 0.5 µm. This study suggests that PVP is well mixed and equally spread within the granules, both when PVP is added in the dry premix or when it is added via the granulation liquid. Even though the residence time in the barrel is very short, PVP is well distributed within the granules. Hence, an inhomogeneous spread of PVP is not the cause of the typical bimodal granule size distribution obtained by continuous wet twin screw granulation.

6.5. REFERENCES

[1] C. Vervaet, J.P. Remon, Continuous granulation in the pharmaceutical industry, Chemical Engineering Science, 60 (2005) 3949-3957.

[2] A.S. El Hagrasy, J.R. Hennenkamp, M.D. Burke, J.J. Cartwright, J.D. Litster, Twin screw wet granulation: Influence of formulation parameters on granule properties and growth behavior, Powder Technology.

[3] R.M. Dhenge, R.S. Fyles, J.J. Cartwright, D.G. Doughty, M.J. Hounslow, A.D. Salman, Twin screw wet granulation: Granule properties, Chemical Engineering Journal, 164 (2010) 322-329.

[4] B. Crean, A. Parker, D. Le Roux, M. Perkins, S.Y. Luk, S.R. Banks, C.D. Melia, C.J. Roberts, Elucidation of the internal physical and chemical microstructure of pharmaceutical granules using X-ray micro-computed tomography, Raman microscopy and infrared spectroscopy, European Journal of Pharmaceutics and Biopharmaceutics, 76 (2010) 498-506.

[5] M. Fonteyne, H. Wickström, E. Peeters, J. Vercruysse, J.P. Remon, C. Vervaet, N. Sandler, J. Rantanen, K. Naelapää, T.D. Beer, Influence of raw material properties upon critical quality attributes of continuously produced granules, in: 6th International Granulation Workshop, Sheffield, UK, 2013.

[6] J. Vercruysse, D. Córdoba Díaz, E. Peeters, M. Fonteyne, U. Delaet, I. Van Assche, T. De Beer, J.P. Remon, C. Vervaet, Continuous twin screw granulation: Influence of process variables on granule and tablet quality, European Journal of Pharmaceutics and Biopharmaceutics, 82 (2012) 205-211.

[7] M. Fonteyne, S. Soares, J. Vercruysse, E. Peeters, A. Burggraeve, C. Vervaet, J.P. Remon, N. Sandler, T. De Beer, Prediction of quality attributes of continuously produced granules using complementary pat tools, European Journal of Pharmaceutics and Biopharmaceutics, 82 (2012) 429-436.

[8] M. Fonteyne, J. Vercruysse, D.C. Díaz, D. Gildemyn, C. Vervaet, J.P. Remon, T.D. Beer, Real-time assessment of critical quality attributes of a continuous granulation process, Pharmaceutical Development and Technology, 18 (2013) 85-97.

[9] E.T. Garbacik, J.L. Herek, C. Otto, H.L. Offerhaus, Rapid identification of heterogeneous mixture components with hyperspectral coherent anti-Stokes Raman scattering imaging, Journal of Raman Spectroscopy, 43 (2012) 651-655.

CHAPTER 7

REAL-TIME ASSESSMENT OF CRITICAL QUALITY ATTRIBUTES OF A CONTINUOUS GRANULATION PROCESS

"Patience is the companion of wisdom."

Aurelius Augustinus (354-430)

Fonteyne M., Vercruysse J., Córdoba Díaz D., Gildemyn D., Vervaet C., Remon J.P., De Beer T. (2013) Real-time assessment of critical quality attributes of a continuous granulation process, Pharmaceutical Development and Technology, 18, 85-97.

ABSTRACT

There exists the intention to shift pharmaceutical manufacturing of solid dosage forms from traditional batch production towards continuous production. The currently applied conventional quality control systems, based on sampling and time-consuming off-line analyses in analytical laboratories, would annul the advantages of continuous processing. It is clear that real-time quality assessment and control is indispensable for continuous production. This manuscript evaluates strengths and weaknesses of several complementary Process Analytical Technology (PAT) tools implemented in a continuous wet granulation process, which is part of a fully continuous from powder-to-tablet production line. The use of Raman and NIR spectroscopy and a particle size distribution analyzer is evaluated for the real-time monitoring of critical parameters during the continuous wet agglomeration of an anhydrous theophylline – lactose blend. The solid state characteristics and particle size of the granules were analyzed in real-time and the critical process parameters influencing these granule characteristics were identified. The temperature of the granulator barrel, the amount of granulation liquid added and, to a lesser extent, the powder feed rate were the parameters influencing the solid state of the active pharmaceutical ingredient (API). A higher barrel temperature and a higher powder feed rate, resulted in larger granules.

CHAPTER 7

REAL-TIME ASSESSMENT OF CRITICAL QUALITY ATTRIBUTES OF A CONTINUOUS GRANULATION PROCESS

7.1. INTRODUCTION

Continuous processing is well established in the chemical, cosmetics and food industry, whilst it is still in its infancy in the pharmaceutical industry. Pharmaceutical companies stick to batch processing, because the machinery required for batch processing is already installed in their production plants. A switch to continuous production would require investments in new equipment, training of the employees, new process validation and co-current regulatory documentation. However, batch processing is a very time-consuming and expensive way of production, which can be overcome by continuous production. For example, the development process of solid dosage forms is generally accomplished by the optimization of its production at several batch scales: first, the product is formulated at lab-scale, after which pilot and clinical batches are produced, followed by production scale manufacturing. This up-scaling process is not only costly and time-consuming; it also prolongs the time-to-market. Process optimization and validation have to be performed at each batch scale since optimal process and formulation settings at small scale process are generally not transferrable to larger scales [1]. Up-scaling does also involve regulatory issues, because larger batches may require new bioequivalence tests, next to dissolution and stability-tests [2]. Alternatively, continuous production processing allows flexible batch sizes as larger amounts of drug products can be produced by simply running the process longer using the same process equipment. (i.e. “up-scaling in the fourth dimension” [3]). Hence, continuous manufacturing can lead to just-in-time production, where products do not longer have to wait in warehouses. Furthermore, continuous manufacturing lines aim to

be fully automated with a minimum of operators, as material transport to the next production step is integrated in the production line. Since pharmaceutical manufacturers are under increasing pressure to reduce expenses and augment efficiency, continuous manufacturing will also have an economical impact.

One of the major reasons for the pharmaceutical industry to be reluctant to move from batch production to continuous production, is the uncertainty of approval by the regulatory bodies. Indeed, the drug quality and safety have to be assessed and assured at any time. Batch production works with the principle of profound product quality control, by means of sampling and testing after each step in the production process. It is obvious that the current conventional quality control systems of production processes, based on off-line analyses in analytical laboratories, would annul the advantages of continuous processing. Real-time quality evaluation and control, using in-line process analyzers, is crucial for the successful implementation of continuous manufacturing of pharmaceutical products.

Based on the PAT guidance for Industry [4], the Process Validation Guidance for Industry [5] and the ICH guidelines Q8, Q9 and Q10 [6-8], a new approach for pharmaceutical development and production has been proposed. In the PAT-guidance, the FDA encourages the industry to improve pharmaceutical development, manufacturing and quality assurance through innovation in product and process development, process analysis and process control by using the latest scientific advances. The aim is to ensure product quality through the design of effective manufacturing processes, where formulation and process factors and their influence on the end-product are fully understood. This profound understanding and control of manufacturing processes must lead to quality built into the product (Quality by Design). The desire within the pharmaceutical industry to shift towards continuous processing strengthens the need to invest in PAT. The recently introduced Guidance for Process Validation [5] focuses on assuring drug quality by effective process validation. A manufacturing process must be capable of consistently delivering a high quality product. The scientific evidence of that should be based on the collection and evaluation of data, from the process design stage through the commercial production. In the ICH Q8 guideline “Pharmaceutical Development” [6], the principles for building quality into products are stated. Real-time release of pharmaceutical products will be possible if quality of the whole

process can be assured by real-time quality control. Q9 “Quality Risk Management” [7] explains the general quality risk assessment and management process and gives examples of possible risk management methods and tools. Naelepää et al. [9] recently showed the application of risk management tools to reveal the critical parameters of a coating process. Q10, “Pharmaceutical Quality System” [8], describes a model for an efficient quality management system for the pharmaceutical industry, based on International Standards Organization (ISO) quality concepts. The present study aimed at applying elements of these five guidelines on a continuous pharmaceutical granulation process.

Gamlen and Eardley [10] were the first in 1986 to describe the advantages of continuous processing compared to batch processing. They used a continuous extruder, equipped with two helical mixing blades, for the production of paracetamol extrudates. Lindberg et al. [11] used a twin screw extruder to granulate. Both powder flow rate and liquid flow rate were regularly tested, but not persistently controlled and monitored. The group of H. Leuenberger (University of Basel) developed a semi-continuous agglomeration process, consisting of a high shear granulation mixer and a fluid bed dryer. This system produced mini-batches in a quasi-continuous way [1, 3, 12, 13]. The terminology ‘quasi-continuous manufacturing’ is used here, since the process principle is based on the granulation of small portions of powder in a high shear mixer. After the first portion is granulated, it is discharged to the fluid bed dryer and a second portion is filled into the mixer. This process can hence be considered as a fast succession of mini-batches, but not as a continuous stream of granules.

As wet granulation is a commonly used unit operation within the pharmaceutical industry to improve compactibility and/or flowability of powder mixtures prior to tableting, several continuous wet granulation techniques were developed which have been reviewed by Vervaet and Remon [14, 15] Their co-workers [16-19] developed a continuous twin-screw granulator, which is now implemented in the commercially available ConsiGma™-system (GEA Pharma Systems nv., Collette™, Wommelgem, Belgium). Systems producing 25, 50 and 100 kg of granules per hour are commercially available.

This study focused on a high shear twin screw granulator, being the granulation unit of the ConsiGma™ 25 continuous production line. Several equipment, formulation and process factors can affect the quality of granules manufactured via this technique. These will affect further downstream processing, such as the fluid bed drying and tableting process step. The continuous granulator parameters were scheduled (Table 7.1) after Aulton and Banks [20], who listed parameters of a fluid bed granulation process in three categories: equipment variables, process variables and product variables. Kristensen and Schaefer used the same categories with emphasis on both fluid bed and high shear mixing-granulation [21]. The important characteristics of agglomerates manufactured via wet granulation are overviewed in Table 7.2.

An evaluation of the equipment, process and formulation parameters having a significant influence upon the critical granule properties is needed in order to find the optimal process conditions. Traditionally, such evaluations are done by trial-and-error, i.e. changing one separate variable at a time (COST-approach). Since this is a time- and product-consuming approach, which does not guarantee finding the optimum conditions [22], the PAT and ICH guidelines recommend the application of organized methods (e.g. design of experiments, DoE) to define the relationship between parameters and quality of the end-product.

A model formulation containing theophylline anhydrate and lactose monohydrate was used to monitor the wet granulation process. Four different polymorphs of theophylline are known: theophylline monohydrate (TH), a metastable form of theophylline and two types of anhydrous forms, one stable at room temperature (TA) and one only occurring at very high temperatures [23]. Pharmaceutical processes can induce (undesired) solid state transformations. Knowledge of the solid state of the API during processing and storage is of the highest importance to assure a safe drug product. Changes in solid state can influence the chemical and physical properties of API's, resulting in different processability (compressibility and powder flow), but also solubility, stability and bioavailability [24]. Norvir, an anti-HIV medicine, was already on the market when in 1998 a polymorphic transformation to a less soluble form of ritonavir was detected [25]. This product had to be reconstituted by the patient, but the dissolution of the capsules failed. Airaksinen et al. [26]

and Wikström et al. [27] studied the conversion of anhydrous theophylline into theophylline monohydrate using a planetary mixer and a high-shear mixer granulator, respectively.

The **aim** of this study was to evaluate which granule properties can be monitored in-line using several PAT tools (Raman and NIR spectroscopy and a particle size analyzer) during a continuous wet granulation process in the granulation module of the ConsiGma™ 25 unit. Furthermore, a DoE was applied to examine the influence of several process and formulation settings upon the granule quality attributes, which were measurable using the implemented PAT tools.

Table 7.2. Granulation responses – Granule characteristics.

Characterization of granules:
- **Particle size distribution**
- **Density (loose and tapped)**
- **Compressibility (Carr's Index)**
- **Flowability**
- **Friability**
- **Residual moisture content**
- **Assay / content uniformity per particle fraction**
- **Particle morphology**
- **Porosity**
- **Solid state**
- **Surface area**

Table 7.1. Equipment, product and process variables influencing the characteristics of a continuous twin screw granulation process.

Equipment variables	Product variables		Process variables
	Starting Powder Properties	Liquid Characteristics	
Screw configuration	Particle size distribution	Viscosity	Powder feed rate
Screw length	Homogeneity of raw material powders	Surface tension	Bridge breaker speed
Length- to-diameter ratio of the screws	Presence of agglomerates in premix	Solid-liquid tension	Filling degree of barrel
Diameter of the granulation liquid inlet nozzels	Segregation during feeding		Screw speed
	Powder density		Barrel temperature
Powder feeding method	Cohesion	Binder type	Liquid feed rate
Place of liquid addition into barrel	Particle shape	Binder concentration	
	Surface roughness	Binder addition method (wet/dry)	
	Surface area		
	Solubility in granulation liquid		
	Hygroscopicity		
	Wettability		
	API/excipient quantitative ratio		
	Concentration		

7.2. MATERIALS AND METHODS

7.2.1. Materials

Anhydrous theophylline (Fagron Iberica, Barcelona, Spain) (30%, w/w) was granulated with lactose monohydrate 200 M (Caldic Belgium NV, Hemiksem, Belgium). Polyvinylpyrrolidone (Kollidon®30, BASF, Burgbernheim, Germany) was added as binder to the dry powder mixture in a concentration of 2.5% (w/w). Distilled water was used as granulation liquid. Sodiumlaurylsulfate (Fagron, Waregem, Belgium) was added to the granulation liquid (0.5% w/v) to improve the wettability of the dry powder mixture.

7.2.2. Wet twin screw granulation

All granules were produced using the ConsiGma™ 25 unit (GEA Pharma Systems nv., Collette™, Wommelgem, Belgium). This study focuses on the continuous twin screw granulator. The screw configuration was kept constant for all experiments (Figure 7.1). The influence of the granulator configuration upon the granule properties is evaluated in other studies. The screws consisted of a long transport zone and two kneading zones of six kneading elements in an angle of 60°. These two kneading zones were separated from each other by a short transport element, with the same length as a kneading zone. Wet granules were unloaded, from the barrel via another identical short transport element.

Figure 7.1. Screw configuration of the twin screws.

Several process parameters can be set for continuous wet granulation (Table 7.1, 4th column). In this study, bridge breaker speed was held constant at 80%. One of the assets that ConsiGma™ offers is the automatic logging, trending and storage of several process parameters (e.g., temperature granulator barrel, weight powder dosing unit, mass flow granulation liquid etc.).

7.2.3. Twin screw granulation process monitoring

An in-house made cuvet was placed under the granulator outlet to collect the granules (Figure 7.2). The cuvet was a box of 10 cm x 10 cm, with a height of 15 cm. One side contained several interfacing places where the NIR diffuse reflectance contact probe could be introduced, while the opposite side of the cuvet contained two interfacing places for the MR Raman probe head. At the inner wall of the cuvet, the Raman probe interfacing holes were covered by quartz-glass, hence allowing non-contact measurements.

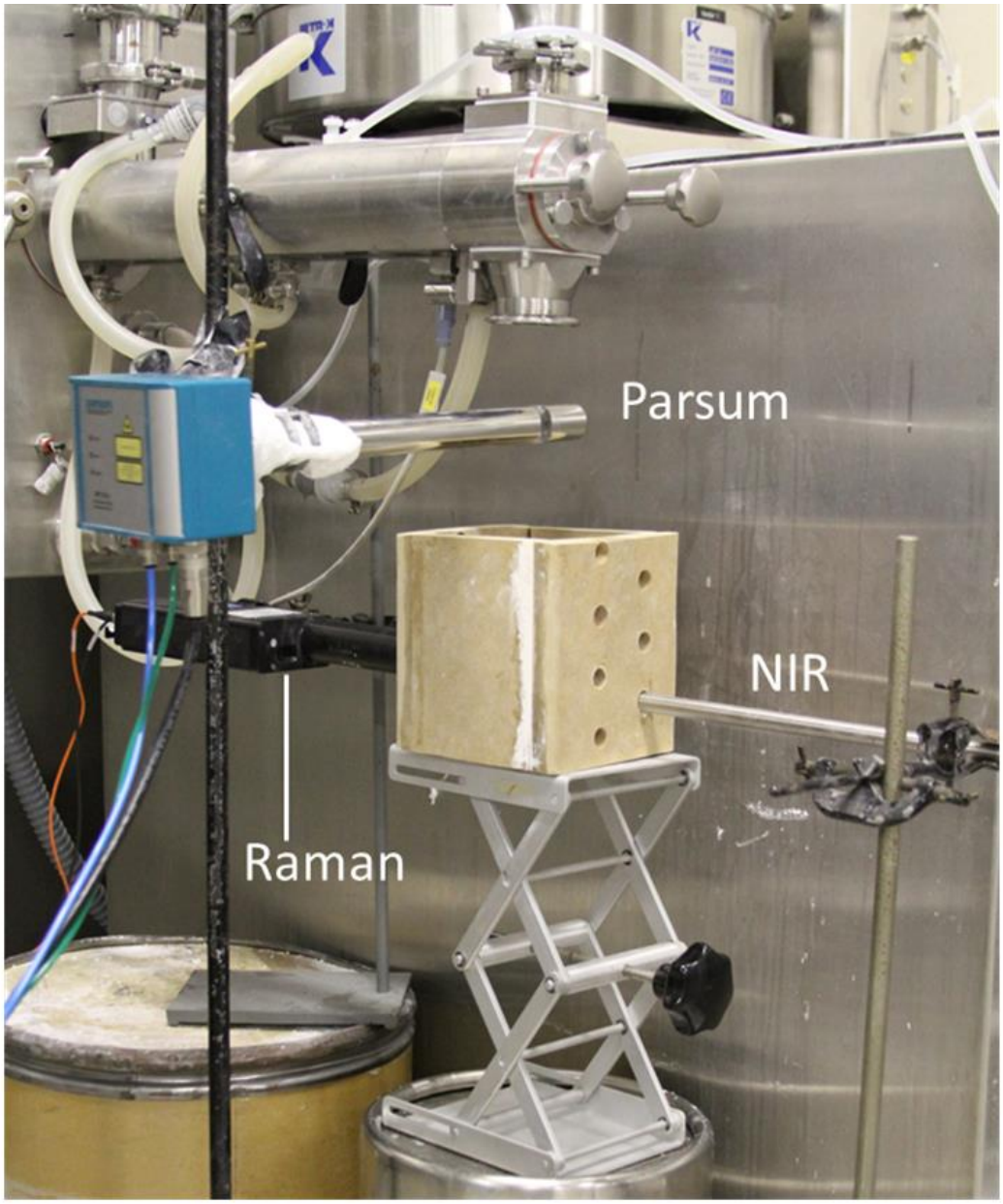

Figure 7.2. In-line twin screw granulation monitoring.

This measurement setup ensured reproducible probe interfacing and sampling of non-moving granules, hence eliminating variation in the spectra due to variable probe positions. At present, a measurement device which can be implemented in the transport lines between the different units of the ConsiGma™ is already developed. Since the equipment produces mainly fines in the start-up phase, the granules produced during the first minute of each granulation experiment were considered as waste and removed. After this first minute, granules were collected in the cuvet for three minutes.

7.2.4. Raman - Spectroscopy

A RamanRxn1 spectrometer (Kaiser Optical Systems, Ann Arbor, Michigan), equipped with an air-cooled CCD detector (back-illuminated deep depletion design) was used. A fiber-optic non-contact probe was placed against the quartz glass at the inner wall of the cuvet in which the granules were collected. Spectra were taken via the different interfacing places of the cuvet. The laser wavelength was the 785 nm line from a 785 nm Invictus NIR diode laser. All spectra were recorded with a resolution of 4 cm^{-1} and an exposure time of 30 seconds, using a laser power of 400 mW. Data collection and data transfer were automated using the HoloGRAMS™ data collection software, the HoloREACT™ reaction analysis and profiling software and the Matlab software (version 7.1, The MathWorks Inc., Natick, Massachusetts).

7.2.5. NIR Spectroscopy

A Fourier-Transform NIR spectrometer (Thermo Fisher Scientific, Zellik, Belgium, Nicolet Antaris II near-IR analyzer) equipped with an InGaAs detector, a quartz halogen lamp and a fiber optic contact probe was used. Spectra of each granulation experiment were taken, through each of the four interfacing places in the cuvet. The probe was mounted into the cuvet in exactly the same way for every measurement. Hence, measurements could be done in a reproducible way. Each spectrum was collected in the 4500 - 10000 cm^{-1} region with a resolution of 16 cm^{-1} and averaged over 16 scans. Data collection and data transfer were done using Thermo Fisher Scientific's Result Software.

7.2.6. In-line Particle Size Analysis

An In-line Spatial Filter Velocimetry probe (Parsum®, Chemnitz, Germany) was used to continuously monitor the particle size of the granules in-process. The probe consisted of a semiconductor laser diode, which radiated visible light at a wavelength of 670 nm. Furthermore the measurement probe was provided with an integrated air-cleaning system to keep the optical surfaces clean. The applicability and technical details of SFV are extensively described in literature [28]. The probe was placed 10 cm under the granulator outlet and in-line measurements were started after one minute. At the beginning of each granulation experiment one can choose virtual 'sieves', which are the ranges that will be used to calculate the particle size distribution. In this study, the virtual sieves were 150 µm, 250 µm, 500 µm, 710 µm, 1000 µm, 1400 µm, 2000 µm, 3150 µm, 5000 µm and 7500 µm and the particle size distribution was calculated in real-time every five seconds. A shortfall of the Parsum system is that once the particle size distribution ranges are chosen, they cannot be adjusted during the process. This means that prescience on the particle size distribution of the investigated granules is required before starting the SFV measurements. All measurement values were continuously stored and visualized in real-time by the IPP 70 software. Data analysis was done using the V 1.6 Macro in Excel 2007.

7.2.7. Design of Experiments (DoE)

A 2-level full factorial design was applied to study the influence of four process variables upon both the solid state and particle size (d50) of the wet granules (i.e. 2^4 + 3 = 19 granulations experiments). The screw speed was varied between 600 and 950 rpm. The temperature of the granulator barrel was altered between 25°C and 40°C. The liquid concentration was varied between 8.38% and 9.94% (w/w). The premixed powder was fed in a range from 10 to 25 kg per hour (Table 7.3). Both the powder feed rate and screw speed determine the barrel filling degree. The center point experiment of the design was repeated three times. All equipment variables (Table 7.1) were kept constant. The excipients, API and granulation liquid were the same for all experiments. All performed DOE granulation experiments are listed in Table 7.3.

Table 7.3. Overview of the DoE – Calculated d50 values obtained after two process minutes.

Run Order	Screw Speed (rpm)	Powder Feed Rate (kg/h)	Water Content (%)	Barrel T (°C)	D50 (µm)
1	950	10	8.38	25	2397
2	600	25	9.94	40	5793
3	950	10	9.94	40	3299
4	950	10	9.94	25	2521
5	950	10	8.38	40	3650
6	600	10	9.94	25	2843
7	775	17.5	9.16	32.5	3787
8	950	25	8.38	40	3966
9	950	25	9.94	40	6153
10	600	25	8.38	25	2463
11	950	25	9.94	25	3188
12	600	10	8.38	25	2051
13	600	25	9.94	25	3053
14	600	10	9.94	40	2437
15	775	17.5	9.16	32.5	3124
16	950	25	8.38	25	3227
17	775	17.5	9.16	32.5	3097
18	600	10	8.38	40	2383
19	600	25	8.38	40	4137

7.2.8. Data-analysis

The results of the DoE granulation experiments were analyzed using Modde 9.0 (Umetrics, Umeå, Sweden). Simca P+ 12.1 (Umetrics, Umeå, Sweden) was used for principal component analysis (PCA) of the NIR and Raman spectra collected during all granulation experiments. The spectral data were Standard Normal Variation (SNV) corrected for baseline-correction and for neutralizing differences in particle size and packing of the granules before applying PCA.

7.3. RESULTS AND DISCUSSION

One characteristic of the ConsiGma™ 25 is that *all* continuously produced wet granules are transferred to the fluid bed dryer. Granules which are not meeting the predetermined specifications cannot be removed, as is possible for batch production systems. Since batches are inspected after production and off-line tests are performed, bad batches can be rejected and will not be processed to the next production step. Therefore knowledge and control of the critical characteristics of the granules is important to guarantee appropriate downstream processing.

7.3.1. Particle size

The in-line particle size analyzer (Parsum®, Chemnitz, Germany) gives a very rapid image of the particle size distribution of the continuously produced wet granules. However, during the DoE experiments, sticking of the ***wet*** granules to the probe window (fouling) was observed despite the integrated air-cleaning system. Therefore, only these distributions in which no fouling was seen were extracted from all obtained distributions per DoE experiment (every 5 s during 3 minutes) for further interpretation. For future studies and more detailed wet granule size distribution evaluation, it will first need to be examined whether fouling can be avoided by optimizing the probe interfacing and cleaning system. Therefore in this study, only the d50 values from the selected distributions were evaluated to observe some trends how the examined parameters influence the granule size. A representative example of a selected particle size distribution obtained during DoE experiment 4 is shown in Figure 7.3. The d50 (50 % of the distribution has a particle size smaller than this value) obtained after two minutes of measurements was used as the DoE-response value. Table 7.3 gives an overview of the d50's after two minutes of production for all DoE-experiments. The influence of the process variables upon the d50 is evaluated in the effect plot, shown in Figure 7.4. Both the powder feed rate and the temperature of the barrel have a significant and positive influence on the d50. Increasing the powder feed rate and increasing the barrel temperature result in large and oversized granules. Also, a significant interaction between these two factors was found. A higher powder feed rate will result in a higher compaction of the powder in the granulator barrel and thus larger

granules. A higher temperature of the granulator barrel will induce a higher solubility of lactose, theophylline and PVP and consequently more bridge formation. Adding more granulation liquid tends to generate larger granules, but only a small range of the amount of added liquid was investigated in this study. Experiments 2, 9 and 19 illustrate these findings, as these three runs produced very large granules (Table 7.3). Experiments 1, 4, 6, 12 and 18 produced the smallest granules, as granulation was done using a low powder feed rate (10 kg/hour) and (except for run 18) a cold granulator barrel.

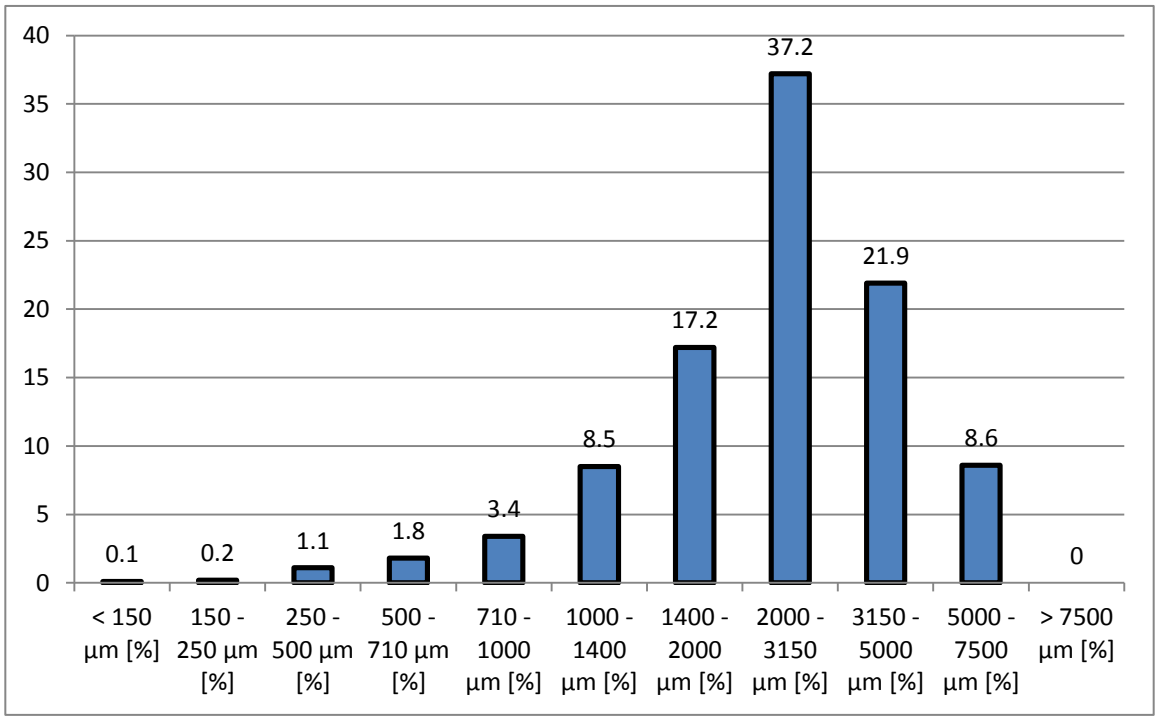

Figure 7.3. Particle size distribution observed during DoE experiment 4.

Overall it can be stated that none of the produced wet granules are satisfactory regarding particle size. The produced granules are too large to obtain good tablets after compression, but some remarks should be made. First off all, this is a measurement of wet granules, the particle size of the granules may reduce during drying. Furthermore the ConsiGma™ 25 is equipped with a discharging unit, which contains a mill to grind oversized granules. Nevertheless, the aim should be to fully understand, monitor and control the granulation and drying process, so that granules with an ideal particle size distribution are obtained and the mill will be redundant.

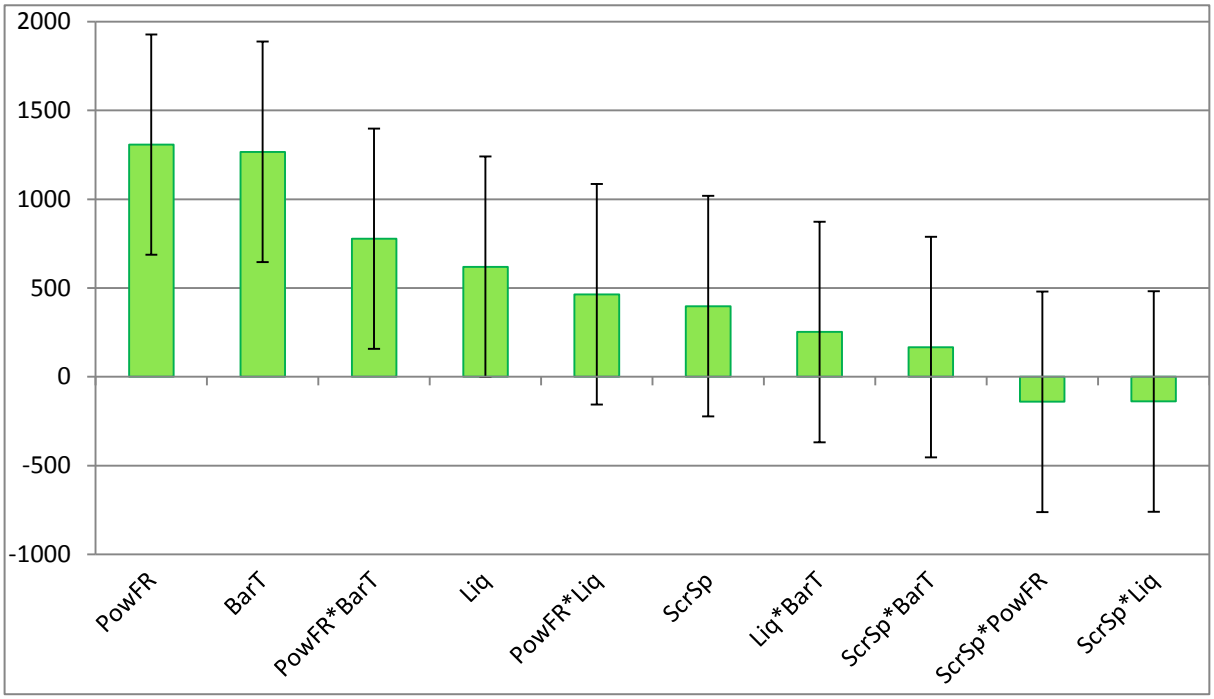

Figure 7.4. Effect plot of the response d50.

7.3.2. Solid State

7.3.2.1. Raman spectroscopy

Wikström et al. [27] found that Raman spectroscopy is an efficient tool to differentiate theophylline monohydrate from anhydrous theophylline, and that the conversion can be followed in real-time. The spectrum (Figure 7.5) of TA has two intense peaks at 1664 and 1706 cm^{-1}, whereas TH has a peak at 1686 cm^{-1}, which is due to C=O stretch of the carbonyl-groups. Furthermore during hydrate formation the O==C—N band shifts from 555 cm^{-1} to 572 cm^{-1} [29]. The excipients in the studied formulation have no overlapping Raman signal in these regions.

Principal component analysis of all spectra collected during the 19 DoE experiments was performed. The spectral regions from 520 cm^{-1} to 600 cm^{-1} and from 1636 cm^{-1} to 1737 cm^{-1} were selected and modeled together, as the solid state information is available in these spectral regions.

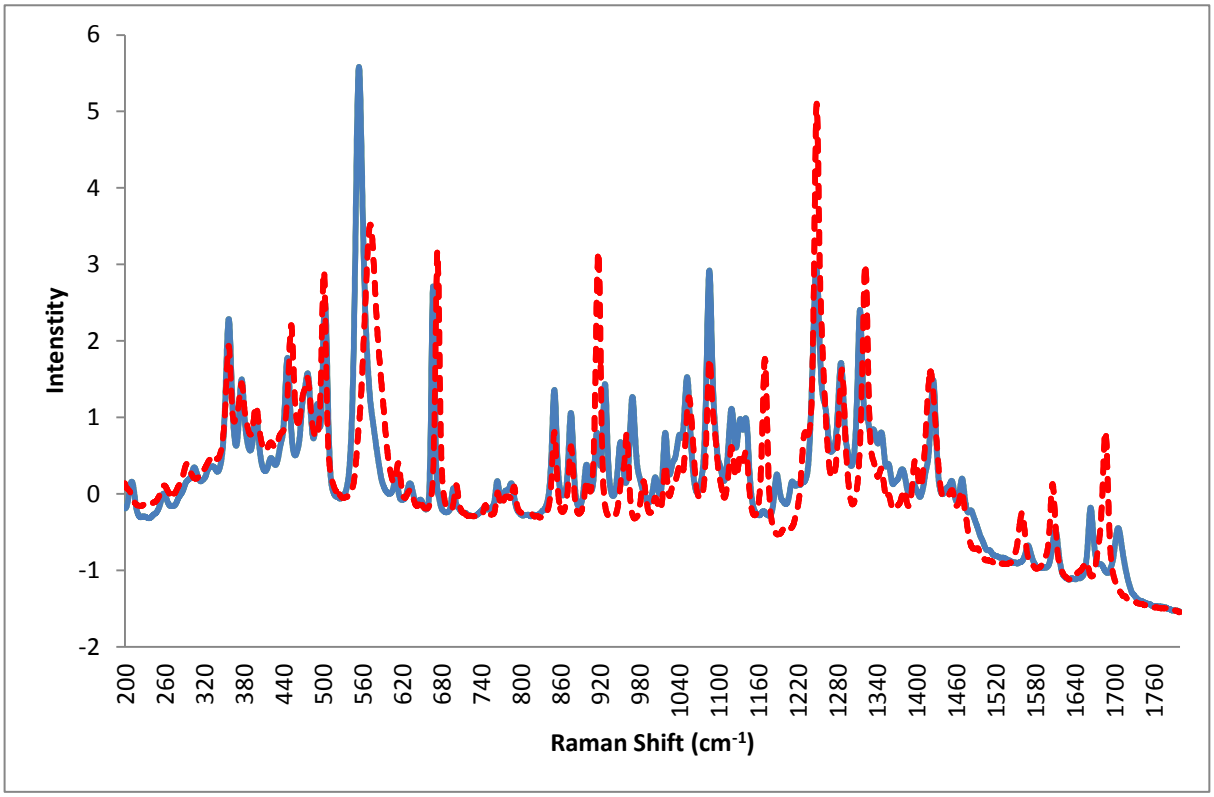

Figure 7.5. SNV-corrected Raman spectra of anhydrous theophylline (full line) and theophylline monohydrate granules (dashed line) in lactose.

Three principal components described 99.4% the spectral variation. The first, second and third PC explained 78.62%, 14.37% and 6.41%, respectively. A PC 1 versus PC 2 scores plot was plotted, and information regarding the solid state can be seen along the PC 2-axis. Secondary observation identifiers (i.e., the applied colors in the scores plots) were assigned to each individual spectrum (score) in order to classify them after used screw speed, barrel temperature, liquid concentration and powder feed rate. When classifying spectra according to the amount of added granulation liquid (Figure 7.6a); the red triangles correspond to the spectra collected from the DoE experiments where 8.38% (w/v) granulation liquid was used, the green crosses to 9.16% (w/v) and the blue squares to 9.94 % (w/v)), clustering can be noticed in the scores plot. Granules, which were produced with a low concentration of granulation liquid, are mainly situated in the positive part of the PC 2, whilst those granulated with a high amount of liquid are situated in the negative part.

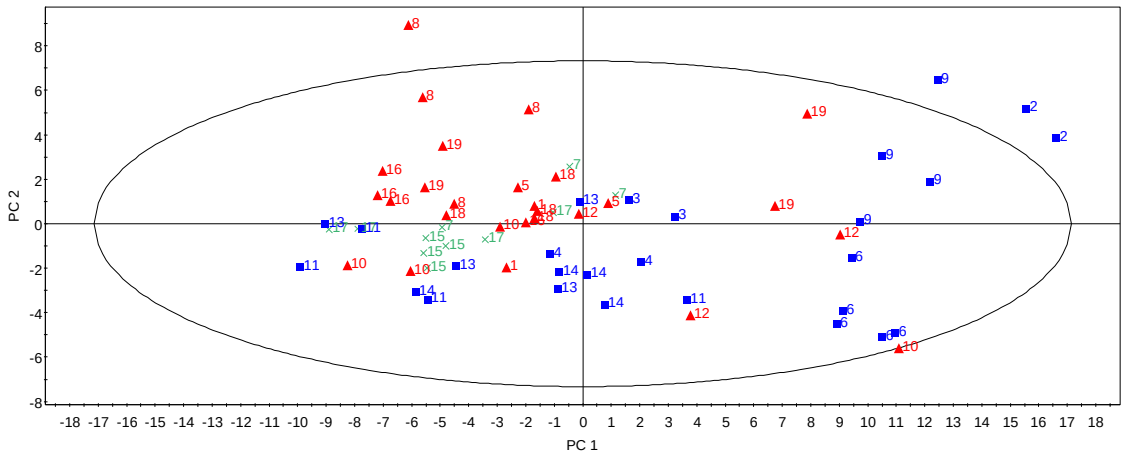

Figure 7.6. a. Raman spectra: PC 1 (78.62 %) versus PC 2 (14.37 %) scores plot (a) colored according to concentration of added granulation liquid. Red triangles – 8.38 %; blue squares – 9.94 %; green crosses centerpoints – 9.16%.

Classification according to the applied barrel temperature (Figure 7.6b) shows, that granules produced in a barrel heated to 40°C result in spectra mainly clustered in the positive half of the PC 2. Granules produced using a cold barrel (25°C) can be found in the negative part of PC 2. Concerning the powder feed rate, the positive part of the PC 2 contains most of the runs, where a powder feed rate of 25 kg/hour was used (Figure 7.6c). When data were classified after screw-speed, no clustering could be seen in the scores plot.

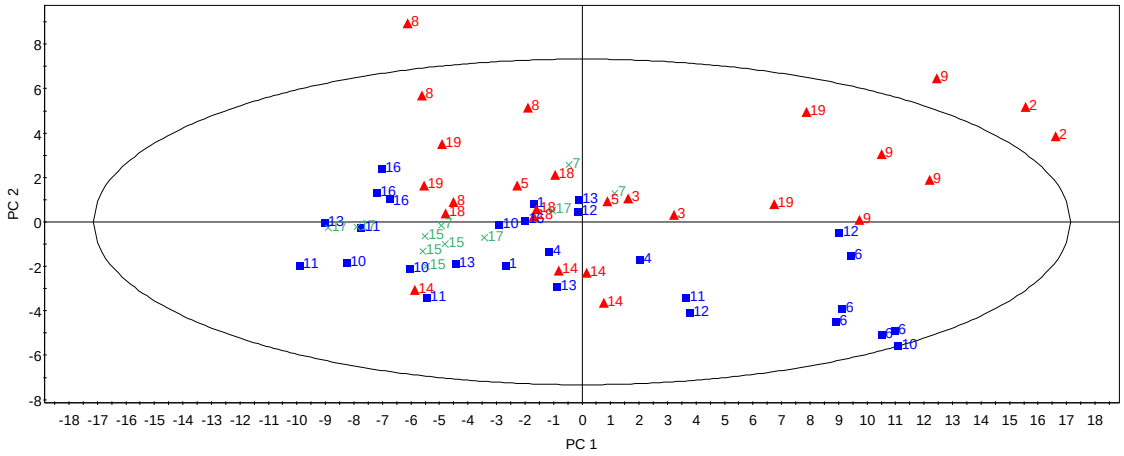

Figure 7.6. b. Raman spectra: PC 1 (78.62 %) versus PC 2 (14.37 %) scores plot (b) colored according to the applied temperature of the barrel. Red triangles – 40°C; blue squares – 25°C; green crosses centerpoints – 32.5 °C.

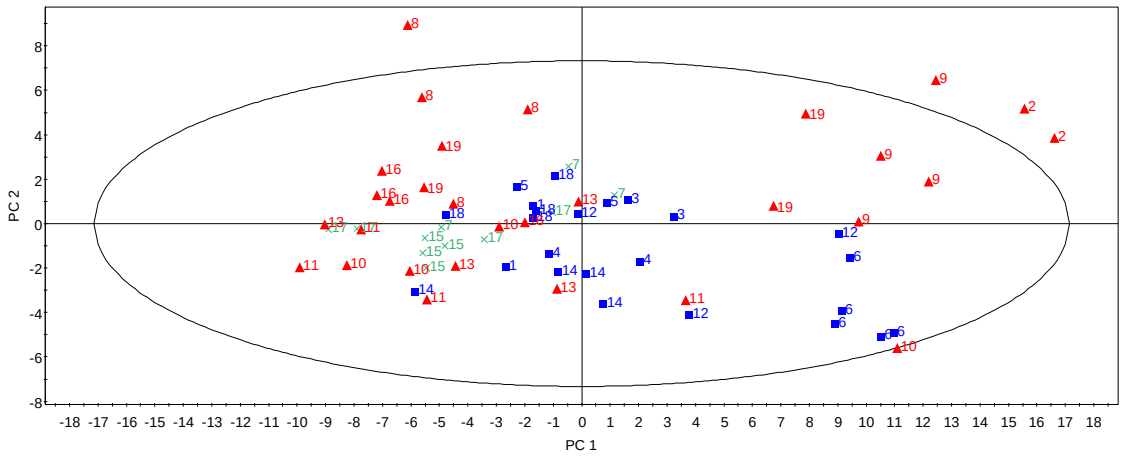

Figure 7.6. **c.** Raman spectra: PC 1 (78.62 %) versus PC 2 (14.37 %) scores plot (c) colored according to powder feed rate. Red triangles – 25 kg/h; blue squares – 10 kg/h; green crosses centerpoints – 17.5 kg/h.

To find an explanation for these clusterings, one should take a look at the loadings plots. No solid state clustering can be seen along the PC 1-axis from the scores plots, but only along the PC 2-axis. This indicates that the variation in solid state is expressed by PC 2. The loadings plot of the first principal component shows basically the joint spectra of theophylline monohydrate and anhydrous theophylline. The variation captured by PC 1 is most probable due to altering measurement conditions between the different analyzed samples (e.g., differences in probe to sample distances, differences in physical properties and granule sizes of the different samples etc.). More interesting is the loadings plot of the second principal component (Figure 7.7). Maxima are found at 555 cm^{-1}, 1665.6 cm^{-1} and 1707.6 cm^{-1}, whereas minima are found at 574.2 cm^{-1} and 1687.5 cm^{-1}. Both minima can be attributed to theophylline monohydrate, while the three maxima can be assigned to anhydrous theophylline. Hence, experiments where the spectra are clustered in the positive part of the PC 2-axis contain a quantity of remaining anhydrous theophylline. These experiments are listed in Table 7.4.

It is clear that water, and a certain water activity is needed for the conversion of anhydrous theophylline to theophylline monohydrate. Hence, the presence of remaining anhydrous theophylline can be explained for the runs with lower liquid concentration. Adding less

water, which results in a lower water activity, leads to a lower conversion rate of anhydrous theophylline to theophylline monohydrate [30, 31].

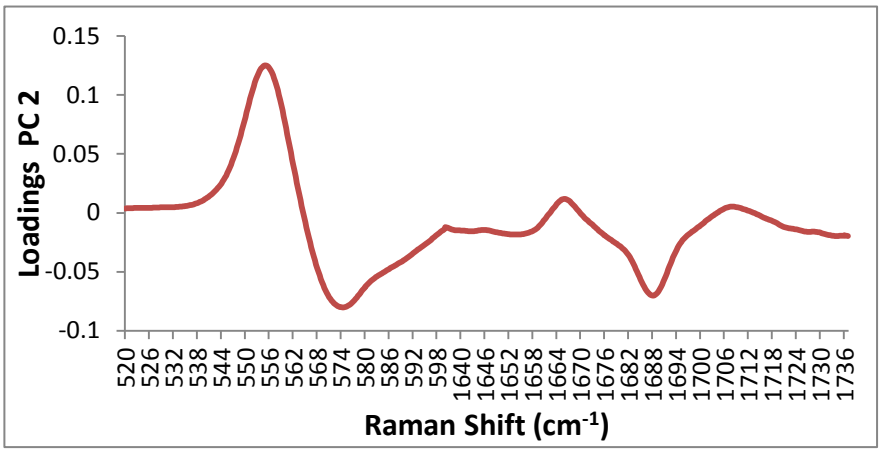

Figure 7.7. Raman spectra: Loadings plot of the second principal component (14.34 %).

Table 7.4. Overview of all DOE granulation experiments. Both significant parameters and spectroscopic responses are listed. Runs in which Raman and/or NIR-spectroscopy show the presence of anhydrous theophylline are indicated with +++.

Run	Water Content Dry - (8,38%)	Barrel T Hot - (40 °C)	Powder Feed Rate Full - (25kg/h)	Raman	NIR
1	X				
2		X	X	+++	
3		X		+++	
4					
5	X	X		+++	
6					
7					
8	X	X	X	+++	+++
9		X	X	+++	+++
10	X		X		
11			X		
12	X				
13			X		
14		X			
15					
16	X		X	+++	+++
17					
18	X	X		+++	+++
19	X	X	X	+++	+++

Ticehurst et al. [30] stated that at higher temperature an increased water activity is required to transform anhydrous theophylline to theophylline monohydrate. This can explain why runs with a higher barrel temperature result in these small remaining amounts of anhydrous theophylline in the granules. Furthermore hydration is an exothermic process, which means adding energy by means of heat will shift the reaction towards the anhydrate form [32].

With a high barrel filling the granulation liquid will have more difficulties to spread well through the powder bed, this can be an explanation of remaining anhydrate when granulating at 25 kg/h. Furthermore a high barrel filling will result in larger granules (as stated earlier), which makes it harder for the granulation liquid to penetrate in the granules.

Raman spectroscopy together with Design of Experiments showed to be valuable tools to investigate and understand solid state transformations in wet granules. Even small amounts of a non-expected polymorph can be detected.

7.3.2.2. NIR spectroscopy

To investigate if the same conclusions can be made when analyzing the granules with NIR spectroscopy, runs 6 till 19 were taken into account (runs 1 till 5 were not taken into account, since inadequate NIR spectra were obtained due to sampling problems). PCA was performed on the complete spectral range (10000 to 4500 cm^{-1}) resulting in three principal components. These explained 97.1 % of the variation. PC 1 explained 69.11 % of the spectral variation, PC 2 18.82% and PC 3 9.13 %. In order to make a distinct classification possible, secondary observation identifiers (i.e., assignment of colors, which are corresponding to certain process settings, to the scores) were added to all spectra.

The first principal component differentiates the granulation experiments after water content (Figure 7.8). Granules produced with a high liquid amount are spread along the positive part of the PC 1-axis, while those produced with a low liquid amount can be found in the negative part of PC 1. This is confirmed by the loadings of this first principal component, which clearly shows two water bands (Figure 7.9). The spectral band at 5222 cm^{-1} corresponds to the OH-stretching and bending vibrations of water molecules, while the 7035 cm^{-1} band can be attributed to first overtone OH-stretching vibrations. Two more

vibration are contributing to these peaks, resulting in two shoulders at 6880 cm^{-1} and 5168 cm^{-1}. These two bands are caused by lactose monohydrate [33].

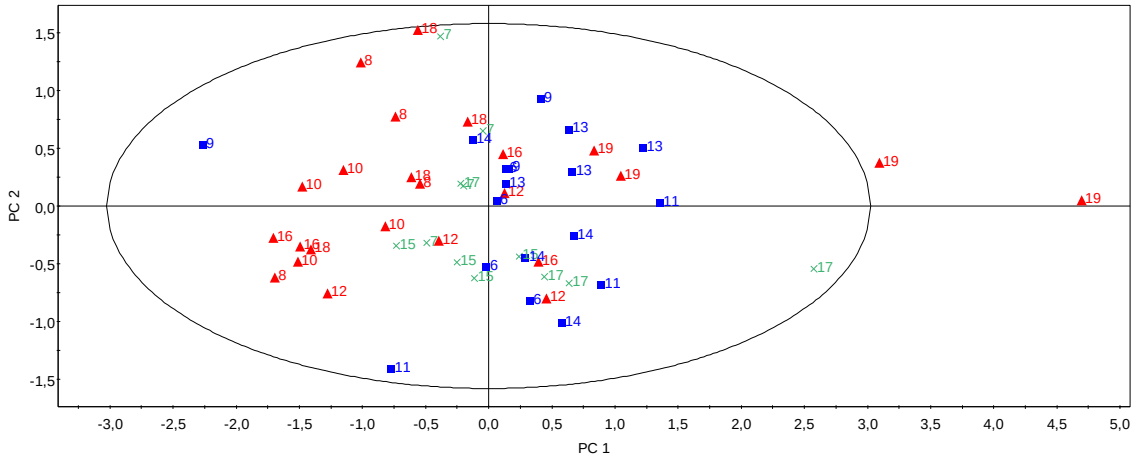

Figure 7.8. NIR spectra: PC 1 (69.11 %) versus PC 2 (18.82 %) scores plot: colored according to added granulation liquid amount. Red triangles – 8.38 %; blue squares – 9.94 %; green crosses centerpoints – 9.16%.

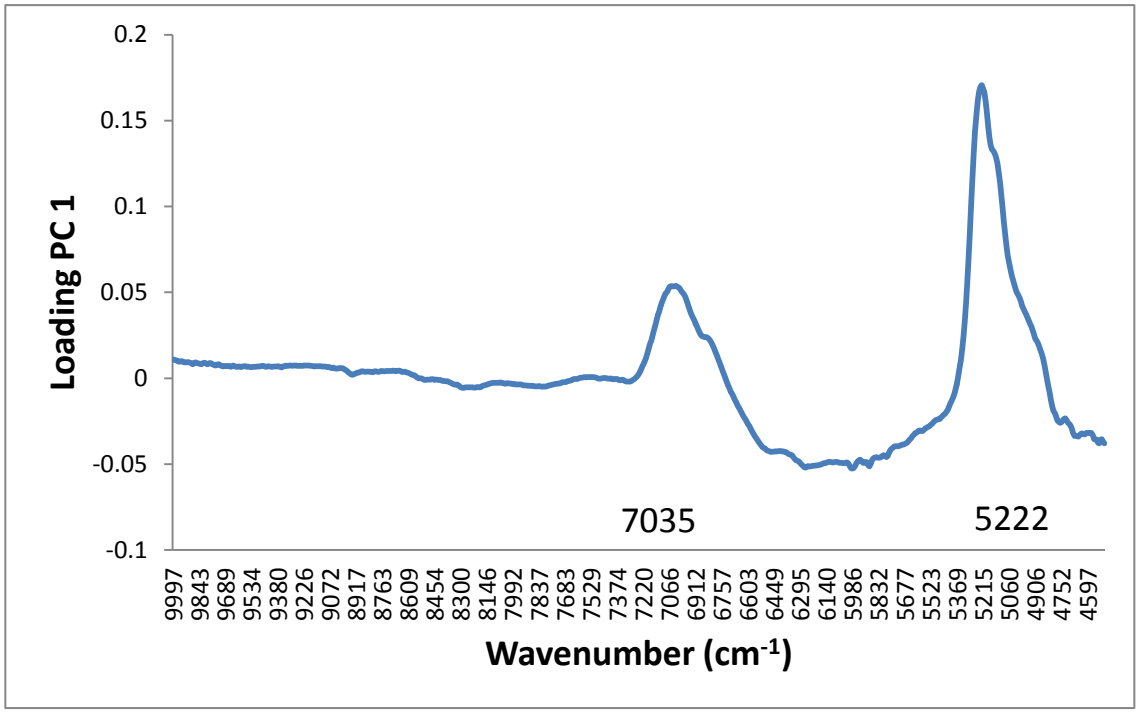

Figure 7.9. NIR spectra: Loadings plot of the first principal component (69.11 %).

In Figure 7.10 a, the PC 2 versus PC 3 scores plot was plotted and data were labeled and examined after secondary observation identifiers. Most spectra of the granules produced

with a low concentration of granulation liquid can be found in the positive part of the PC 3-axis. The same trend can be seen for granules produced in a warm granulation barrel (Figure 7.10b). Classifying data after powder feed rate or screw speed did not result in any clear clustering.

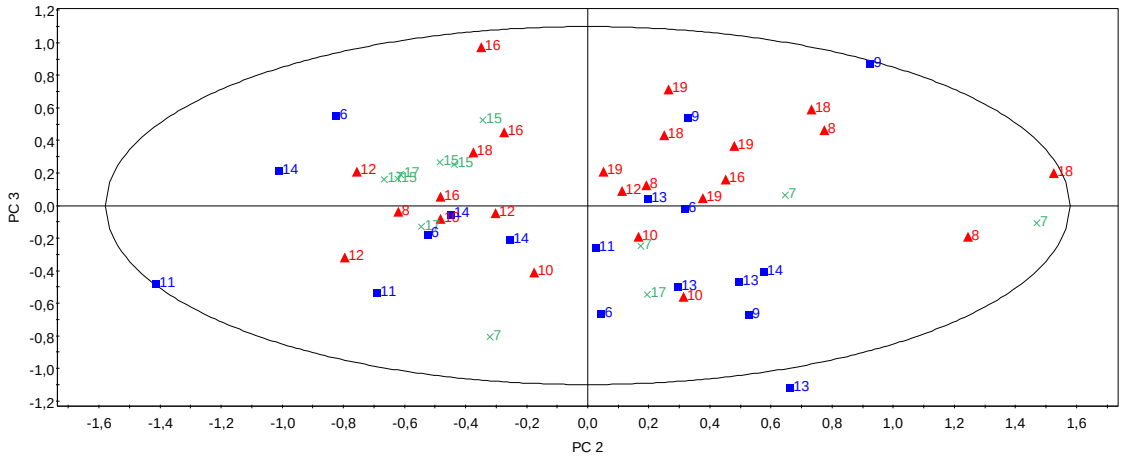

Figure 7.10. a. NIR spectra: PC 2 (18.82 %) versus PC 3 (9.13 %) scores plot colored according to concentration of added granulation liquid. Red triangles – 8.38 %; blue squares – 9.94 %; green crosses centerpoints – 9.16%.

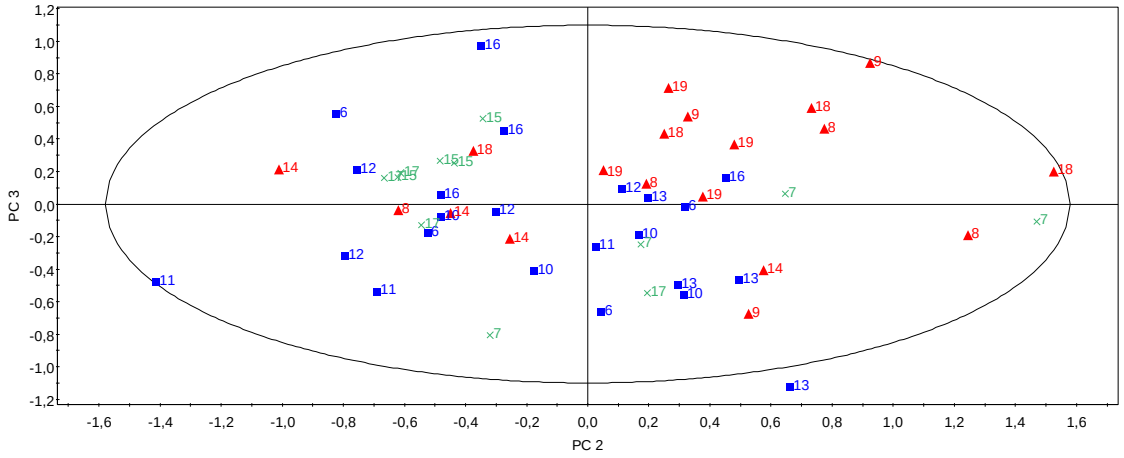

Figure 7.10. b. NIR spectra: PC 2 (18.82 %) versus PC 3 (9.13 %) scores plot coloured according to the applied temperature of the barrel. Red triangles – 40°C; blue squares – 25°C; green crosses centerpoints – 32.5 °C.

The loadings plot of PC 3 (Figure 7.11) shows an absorption band of OH-vibrations at 7035 cm^{-1}. This water-band is oppositely directed, compared to the bands at 5947 cm^{-1} and 6009

cm^{-1}, which are specific peaks for anhydrous theophylline. Furthermore, a remarkable peak at 5168 cm^{-1} can be attributed to lactose monohydrate, which has the same concentration in all granules [33]. NIR confirms hence the Raman analysis findings. The granulation experiments corresponding to the scores in the positive part of the PC 3-axis most likely contain remaining anhydrous theophylline. NIR only shows the variation in solid state, when different barrel temperatures or liquid concentrations are applied.

An overview of the runs containing an amount of anhydrous theophylline is given in Table 7.4. Runs (6-19) which were thought to contain anhydrous theophylline when investigated with Raman are all confirmed by NIR.

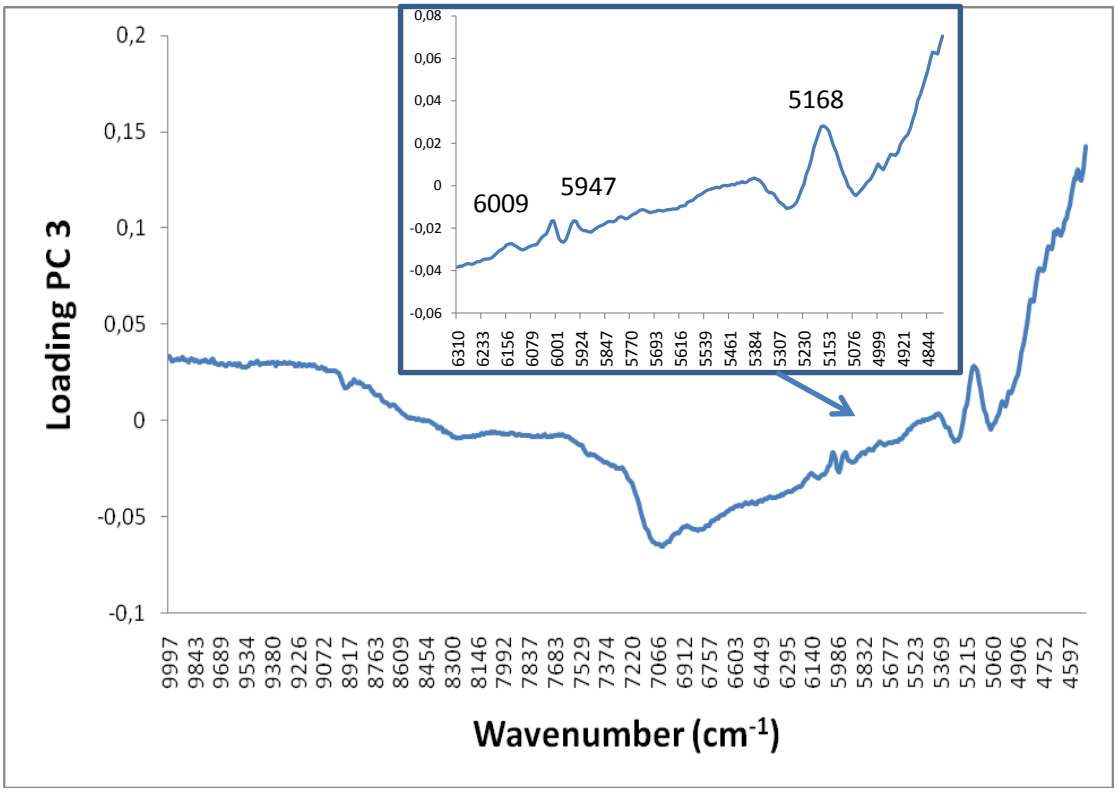

Figure 7.11. NIR spectra: Loadings plot of the third principal component (9.13 %) with a zoom on the 6310 cm^{-1}-4800 cm^{-1} region.

7.4. CONCLUSIONS

This study gave an insight in the possibilities of implementing PAT tools in a continuous twin screw granulation process. Both Raman and NIR showed to be appropriate tools for understanding the solid state behavior of theophylline during wet granulation. Peak differentiation and polymorph differentiation was more definite in Raman spectra than in NIR spectra.

The In-Line Particle Probe showed to be a promising tool for the in-line measurement of particle size distribution. More investigation on the measurement technique will be necessary to obtain adequate measurements of wet granules. The main challenge is to avoid fouling of the optical surfaces.

Performing a DoE, allowed to reveal the most influencing granulation parameters upon granule size and the solid state of the API. The temperature of the barrel and the added amount of granulation liquid, and to a lesser extent the powder feed rate showed to have an effect upon the solid state of the wet granules. The powder feed rate and the barrel temperature had significant effects upon the granule size.

This study proves that at-line measurements of both solid state and particle size during a continuous twin screw granulation process are feasible. Given these promising results of the presented tools, the next step is the design of a new process analyzer interfacing device. This device permits integration of PAT tools in the ConsiGma™ 25, allowing them to provide real-time information. Future studies will focus on the use of the in-line measured critical process and product information to steer the next process steps (e.g., feed forward adjustment of process settings of further process steps).

7.5. REFERENCES

[1] H. Leuenberger, New trends in the production of pharmaceutical granules: batch versus continuous processing, European Journal of Pharmaceutics and Biopharmaceutics, 52 (2001) 289-296.

[2] M. Levin, Introduction, in: Pharmaceutical Process Scale-up, Marcel Dekker, New York, 2001, pp. vii-x.

[3] H. Leuenberger, Scale-up in the 4th dimension in the field of granulation and drying or how to avoid classical scale-up, Powder Technology, 130 (2003) 225-230.

[4] FDA-Adminstration, Guidance for Industry - PAT - A Framework for Innovative Pharmaceutical Development, Manufacturing, and Quality Assurance, in, 2004.

[5] Guidance for Industry - Process Validation: General Principles and Practices - January 2011, in, 2011.

[6] International Conference on Harmonisation of Technical Requirements for Registration of Pharmaceuticals for Human Use. Pharmaceutical Development Q8, in, 2009.

[7] International Conference on Harmonisation of Technical Requirements of Registration of Pharmaceuticals for Human Use. Quality Risk Management Q9, in, 2005.

[8] International Conference on Harmonisation of Technical Requirements for Registration of Pharmaceuticals for Human Use. Pharmaceutical Quality System Q10., in, 2008.

[9] K. Naelapaa, P. Veski, H.G. Kristensen, J. Rantanen, P. Bertelsen, Building quality into a coating process, Pharmaceutical Development and Technology, 15 (2010) 35-45.

[10] M.J. Gamlen, C. Eardley, CONTINUOUS EXTRUSION USING A BAKER PERKINS MP50 (MULTIPURPOSE) EXTRUDER, Drug Dev. Ind. Pharm., 12 (1986) 1701-1713.

[11] N.O. Lindberg, C. Tufvesson, L. Olbjer, EXTRUSION OF AN EFFERVESCENT GRANULATION WITH A TWIN SCREW EXTRUDER, BAKER PERKINS MPF 50-D, Drug Dev. Ind. Pharm., 13 (1987) 1891-1913.

[12] J. Werani, M. Grunberg, C. Ober, H. Leuenberger, Semicontinuous granulation - the process of choice for the production of pharmaceutical granules?, Powder Technology, 140 (2004) 163-168.

[13] G. Betz, P. Junker-Burgin, H. Leuenberger, Batch and continuous processing in the production of pharmaceutical granules, Pharmaceutical Development and Technology, 8 (2003) 289-297.

[14] C. Vervaet, J.P. Remon, Continuous Granulation, in: D.M. Parikh (Ed.) Handbook of Pharmaceutical Granulation Technology, Informa Healthcare, New York, 2009, pp. p. 308-322.

[15] C. Vervaet, J.P. Remon, Continuous granulation in the pharmaceutical industry, Chemical Engineering Science, 60 (2005) 3949-3957.

[16] E.I. Keleb, A. Vermeire, C. Vervaet, J.P. Remon, Continuous twin screw extrusion for the wet granulation of lactose, International Journal of Pharmaceutics, 239 (2002) 69-80.

[17] E.I. Keleb, A. Vermeire, C. Vervaet, J.P. Remon, Twin screw granulation as a simple and efficient tool for continuous wet granulation, International Journal of Pharmaceutics, 273 (2004) 183-194.

[18] B. Van Melkebeke, C. Vervaet, J.P. Remon, Validation of a continuous granulation process using a twin-screw extruder, International Journal of Pharmaceutics, 356 (2008) 224-230.

[19] D. Djuric, B. Van Melkebeke, P. Kleinebudde, J.P. Remon, C. Vervaet, Comparison of two twin-screw extruders for continuous granulation, European Journal of Pharmaceutics and Biopharmaceutics, 71 (2009) 155-160.

[20] M.E. Aulton, B. M., Fluidised bed granulation—factors influencing the quality of the product., Int. J. Pharm. Technol. Prod. Manuf., 2 (1981) 24-29.

[21] H.G. Kristensen, T. Schaefer, GRANULATION - A REVIEW OF PHARMACEUTICAL WET-GRANULATION, Drug Dev. Ind. Pharm., 13 (1987) 803-872.

[22] L. Eriksson, E. Johansson, N. Kettaneh-Wold, C. Wikström, W. S, Design of Experiments - Principles and Applications, Umetrics, Umea, 2008.

[23] E. Suzuki, K. Shimomura, K. Sekiguchi, THERMOCHEMICAL STUDY OF THEOPHYLLINE AND ITS HYDRATE, Chemical & Pharmaceutical Bulletin, 37 (1989) 493-497.

[24] A. Heinz, C.J. Strachan, K.C. Gordon, T. Rades, Analysis of solid state transformations of pharmaceutical compounds using vibrational spectroscopy, Journal of Pharmacy and Pharmacology, 61 (2009) 971-988.

[25] J. Bauer, S. Spanton, R. Henry, J. Quick, W. Dziki, W. Porter, J. Morris, Ritonavir: An extraordinary example of conformational polymorphism, Pharmaceutical Research, 18 (2001) 859-866.

[26] S. Airaksinen, P. Luukkonen, A. Jorgensen, M. Karjalainen, J. Rantanen, J. Yliruusi, Effects of excipients on hydrate formation in wet masses containing theophylline, J. Pharm. Sci., 92 (2003) 516-528.

[27] H. Wikstrom, P.J. Marsac, L.S. Taylor, In-line monitoring of hydrate formation during wet granulation using Raman spectroscopy, J. Pharm. Sci., 94 (2005) 209-219.

[28] A. Burggraeve, T. Van Den Kerkhof, M. Hellings, J.P. Remon, C. Vervaet, T. De Beer, Evaluation of in-line spatial filter velocimetry as PAT monitoring tool for particle growth during fluid bed granulation, European Journal of Pharmaceutics and Biopharmaceutics, 76 (2010) 138-146.

[29] A. Jorgensen, J. Rantanen, M. Karjalainen, L. Khriachtchev, E. Rasanen, J. Yliruusi, Hydrate formation during wet granulation studied by spectroscopic methods and multivariate analysis, Pharmaceutical Research, 19 (2002) 1285-1291.

[30] M.D. Ticehurst, R.A. Storey, C. Watt, Application of slurry bridging experiments at controlled water activities to predict the solid state conversion between anhydrous and hydrated forms using theophylline as a model drug, International Journal of Pharmaceutics, 247 (2002) 1-10.

[31] Y. Yoshihashi, M. Makita, S. Yamamura, E. Fukuoka, K. Terada, Determination of heat of hydration and hydration kinetics of theophylline by thermal analysis, Chemical & Pharmaceutical Bulletin, 46 (1998) 1148-1152.

[32] G.G.Z. Zhang, D. Law, E.A. Schmitt, Y.H. Qiu, Phase transformation considerations during process development and manufacture of solid oral dosage forms, Advanced Drug Delivery Reviews, 56 (2004) 371-390.

[33] H.R.H. Ali, H.G.M. Edwards, I.J. Scowen, Noninvasive in situ identification and band assignments of some pharmaceutical excipients inside USP vials with FT-near-infrared spectroscopy, Spectrochimica Acta Part a-Molecular and Biomolecular Spectroscopy, 72 (2009) 890-896.

CHAPTER 8

MOISTURE AND DRUG SOLID STATE MONITORING DURING A CONTINUOUS DRYING PROCESS USING EMPIRICAL AND MASS BALANCE MODELS

"Science is the systematic classification of experience."

George Henry Lewes (1817-1878)

Fonteyne M., Gildemyn D., Peeters E., Mortier S., Vercruysse J., Gernaey K.V., Vervaet C., Remon J.P., Nopens, I., De Beer T. (2014). Moisture and drug solid state monitoring during a continuous drying process using empirical and mass balance models, European Journal of Pharmaceutics and Biopharmaceutics, doi:10.1016/j.ejpb.2014.02.015

ABSTRACT

Classically, the end point detection during fluid bed drying has been performed using indirect parameters, such as the product temperature or the humidity of the outlet drying air. This chapter aims at comparing those classic methods to both in-line moisture and solid state determination by means of PAT tools (Raman and NIR spectroscopy) and a mass balance approach. The six-segmented fluid bed drying system being part of a fully continuous from-powder-to-tablet production line (ConsiGma™ 25) was used for this study. A theophylline:lactose:PVP (30:67.5:2.5) blend was chosen as model formulation. For the development of the NIR-based moisture determination model, 15 calibration experiments in the fluid bed dryer were performed. Six test experiments were conducted afterwards, and the product was monitored in-line with NIR and Raman spectroscopy during drying. The results (drying end point and residual moisture) obtained via the NIR-based moisture determination model, the classical approach by means of indirect parameters and the mass balance model were then compared. Our conclusion is that the PAT-based method is most suited for use in a production set-up.

CHAPTER 8

MOISTURE AND DRUG SOLID STATE MONITORING DURING A CONTINUOUS DRYING PROCESS USING EMPIRICAL AND MASS BALANCE MODELS

8.1. INTRODUCTION

About 80% of the currently available pharmaceuticals are formulated as solid dosage forms, the majority of them being tablets. In many cases tableting requires granulation of the starting materials (powders) prior to compaction. As a consequence industrial tableting is still a multi-step process nowadays. In case of wet granulation, a drying step follows the granulation step. Afterwards the dry granules may be mixed with an external phase (i.e. lubricant, disintegrant). The final blend is then fed to the tableting machine for compaction, which might be followed by coating, before the tablets are blistered and packed. *After* each step of this production chain the critical (intermediate) product characteristics of random samples of the batch are generally evaluated by means of off-line analyses in analytical laboratories. Batches will either proceed to the next processing step or will be rejected in case of failure of these analysis tests. Hence, traditional batch production is a time-consuming and expensive production method. Partly due to the increasing competition and decreasing profits in the pharmaceutical industry (i.e. generics, smaller pipelines, expiring patents,…), innovative manufacturing models are more and more desired in order to make the production processes faster, cheaper, more efficient and hence more competitive. Therefore, continuous production gains increasing interest in the pharmaceutical industry, also in tableting applications. Recent manufacturing technology advances have already shown the advantages of this approach [1-6].

Recently, full continuous from-powder-to-tablet production lines became commercially available [7-11]. The traditionally applied quality assessment approach based on off-line analysis is not applicable in a continuous manufacturing environment, since the process cannot be stopped and immediate and continuous process and product quality information is required. The need for off-line tests would counterbalance the advantages of continuous manufacturing. Therefore, continuous real-time quality control should be ensured by means of in-process analysis methods as it is advised in the Food and Drug Administration's PAT guideline [12].

Conventionally, the end point of a drying process - usually performed in a fluid bed dryer - after wet granulation is determined by means of *indirect* parameters. The humidity and the temperature of the outgoing drying air, the product temperature and the pressure difference over the fluidized bed can be evaluated in order to control the fluidized bed drying of wet granules [13, 14]. These methods give an idea about the water evaporation progress. The drying process is considered as finished when water evaporation is no longer detected. However, the in-line monitoring of residual moisture content during drying using near infrared (NIR) spectroscopy is beneficial for two reasons: (i) monitoring the moisture content allows end point detection of the drying process and makes real-time decision making possible, hence preventing over-drying; and (ii) information regarding possible structural changes of the active pharmaceutical ingredient (API) or/and excipients can be obtained.

The utility of NIR spectroscopy for the in-line monitoring and moisture assessment during fluid bed and spray drying processes has been demonstrated extensively in the literature [15-23]. Furthermore, NIR spectroscopy has also recently been used for the monitoring of a continuous granulation and drying process [10]. However, in this study the measurements were performed after the drying unit and not during drying. Besides monitoring of the drying process, NIR spectroscopy can also be used for the continuous evaluation of process induced solid state transformations of both APIs and excipients. Römer et al. [24] monitored the solid state conversions of erythromycin dehydrate using an in-line NIR spectrometer in a miniaturized fluid bed dryer. Aaltonen et al. [14] used both NIR and Raman spectroscopy to monitor the solid state changes of theophylline using the same mini-dryer. They linked the

in-line obtained spectra to the traditionally monitored fluid bed parameters such as absolute humidity of the outlet air and pressure difference over the fluidized bed. The solid state changes were quantified in real-time, which is impossible with the traditional indirect parameters. Furthermore, the same micro scale fluid bed dryer was used by Kogerman et al. [25] to quantify the solid state changes of piroxicam and carbamazepine in-line using Raman spectroscopy.

The presented study **aim**s at evaluating Raman and NIR spectroscopy for the in-line monitoring of the drying process and determination of the end point, the residual moisture content and the product solid state *during* continuous drying *in* a six-segmented continuous fluid bed drying unit, which is part of a fully continuous from-powder-to-tablet manufacturing line (ConsiGma™ 25, GEA Pharma Systems nv., Collette™, Wommelgem, Belgium). Furthermore, data derived from the in-line acquired spectroscopic data are compared with the conclusions obtained from the conventional *indirect* approach using the logged univariate parameters such as humidity of the outlet air and product temperature. Additionally, the spectroscopic observations are compared with the residual moisture content conclusions that can be derived from a mass balance model, which was recently developed for the six-segmented continuous fluid bed dryer [26]. This mass balance model is based on the physics governing the continuous drying process, hence forcing fundamental process understanding. Mass balance modeling requires the definition of the composition of the physical in- and outgoing gas (moisture content) and the liquid and solid streams in the process. It is examined whether feeding the continuously logged process parameters (e.g., humidity and temperature of inlet and outlet air, product temperature,…) into this mass balance model allows visualizing the drying process progress and calculating the end point of drying and the corresponding residual moisture content. By comparing these results to the spectroscopic results, the necessity of using spectroscopic monitoring during drying is evaluated and discussed.

8.2. MATERIALS AND METHODS

8.2.1. Materials

Anhydrous theophylline (Farma-Quimica Sur S.L., Malaga, Spain) (30%, w/w) was used as a model drug and granulated together with lactose monohydrate 200M (Caldic Belgium NV, Hemiksem, Belgium) as filler. Polyvinylpyrrolidone (Kollidon 30®, BASF, Burgbernheim, Germany) was added as a binder to the dry powder mixture in a concentration of 2.5% (w/w). Distilled water was used as granulation liquid. Sodium lauryl sulfate (Fagron, Waregem, Belgium) was added to the granulation liquid (0.5% w/v) to improve the wettability of the dry powder mixture.

8.2.2. Continuous twin screw granulation and fluid bed drying

Continuous granulation and drying was performed using the ConsiGma™ 25 unit (GEA Pharma Systems nv., Collette™, Wommelgem, Belgium) [7, 11]. One of the assets that ConsiGma™ offers is the continuous logging and storage of numerous process parameters and outcomes in each unit (i.e., temperature granulator barrel, torque on twin screws, weight powder dosing unit, temperature of product in the dryer, etc.).

8.2.3. NIR spectroscopy

A Fourier-Transform NIR spectrometer (Thermo Fisher Scientific, Zellik, Belgium, Nicolet Antaris II near-IR analyzer) equipped with an InGaAs detector, a quartz halogen lamp and a fiber optic contact probe was used. The probe was inserted in cell 5 of the six-segmented fluid bed dryer by means of an in-house developed accessory (Figure 8.1). Each spectrum was collected in the 10000-4500 cm^{-1} spectral region with a resolution of 16 cm^{-1} and was averaged over 16 scans. Spectra were recorded continuously during drying and a spectrum was collected approximately each ten seconds. The same fiber optic contact probe and spectrometer settings were used for off-line measurements. Spectra were mean centered and standard normal variate (SNV)-corrected prior to multivariate data-analysis. Data collection and data transfer were done using Thermo Fisher Scientific's Result Software.

Figure 8.1. NIR fiber optic contact probe mounted in cell 5 of the dryer by means of an in-house made accessory.

8.2.4. Raman spectroscopy

A RamanRxn1 spectrometer (Kaiser Optical Systems, Inc., Ann Arbor, Michigan, US) equipped with an air-cooled CCD detector (back-illuminated deep depletion design) was used. For the in-line measurements, an immersion optic (IO), connected to an MR Probe (Kaiser Optical Systems, Ann Arbor, Michigan) was inserted in cell 2 of the six-segmented continuous fluid bed dryer by means of an in-house developed accessory. An IO with a working distance of 3 mm was used (i.e. “long”). All spectra were recorded with a resolution of 4 cm^{-1} and an exposure time of 10 seconds, using a laser power of 400 mW. In-line spectra were taken continuously during the 20 minutes of drying. The system was not paused in between two spectra, resulting in a spectrum each 10 seconds approximately. Spectra were mean centered and SNV-corrected before data analysis in the spectral region from 200 to 1800 cm^{-1}. Data collection and data transfer were automated using the HoloGRAMS™ data collection software, the HoloREACT™ reaction analysis and profiling software and the Matlab software (version 7.1, The MathWorks Inc., Natick, Massachusetts, US).

8.2.5. In-process moisture and drug solid state monitoring

This study focuses on the continuous fluid bed dryer of the ConsiGma™ 25-system, which consists of six parallel cells. Wet granules are loaded into the first cell during a user defined time period, after which wet granules are loaded into the second cell, etc. While the second cell is being filled, wet granules continue to dry inside the first cell for a user defined drying time after which they are unloaded and discharged to the discharge module. Every cell repeats this cycle of loading, drying and discharging, hence enabling the continuous drying of the continuously produced wet granules. Two of the dryer cells (cell 2 and cell 5) contain an interfacing opening for PAT tools. In-house designed accessories were used to insert the Raman (cell 2) and NIR (cell 5) spectroscopic probes in these interfacing places (Figure 8.1).

One of the aims of this study is to evaluate the applicability of in-line NIR spectroscopy for the in-process monitoring of the drying progress and for the granule moisture content prediction at the end of drying. To develop an NIR calibration model for residual moisture content, granules with different residual moisture contents were produced. Therefore, wet granules were manufactured using a powder feed rate of 10 kg/h, a screw speed of 950 rpm, 9.94 % (w/w) granulation liquid and a granulator barrel temperature of 25°C. During the consecutive drying step, the inlet airflow and temperature of the drying air were varied as well as the filling and drying time, hence generating granules with different residual moisture contents (Table 8.1). Immediately after drying, the granules were collected and twenty NIR spectra were measured off-line. Karl Fischer moisture determination was also performed directly after the NIR measurements of each calibration experiment. These data (i.e., the off-line collected NIR spectra (X) and the corresponding Karl Fischer determined residual moisture contents (Y)) were used for the construction of a Partial Least Squares (PLS) model. Afterwards, six test experiments were performed, where NIR and Raman spectra were collected in-line during drying, for both moisture and drug solid state monitoring. These test experiments were performed using a powder feed rate of 17.5 kg/h, a liquid rate of 9.94 % (w/w), a granulator barrel temperature of 25°C and a screw speed of 950 rpm. The filling time and the drying time were 5 and 20 minutes respectively. An airflow of 360 m^3/h was blown through the bottom plate of the dryer. The test experiments differed regarding the applied drying air temperature varying from 30°C to 80°C in steps of 10°C

(Table 8.1). No other cells, besides 2 and 5 were filled with granules. Directly after each in-line measurement, the moisture content of the dried granules of cell 2 and cell 5 was measured in triplicate by means of Karl Fisher titration.

8.2.6. Karl Fischer moisture determination

The residual moisture of samples was determined by volumetric Karl Fischer titration (KF) using a V30 volumetric Karl Fischer titrator (Mettler Toledo, Zaventem, Belgium). Methanol (Hydranal, Sigma Aldrich, Germany) was used as a solvent. Before titration, granules were stirred and dissolved during 5 minutes.

8.2.7. Data analysis

The analysis of the spectra and the development of the Principal Component Analysis (PCA) and Partial Least Squares (PLS) models was done using the Simca P+ 12.0.1 software (Umetrics AB, Umeå, Sweden).

Table 8.1. Experiments for the development of the NIR moisture calibration model and the test experiments.

Exp	Flow drying air (m^3/h)	Temperature drying air (°C)	Filling time (s)	Drying time (s)	Moisture content (%)
0		Wet granules			11.54
1	360	45	75	75	5.17
2	360	45	45	45	6.24
3	360	45	30	30	5.34
4	360	45	30	30	6.05
5	200	45	75	75	7.08
6	360	45	60	90	6.16
7	360	45	60	150	5.75
8	360	45	60	380	5.03
9	360	45	120	600	3.95
10	360	45	300	900	4.26
11	360	60	150	900	3.62
12	360	60	60	900	3.78
13	360	60	300	900	3.53
14	360	60	300	1500	3.60
	Test experiments				
T X	360	X=30,40,50,60, 70,80	300	1200	varied

8.3. RESULTS AND DISCUSSION

8.3.1. In-line moisture calibration model and mass balance approach

Fifteen different loads of granules (i.e., calibration set) were produced for the development of the moisture calibration model. The process parameters of these 15 runs were varied to obtain granules with different residual moisture contents (see materials and methods and Table 8.1). Twenty NIR spectra were collected per calibration sample, resulting in 20 x 15 = 300 spectra. A PLS model was developed by regressing these NIR spectra versus the residual moisture contents of the calibration samples, assessed via Karl Fischer titration. Subsequently, six test experiments were performed hereby using in-line NIR and Raman spectroscopic monitoring in order to assess moisture content during drying (using the developed NIR moisture PLS model) as well as the drug solid state. The optimal number of PLS components for the NIR moisture model was evaluated according to the cumulative fraction of the variation of the y-variable explained ($R^2[Y]$), the fraction of the total variation that can be predicted estimated by cross-validation (Q^2) and the Root Mean Square Error of Prediction (RMSEP) for the predictions in the test set. The RMSEP was determined in two ways: (i) comparing the moisture content predicted from the last five collected in-line NIR spectra of each test-experiment. Then the average of the five obtained predictions was compared to the actual moisture content determined via Karl Fischer-titration immediately after each experiment; (ii) comparing the moisture content predicted from only the last NIR spectrum of each test-experiment to the same KF results. Applying the spectral range of 10000 to 4500 cm^{-1} of the 300 calibration spectra resulted in a three PLS components model, with an $R^2[X]$ of 0.936, an $R^2[Y]$ of 0.94 and a Q^2 of 0.916. Applying this model for the moisture prediction based on the last 5 in-line collected NIR spectra of the 6 test experiments (6x5) resulted in an RMSEP of 0.5659%. When only the last spectrum (6x1) of each test experiment was used, a similar RMSEP of 0.5676% was obtained. The model was optimized by removing calibration runs 0, 7 and 8 (these runs had a high standard deviation on the Karl Fischer measurements, hence creating doubt on the correctness of the reference measurements for these experiments). The $R^2[X]$ was 0.994 and both the $R^2[Y]$ and the Q^2 of this model were 0.962. The final model consisted out of four PLS components and an RMSEP (6x5) of 0.5608% and (6x1) 0.5649% was obtained. This model, including the spectral range

from 10000 to 4500 cm^{-1}, but excluding calibration experiment 0, 7 and 8 was used for further calculations (Figure 8.2).

The six in-line test experiments were performed at six different drying temperatures varying from 30°C to 80°C in steps of 10°C per experiment (Table 8.1). The end point of the drying cycle could be determined by means of real-time NIR monitoring of the granule's moisture content. The actual moisture content values, determined with Karl Fischer at the end of the drying cycle of each test experiment are shown in Figure 8.2 (red dashed line). The granules are considered as dry when a moisture content of 3.6% is reached, since this is the moisture content of the premix used to produce the granules. The in-line NIR predicted moisture contents during the entire drying process of each test experiment are also plotted in Figure 8.2 (blue full lines). During the first five drying minutes of each test experiment, the cell was loaded with granules and the NIR probe was not embedded in granules. The probe was measuring air and the resulting noisy spectra were therefore excluded. As drying proceeds, the moisture content, measured by means of NIR, reaches a steady state for all six test experiments. One can notice certain "plateaus" of the blue lines in the graphs (during the first part of drying), where for different time points exactly the same predicted moisture contents were obtained. The plateaus were caused by fouling of the NIR probe. When wet particles got stuck on the probe window, similar spectra were captured for several time points. This phenomenon can clearly be seen at the start of the cycles with low drying temperatures (T 30 and T 40). For the granule loads that were dry after the drying cycle (T 60, T 70 and T 80), the drying process end points can be clearly detected and are indicated in Figure 8.2.

Next page: **Figure 8.2.** Moisture content (%) in function of time (min). Prediction of moisture content according to in-line NIR measurements (full blue line) and residual moisture content as obtained by means of Karl Fischer after each test-experiment (red dashed line).

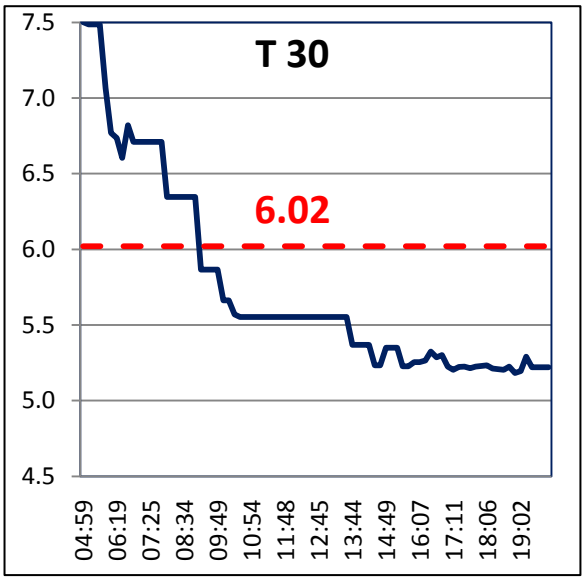
T 30
6.02
7.5
7.0
6.5
6.0
5.5
5.0
4.5
04:59
06:19
07:25
08:34
09:49
10:54
11:48
12:45
13:44
14:49
16:07
17:11
18:06
19:02

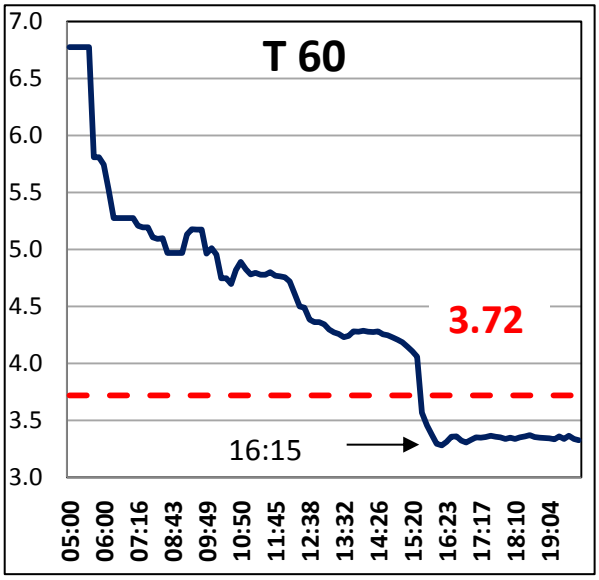
T 60
3.72
16:15
7.0
6.5
6.0
5.5
5.0
4.5
4.0
3.5
3.0
05:00
06:00
07:16
08:43
09:49
10:50
11:45
12:38
13:32
14:26
15:20
16:23
17:17
18:10
19:04

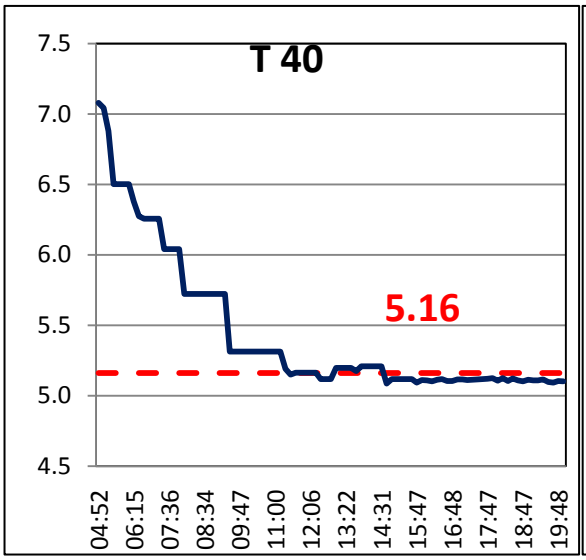
T 40
5.16
7.5
7.0
6.5
6.0
5.5
5.0
4.5
04:52
06:15
07:36
08:34
09:47
11:00
12:06
13:22
14:31
15:47
16:48
17:47
18:47
19:48

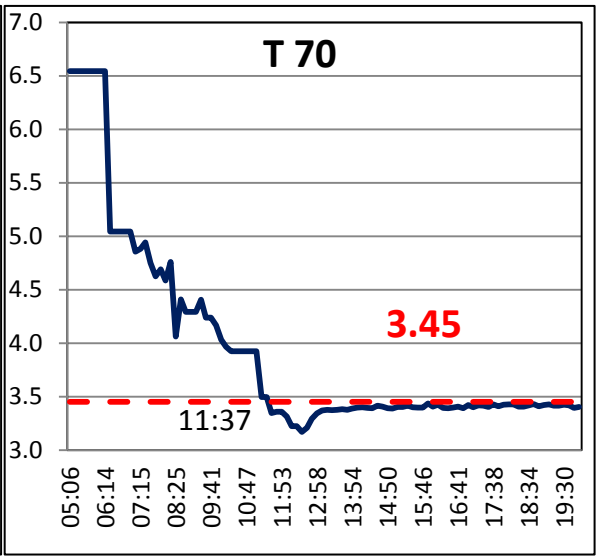
T 70
3.45
11:37
7.0
6.5
6.0
5.5
5.0
4.5
4.0
3.5
3.0
05:06
06:14
07:15
08:25
09:41
10:47
11:53
12:58
13:54
14:50
15:46
16:41
17:38
18:34
19:30

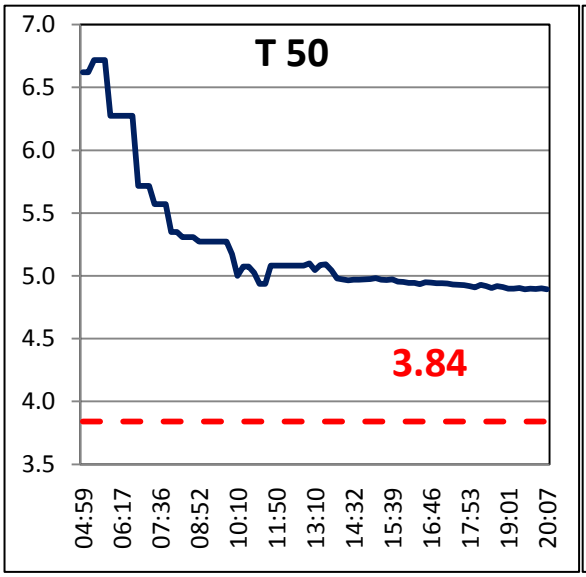
T 50
3.84
7.0
6.5
6.0
5.5
5.0
4.5
4.0
3.5
04:59
06:17
07:36
08:52
10:10
11:50
13:10
14:32
15:39
16:46
17:53
19:01
20:07

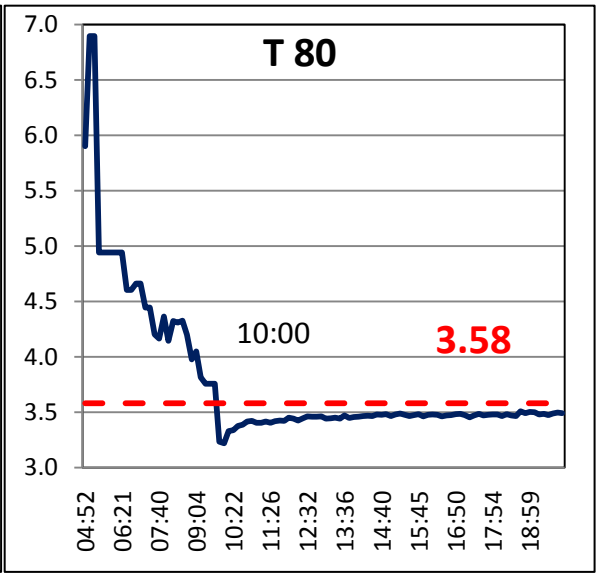
T 80
10:00
3.58
7.0
6.5
6.0
5.5
5.0
4.5
4.0
3.5
3.0
04:52
06:21
07:40
09:04
10:22
11:26
12:32
13:36
14:40
15:45
16:50
17:54
18:59

Conventionally, the end point of drying is estimated based on the measurement of the humidity of the outlet air or by evaluating the temperature of the drying product. These data are plotted in Figure 8.3 for the test experiments, which resulted in a dry product (i.e., test experiments which were dried at 60, 70 and 80°C). The time points when the humidity of the outlet air and the product temperature reach steady state are indicated as well as the end point predicted by the in-line NIR measurements (vertical blue line). Regarding the humidity of the outlet air, no steady state can be observed for the experiment conducted at 60°C. The humidity of the outlet air reaches a steady state for the experiments run at 70°C and 80°C, but this is at a later time instant compared to the drying process end point as indicated by the NIR moisture determination model. The product temperature seems to be a more reliable parameter for the drying endpoint determination of the six-segmented fluid bed dryer since each cell has its own temperature sensor installed, and the sensor is really embedded in the product. The determined product temperature steady states are indicated as well in Figure 8.3.

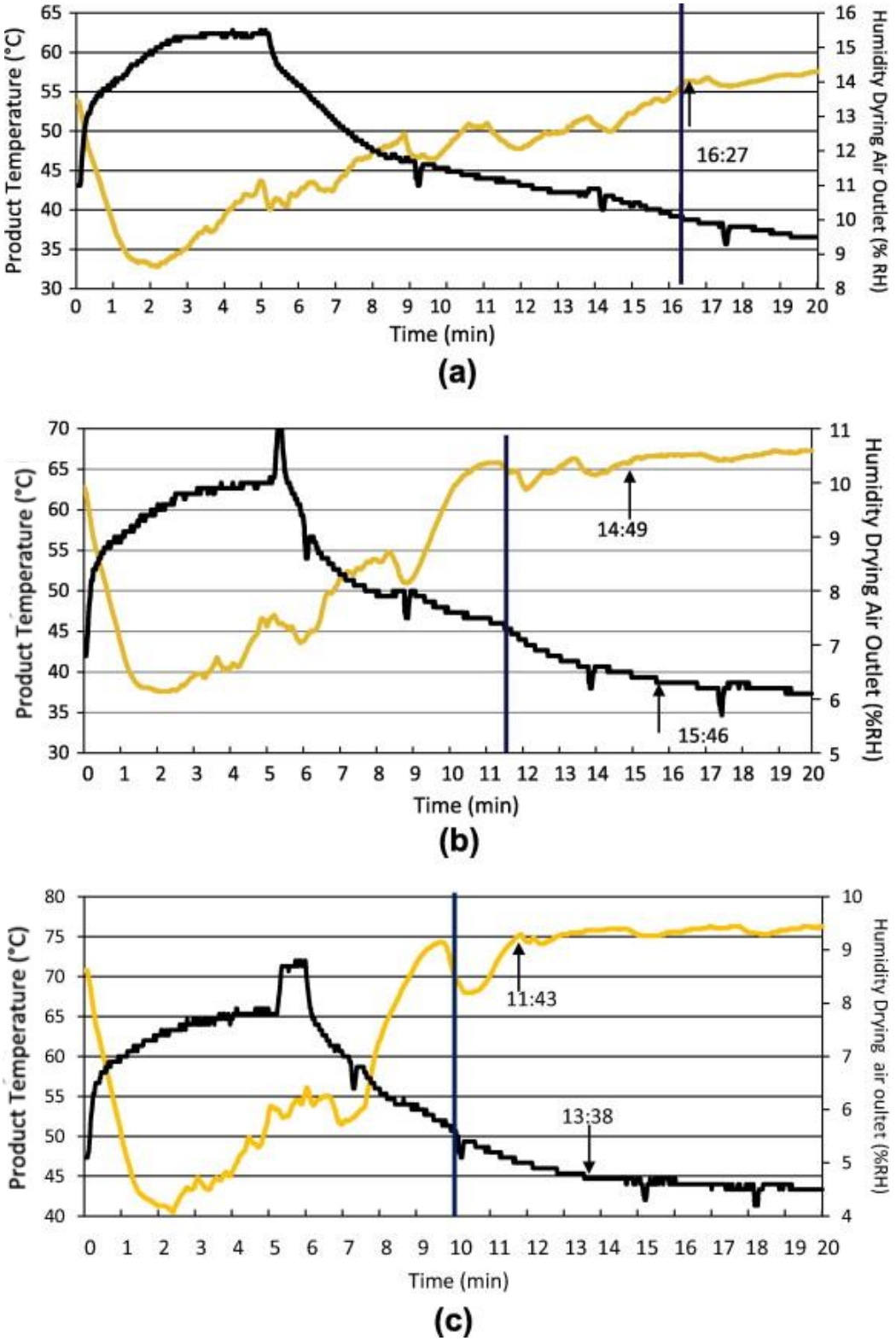

Figure 8.3. Product temperature (yellow line) and humidity of the outlet air (black line) during the test experiments dried at **a.** 60°C, **b.** 70°C and **c.** 80°C. The vertical blue line indicates the end-point as determined by the NIR-based moisture determination model.

The evolution of the granules' residual moisture content during drying can also be calculated using a mass balance, which was recently developed by our group for the six-segmented fluid bed drying system of the ConsiGma™-25 system [26]. Using this mass balance, univariate data (e.g., temperature of inlet and outlet air, product temperature during drying, humidity of inlet and outlet air), which are automatically and continuously logged by the ConsiGma™ 25-system are processed to calculate the amount of water, which evaporates from the granules during drying. Therefore, the water content of the dry premix - being 3.6% - has to be added to the moisture content values predicted via the mass balance model.

The drying curves obtained through the mass balance model are plotted in Figure 8.4. At the end of the drying cycle, the granules dried at 60, 70 and 80°C are considered to be dry according to the model (they reach 0%). This is confirmed by both the off-line Karl Fischer measurements and the NIR-based drying curves (Figure 8.2). The mass balance model predicted moisture content values at the end of the drying cycle when drying at 30, 40 and 50 °C are comparable to Karl Fischer findings (6.69 %, 5.93% and 4.3% respectively). The typical shape of the drying curves in Figure 8.4 can unfortunately not be compared with the curve obtained via NIR predictions (Figure 8.2), since it was only possible to collect good spectra after five drying minutes in the used experimental set-up (cfr. supra). When comparing the NIR model and mass balance model based obtained moisture content values after five minutes of drying, mass balance model predictions are approximately 2% (absolute value) higher than the values obtained by means of NIR prediction, when granules are dried at 30, 40 and 50°C. When granules are dried at 60, 70 an 80°C the predicted moisture value by the NIR method is comparable to the moisture value calculated via the mass balance model.

As an example, in Figure 8.5, the moisture contents as predicted by the NIR calibration model and the mass balance model for the experiment performed at 70°C are presented in an overlay plot. A value of 3.6% (i.e. moisture content of the dry premix) is added to the mass balance model predictions for better comparison.

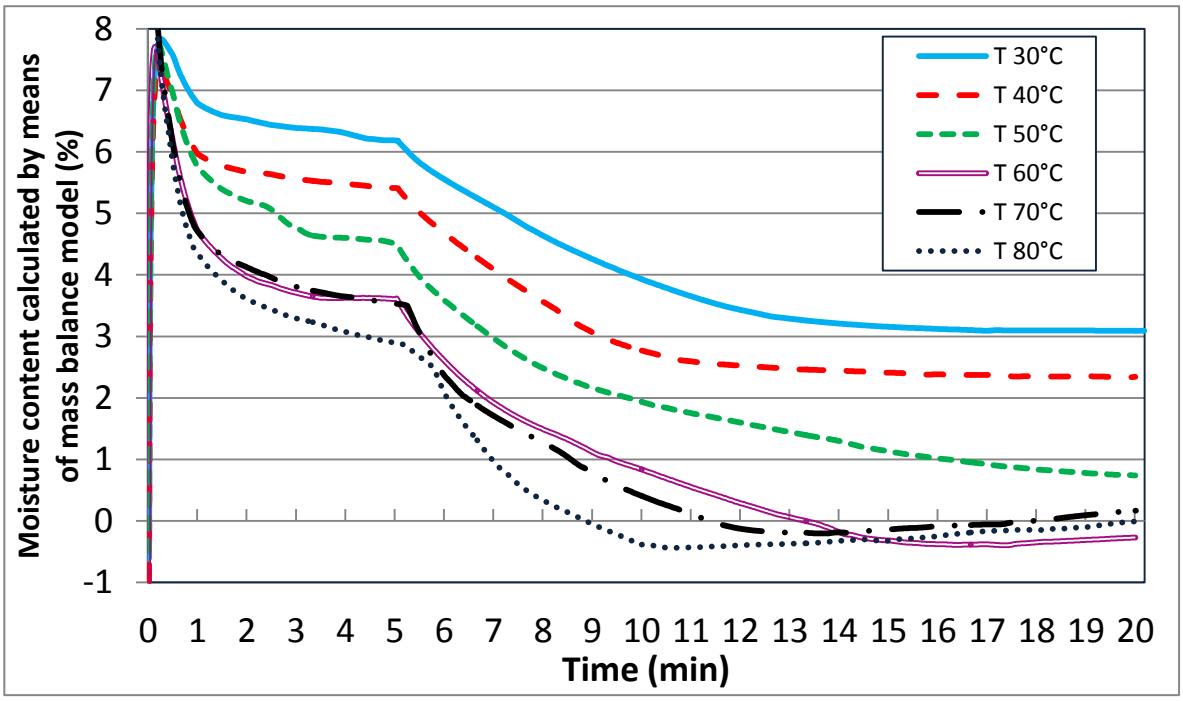

Figure 8.4. Drying curves of the six different test experiments as calculated with the mass balance model.

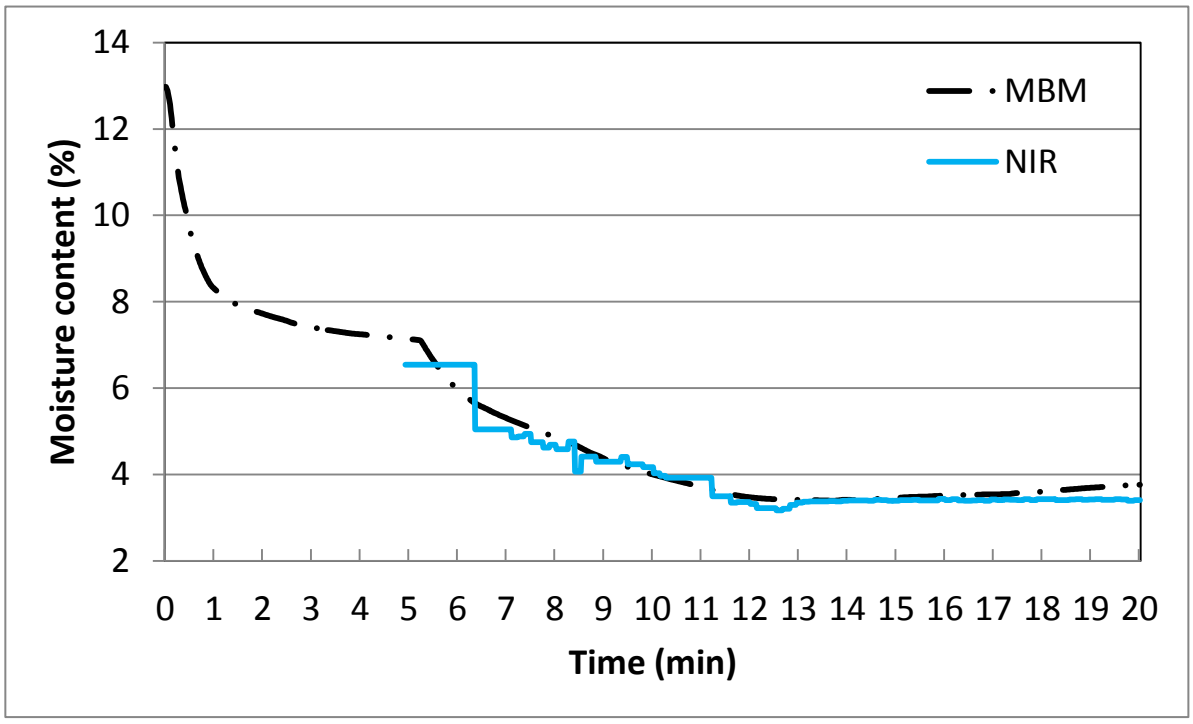

Figure 8.5. Experiment at 70°C: Overlay of the predicted moisture content via the mass balance model (MBM, dotted black line) and the NIR-calibration model (NIR, full blue line).

Even though the granules are not dry when a temperature of 30°C or 40°C is applied, a steady-state in the drying curves can be observed in Figure 8.4. The same steady-state can be seen in the NIR prediction curves, which suggests that at lower temperatures after a given time no extra water evaporates from the granules, even though they are not dry yet and still fluidizing. The experiment ran at 50°C does not show this steady-state, but a slow decrease in water moisture content during the last five minutes in both the moisture curves obtained by the NIR-model as the mass balance model can be detected. This means the results of the mass balance model and the NIR based model are in line.

8.3.2. In-line solid state monitoring

8.3.2.1. In-line Raman spectroscopy

The theophylline solid state changes were monitored using in-line Raman spectroscopy during the six test experiments (Figures 8.6a-f). Some spectral differences can be noted according to the applied temperature of the drying air. To evaluate the solid state of theophylline, one should focus on the spectral region from 1650 to 1750 cm^{-1}, since theophylline monohydrate shows a band at 1687.5 cm^{-1}, whereas a spectrum of anhydrous theophylline shows two peaks, one at 1665 cm^{-1} and one at 1707 cm^{-1} [7]. Furthermore, a metastable form of theophylline exists, which shows a typical Raman band at 1692 cm^{-1} [27]. When granules were dried at 30°C, no spectral changes (i.e. changes in solid state) can be noticed (Figure 8.6a). Only a band at 1687.5 cm^{-1} can be seen indicating that theophylline remains in the monohydrate form from the start till the end of the drying cycle at 30°C. In the spectra, collected during drying at 50°C (Figure 8.6c), two extra peaks can be noticed at 1665 cm^{-1} and 1707 cm^{-1}, indicating that an amount of theophylline is dehydrated to the anhydrous form. This can also be noted, when granules are dried at 40°C albeit to a much lesser extent (Figure 8.6b). The test experiments with drying temperatures of 60°C and up (Figures 8.6d, 8.6e and 8.6f) show a shift of the Raman band at 1687.5 cm^{-1} to 1692 cm^{-1}. This shift denotes a polymorphic change from theophylline monohydrate to metastable theophylline. When comparing Figure 8.6d to Figures 8.6e and 8.6f, the color code of the spectra shows that the higher the temperature of the incoming air is, the faster this conversion takes place. Furthermore, additional peaks at 1665 cm^{-1} and 1707 cm^{-1} appear during these test experiments, indicating the formation of anhydrous theophylline. This

means that the dried granules of these test experiments contain both metastable and anhydrous theophylline.

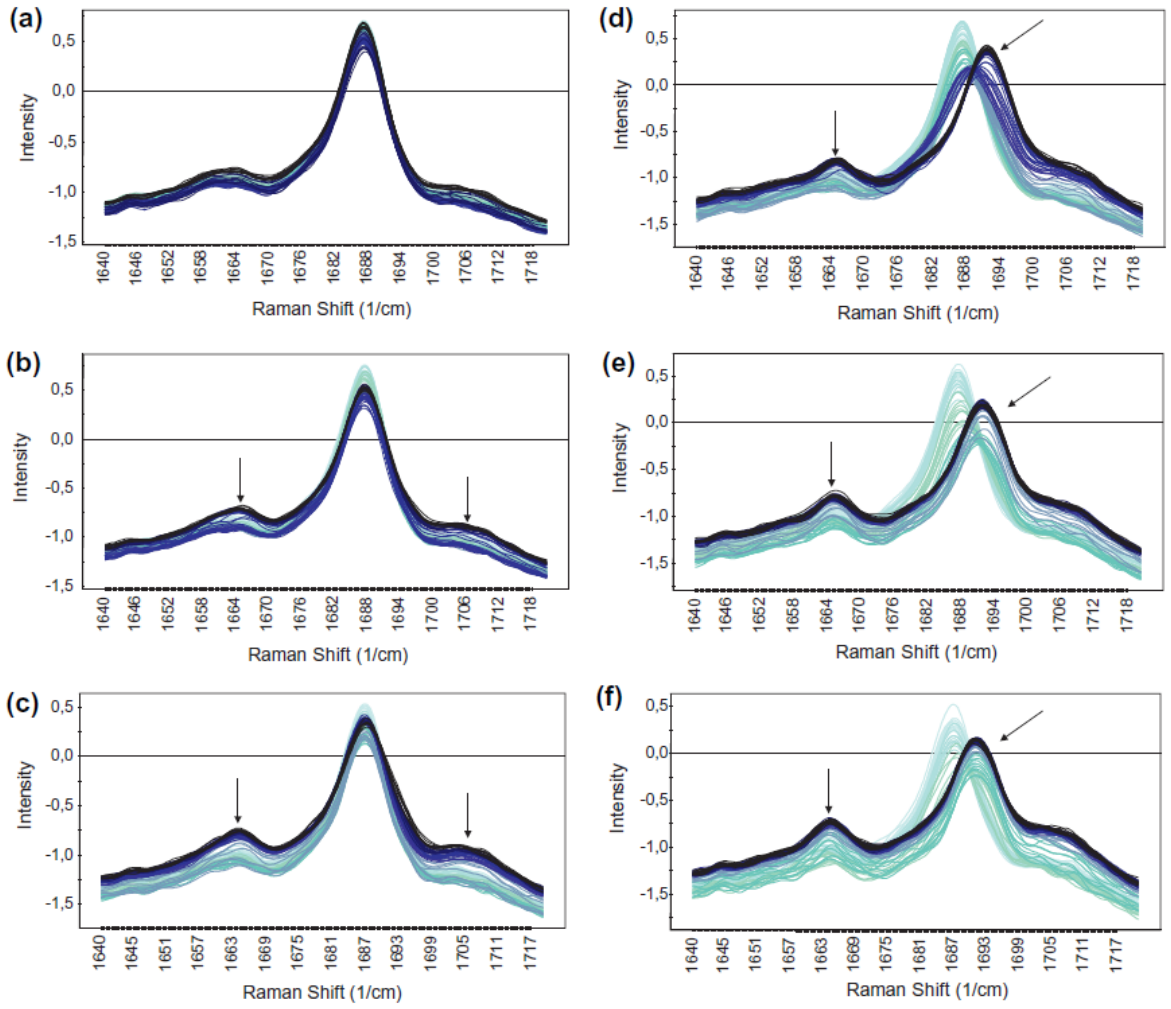

Figure 8.6. In-line Raman spectra collected during the six test experiments. The spectra are colored from light blue to black according to drying time. The first spectrum is light blue while the last collected spectrum is black. Test experiments dried at **a.** 30°C, **b.** 40°C, **c.** 50°C, **d.** 60°C, **e.** 70°C, **f.** 80°C.

The findings regarding the solid state of theophylline correspond with the detected steady-states in the drying curves (Figures 8.2 and 8.4) of the test-experiments conducted at 30 and 40°C. From a certain timepoint, no more water is evaporating during these experiments, furthermore theophylline stays in the monohydrate form. These findings suggest that, when drying at 30 or 40°C the theophylline hydrate water will stay bound to the theophylline

molecule and hence no extra water will evaporate. For the test experiment conducted at 50°C a slow conversion from theophylline monohydrate to anhydrous theophylline can be noted. This can be correlated with the slightly decreasing slope in the NIR predicted drying curve (minute 13 till end) and the slope in the mass balance calculated curve (minute 10 till end).

The spectra collected during the drying test experiment at 60°C were analyzed using principal component analysis (PCA). The spectral region from 200 cm^{-1} to 1800 cm^{-1} was centered and SNV-corrected. The resulting principal component 1 vs. principal component 2 scatter scores plot (Figure 8.7) shows the transition from theophylline monohydrate towards a mixture of metastable and anhydrous theophylline.

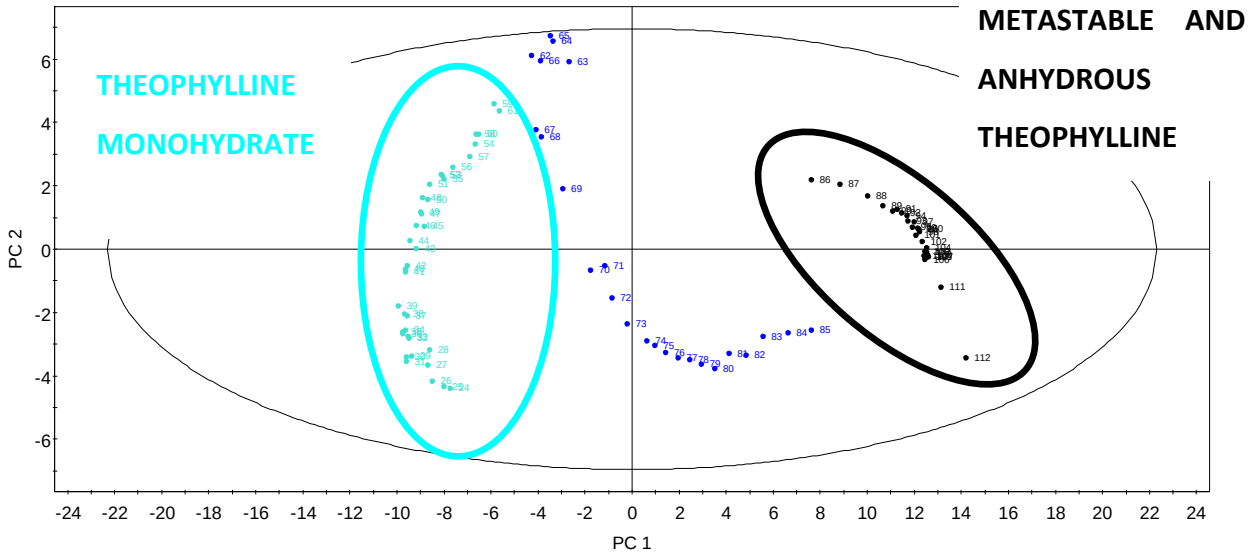

Figure 8.7. PC 1 versus PC 2 scores plot of the Raman spectra of the test experiment at 60°C.

The first principal component represented 84.65% of the spectral variance, the second 8.25%. The spectra taken in the first 12 minutes only show a band at 1687.5 cm^{-1} indicating that theophylline remained in the monohydrate state. After 15 minutes the band has clearly shifted to 1692 cm^{-1}, and bands at 1665 cm^{-1} and 1707 cm^{-1} appear as well. From minute 12 to minute 15, one can observe a transition period in the plotted data and the Raman spectra. When drying at 70°C it took 11m30s to convert theophylline monohydrate to a mixture of metastable and anhydrous theophylline and the transition period started after 8 minutes. A mixture of metastable theophylline and anhydrous theophylline could be

detected after 11 minutes of drying at 80°C. A transition period from the eighth till the eleventh minute could be observed. These findings are different compared to the results obtained by others, since some found the metastable theophylline at lower drying temperatures (40°C) [28] when heating theophylline monohydrate powder in a variable temperature X-ray powder diffractometer. Morris et al. [29] stated that the metastable form of theophylline most likely occurs at low temperatures (< 60°C) when fluid bed drying is applied after wet granulation. These findings were confirmed when theophylline was wet-massed, followed by drying at 60°C during 50 minutes [30]. Airaksinen et al. [31] already found metastable theophylline when drying at a temperature as low as 30°C and using dry inlet air. When using ambient air for drying the highest relative amount of metastable theophylline was found when drying at 40°C. The differences in observations compared to this study, where metastable theophylline could only be found at 60°C, might be due to the fact that all other mentioned authors used pure theophylline or pure theophylline granules and did not use any excipients.

8.3.2.2. In-line NIR spectroscopy

When evaluating the in-line recorded NIR spectra, not only the disappearing water bands attract attention. As for Raman spectroscopy, the changes in solid state of the API can also be identified in the NIR spectra. Two extra bands appear during dehydration, which can be attributed to appearance of anhydrous theophylline: one at 5962 cm^{-1} and one, less obvious at 6009 cm^{-1} [7]. Near-infrared spectroscopy is incapable of differentiating between stable and metastable anhydrous theophylline [14]. In Figure 8.8, the spectral range from 5900 to 6100 cm^{-1} of the in-line collected spectra (T=60°C) was selected and was corrected using SNV. PCA was applied on these corrected spectra. Figure 8.9 shows the resulting PC 1 versus PC 2 scores plot for this test experiment. The PC 1 represented 95.1% of the variance and PC 2 represented 3.91%. Three clusters can be distinguished in the scores plot: (i) the spectra of the first 12m30s, (ii) the spectra collected between 12m30s and 15m45s (iii) the spectra collected after 15m45s minutes of drying. During the first 12m30s no bands can be seen at 5962 cm^{-1} and 6009 cm^{-1}, indicating that all theophylline remained in the monohydrate form. After 15m45s, the two extra bands appear clearly, indicating the transformation to anhydrous theophylline. Between 12m30s and 15m45s a mixture of theophylline anhydrate

and monohydrate was found. For the test experiment conducted at 70°C, anhydrous theophylline could be found after 11m15s. When granules were dried at 80°C, the anhydrous theophylline bands appeared after 9 minutes.

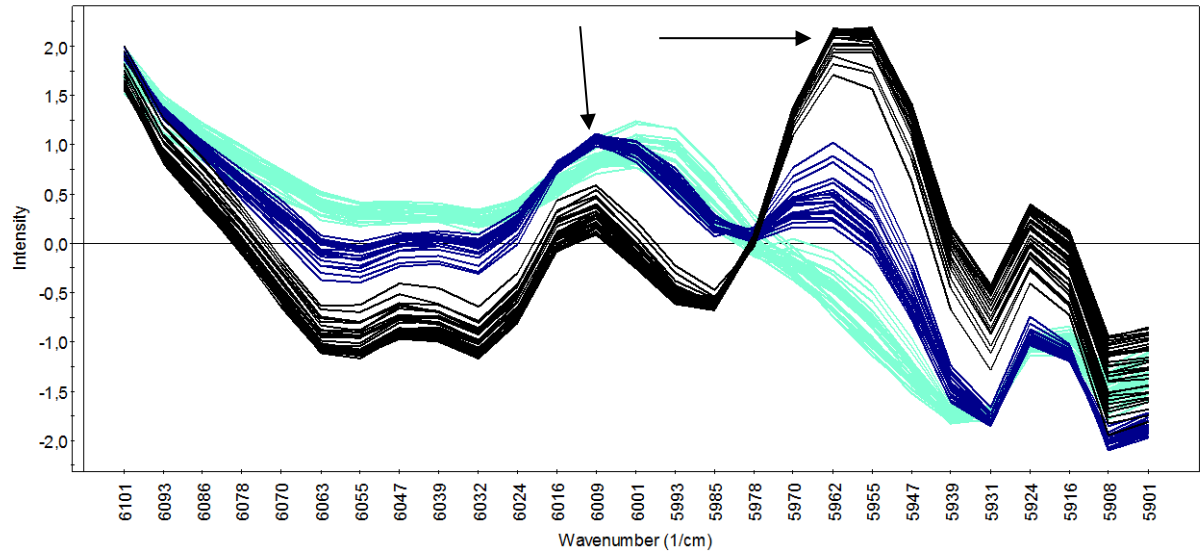

Figure 8.8. In-line collected NIR spectra, SNV-corrected in the spectral range from 6100 to 5900 cm^{-1}. The earliest spectrum is light blue changing to black for the last spectrum, test experiment at 60°C.

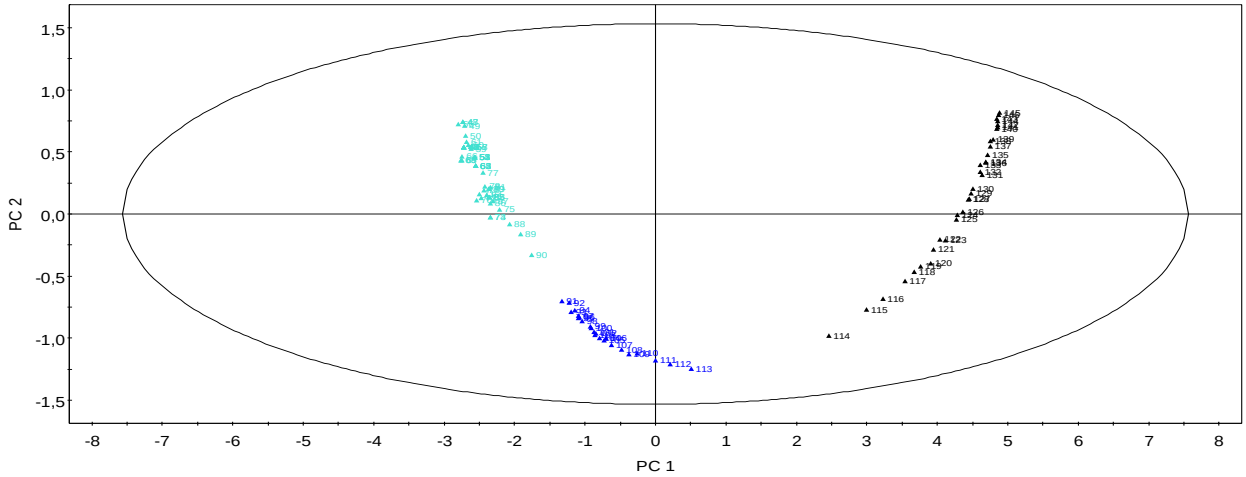

Figure 8.9. PCA of In-line collected NIR spectra, SNV-corrected in the spectral range from 6100 to 5900 cm^{-1}. PC 1 vs PC 2 scores plot, test experiment at 60°C.

8.3.2.3. End point detection during drying and solid state monitoring: evaluation of different techniques

Four different methods to detect the end point of a drying cycle have been presented: (i) by means of an NIR-based PLS model, (ii) by logging of the humidity of the outlet air, (iii) by logging of the product temperature and (iv) by means of a mass balance model. Secondly, NIR and Raman proved to be able to monitor the solid state changes of the API in real-time during drying. Table 8.2 shows an overview of the time points (end of drying or solid state change) as calculated using the different methods. For the indirect methods (ii) and (iii), a clear steady state can be found for the product temperature, but not for the humidity of the outlet drying air. Both the NIR prediction model and the mass balance model indicate the drying process end point sooner than the two indirect methods. The dehydration of theophylline monohydrate was monitored with both NIR and Raman spectroscopy. The time points of conversion from theophylline monohydrate to anhydrous theophylline, derived from the Raman and NIR spectra respectively, are comparable. It is important to emphasize that both measurements were conducted in different cells of the dryer, and thus a small deviation between the results obtained from both spectroscopic methods is understandable. These time points are also comparable with the drying process end points calculated using the NIR-based PLS model. It can be concluded that the in-line monitoring of moisture content by means of PAT tools and mass balance models is beneficial. The indirect methods seem to overestimate the needed drying time. It should be remarked that, unlike a conventional fluid bed dryer where only one load is dried at a time, the Consigma™ 25 consists of six parallel drying cells, and that only one humidity sensor is placed on top of the dryer. For this reason, the NIR method is to be preferred over the mass balance approach in a production set-up, since the measured humidity of the outlet air will correspond to the average value of the six cells when all drying cells are filled with product. Secondly, NIR spectroscopy DoEs not only provide information regarding residual moisture, but also regarding the solid state of the API (and excipients). Raman spectroscopy will give information regarding the solid state, and is able to differentiate between anhydrous theophylline and metastable theophylline. Challenges for a successful integration of in-line NIR and Raman spectroscopy are (i) the avoidance of fouling of the probe; and, (ii) an adequate method to mount the probe in the dryer should be found as well, so that spectra

can be collected from the very start of the drying cycle. Furthermore software packages with high performances for the fast collection and processing of in-line data would be beneficial.

Table 8.2. Summary and comparison between the different detected drying process end points and solid state changes from theophylline monohydrate towards metastable and anhydrous theophylline.

		Drying endpoint according to					**Timepoint of solid state shift according to**	
Applied Temperature (°C)		NIR PLS model	Mass balance model	Humidity of the outlet air	Product temperature		Raman	NIR
60		16:08	13:30	/	16:27		15:00	15:45
70		11:37	11:15	15:46	14:49		11:30	11:15
80		10:00	9:00	13:38	11:43		11:00	9:00

8.4. CONCLUSION

Raman and NIR spectroscopy were used successfully for the real-time monitoring of a fluid bed drying process. The drying process end point could be predicted by means of an NIR-based PLS model. NIR spectroscopy proved to be superior to conventional end point determination by means of indirect process parameters or mass balance modeling in a production set-up. NIR and Raman spectroscopy proved to be capable of in-line solid state monitoring as well. The time point of conversion to the dehydrated state of the API was comparable to the drying process end point.

8.5. REFERENCES

[1] C. Vervaet, J.P. Remon, Continuous granulation in the pharmaceutical industry, Chemical Engineering Science, 60 (2005) 3949-3957.

[2] G. Betz, P. Junker-Burgin, H. Leuenberger, Batch and continuous processing in the production of pharmaceutical granules, Pharmaceutical Development and Technology, 8 (2003) 289-297.

[3] H. Leuenberger, New trends in the production of pharmaceutical granules: batch versus continuous processing, European Journal of Pharmaceutics and Biopharmaceutics, 52 (2001) 289-296.

[4] H. Leuenberger, Scale-up in the 4th dimension in the field of granulation and drying or how to avoid classical scale-up, Powder Technology, 130 (2003) 225-230.

[5] H. Leuenberger, New trends in the production of pharmaceutical granules: the classical batch concept and the problem of scale-up, European Journal of Pharmaceutics and Biopharmaceutics, 52 (2001) 279-288.

[6] J. Werani, M. Grunberg, C. Ober, H. Leuenberger, Semicontinuous granulation - the process of choice for the production of pharmaceutical granules?, Powder Technology, 140 (2004) 163-168.

[7] M. Fonteyne, J. Vercruysse, D.C. Díaz, D. Gildemyn, C. Vervaet, J.P. Remon, T.D. Beer, Real-time assessment of critical quality attributes of a continuous granulation process, Pharmaceutical Development and Technology, 18 (2013) 85-97.

[8] M. Fonteyne, S. Soares, J. Vercruysse, E. Peeters, A. Burggraeve, C. Vervaet, J.P. Remon, N. Sandler, T. De Beer, Prediction of quality attributes of continuously produced granules using complementary pat tools, European Journal of Pharmaceutics and Biopharmaceutics, 82 (2012) 429-436.

[9] J. Vercruysse, D. Córdoba Díaz, E. Peeters, M. Fonteyne, U. Delaet, I. Van Assche, T. De Beer, J.P. Remon, C. Vervaet, Continuous twin screw granulation: Influence of process variables on granule and tablet quality, European Journal of Pharmaceutics and Biopharmaceutics, 82 (2012) 205-211.

[10] L. Chablani, T.M. K, M. Amit, R. Patrick, S.W. C, Inline Real-Time Near-Infrared Granule Moisture Measurements of a Continuous Granulation-Drying-Milling Process, AAPS PharmsciTech, 12 (2011) 1050-1055.

[11] J. Vercruysse, U. Delaet, I. Van Assche, P. Cappuyns, F. Arata, G. Caporicci, T. De Beer, J.P. Remon, C. Vervaet, Stability and repeatability of a continuous twin screw granulation and drying system., European Journal of Pharmaceutics and Biopharmaceutics, 85 (2013) 1031-1038.

[12] FDA-Adminstration, Guidance for Industry - PAT - A Framework for Innovative Pharmaceutical Development, Manufacturing, and Quality Assurance, in, 2004.

[13] K. Wöstheinrich, P.C. Schmidt, Evaluation and validation of a fully instrumented Hüttlin HKC 05-TJ laboratory-scale fluidized bed granulator, Drug Development and Industrial Pharmacy, 26 (2000) 621-633.

[14] J. Aaltonen, K. Kogermann, C.J. Strachan, J. Rantanen, In-line monitoring of solid state transitions during fluidisation, Chemical Engineering Science, 62 (2007) 408-415.

[15] P. Frake, D. Greenhalgh, S.M. Grierson, J.M. Hempenstall, D.R. Rudd, Process control and end-point determination of a fluid bed granulation by application of near infra-red spectroscopy, International Journal of Pharmaceutics, 151 (1997) 75-80.

[16] R.L. Green, G. Thurau, N.C. Pixley, A. Mateos, R.A. Reed, J.P. Higgins, In-line monitoring of moisture content in fluid bed dryers using near-IR spectroscopy with consideration of sampling effects on method accuracy, Analytical Chemistry, 77 (2005) 4515-4522.

[17] A. Hartung, M. Knoell, U. Schmidt, P. Langguth, Role of continuous moisture profile monitoring by inline NIR spectroscopy during fluid bed granulation of an Enalapril formulation, Drug Development and Industrial Pharmacy, 37 (2011) 274-280.

[18] F.J.S. Nieuwmeyer, M. Damen, A. Gerich, F. Rusmini, K. van der Voort, H. Vromans, Granule characterization during fluid bed drying by development of a near infrared method to determine water content and median granule size, Pharmaceutical Research, 24 (2007) 1854-1861.

[19] A. Peinado, J. Hammond, A. Scott, Development, validation and transfer of a Near Infrared method to determine in-line the end point of a fluidised drying process for commercial production batches of an approved oral solid dose pharmaceutical product, Journal of Pharmaceutical and Biomedical Analysis, 54 (2011) 13-20.

[20] J. Rantanen, S. Lehtola, P. Ramet, J.P. Mannermaa, J. Yliruusi, On-line monitoring of moisture content in an instrumented fluidized bed granulator with a multi-channel NIR moisture sensor, Powder Technology, 99 (1998) 163-170.

[21] J. Rantanen, O. Antikainen, J.P. Mannermaa, J. Yliruusi, Use of the near-infrared reflectance method for measurement of moisture content during granulation, Pharmaceutical Development and Technology, 5 (2000) 209-217.

[22] J. Rantanen, A. Jorgensen, E. Rasanen, P. Luukkonen, S. Airaksinen, J. Raiman, K. Hänninen, O. Antikainen, J. Yliruusi, Process analysis of fluidized bed granulation, AAPS PharmsciTech, 2 (2001) article 21.

[23] E. Rasanen, J. Rantanen, J.P. Mannermaa, J. Yliruusi, H. Vuorela, Dehydration studies using a novel multichamber microscale fluid bed dryer with in-line near-infrared measurement, Journal of Pharmaceutical Sciences, 92 (2003) 2074-2081.

[24] M. Romer, J. Heinamaki, I. Miroshnyk, N. Kivikero, N. Sandler, J. Rantanen, J. Yliruusi, Phase transformation of erythromycin a dihydrate during fluid bed drying, Journal of Pharmaceutical Sciences, 97 (2008) 4020-4029.

[25] K. Kogermann, J.A. Zeitler, J. Rantanen, T. Rades, P.F. Taday, M. Pepper, J. Heinamaki, C.J. Strachan, Investigating dehydration from compacts using terahertz pulsed, Raman, and near-infrared spectroscopy, Applied Spectroscopy, 61 (2007) 1265-1274.

[26] S.T.F.C. Mortier, K.V. Gernaey, T. De Beer, I. Nopens, Analysing drying unit performance in a continuous pharmaceutical manufacturing line by means of mass - energy balances European Journal of Pharmaceutics and Biopharmaceutics, *submitted* (2013).

[27] A. Dukic-Ott, T. De Beer, J.P. Remon, W. Baeyens, P. Foreman, C. Vervaet, In-vitro and in-vivo evaluation of enteric-coated starch-based pellets prepared via extrusion/spheronisation, European Journal of Pharmaceutics and Biopharmaceutics, 70 (2008) 302-312.

[28] N.V. Phadnis, R. Suryanarayanan, Polymorphism in anhydrous theophylline - Implications on the dissolution rate of theophylline tablets, Journal of Pharmaceutical Sciences, 86 (1997) 1256-1263.

[29] K.R. Morris, U.J. Griesser, C.J. Eckhardt, J.G. Stowell, Theoretical approaches to physical transformations of active pharmaceutical ingredients during manufacturing processes, Advanced Drug Delivery Reviews, 48 (2001) 91-114.

[30] M. Alleso, F. Tian, C. Cornett, J. Rantanen, Towards Effective Solid Form Screening, Journal of Pharmaceutical Sciences, 99 (2010) 3711-3718.

[31] S. Airaksinen, M. Karjalainen, E. Rasanen, J. Rantanen, J. Yliruusi, Comparison of the effects of two drying methods on polymorphism of theophylline, International Journal of Pharmaceutics, 276 (2004) 129-141.

CHAPTER 9

NIR SPECTROSCOPIC METHOD FOR IN-LINE MOISTURE ASSESSMENT: VALIDATION OF QUANTIFYING ABILITIES AND UNCERTAINTY ASSESSMENT

"The logic of validation allows us to move

between the two limits of dogmatism and skepticism."

Paul Ricœur (1913-2005)

Fonteyne M., Arruabarrena J., De Beer J., Hellings M., Van den Kerkhof T., Burggraeve A., Vervaet C., Remon J.P., De Beer T. (2014) NIR spectroscopic method for the in-line assessment during drying in a six-segmented fluid bed dryer of a continuous tablet production line: validation of quantifying abilities and uncertainty assessment, Journal of Pharmaceutical and Biomedical Analysis, *submitted (moderate revision)*.

ABSTRACT

This study focuses on the thorough validation of an in-line NIR based moisture quantification method in the six-segmented fluid bed dryer of a continuous from-powder-to-tablet manufacturing line (ConsiGma™ 25, GEA Pharma Systems nv, Wommelgem, Belgium). The moisture assessment ability of an FT-NIR spectrometer (Matrix™-F Duplex, Bruker Optics Ltd, UK) equipped with a fiber-optic Lighthouse Probe™ (LHP, GEA Pharma Systems nv, Wommelgem, Belgium) was investigated. Although NIR spectroscopy is a widely used technique for in-process moisture determination, a minority of NIR spectroscopy methods is thoroughly validated.

A moisture quantification PLS model was developed. Twenty calibration experiments were conducted, during which spectra were collected at-line and then regressed versus the corresponding residual moisture values obtained via Karl Fischer measurements. The developed NIR moisture quantification model was then validated by calculating the accuracy profiles on the basis of the analysis results of independent in-line validation experiments. Furthermore, as the aim of the NIR method is to replace the destructive, time-consuming Karl Fischer titration, it was statistically demonstrated that the new NIR method performs at least as good as the Karl Fischer reference method.

CHAPTER 9

NIR SPECTROSCOPIC METHOD FOR IN-LINE MOISTURE ASSESSMENT: VALIDATION OF QUANTIFYING ABILITIES AND UNCERTAINTY ASSESSMENT

9.1. INTRODUCTION

In 2004, the Food and Drug Administration (FDA) launched their PAT-Guidance for Industry' [1]. One of the goals of this guidance is to encourage the pharmaceutical industry to imply innovative methods for quality assurance, based on measurements during processing and enhancing in-depth process understanding. It is stated that the use of PAT tools and -principles will lead to an increased process knowledge which should allow better process control. Real-time process information can be used to overcome the limitations of time-defined process end points, which are commonly used in pharmaceutical industry. In case of fluid bed drying for example, it is not opportune to dry longer than necessary. Thanks to industrial drivers, recent technological advances in process analyzers make real-time measurement of critical process parameters and quality attributes possible. To allow in-line monitoring, analyzers should be non-destructive, fast and mountable in the process. Furthermore, the analyzer should be capable of collecting data without sample-pretreatment. Therefore, near infrared (NIR) spectroscopy has found its way to the pharmaceutical industry already for a long time.

NIR has been reported to be a powerful tool for water determination. It has found multiple applications for the quantitative determination of moisture content during the manufacturing of pharmaceutical solid dosage forms [2]. Several authors reported the in-

line, on-line and at-line use of NIR spectroscopy to determine the moisture content of pharmaceutical products during granulation and drying [3-18]. These authors developed multivariate calibration models, e.g. Partial Least Squares (PLS)-models, for the prediction of moisture content, using either Loss on Drying or Karl Fischer titration as reference method. They validated their models by means of validation parameters, such as the Standard Error of Calibration (SEC), the Standard Error of Prediction (SEP) as well as the Root Mean Square Error of Calibration (RMSEC), the RMSE of Cross Validation (RMSECV), the RMSE of Prediction (RMSEP) and the R^2. Among these, the best measure for the predictive power of the model is the RMSEP, since this includes the evaluation of an external test-set.

However, all these validation parameters do not guarantee that future measures will be inside predefined acceptance limits [19]. Hubert et al. presented a validation strategy allowing to evaluate the proportion of expected future measures that will fall inside the acceptance limits. The acceptance limit is the accepted difference between the 'measured value' and the unknown true value [20-22]. This validation strategy is based on the use of accuracy profiles and is in full compliance with the regulatory quality guidelines. Mantanus et al. for example constructed a PLS model, which predicted the moisture content in pellets by means of NIR spectroscopy [23]. They concluded that the SEC and SEP were not sufficient to validate the method and therefore applied the accuracy profile approach. More case studies for the application of accuracy profiles to mainly off-line NIR spectroscopic methods have been reported by De Bleye et al. [19]. Raman spectroscopic methods for the determination of medroxyprogesterone in pharmaceutical suspensions [24] and metoprolol tartrate during hot-melt extrusion [25] have been validated using accuracy profiles as well.

The **aim** of this study was to validate a method for the in-line moisture determination of granules via NIR spectroscopy in the six-segmented fluid bed dryer of a fully continuous from powder-to-tablet production line. An NIR system equipped with a fiber-optic Lighthouse Probe™ was implemented in the dryer. The granulas were produced via high shear twin screw wet granulation. The validation of the NIR based moisture assessment was based on the use of accuracy profiles as presented by the SFSTP (La Societé Française des Sciences et Techniques Pharmaceutiques) [20-22]. Furthermore, from the validation measurements performed to apply the accuracy profile validation strategy, the measurement uncertainty

was estimated as described by Feinberg et al. [26, 27]. As the final aim was to evaluate whether the in-line NIR method is able to replace the off-line Karl Fischer method, the proposed method must perform at least as good as the reference method. Therefore, a comparison of the performance (precision and bias) of both methods was made via the approach proposed by [28, 29].

9.2. MATERIALS AND METHODS

9.2.1. Materials

All continuous granulation and fluid bed drying experiments were performed with the same powder premix. Anhydrous theophylline (Farma-Quimica sur SL, Malaga, Spain) (30%, w/w) was granulated with lactose monohydrate 200M (Caldic, Hemiksem, Belgium). Polyvinylpyrrolidone (Kollidon 30®, BASF, Burgbernheim, Germany) was used as a binder and added to the dry powder mixture at a concentration of 2.5% (w/w). Distilled water was used as granulation liquid.

9.2.2. NIR equipment

An FT-NIR spectrometer (Matrix^{TM}-F Duplex, Bruker Optics Ltd, UK) equipped with a fiber optic Lighthouse Probe^{TM} (LHP, GEA Pharma Systems nv, Wommelgem, Belgium) was used for this study. The Lighthouse Probe^{TM} was mounted in cell 2 of the fluid bed dryer (see description of the continuous system below). For all spectra a resolution of 8 cm^{-1} was applied and each spectrum was the average of 32 scans. This resulted in one spectrum collected every 20 seconds. The applied spectral range was 10,000 to 4,500cm^{-1}.

9.2.3. Karl Fischer moisture determination

The residual moisture content of the granules after drying was determined by volumetric Karl Fischer titration using a V30 volumetric Karl Fischer titrator (Mettler Toledo, USA). Methanol (Hydranal, Sigma Aldrich, Germany) was used as solvent. Before titration, granules were stirred and dissolved during three minutes. Measurements were done in triplicate.

9.2.4. Continuous granulation and drying

For continuous granulation and drying, the ConsiGma™ 25 unit (GEA Pharma Systems nv., Collette™, Wommelgem, Belgium) was used [30]. The six-segmented dryer is equipped with two probe interfacing places, namely in cell 2 and cell 5. PAT probes can be mounted in these cells, hence enabling in-line measurements. For both the calibration and validation experiments (see below), the granulator settings were kept constant. The raw material premix was fed at a rate of 17.5 kg/h, a screw speed of 950 rpm was applied and the barrel

temperature was kept constant at 25°C. The distilled water was added with a rate of 32 g/min. The same airflow was applied in the fluid bed dryer for all experiments: 360 m^3/h.

9.2.5. Development of the NIR moisture determination calibration model

For the development of the calibration model, granules with five different moisture levels were prepared (Figure 9.1). To obtain these granules, five granulation runs were performed in which the applied drying air temperature was varied between 35°C and 80°C. The cell filling time was kept constant at 180s and granules were dried during 600s. The granules for which the highest moisture content was aimed, were only dried for 300s. Each moisture level experiment was repeated four times, spread over two days (hence resulting in a total of 5 x 4 = 20 calibration experiments). After each calibration experiment, five NIR spectra were immediately collected at-line. Simultaneously, three samples were collected for Karl Fischer measurements. These measurements were performed immediately. Nevertheless, since only one Karl Fischer titrator was available, the second and third Karl Fischer measurement had a certain 'lag time' before they were measured. Spectra were Standard Normal Variate (SNV) corrected prior to further analysis and the three Karl Fischer measurements were averaged in order to obtain one moisture content value for each calibration experiment that was then correlated to the five corresponding collected NIR spectra from that run. Taking the 20 calibration experiments into account, the obtained KF moisture contents varied between 3.4% and 7.21%.

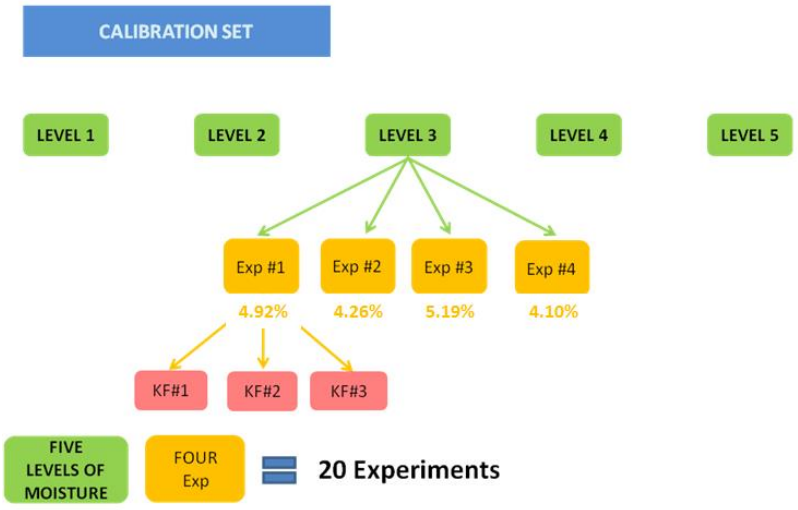

Figure 9.1. Overview of the performed calibration experiments.

9.2.6. Validation of the in-line NIR moisture assessment method

For the validation experiments the drying cells were filled during 300s and a total drying time of 900s was applied. The temperature of the drying air was changed between 35°C and 75°C in order to obtain three different moisture content (Figure 9.2). The low level had an average moisture content of 3.67%, the medium moisture content was 4.79% and the highest moisture content was 6.13% (determined by KF). Each level was performed in triplicate and repeated on four different days. A total of four blocks of three experiments resulted in twelve experiments per moisture level. The validation experiments were repeated on four different days in order to evaluate the intermediate precision. Karl Fischer measurements were performed after each validation experiment, as was done for the calibration experiments.

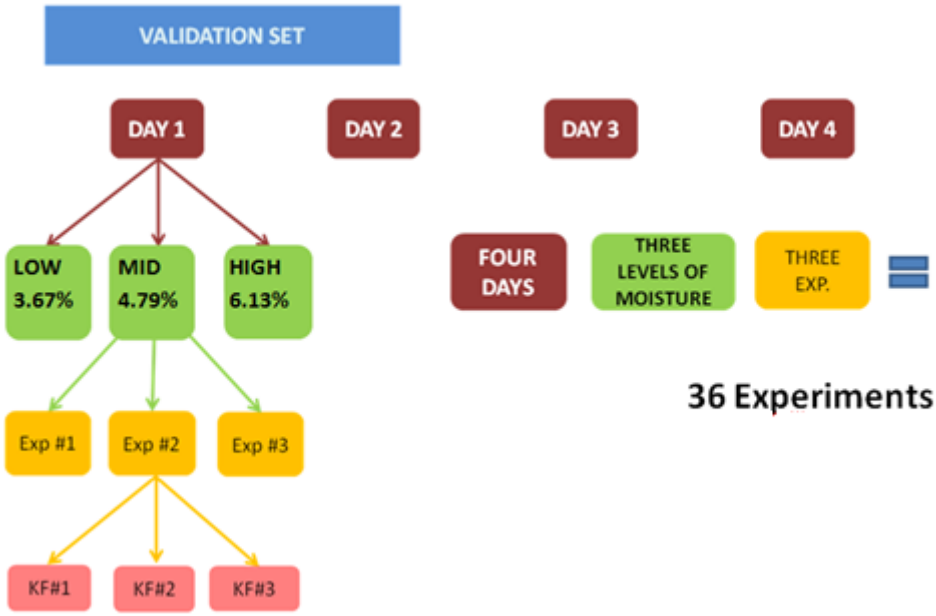

Figure 9.2. Overview of the performed validation experiments.

NIR spectra were collected in-line during drying. One spectrum was collected each 20 seconds, hence providing real-time spectral information. Each collected NIR spectrum was fed into the PLS model calibration model resulting in a predicted moisture content each time an NIR spectrum was collected during processing. After each validation experiment, five at-line spectra were collected (and also fed into the calibration model resulting in predicted moisture contents) as well as three samples for Karl Fischer titration.

Due to process variation it was not possible to obtain the exact same moisture content when repeating the validation runs. (e.g. the low level moisture content validation experiment of day 1 resulted in a slightly different moisture content compared to the low level moisture content experiment of day 2). Therefore, at each validation moisture level all the NIR predicted moisture content values were normalized as follows (see Table 9.1):

Equation 9.1.

$$y_{inor} = \frac{y_{ipred} * mean}{y_{iref}}$$

With

y_{inor}= normalized NIR predicted moisture content of validation experiment *i*

y_{ipred}= moisture content as predicted by the NIR calibration model

mean= mean Karl Fischer moisture content at each moisture level: 3.67%, 4.76% or 6.13%, respectively

y_{iref}= moisture content as obtained via the Karl Fischer titration for validation experiment *i*

In order to evaluate the in-line collected spectra, Principal Component Analysis was performed on all in-line spectra per experiment. Scatter plots of the first and second component were used in order to detect and exclude outliers. With this information the last 'valid' spectrum of each run was selected. In this manner a set of 36 in-line spectra were constructed as validation test-set.

9.2.7. Multivariate data-analysis and modeling

Principal Component Analysis (PCA) and Partial least squares (PLS) calibration models were developed using a multivariate data analysis software package (Simca P+ 12.0, Umetrics AB, Umeå, Sweden).

Table 9.1. The moisture content obtained after each validation experiment by means of Karl Fischer (y_{iref}), the value predicted by the PLS-calibration model (y_{ipred}) and the normalized value (y_{inor}).

Experiment	y_{iref}	y_{ipred}	y_{inor}
Low Day 1	3.51	3.56	3.73
Low Day 1	3.53	3.43	3.57
Low Day 1	3.73	3.49	3.43
Low Day 2	3.63	3.50	3.54
Low Day 2	3.58	3.46	3.54
Low Day 2	3.57	3.45	3.55
Low Day 3	3.78	3.48	3.38
Low Day 3	3.54	3.38	3.50
Low Day 3	3.73	3.45	3.40
Low Day 4	3.72	3.83	3.78
Low Day 4	3.79	3.78	3.66
Low Day 4	3.95	3.81	3.55
Mid Day 1	4.74	4.80	4.85
Mid Day 1	4.81	4.74	4.71
Mid Day 1	4.77	4.77	4.78
Mid Day 2	5.07	4.94	4.66
Mid Day 2	5.14	4.87	4.53
Mid Day 2	4.87	4.62	4.54
Mid Day 3	4.28	4.03	4.50
Mid Day 3	4.89	4.33	4.24
Mid Day 3	4.75	4.29	4.32
Mid Day 4	4.15	3.85	4.44
Mid Day 4	5.19	4.94	4.56
Mid Day 4	4.77	4.69	4.71
High Day 1	5.71	5.69	6.11
High Day 1	5.85	5.81	6.08
High Day 1	5.69	5.38	5.80
High Day 2	6.7	6.44	5.89
High Day 2	6.5	6.23	5.87
High Day 2	6.44	6.07	5.77
High Day 3	5.7	5.91	6.36
High Day 3	6.28	5.98	5.83
High Day 3	6.09	6.15	6.19
High Day 4	6.09	6.10	6.14
High Day 4	6.16	6.12	6.09
High Day 4	6.33	6.14	5.94

9.2.8. Validation of the in-line moisture assessment method

The validation strategy introduced by Hubert et al. [20-22] proposed to review the objectives of the validation according to the intended use of the analytical procedure: to ensure that the difference between the "measured value" (y_i) and the unknown "true value" (μT), is at least lower than an acceptance limit (λ):

$$|y_i - \mu T| < \lambda$$

In this paper, λ is set at 20% for the in-line determination of the moisture content of granules during drying. Thus, as the aim of validation is to determine if an analytical procedure can be guaranteed as acceptable, it must be assured that the probability that a measurement will fall outside the acceptance limits is less or equal to the maximum risk (5%) that the analyst is able to take during routine use:

$$\Pr(|y_i - \mu T| < \lambda) \geq \beta$$

If so, the analytical procedure can be considered as acceptable. In this study, the wished proportion of measurements inside the acceptance limits was set at 95%. It is clear that the classical determinations of trueness, precision, linearity etc. as they are described in the ICH Q2 are not sufficient to decide whether the objectives of an analytical procedure are guaranteed. The adapted decision tool therefore is the accuracy profile of the analytical procedure, which is constructed from the total error (bias + standard deviation) of the procedure. This is obtained by computing the β-expectation tolerance interval at each concentration level and allows evaluating the proportion of expected future measurements that will fall inside the acceptance limits. This enables to control the risk associated to the use of the method. Using the data collected for the development of the accuracy profile, the measurement uncertainty was estimated as described by Feinberg et al [26, 27]. During validation, the within day and between day variability were taken into account (Figure 9.2).

9.2.9. Comparison of the NIR method with the KF reference method

The final aim of the present work is to replace the slow and destructive Karl Fischer reference method for the quantitative moisture assessment during drying by a fast and non-destructive alternative in-line analysis method. Therefore, it is necessary to demonstrate that the envisaged method does not have worse performance characteristics than the reference method. Therefore, a comparison of the two fundamental performance parameters, precision and bias, was performed as described by [28, 29] The approach for method comparison proposed in those papers, calculates the number of measurements needed to assure the preset probability (1-β) of not adopting an alternative method with unacceptable performance (α and β error are under control). This may require a higher number of measurements than a laboratory can perform. This was the case in our study (15 measurement days required) due to practical, time and cost reasons. Therefore, a user-defined number of measurements was used and only the α-error (risk to reject the null hypothesis, when it should be accepted) was under control. On the other hand, it was possible to calculate the β-error [31]. The comparison of the precision parameters (repeatability and intermediate precision) between both methods was done using F-tests. Bias was compared using the interval hypothesis t-test instead of the point hypothesis t-test, as it is more relevant to test whether bias between two methods is not too large (for this study, smaller than or equal to 0.5%) instead of testing that the bias between methods is zero [32]. From a chemical point of view, there is always a bias. Furthermore, the traditional null and alternative hypotheses were exchanged (thus the α- and β-error are exchanged too) for the interval hypothesis testing. This is, since it is more important to control the risk to wrongly accept there is no bias while in fact here is, instead of wrongly accepting there is bias, while there is none. For this study the 'new' α risk (= risk to wrongly accept that there is no bias) was chosen at 0.05.

9.3. RESULTS AND DISCUSSION

9.3.1. Development of a NIR based calibration model

Hundred spectra were obtained during the calibration experiments and used to build the calibration model (5 moisture levels * 4 repetitions * 5 spectra/experiment = 100 spectra, see Figure 9.1). All spectra were centered and SNV-corrected after which a principal component analysis (PCA) was performed, using the full spectral region from 10000 to 4500 cm^{-1}. The first principal component, capturing a variance of 90.58%, represented moisture content. The loadings of the first principal component clearly indicated the spectral region between 5350 cm^{-1} and 4775 cm^{-1} enclosed the most variance, which is indeed where the water bands are expected. Hence, the 5350 to 4775 cm^{-1} spectral region was selected, centered and SNV-corrected to build a PLS calibration model for the prediction of moisture content. This PLS model consisted of two principal components, resulting in an R^2 of 99.7%, a Q^2 of 96.4% and an RMSEE of 0.2342% and an RMSECV of 0.2331%.

9.3.2. Validation of the in-line moisture assessment method

Using the above developed PLS moisture calibration model, the moisture content at the end of each drying validation experiment was predicted based on the last valid in-line collected spectrum (Table 9.1, y_{ipred}) and normalized (Table 9.1, y_{inor}). Based on these results, the trueness, precision, accuracy (Table 9.2) and accuracy profile (Figure 9.3) were calculated for each validated residual moisture level. It can be noticed from the accuracy profile that the β-expectation tolerance intervals do not exceed the acceptance limits of 20% over the validated concentration range. Ninety-five times out of 100, the future in-line measurements will be included within the acceptance limits of 20%. Thus, using this validation strategy, the accuracy profile is used to *decide* whether the in-line NIR method can be declared valid or not. The validation data calculated in Table 9.2 help to make a *diagnosis*.

From the data used for the calculation of the accuracy profile, the measurement uncertainty was estimated [26]. The uncertainty results are presented in Table 9.3. The expanded uncertainty defines an interval around the mean value in which the unknown 'true value' is retrieved with a probability of 95%. From the relative expanded uncertainties, it can be seen

that for each examined moisture level, the interval in which there is a probability of 95% that the true value, estimated by the measured value, occurs, is larger than 5%.

Table 9.2. Calculated in-line NIR method validation parameters.

Trueness

Level	Relative bias	Recovery
Low	-3.25 %	96.75 %
Mid	-4.50 %	95.50 %
High	-1.99 %	98.01 %

Precision

Level	Repeatability	Intermediate precision
Low	2.78 %	3.55 %
Mid	2.30 %	4.24 %
High	2.85 %	3.05 %

Accuracy

Level	Absolute total error	Relative total error	Relative β-expectation tolerance limits
Low	0.245 %	6.68 %	[-11.94; 5.43] %
Mid	0.409 %	8.54 %	[-16.81; 7.81] %
High	0.305 %	4.98 %	[-9.11; 5.12] %

Table 9.3. Point estimates of the different uncertainties related to moisture content at each moisture content level of the accuracy profile

Level	Uncertainty of the bias (%)	Uncertainty (%)	Expanded uncertainty (%)	Relative expanded uncertainty (%)
Low	0.048	0.135	0.270	7.35
Mid	0.087	0.212	0.424	8.87
High	0.060	0.193	0.386	6.29

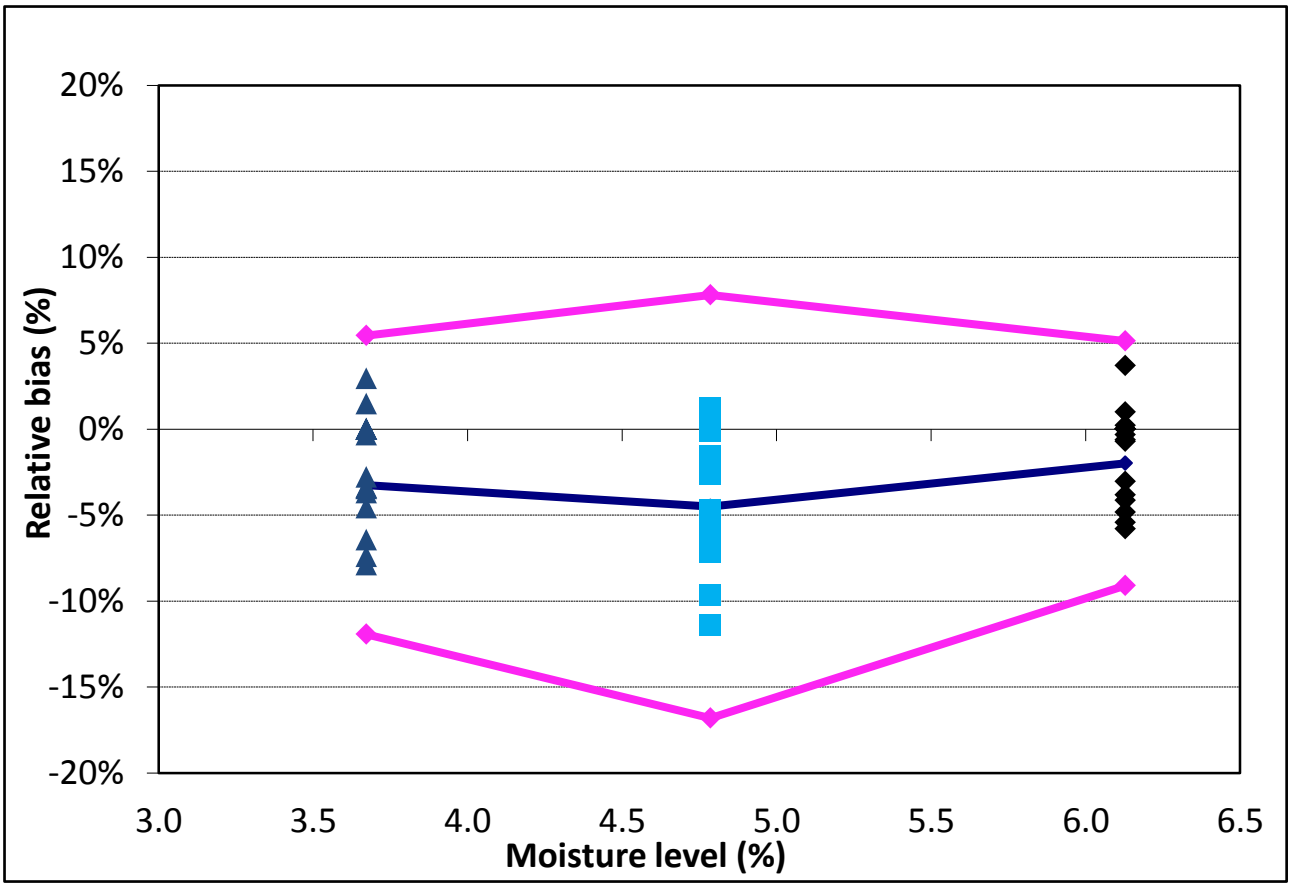

Figure 9.3. Accuracy profile.

9.3.3. Comparison of alternative in-line NIR method with Karl Fischer reference method

The NIR as well as the Karl Fischer validation data used for the comparison of both methods at the lowest examined residual moisture content level are mentioned in Table 9.4. In a first step, the different types of variances at this low level were calculated (Table 9.5). These variances were used for the calculation of the F-tests for the evaluation of the different precision parameters (Table 9.6). From these tests, it can be concluded that the repeatability as well as the intermediate precision are at least as good as those of the KF reference method. The α error of these F-tests (risk to wrongly reject the conclusion that the precision parameters of the NIR based prediction method are better or equal to the precision parameters of the KF reference method) was set at 5%. For the evaluation of the bias, the estimated bias *d* (grand mean of alternative validation data – **grand** mean of reference validation data = 0.12%), was calculated together with its 95% upper confidence limit (UCL = 0.317%) and lower confidence limit (LCL = -0.077%). If UCL is smaller or equal or LCL is higher or equal to the acceptable bias (0.5%), the bias is acceptable since there is probability

smaller than 5% that the absolute bias as estimated by d is larger than 0.5%. Using the interval hypothesis, the risk to wrongly accept that there is no bias ('new' α error) was kept at 5%. The probability to reject wrongly a non biased method was calculated as 2.40% ('new' β error).

Table 9.4. KF reference data and NIR validation data used for method comparison.

			KF	**predicted by NIR calibration model**
day 1	low (3.6%)	exp 1	3.51	3.56
day 1	low (3.6%)	exp 2	3.53	3.43
day 1	low (3.6%)	exp 3	3.73	3.49
day 1	mid (4.5%)	exp 1	4.74	4.80
day 1	mid (4.5%)	exp 2	4.81	4.74
day 1	mid (4.5%)	exp 3	4.77	4.77
day 1	high (6.0%)	exp 1	5.71	5.69
day 1	high (6.0%)	exp 2	5.85	5.81
day 1	high (6.0%)	exp 3	5.69	5.38
day 2	low (3.6%)	exp 1	3.63	3.50
day 2	low (3.6%)	exp 2	3.58	3.46
day 2	low (3.6%)	exp 3	3.57	3.45
day 2	mid (4.5%)	exp 1	5.07	4.94
day 2	mid (4.5%)	exp 2	5.14	4.87
day 2	mid (4.5%)	exp 3	4.87	4.62
day 2	high (6.0%)	exp 1	6.70	6.44
day 2	high (6.0%)	exp 2	6.50	6.23
day 2	high (6.0%)	exp 3	6.44	6.07
day 3	low (3.6%)	exp 1	3.78	3.48
day 3	low (3.6%)	exp 2	3.54	3.38
day 3	low (3.6%)	exp 3	3.73	3.45
day 3	mid (4.5%)	exp 1	4.28	4.03
day 3	mid (4.5%)	exp 2	4.89	4.33
day 3	mid (4.5%)	exp 3	4.75	4.29
day 3	high (6.0%)	exp 1	5.70	5.91
day 3	high (6.0%)	exp 2	6.28	5.98
day 3	high (6.0%)	exp 3	6.09	6.15
day 4	low (3.6%)	exp 1	3.72	3.83
day 4	low (3.6%)	exp 2	3.79	3.78
day 4	low (3.6%)	exp 3	3.95	3.81
day 4	mid (4.5%)	exp 1	5.19	4.94

day 4	mid (4.5%)	exp 2	4.77	4.69
day 4	mid (4.5%)	exp 3	4.15	3.85
day 4	high (6.0%)	exp 1	6.09	6.10
day 4	high (6.0%)	exp 2	6.16	6.12
day 4	high (6.0%)	exp 3	6.33	6.14

Table 9.5. Overview of the different types of variances of the in-line NIR and KF validation used for method comparison.

Variance estimates	**KF method**	**NIR method**
Repeatability variance (s_r^2)	0.0114	0.0021
(Operator + day) variance (s_{OD}^2)	0.0078	0.0289
(Operator + day) intermediate precision	0.0193	0.0310
Variance of the day means	0.0116	0.0296

Table 9.6. Overview of the F-test results for the comparison of the repeatability and intermediate precision between the in-line NIR and KF reference method.

Evaluated precision comparison	**Calculated F-value**	**Tabulated F-value**	**Conclusion**
Repeatability	0.186	3.44	Repeatability of the in-line NIR method is acceptable
Time + operator different intermediate precision	1.61	4.35	Operator + time-different intermediate precision of the in-line NIR method is acceptable

9.4. CONCLUSION

The results show that the developed fast and non-destructive in-line NIR method is a reliable alternative for the traditionally used destructive and time-consuming KF method for the in-line moisture determination of granules in the six-segmented fluid bed dryer of a continuous from-powder-to-tablet production line. The NIR spectra were collected in-line by means of a Lighthouse Probe^{TM}, connected to a Brüker-system. The accuracy profile, calculated during the validation of the in-line NIR method, assures that at least 95% of future routine experiments will be included within the preset acceptance limits (20%), which suits with the aim of the developed analytical procedure. Moreover, the data used in this validation approach were also used to estimate the uncertainty of the bias as well as the expanded uncertainty at each concentration level. Finally, the new NIR method has at least as good performance characteristics (precision and bias) as the KF method.

9.5. REFERENCES

[1] FDA-Adminstration, Guidance for Industry - PAT - A Framework for Innovative Pharmaceutical Development, Manufacturing, and Quality Assurance, in, 2004.

[2] T. De Beer, A. Burggraeve, M. Fonteyne, L. Saerens, J.P. Remon, C. Vervaet, Near infrared and Raman spectroscopy for the in-process monitoring of pharmaceutical production processes, International Journal of Pharmaceutics, 417 (2011) 32-47.

[3] W. Paul Findlay, G.R. Peck, K.R. Morris, Determination of fluidized bed granulation end point using near-infrared spectroscopy and phenomenological analysis, J. Pharm. Sci., 94 (2005) 604-612.

[4] J. Rantanen, M. Kansakoski, J. Suhonen, J. Tenhunen, S. Lehtonen, T. Rajalahti, J.P. Mannermaa, J. Yliruusi, Next Generation Fluidized Bed Granulator Automation, AAPS PharmsciTech, 1 (2000) article 10.

[5] J. Rantanen, A. Jorgensen, E. Rasanen, P. Luukkonen, S. Airaksinen, J. Raiman, K. Hänninen, O. Antikainen, J. Yliruusi, Process Analysis of Fluidized Bed Granulation, AAPS PharmsciTech, 2 (2001) article 21.

[6] F.J.S. Nieuwmeyer, M. Damen, A. Gerich, F. Rusmini, K. van der Voort, H. Vromans, Granule characterization during fluid bed drying by development of a near infrared method to determine water content and median granule size, Pharmaceutical Research, 24 (2007) 1854-1861.

[7] M. Alcalà, M. Blanco, M. Bautista, J.M. González, On-line monitoring of a granulation process by NIR spectroscopy, J. Pharm. Sci., 99 (2010) 336-345.

[8] J. Rantanen, S. Lehtola, P. Ramet, J.P. Mannermaa, J. Yliruusi, On-line monitoring of moisture content in an instrumented fluidized bed granulator with a multi-channel NIR moisture sensor, Powder Technology, 99 (1998) 163-170.

[9] J. Rantanen, O. Antikainen, J.P. Mannermaa, J. Yliruusi, Use of the near-infrared reflectance method for measurement of moisture content during granulation, Pharmaceutical Development and Technology, 5 (2000) 209-217.

[10] R.A. Mattes, In-line process analysis of residual moisture in a fluid bed granulator-dryer using NIR spectroscopy, Spectroscopy, January (2005).

[11] J.G. White, On-line moisture detection for a microwayve vacuum dryer, Pharmaceutical Research, 11 (1994) 728-732.

[12] R.L. Green, G. Thurau, N.C. Pixley, A. Mateos, R.A. Reed, J.P. Higgins, In-line monitoring of moisture content in fluid bed dryers using near-IR spectroscopy with consideration of sampling effects on method accuracy, Analytical Chemistry, 77 (2005) 4515-4522.

[13] P. Frake, D. Greenhalgh, S.M. Grierson, J.M. Hempenstall, D.R. Rudd, Process control and end-point determination of a fluid bed granulation by application of near infra-red spectroscopy, International Journal of Pharmaceutics, 151 (1997) 75-80.

[14] L. Chablani, T.M. K, M. Amit, R. Patrick, S.W. C, Inline Real-Time Near-Infrared Granule Moisture Measurements of a Continuous Granulation-Drying-Milling Process, AAPS PharmsciTech, 12 (2011) 1050-1055.

[15] A. Hartung, M. Knoell, U. Schmidt, P. Langguth, Role of continuous moisture profile monitoring by inline NIR spectroscopy during fluid bed granulation of an Enalapril formulation, Drug Dev. Ind. Pharm., 37 (2011) 274-280.

[16] A. Burggraeve, A.F.T. Silva, T. Van Den Kerkhof, M. Hellings, C. Vervaet, J. Paul Remon, Y. Vander Heyden, T. De Beer, Development of a fluid bed granulation process control strategy based on real-time process and product measurements, Talanta, 100 (2012) 293-302.

[17] M. Fonteyne, S. Soares, J. Vercruysse, E. Peeters, A. Burggraeve, C. Vervaet, J.P. Remon, N. Sandler, T. De Beer, Prediction of quality attributes of continuously produced granules using complementary pat tools, European Journal of Pharmaceutics and Biopharmaceutics, 82 (2012) 429-436.

[18] A. Peinado, J. Hammond, A. Scott, Development, validation and transfer of a Near Infrared method to determine in-line the end point of a fluidised drying process for commercial production batches of an approved oral solid dose pharmaceutical product, Journal of Pharmaceutical and Biomedical Analysis, 54 (2011) 13-20.

[19] C. De Bleye, P.F. Chavez, J. Mantanus, R. Marini, P. Hubert, E. Rozet, E. Ziemons, Critical review of near-infrared spectroscopic methods validations in pharmaceutical applications, Journal of Pharmaceutical and Biomedical Analysis, 69 (2012) 125-132.

[20] P. Hubert, J.J. Nguyen-Huu, B. Boulanger, E. Chapuzet, P. Chiap, N. Cohen, P.A. Compagnon, W. Dewé, M. Feinberg, M. Lallier, M. Laurentie, N. Mercier, G. Muzard, C. Nivet,

L. Valat, Validation of quantitative analytical procedure, Harmonization of approaches, STP Pharma Pratiques, 13 (2003) 101-138.

[21] P. Hubert, J.J. Nguyen-Huu, B. Boulanger, E. Chapuzet, N. Cohen, P.A. Compagnon, W. Dewé, M. Feinberg, M. Laurentie, N. Mercier, G. Muzard, L. Valat, Quantative analytical procedures: Harmonization of the approaches Part II: Statistics, STP Pharma Pratiques, 16 (2006) 28-58.

[22] P. Hubert, J.J. Nguyen-Huu, B. Boulanger, E. Chapuzet, N. Cohen, P.A. Compagnon, W. Dewé, M. Feinberg, M. Laurentie, N. Mercier, G. Muzard, L. Valat, Quantitative analytical procedures validation: harmonization of the approaches Part III. Examples of application, STP Pharma Pratiques

16 (2006) 87-121.

[23] J. Mantanus, E. Ziémons, P. Lebrun, E. Rozet, R. Klinkenberg, B. Streel, B. Evrard, P. Hubert, Moisture content determination of pharmaceutical pellets by near infrared spectroscopy: Method development and validation, Analytica Chimica Acta, 642 (2009) 186-192.

[24] T. De Beer, W. Baeyens, A. Vermeire, D. Broes, J.P. Remon, C. Vervaet, Raman spectroscopic method for the determination of medroxyprogesterone acetate in a pharmaceutical suspensions: validation of quantifying abilities, uncertainty assessment and comparison with the high performance liquid chromatography reference method, Analytica Chimica Acta, 589 (2007) 192-199.

[25] L. Saerens, N. Segher, C. Vervaet, J.P. Remon, T. De Beer, Thorough validation of an in-line Raman spectroscopic method for continuous API quantification during pharmaceutical hot-melt extrusion., Analytica Chimica Acta, 806 (2014) 180-7.

[26] M. Feinberg, B. Boulanger, W. Dewé, P. Hubert, New advances in method validation and measurement uncertainty aimed at improving the quality of chemical data, Anal Bioanal Chem, 380 (2004) 502-514.

[27] M. Feinberg, M. Laurentie, A global approach to method validation and measurement uncertainty, Accred Qual Assur, 11 (2006) 3-9.

[28] S. Kuttatharmmakul, D.L. Massart, J. Smeyers-Verbeke, Comparison of alternative measurement methods, Analytica Chimica Acta, 391 (1999) 203-225.

[29] S. Kuttatharmmakul, D.L. Massart, J. Smeyers-Verbeke, Comparison of alternative measurement methods: determination of the minimal number of measurements required for the evaluation of the bias by means of interval hypothesis testing, Chemometrics and Intelligent Laboratory Systems, 52 (2000) 61-73.

[30] M. Fonteyne, J. Vercruysse, D.C. Díaz, D. Gildemyn, C. Vervaet, J.P. Remon, T.D. Beer, Real-time assessment of critical quality attributes of a continuous granulation process, Pharmaceutical Development and Technology, 18 (2013) 85-97.

[31] A.N.M. Nguyet, A.M. van Nederkassel, L. Tallieu, S. Kuttatharmmakul, E. Hund, Y. Hu, J. Smeyers-Verbeke, Y.V. Heyden, Statistical method comparison: short- and long-column liquid chromatography assays of ketoconazole and formaldehyde in shampoo, Analytica Chimica Acta, 516 (2004) 87-106.

[32] C. Hartmann, J. Smeyersverbeke, W. Penninckx, Y. Vanderheyden, P. Vankeerberghen, D.L. Massart, REAPPRAISAL OF HYPOTHESIS-TESTING FOR METHOD VALIDATION - DETECTION OF SYSTEMATIC-ERROR BY COMPARING THE MEANS OF 2 METHODS OR OF 2 LABORATORIES, Analytical Chemistry, 67 (1995) 4491-4499.

CHAPTER 10

MOISTURE AND DRUG SOLID STATE EVALUATION OF CONTINUOUSLY PRODUCED GRANULES CONSIDERING DIFFERENT SIZE FRACTIONS

"The pessimist complains about the wind;
the optimist expects it to change;
the realist adjusts the sails."
William Arthur Ward (1921-1994)

Fonteyne M., Gildemyn D., Peeters E., Mortier S., Vercruysse J., Gernaey K.V., Vervaet C., Remon J.P., Nopens, I., De Beer T. (2014). Moisture and drug solid state monitoring during a continuous drying process using empirical and mass balance models, European Journal of Pharmaceutics and Biopharmaceutics, doi:10.1016/j.ejpb.2014.02.015

ABSTRACT

When PAT tools are implemented in pharmaceutical processes, they provide information on the total product load. No specific information regarding, for example, separate size fractions of granules is gained. In this study, granules were produced during 19 different experiments, and process settings were changed. A model formulation of 30% of theophylline anhydrate, together with lactose monohydrate (67.5%) and PVP (2.5%) was used. From the dried granules, Raman spectra were collected in order to evaluate the solid state of the API and the residual moisture content was determined. Afterwards, granules were split into three size categories: fine granules (< 150 µm), yield (150 – 1400 µm) and oversized granules (>1400 µm). Again, Raman spectra and residual moisture data were retrieved from each size fraction. It was revealed that the overall determined moisture content and solid state information of the API is not spread homogenously over the size fractions. Fine granules will dry faster and contain theophylline anhydrate, whilst the oversized granules are characterized by a higher residual moisture content and theophylline in the monohydrate or metastable form.

CHAPTER 10

MOISTURE AND DRUG SOLID STATE EVALUATION OF CONTINUOUSLY PRODUCED GRANULES CONSIDERING DIFFERENT SIZE FRACTIONS

10.1. INTRODUCTION

In 2011, Lee et al. [1] reported solid state variation of spray-dried mannitol formulations as a function of particle size. Mannitol can exist in four different states: the α-, β- and δ- form as well as the hemi-hydrate form. XRPD, Raman and NIR spectroscopy were used in order to determine the solid state of mannitol in the different size fractions. Smaller droplets dried faster and a faster loss of solvent occurred. More metastable α-mannitol was found in the smaller droplets, whereas the larger droplets contained more stable β-mannitol. The opposite findings were reported when 10% lysozyme was added to the formulation. Clearly, the polymorphic forms of spray-dried mannitol changes as a function of droplet size.

In this chapter, theophylline was used a model drug. It can occur in four different solid states: theophylline monohydrate, a metastable form of theophylline and two types of anhydrous forms, one stable at room temperature and one only occurring at very high temperatures [2]. Two critical quality attributes of the dried granules were evaluated, both for the total granule load and for different size fractions, namely the residual moisture content and the solid state of the API. The **aim** of this study is to evaluate how the moisture content and solid state determinations conducted on the total granule load agree or differ from the same information determined on specific granule size fractions.

10.2. MATERIALS AND METHODS

10.2.1. Materials

Anhydrous theophylline (Farma-Quimica Sur S.L., Malaga, Spain) (30%, w/w) was used as a model drug and granulated together with lactose monohydrate 200M (Caldic Belgium nv., Hemiksem, Belgium) as filler. Polyvinylpyrrolidone (Kollidon 30®, BASF, Burgbernheim, Germany) was added as a binder to the dry powder mixture in a concentration of 2.5% (w/w). Distilled water was used as granulation liquid. Sodium lauryl sulfate (Fagron, Waregem, Belgium) was added to the granulation liquid (0.5% w/v) to improve the wettability of the dry powder mixture.

10.2.2. Continuous twin-screw granulation and fluid bed drying

Continuous granulation and drying was performed using the ConsiGma™ 25 unit (GEA Pharma Systems nv., Collette™, Wommelgem, Belgium). In order to obtain granules with diverse characteristics (i.e. granule size distribution, residual moisture content, solid state of the API), an experimental design (DoE) was performed. A 4-factor full factorial design with high and low levels and three centerpoints, resulting in 19 experiments, was performed (Table 10.1).

Table 10.1. Overview of the DoE parameters.

Parameter	-1	0	1
Temperature granulator barrel (°C)	25	32.5	40
Powder feed rate (kg/h)	10	17.5	25
Temperature drying air (°C)	35	55	75
Air flow drying air (m^3/h)	350	400	450

The temperature of the granulator barrel was varied between 25°C and 40°C and powder feed rates of 10 and 25 kg/h were used. The screw speed was kept constant at 950 rpm and the granulation liquid was added at 9.16% (w/w). For the drying unit the drying air temperature was varied between 35°C and 75°C and an air flow between 350 and 450 m^3/h was applied. Two of the 19 experiments, namely experiment 8 and 12, could practically not

be performed, since the produced granules consisted mainly of fines and the high air flow (450 m^3/h) blew the fines in the filters, leading to blockage of the filters. The remaining 17 experiments were performed in randomized order. An amount of 1.25 kg was dried in each cell during 10 minutes and each DoE experiment was done in duplicate.

After each DoE experiment, the moisture content and the solid state of the API were determined for separate sieve fractions: fines (<150 µm), yield (151 µm – 1400 µm) and oversized granules (>1400 µm). The granules were separated in these three fractions by means of a sieve tower. For each experiment and its duplicate, five Raman spectra were taken from the total granule load as well as from the three sieve fractions, resulting in 40 spectra per DoE experiment. Furthermore, the residual moisture content was determined for both the total fractions of granules and the three sieve fractions individually by means of Karl Fischer titration (n=2).

10.2.3. Raman spectroscopy

A RamanRxn1 spectrometer (Kaiser Optical Systems, Inc., Ann Arbor, Michigan, US) equipped with an air-cooled CCD detector (back-illuminated deep depletion design) was used. The spectra were collected with a non-contact optic (NCO), being connected to an MR probe (Kaiser Optical Systems, Inc., Ann Arbor, Michigan, US). All spectra were recorded with a resolution of 4 cm^{-1} and an exposure time of 10 seconds, using a laser power of 400 mW. Spectra were mean centered and SNV-corrected before data analysis in the spectral region from 200 to 1800 cm^{-1}. Data collection and data transfer were automated using the HoloGRAMS™ data collection software, the HoloREACT™ reaction analysis and profiling software and the Matlab software (version 7.1, The MathWorks Inc., Natick, Massachusetts, US).

10.2.4. Karl Fischer moisture determination

The residual moisture of samples was determined by volumetric Karl Fischer titration (KF) using a V30 volumetric Karl Fischer titrator (Mettler Toledo, Zaventem, Belgium). Methanol (Hydranal, Sigma Aldrich, Germany) was used as a solvent. Before titration, granules were stirred and dissolved during 5 minutes.

10.2.5. Data analysis

The analysis of the spectra and the development of the Principal Component Analysis (PCA) was done using the Simca P+ 12.0.1 software (Umetrics AB, Umeå, Sweden).

10.3. RESULTS AND DISCUSSION

To obtain granules with diverse characteristics, a 4-factor full factorial design (19 experiments) was performed. Based on the residual moisture content of the granules of the 19 experiments, they can be classified in three groups (Table 10.2): (i) granules, which are 'dry' after drying, with a moisture content of 4% or lower (experiments 1, 2, 6, 13, 16, 18 and 19); (ii) granules with a residual moisture content higher than 5% (experiments 3, 4, 7, 9, 11, 14, 15 and 17); and (iii), granules having a residual moisture content that is in between 4% and 5% (experiments 5 and 10). These three groups, except experiment 9, correspond to the applied drying air temperature. The ones with residual moisture contents higher than 5% were dried at 35°C, while the granules having residual moisture contents below 4% were dried at 75°C. The latter group does not show significant differences in residual moisture content between the oversized fraction, the yield and the fines (Figure 10.1). The residual moisture content of the granules dried at 55°C and 35°C increases with increasing granule size (Figure 10.1). The fines fraction has a lower residual moisture content compared to the yield and oversized fraction. This is because fine particles can dry much faster due to a higher surface to volume ratio. Furthermore, water in the core of the granule will reach the surface of the granule faster in small granules compared to larger granules.

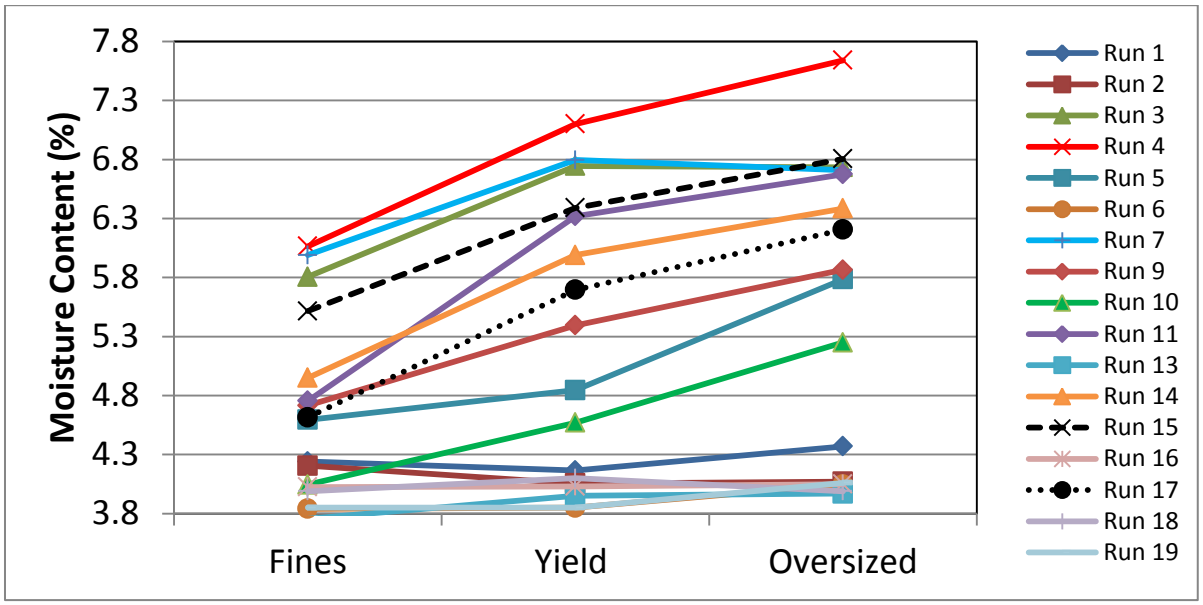

Figure 10.1. Residual moisture content (KF titration) of the different granule size fractions.

Table 10.2. Overview of the design experiments. Average moisture content of the total granule load and its granule size fractions.

Run	1	2	3	4	5	6	7	8	9	10	11	12	13	14	15	16	17	18	19
Temperature granulator barrel (°C)	40	40	40	40	32.5	25	25	25	32.5	32.5	25	25	25	25	40	40	40	40	25
Powder feed rate (kg/h)	10	25	10	25	17.5	25	10	10	17.5	17.5	25	10	10	25	25	10	10	25	25
Temperature drying air (°C)	75	75	35	35	55	75	35	75	55	55	35	35	75	35	35	75	35	75	75
Air flow drying air (m^3/h)	350	450	450	350	400	350	350	450	400	400	450	450	350	350	450	450	350	350	450
Moisture content (w/w %) of																			
total granule load	4.00	3.68	6.51	7.34	4.96	3.88	6.39		5.40	4.26	5.76		3.79	5.48	6.46	3.87	5.13	3.85	3.73
oversized granules	4.37	4.07	6.74	7.64	5.79	4.05	6.71		5.87	5.25	6.68		3.97	6.39	6.81	4.05	6.21	3.99	4.06
yield	4.17	4.06	6.75	7.10	4.85	3.85	6.80		5.40	4.57	6.32		3.95	5.99	6.39	4.03	5.70	4.10	3.85
fines	4.24	4.21	5.81	6.07	4.60	3.84	5.99		4.72	4.05	4.76		3.76	4.95	5.52	4.03	4.62	3.99	3.85

Since the moisture content of each size fraction is different, there might be a difference in solid state of the API as well. Experiment 4 shows the largest differences in residual moisture content according to granule size. The Raman spectral region from 200 cm^{-1} to 1800 cm^{-1} was selected to perform PCA on the 40 collected and SNV preprocessed Raman spectra resulting from experiment 4. PC 1 explained 79.65% of the variance, whereas PC 2 represented 12.01%. Figure 10.2 shows the resulting PC 1 versus PC 2 scores plot. The Raman spectra corresponding to the fine fraction are clearly isolated along PC 1 from the spectra corresponding to the other size fractions. The information regarding the solid state of theophylline is reflected in the Raman spectral region from 520 cm^{-1} to 600 cm^{-1} [3] and from 1650 cm^{-1} to 1750 cm^{-1} [4, 5]. The loadings plot of the first principal component (Figure 10.3) in these regions show three maxima: at 554 cm^{-1}, 1685 cm^{-1} and 1707 cm^{-1}, which indicates that the fraction of fines contains anhydrous theophylline. The minima at 573 cm^{-1} and 1687 cm^{-1} on the other hand, imply that the other size fractions mainly contain theophylline monohydrate. Similar solid state conclusions were obtained for experiment 3, 5, 7, 9, 10, 11, 14, 15 and 17 (fine fraction = anhydrate; other fractions = mainly monohydrate).

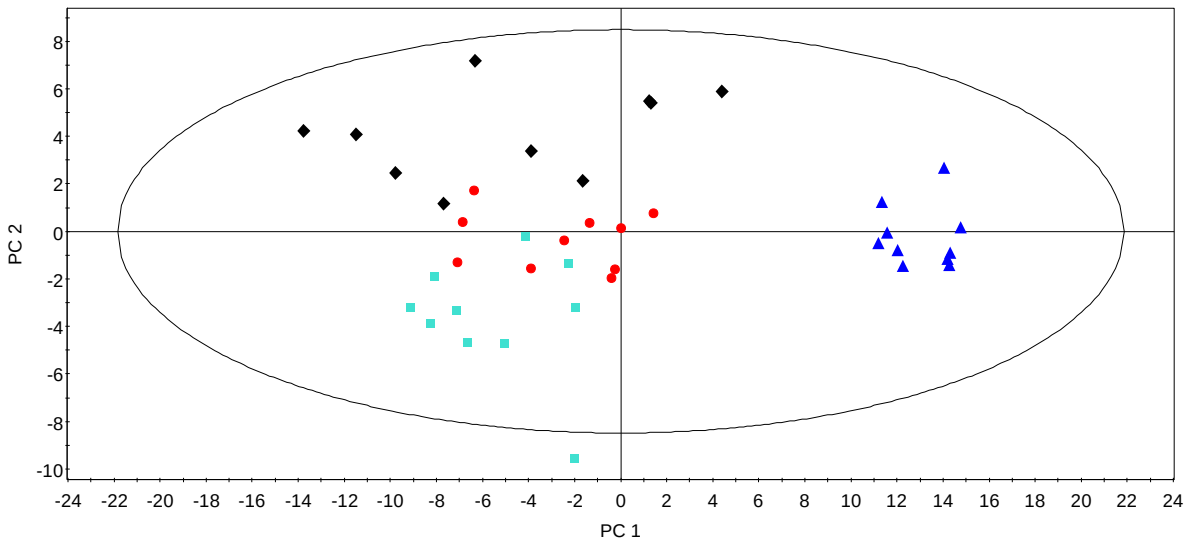

Figure 10.2. Experiment 4: PCA of the Raman spectra of the different granule size fractions: PC 1 versus PC 2 scores plot. Spectra of fines (blue triangles), yield (red dots), oversized granules (turquoise blue squares) and total granule load (black diamonds).

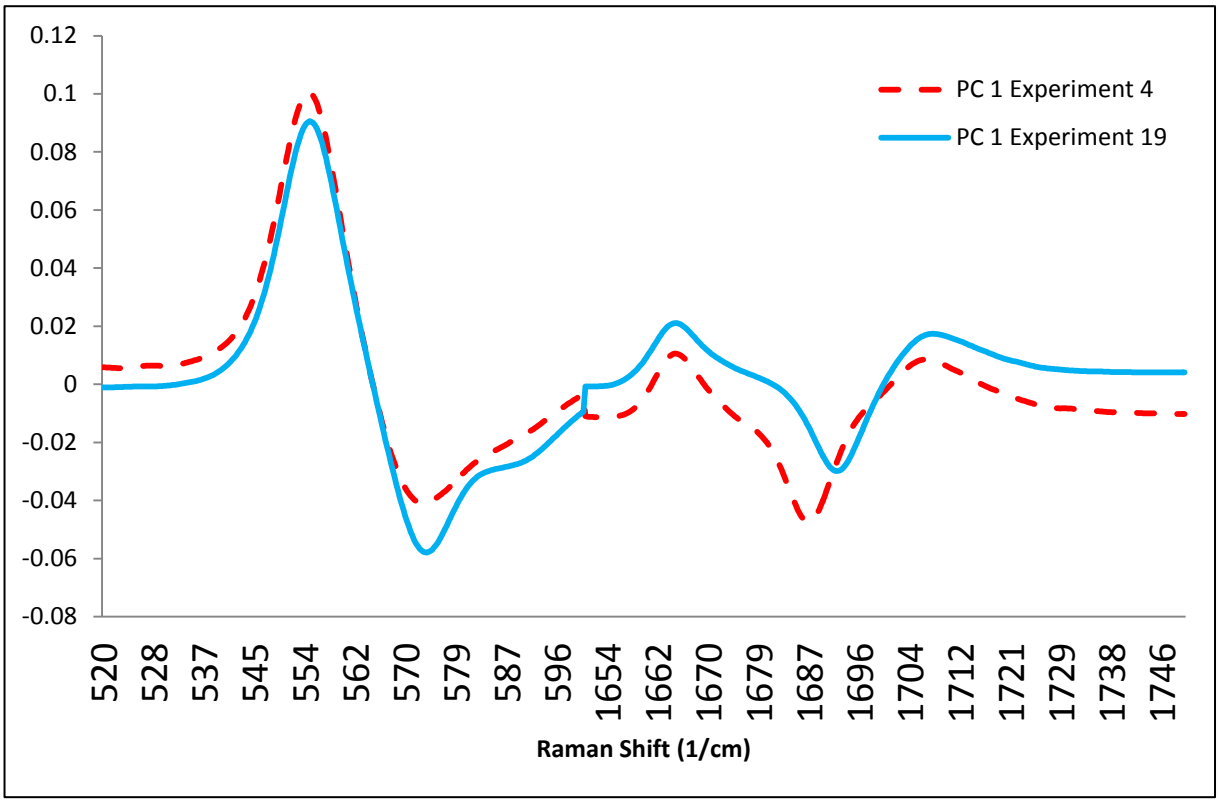

Figure 10.3. Loadings plot of the first PC of the PCA of the Raman spectra of the different granule size fractions for Experiment 4 and 19.

Although the 'dry' runs (experiment 1, 2, 6, 13, 16, 18 and 19) do not show differences in residual moisture content between the different granule size fractions, similar solid state observations were made (Figure 10.4). The PCA of the spectra obtained after experiment 19, resulted in PC 1 representing 61.28% and PC 2 representing 23.84% of the spectral variance, respectively. Again, fines were mostly clustered in the positive part along the PC 1-axis, whereas oversized granules are located in the negative part. The spectra of the yield fraction can be found central. The loadings plot of the first principal component of experiment 19 (Figure 10.3) shows again three maxima, attributable to theophylline anhydrate, and indicating that the fines consist of anhydrous theophylline. The minimum in the PC 1 loadings plot on the other hand has shifted from 1687 cm^{-1} to 1692 cm^{-1}, indicating that the oversized granules from the runs dried at higher temperatures contain metastable theophylline.

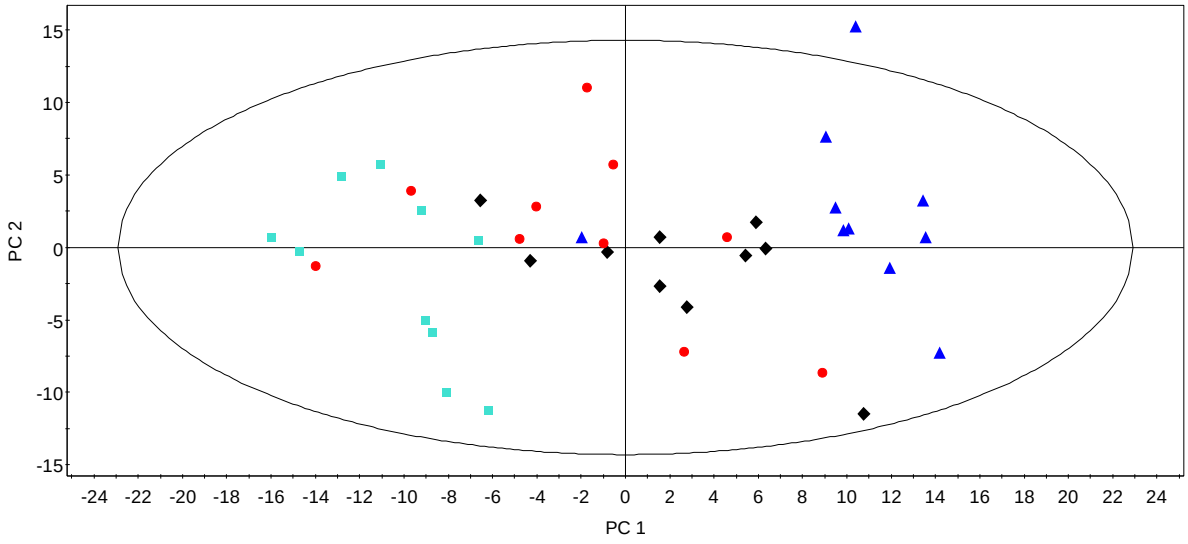

Figure 10.4. Experiment 19: PCA of the Raman spectra of the different granule size fractions: PC 1 versus PC 2 scores plot. Spectra of fines (blue triangles), yield (red dots), oversized granules (turquoise blue squares) and total granule load (black diamonds).

10.4. CONCLUSIONS

These experiments showed that the overall determined moisture content and the solid state information derived from the total granule load differ from moisture content and solid state of the different granule size fractions. Fines tend to dry faster and will contain theophylline anhydrate, whereas the oversized granules will consist of theophylline monohydrate or metastable theophylline. Care should be taken when evaluating the average moisture content and solid state values obtained on the total granule load, since significant differences between the different sieve fractions of the granules were observed.

10.5. REFERENCES

[1] Y.Y. Lee, J.X. Wu, M.S. Yang, P.M. Young, F. van den Berg, J. Rantanen, Particle size dependence of polymorphism in spray-dried mannitol, European Journal of Pharmaceutical Sciences, 44 (2011) 41-48.

[2] E. Suzuki, K. Shimomura, K. Sekiguchi, THERMOCHEMICAL STUDY OF THEOPHYLLINE AND ITS HYDRATE, Chemical & Pharmaceutical Bulletin, 37 (1989) 493-497.

[3] A. Jorgensen, J. Rantanen, M. Karjalainen, L. Khriachtchev, E. Rasanen, J. Yliruusi, Hydrate formation during wet granulation studied by spectroscopic methods and multivariate analysis, Pharmaceutical Research, 19 (2002) 1285-1291.

[4] H. Wikstrom, P.J. Marsac, L.S. Taylor, In-line monitoring of hydrate formation during wet granulation using Raman spectroscopy, J. Pharm. Sci., 94 (2005) 209-219.

[5] A. Dukic-Ott, T. De Beer, J.P. Remon, W. Baeyens, P. Foreman, C. Vervaet, In-vitro and in-vivo evaluation of enteric-coated starch-based pellets prepared via extrusion/spheronisation, European Journal of Pharmaceutics and Biopharmaceutics, 70 (2008) 302-312.

CHAPTER 11

PREDICTION OF QUALITY ATTRIBUTES OF CONTINUOUSLY PRODUCED GRANULES USING COMPLEMENTARY PAT TOOLS

"Most people say it is the intellect which makes a great scientist.

They are wrong:

It is character."

Albert Einstein (1879-1955)

Fonteyne M., Soares S., Vercruysse J., Peeters E., Burggraeve A., Vervaet C., Remon J.P., Sandler, N., De Beer T. (2012). Prediction of quality attributes of continuously produced granules using complementary PAT tools, European Journal of Pharmaceutics and Biopharmaceutics, 82, 429-436

ABSTRACT

Manufacturers of pharmaceutical solid dosage forms aim for a reduced production time and a shorter 'time-to-market'. Therefore continuous manufacturing gains increasing interest in the pharmaceutical industry. For continuous manufacturing, the quality of produced pharmaceuticals should be assessed in real-time (in-line, on-line and at-line) and not via the traditional off-line, often destructive and time-consuming analysis methods which supply the desired information only hours after sampling. This research paper evaluates three PAT tools for the real-time at-line analysis of granules, which were produced using a continuous wet twin-screw granulator being part of a from powder-to-tablet production line (ConsiGma™ 25). A Raman and NIR spectrometer were used together with a photometric imaging technique in order to acquire solid state information and granule size data. These multivariate data were then used to predict the granules' moisture content, tapped and bulk density and flowability. The three PAT tools provided complementary information for predicting these quality attributes of the continuously produced granules. The residual moisture content was mostly correlated with the spectroscopic data, whereas the imaging data had the highest predictive capability for the flowability of the granules.

CHAPTER 11

PREDICTION OF QUALITY ATTRIBUTES OF CONTINUOUSLY PRODUCED GRANULES USING COMPLEMENTARY PAT TOOLS

11.1. INTRODUCTION

Nowadays, the pharmaceutical industry aims at shifting its manufacturing of solid dosage forms from batch production towards continuous production. The ideal continuous process should be capable of producing both small amounts of product (e.g. lab scale or clinical scale) as well as full production scale [1]. Hence, the time-consuming, labor-intensive and expensive scaling-up studies can be avoided. Consequently, the production time of solid dosage forms will shorten and the time-to-market will decrease significantly. Whereas for batch production the actual processing time is only two days, the total elapsed time can take up to 60 days [2]. The protracting delays in between the different processing steps of a batch process are eliminated using a continuous production line. Furthermore, continuous manufacturing lines are designed to be fully automated, so the lines can produce 24 hours a day in a "lights-out" manner. Other important advantages are that continuous pharmaceutical manufacturing equipment requires less floor space and less energy.

Granulation is often used in the pharmaceutical industry as an intermediate step prior to tableting to improve the processability of the starting powder materials. Compared to powders, granules flow better, produce less dust, have a higher density and segregate less [3]. A number of quality attributes can therefore be defined for granules such as flow properties, mechanical durability, porosity, particle size and residual moisture content.

With regard to flow properties several off-line tests for the determination of the flowability of granules exist. For example, the dry funnel method measures the time a weighted amount

of powder/granules needs to fall through a funnel. Another example is the ring-shear tester, which has a specially designed large shear cell for granules, and the working principles have been described in literature [4]. Tapped and bulk density measurements allow to calculate the Hausner ratio (H) of the inspected powder or granules (H = tapped density/bulk density). According to the classification, a Hausner ratio higher than 1.25 indicates that powders or granules are flowing poorly. The residual moisture content of granules is mostly determined via Karl Fischer titration or loss on drying measurements.

The currently applied conventional quality control systems are often based on sampling and time-consuming off-line analyses in analytical laboratories, and they annul the advantages of continuous processing. Continuous manufacturing requires continuous evaluation of the critical process and formulation quality attributes *during* processing. This approach fits into the Process Analytical Technology framework, as launched by the Food and Drug Administration (FDA) in 2004. The FDA states in its guidance for industry [5] that '*quality cannot be tested into products; it should be built-in or should be by design'*. Therefore this study aims to rapidly assess granule size, roughness and solid state information using at-line photometric imaging and Raman and NIR spectroscopy during continuous granulation. These data are then used to calculate and predict the critical granule attributes namely flowability and residual moisture content.

Several non-destructive measurement techniques have been recently developed for the (in-process) determination of granule size distributions. Spatial Filtering Velocimetry (SFV) measures simultaneously particle size and velocity of flowing material as it passes through a laser beam, causing shadows onto a linear array of optical fibers. This technique was already applied in both twin screw [6] and fluid bed granulation [7]. Another technique using a laser beam on moving particles is Focused Beam Reflectance Measurement (FBRM). Here, a moving particle will cause backscattering of the laser light back into the probe and hence the chord length of the particle can be calculated. An FBRM probe, equipped with a mechanical scraper to avoid fouling, was used for the monitoring of a high shear wet granulation process [8]. Liew et al. [9] captured the particle movement in a fluid bed coater by means of a high-speed video camera. Dynamic digital image processing (Camsizer, Retsch Technology) was used by Patchigolla and Wilkinson [10] for the size and shape monitoring during glutamate-

crystallization. Naervanen et al. [11] reconstructed three-dimensional topographic images by means of red, green and blue led light illumination. These topographic data were then used to calculate the size of separate granules. They managed to monitor trends of the median granule size during fluid bed granulation processing. Yu and Hancock [12] evaluated the ability of a dynamic imaging analysis (DIA) technique (QicPic, Sympatec) for adequate particle size and particle shape determination. They evaluated both spherical and rod-shaped samples with the DIA and compared them with laser diffraction and scanning electron microscopy respectively. This DIA apparatus has been used to determine the particle size and particle shape of both powders [13] and granules [14] in order to predict the flowability of the investigated particles.

In this study, photometric stereo imaging (FlashSizer 3D) [15] was used for the evaluation of the granule size distribution, the roughness and the shape of continuously produced wet granules. The technique is based on the illumination of the sample with two different white-light sources which are placed in an angle of 180° in a horizontal plane. These two images are then combined in order to obtain a 3D surface image of the measured sample. The surface images are not only used to determine the particle size distribution and the particle shape, but the digital images give information about the surface roughness as well. Therefore the image is seen as a combination of pixels, every pixel being a spatial coordinate with a certain light intensity. The grey level of this brightness of the pixel is then characterized with a value, going from 0 to 255, 0 being totally black and 255 fully white. The surface roughness calculation is based on differences in the grey scale values. Soppela et al. [16] evaluated the ability of photometric stereo imaging (FlashSizer 3D) for particle size and flowability measurements of granules. Furthermore, the particle size determination was compared with SFV (Parsum®) and conventional sieving.

NIR spectroscopy has been extensively studied for moisture analysis of granules. For instance, Hartung et al. [17] used NIR spectroscopy for the in-line moisture monitoring during a spray drying and tableting process of enalapril maleate. The in-line moisture measurements were then used to evaluate the influence of moisture on the final tablet hardness. To study the end point of a fluid bed drying cycle, a PLS model was developed in order to predict the moisture content by means of in-line NIR-spectra, with loss on drying as

reference method [18]. Nieuwmeyer et al. [19] did similar work, using Karl Fischer as a reference method. Furthermore, based on the same NIR-spectra a PLS model was built in order to predict the median granule size. In-line NIR-measurements for residual moisture prediction have already been performed on the ConsiGma™-system [20]. Only a limited amount of tests was performed, which was covering a small range of residual moisture content (0.43-1.06 % w/w). NIR spectroscopy in combination with multivariate data analysis has also been investigated in order to predict the flowability of both powders [21] and granules [22]. An overview of the applications of NIR and Raman spectroscopy in pharmaceutical production processes has been provided by De Beer et al. [23].

Multiple papers report on the usefulness of Raman spectroscopy in detecting changes in the API and excipient solid state properties during pharmaceutical granulation processes. The API, theophylline, used in the present study has been thoroughly investigated during pharmaceutical processing. Theophylline can occur in several solid state forms during wet granulation and drying [24]. Anhydrous theophylline was mixed in the dry premix, and as expected, this was converted to theophylline monohydrate during wet granulation [6]. Drying induces the conversion from the hydrated form of theophylline to either anhydrous theophylline or a metastable form of theophylline, depending on the applied temperature and drying technique [25].

In the advent of increasing interest in continuous granulation in pharmaceutical manufacturing it is evident that studies are needed to assess the quality of the intermediate and final products. The present study **aim**s to combine solid state, moisture, granule size and roughness data obtained from at-line Raman and NIR spectroscopic and photometric imaging measurements to predict flow properties and residual moisture content of continuously produced granules. All three PAT tools measure different granule properties, which all might contribute to granule flowability and downstream processability.

11.2. MATERIALS AND METHODS

11.2.1. Materials

Anhydrous theophylline (Farma-Quimica sur SL, Malaga, Spain) (30%, w/w) was granulated with lactose monohydrate 200M (Caldic, Hemiksem, Belgium). Polyvinylpyrrolidone (Kollidon®30, BASF, Burgbernheim, Germany) was added as a binder to the dry powder mixture in a concentration of 2.5% (w/w). Distilled water was used as granulation liquid. Sodium lauryl sulfate (Fagron, Waregem, Belgium) was added to the granulation liquid (0.5% w/v) to improve the wettability of the dry powder mixture.

11.2.2. Wet granulation

All granules were produced using the ConsiGma™ 25 unit (GEA Pharma Systems nv., Collette™, Wommelgem, Belgium)[6].

Table 11.1. Experimental design.

Experiment	Barrel temperature (°C)	Powder feed rate (kg/h)	Drying temperature (°C)
1	40	25	35
2	25	25	75
3	32.5	17.5	55
4	25	10	75
5	32.5	17.5	55
6	25	10	35
7	25	25	35
8	40	10	75
9	40	25	75
10	32.5	17.5	55
11	40	10	35

In order to obtain granules with different characteristics, a 3-factor 2-level full factorial design (DoE) was performed in randomized order (Table 11.1). Three centerpoint experiments were performed as well, resulting in $2^3 + 3 = 11$ experiments. The temperature of the granulator barrel, the powder feed rate and the temperature of the drying air were varied in order to obtain granules of different size distributions, solid state and moisture content. Preliminary experiments showed that – besides the screw configuration – these three factors significantly influenced the granule properties [6, 25]. The screw speed was held constant at 950 rpm and granulation liquid was added (9.16% (w/w), based on the wet mass). For each experiment, one drying cell of the six-segmented fluid bed dryer was filled with 1 kg of granules and an airflow of 400 m^3/h was used.

11.2.3. Photometric imaging technique

A photometric stereo camera system (FlashSizer3D, Intelligent Pharmaceutics Ltd, Finland) was used for particle size measurement and surface characterization (roughness and shape) of the produced granules. All data were collected using the FlashSizer3D Process Interface Software. The size ranges used for the calculation of the particle size distribution were: 0-150 µm, 151-250 µm, 251-500 µm, 501-710 µm, 711-1000 µm, 1001-1400 µm, 1401-2000 µm and 2001-3150 µm and >3150 µm. The FlashSizer 3D was equipped with a steel chute and glass window. The produced granules were poured into this chute and images were taken through the glass window. Due to the high amount of fines, which were present in most granule loads of the design experiments, the glass window of the imaging system was covered by fines, which resulted in an underestimation of the granules' particle size. Therefore, during each DoE experiment granules were, prior to the measurement, carefully derived from the manufacturing line into transparent rectangular plastic flasks, by means of a glass funnel. Three samples were collected per DoE experiment and each sample was analyzed in triplicate using the calculation mode "3D Surface", which calculates the particle size and global image roughness as described by Soppela et al. [16]. The averages of these nine granule size distribution and roughness measurements per DoE experiment were then used for data interpretation. Data were Unit Variance (UV)-scaled before applying PCA.

11.2.4. Raman spectroscopy

A RamanRxn1 spectrometer (Kaiser Optical Systems, Ann Arbor, Michigan), equipped with an air-cooled CCD detector (back-illuminated deep depletion design) was used with a fiber-optic non-contact MR probe. The laser wavelength was the 785 nm line from a 785 nm Invictus NIR diode laser. For each DoE experiment 20 spectra were statically recorded at-line with a resolution of 4 cm^{-1} and an exposure time of 20 seconds, using a laser power of 400 mW. Data collection and data transfer were automated using the HoloGRAMS™ data collection software and the HoloREACT™ reaction analysis and profiling software. The spectral data were centered and Standard Normal Variation (SNV) corrected before applying PCA.

11.2.5. NIR spectroscopy

A Fourier-Transform NIR spectrometer (Thermo Fischer Scientific, Zellik, Belgium, Nicolet Antaris II near-IR analyzer) equipped with an InGaAs detector, a quartz halogen lamp and a fiber optic diffuse reflectance probe was used. Again, 20 spectra of each granulation experiment were statically collected at-line in the 10000 - 4500 cm^{-1} region with a resolution of 16 cm^{-1} and averaged over 16 scans. Data collection and data transfer were done using Thermo Fischer Scientifics' Result Software. NIR spectra were centered and SNV-corrected prior to chemometric analysis.

11.2.6. Residual moisture determination

The residual moisture content of the granules of each DoE experiment was determined by volumetric Karl Fischer titration using a V30 volumetric KF titrator (Mettler Toledo, USA). Methanol (Hydranal, Sigma Aldrich, Germany) was used as a solvent. Before titration, approximately 50 mg of granules were stirred and dissolved in methanol during 5 minutes. Measurements were performed in triplicate.

11.2.7. Granule flow measurements

After production, the bulk density, tapped density and Hausner ratio of each DoE experiment were determined. Approximately 40 g of granules were poured into a 100 ml graduated cylinder. The granule weight and volume were used to calculate bulk density.

Then, each sample was tapped 1250 times using an automatic tapping instrument (J. Engelsmann AG, Ludwigshafen am Rhein, Germany) and the volume reading was then used to determine the tapped density. All density measurements were performed in triplicate and the average density was calculated. Bulk and tapped densities were used to determine granule flow characteristics via calculation of Hausner ratio values.

11.2.8. Data analysis

Several principal components analysis (PCA) and partial least squares (PLS) models were developed using a multivariate data analysis software package (Simca P+ 12.0, Umetrics AB, Umeå, Sweden). PCA was performed on all collected NIR and Raman spectra and imaging data to gain a first insight into the variation between the differently processed granules. Afterwards, three prediction models were built by means of PLS regression as an attempt to predict moisture content, Hausner ratio and bulk and tapped density of the granules (y) from the combined spectral and FlashSizer information (X). The number of PCA and PLS components was selected providing the highest Q^2 value. The Q^2 value is the part of the total variation of X (PCA models) or y (PLS models) that can be predicted by a component, as estimated by cross-validation [26].

11.3. RESULTS AND DISCUSSION

11.3.1. Principal Component Analysis

PCA was applied on the spectral data of all 220 observations (20 spectra per DoE experiment, 11 DoE experiments) to investigate the spectral variation caused by differences in solid state properties and moisture content of the differently prepared granules.

11.3.1.1. Raman spectroscopy

The spectral region from 200 cm^{-1} to 1800 cm^{-1} was selected to perform PC analysis on all collected and SNV preprocessed Raman spectra. Four principal components described 97.6% of the spectral variation. The first, second, third and fourth PC explained 47.12%, 26.95%, 16.24% and 7.25 %, respectively. Figure 11.1 shows the PC 1 versus PC 2 scores plot. Two obvious clusters were identified. Cluster A contains all granules dried at 55°C and 75°C, whereas cluster B derived from granules dried at 35°C. The same clusters were obtained by plotting PC 2 versus PC 3 (Figure 11.2).

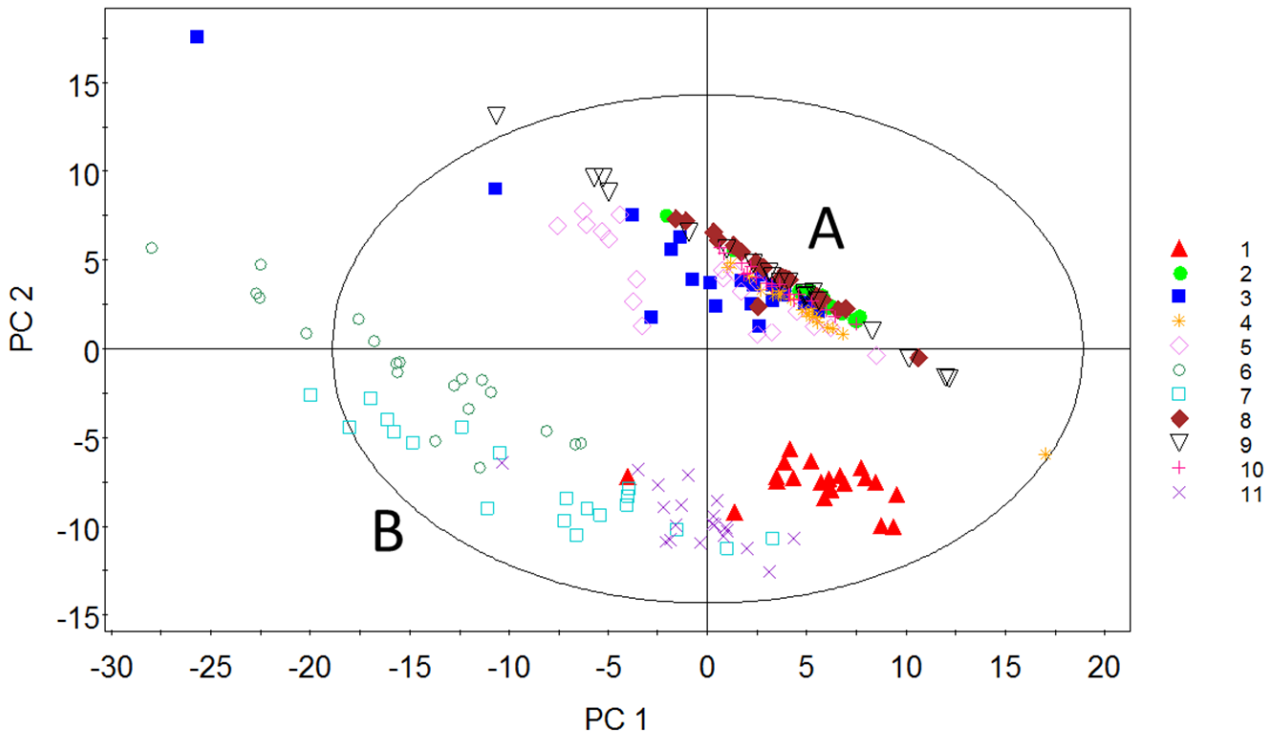

Figure 11.1. Raman spectra: PC 1 (47.12%) versus PC 2 (26.95%) scores plot.

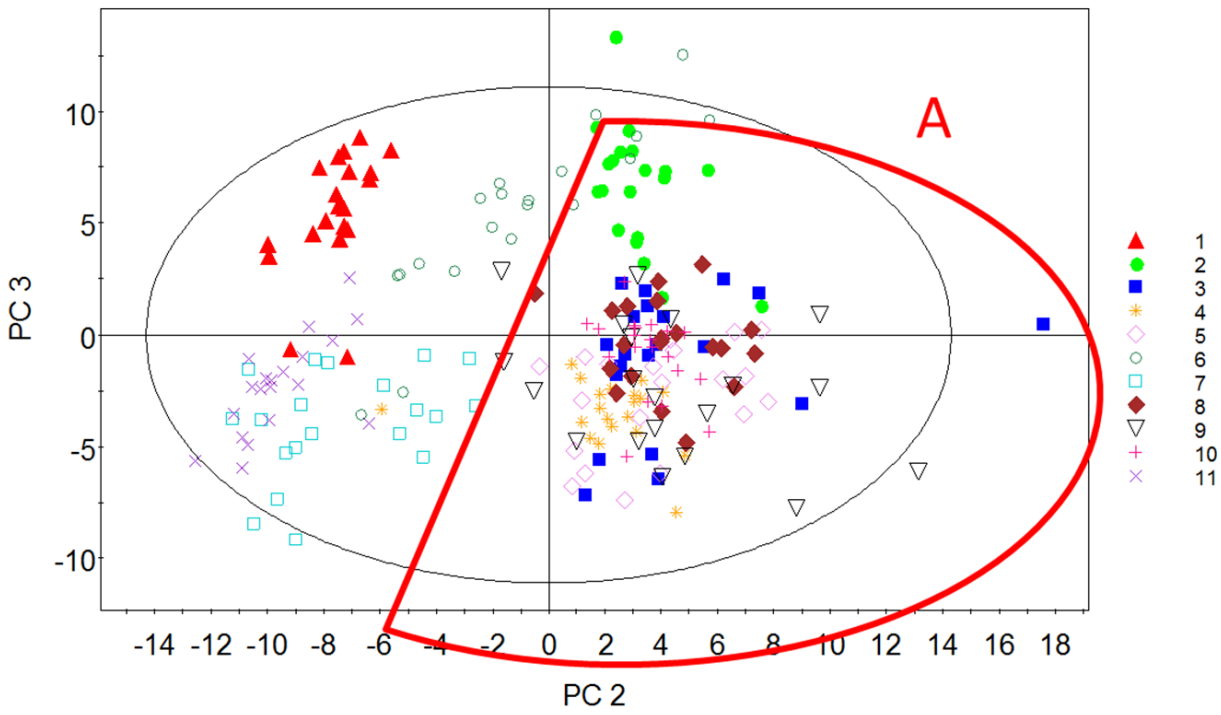

Figure 11.2. Raman spectra: PC 2 (26.95%) versus PC 3 (16.24%) scores plot.

To explain why these two groups are clustered one should look at the loadings. Meaningful information regarding the solid state of theophylline can for example be found in the spectral range from 1636 cm^{-1} to 1737 cm^{-1}. The spectrum of anhydrous theophylline shows two intense peaks at 1664 and 1706 cm^{-1}, whereas theophylline monohydrate has a peak at 1686 cm^{-1}, which is due to C=O stretch of the carbonyl-groups [27]. Dukic-Ott et al. [28] presented the Raman-spectrum of metastable theophylline, showing a signal at 1692 cm^{-1}. The PCA loadings plots of PC 1, PC 2 and PC 3 at this spectral region (1636 cm^{-1} to 1737 cm^{-1}) can be found in Figure 11.3. The positive and negative peaks in the loadings plots of PC 1, PC 2 and PC 3 are listed in Table 11.2. Cluster A has mainly positive PC 1 and PC 2 score values, while cluster B has mainly negative PC 1 (except for DoE experiment 1) PC 2 score values. Hence, Cluster A mainly contains anhydrous and metastable theophylline granules, whereas cluster B mainly contains granules with theophylline monohydrate. The applied ConsiGma™ 25 unit uses untreated ambient air for drying. At ambient inlet air, metastable theophylline will only occur at elevated temperatures (50° and up) whereas at lower temperatures the granules will hardly dry and stay in the monohydrate-form [25]. Cluster A contains DoE experiments 2, 3, 4, 5, 8, 9 and 10, which were all dried at 55° or 75°C, resulting in granules

consisting of anhydrous and metastable anhydrous theophylline. Cluster B includes experiments 1, 6, 7 and 11, dried at 35°C, which is not high enough to remove the hydrate water from the granules.

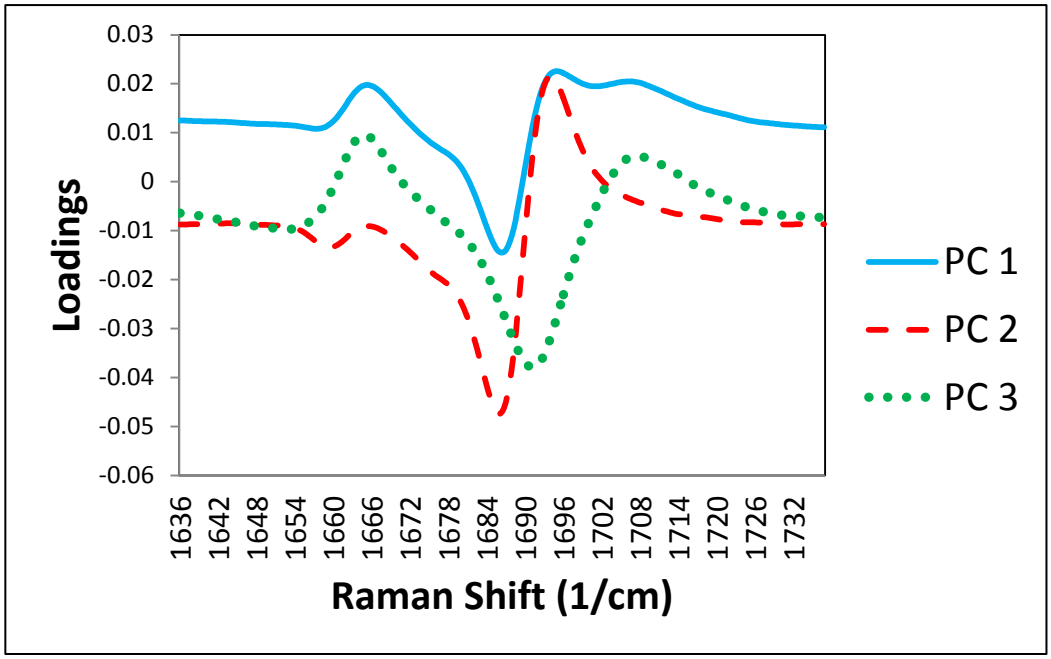

Figure 11.3. Raman spectroscopy: PC A loadings plots of PC 1, PC 2 and PC 3.

Table 11.2. Raman spectroscopy: Overview and interpretation of the positive and negative peaks in the loadings plots of PC 1, PC 2 and PC 3.

Loading	Positive	Negative
1	1665 – 1695 – 1707 Anhydrous + Metastable	1686 Monohydrate
2	1693 Metastable	1686 Monohydrate
3	1665 & 1707 Anhydrous	1692 Metastable

In cluster B, the PC 1 score values of experiment 1 (red full triangles, Figure 11.1) are positive, unlike the score values of the other experiments of cluster B. Furthermore, the PC 3 score values of experiment 1 are clearly positive as well. This indicates that the granules of experiment 1 contain a significant amount of anhydrous theophylline besides theophylline monohydrate. This can clearly be seen in the Raman spectra of experiment 1, showing distinct anhydrous theophylline signals at 1664 and 1706 cm^{-1} and 555 cm^{-1} besides the monohydrate signal at 1686 cm^{-1} (Figure 11.4). The residual moisture content of the granules of all experiments was measured directly after drying. Indeed, experiment 1 was found to have a slightly lower moisture content (5.43%) after drying compared to the other three experiments of cluster B (6.38%, 6.76% and 6.62%). Earlier work performed on the ConsiGma™ 25 system revealed that small amounts of theophylline can remain anhydrous after wet granulation, when high barrel temperatures and high powder feed rates are applied (as is the case for experiment 1) [6]. Hence the significantly larger amount of anhydrous theophylline might not be caused by the drying process, but might be a matter of formation of smaller amounts of theophylline monohydrate in the first place. In cluster A, experiment 2 has higher PC 3 score values (green full dots) compared to the other experiments of cluster A (Figure 11.2). This indicates that run 2 contains more anhydrous theophylline and less metastable theophylline compared to the other experiments of cluster A. Again, this was confirmed by the pure Raman-spectra of the granules in cluster A (spectra not shown).

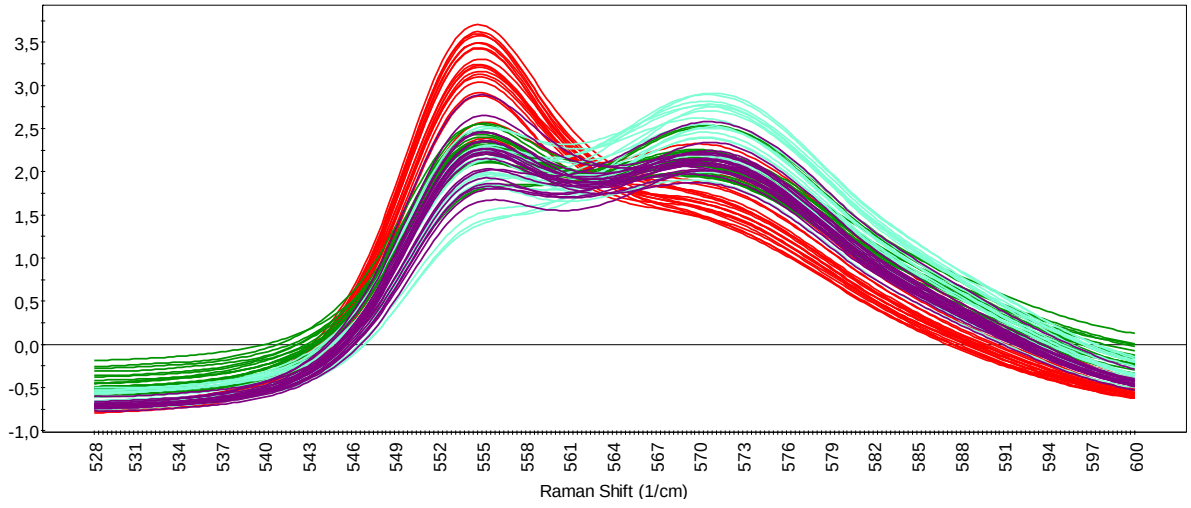

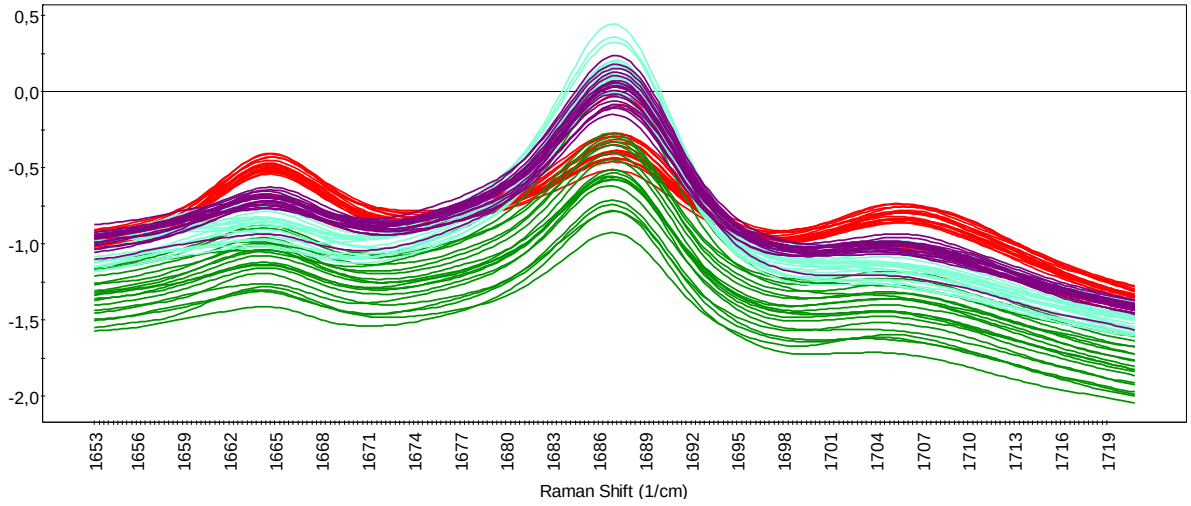

Figure 11.4. SNV-corrected Raman spectra of the granules of all DoE experiments in Cluster B, (experiment 1: red, experiment 6: green, experiment 7: blue and experiment 11: purple). Experiment 1 (red) clearly shows more intense anhydrous theophylline Raman signals (555, 1664 and 1706 cm^{-1}) in comparison to the other experiments of Cluster B.

11.3.1.2. NIR spectroscopy

The spectral region from 8500 cm^{-1} to 4500 cm^{-1} was taken into account to perform a PC analysis on all collected NIR spectra, resulting in three principal components. These explained 96.8 % of the spectral variation. PC 1 explained 69.34 % of the spectral variation, PC 2 21.19% and PC 3 6.24%. In Figure 11.5, the PC 1 versus PC 2 scores plot shows two distinct clusters along the PC 2-axis. Cluster B, having positive PC 2 score values, comprises experiments 1, 6, 7 and 11, whereas cluster A has negative PC 2 score values. The loadings plot (Figure 11.6) of the second principal component shows a positive band at 5068 cm^{-1} and 6749 cm^{-1}, which can be attributed to the hydrate water of theophylline monohydrate [29]. This confirms the Raman analysis, which also showed that experiments 1, 6, 7 and 11 resulted in granules containing theophylline monohydrate. Furthermore, these granules contain higher residual moisture after drying, as is confirmed by the Karl Fischer moisture determinations. One run in cluster A tends to be partly in the positive part of the PC 2-axis, namely run 3 (full blue squares). This can easily be explained by means of the Karl Fischer values, run 3 has the highest moisture content after drying compared to the other granules of cluster A.

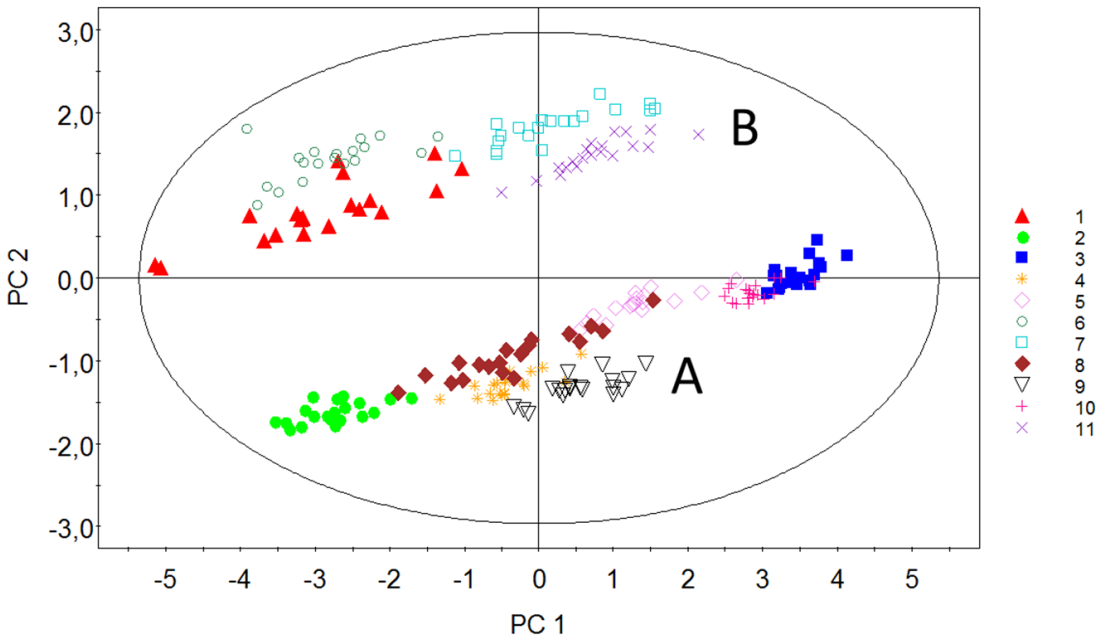

Figure 11.5. NIR spectroscopy: PC 1 (69.34%) versus PC 2 (21.19%) scores plot.

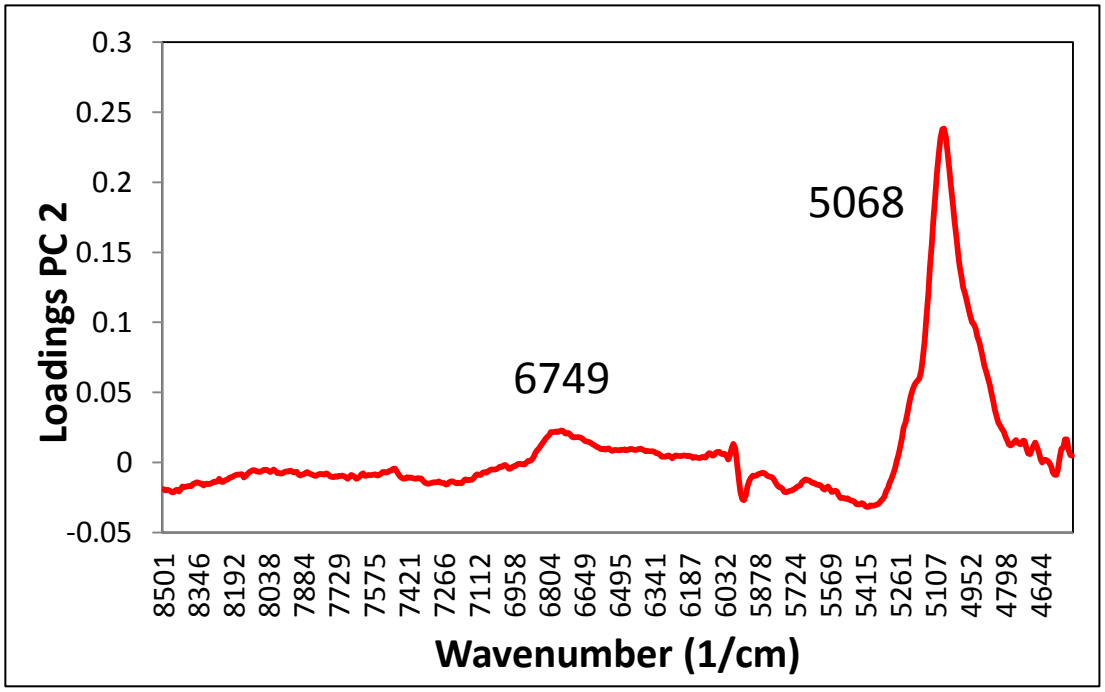

Figure 11.6. NIR spectroscopy: Loadings plot of the second principal component (21.19%).

In the near infrared region, water has large absorption bands. In particular the combination bands of O-H are very strong. The wavenumber and width of these bands may vary slightly, depending on the chemical and physical environment. Maxima were for example found

around 7042 cm^{-1} (overtones) and 5208 cm^{-1} (combination bands) [30]. Rasanen et al. [29] reported the bands of free water around 7092 cm^{-1} and 5249 cm^{-1}. They also describe how free water can be distinguished from hydrate water in the 2nd derivatives of the NIR spectra of theophylline granules by means of the free water band around 5249 cm^{-1} and a hydrate band around 5070 cm^{-1}. Furthermore, Luukkonen et al. [31] describe that lactose monohydrate shows a hydrate band around 5168 cm^{-1}. The 2nd derivatives of all collected NIR spectra of the DoE experiments clearly show a *lactose* monohydrate signal around 5168 cm^{-1} while only experiments 1, 6, 7 and 11 show a theophylline monohydrate signal around 5068 cm^{-1} (Figure 11.7), confirming the Raman findings. Free water bands cannot be seen in any of the NIR spectra.

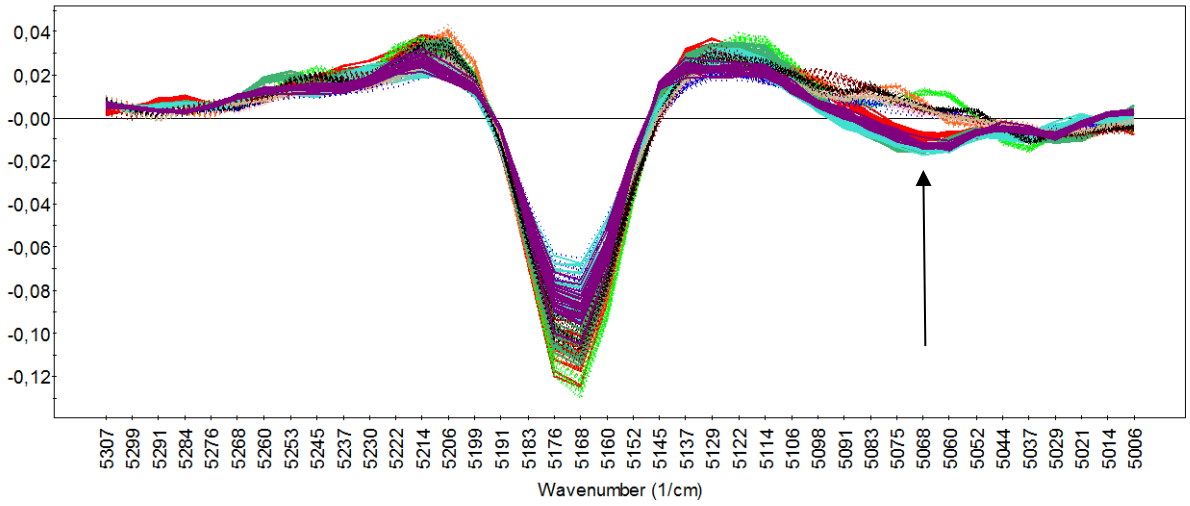

Figure 11.7. NIR spectroscopy: Second derivative of NIR spectra. Colored applied as above for Cluster A (dashed line) and Cluster B (full line).

11.3.1.3. Particle size distribution and roughness

The FlashSizer 3D process analyzer provided granule size distribution and granule surface roughness information. A PC analysis was performed on the imaging data of all 11 DoE experiments. The granule size distributions were derived from nine sieve fractions (see method section) and one average roughness value was obtained per experiment, leading to an 11x10 data matrix. PCA resulted in a three component model, explaining 73.35% (PC 1), 17.88% (PC 2) and 6.26% (PC 3) of variation respectively. The PC 1 versus PC 2 loadings bi-plot shows 4 clusters: a cluster containing experiments 9 and 11; a cluster containing

experiments 5, 7 and 8; a cluster containing experiments 1, 2, 3 and 10 and a cluster containing experiments 4 and 6 (Figure 11.8). The clustered experiments indicate granules having similar size and roughness properties, whereas those experiments which are located far from each other are dissimilar with respect to granule size distribution and roughness values. The loadings in the bi-plot also display the relationships between all 10 variables (9 sieve fractions + 1 roughness value). The variables contributing similar information are grouped together, meaning they are correlated. The lower sieve fractions (< 150 µm, 150-250 µm and 250-500µm) are positively correlated. A similar conclusion can be made for the higher sieve fractions. Furthermore, the roughness value is positively correlated with the higher sieve fractions, indicating that higher roughness values are obtained for larger granules. This is expected as the roughness value is a value describing the global roughness of the image. When there are larger particles present there is more shading effect, thus more variation in the surface images.

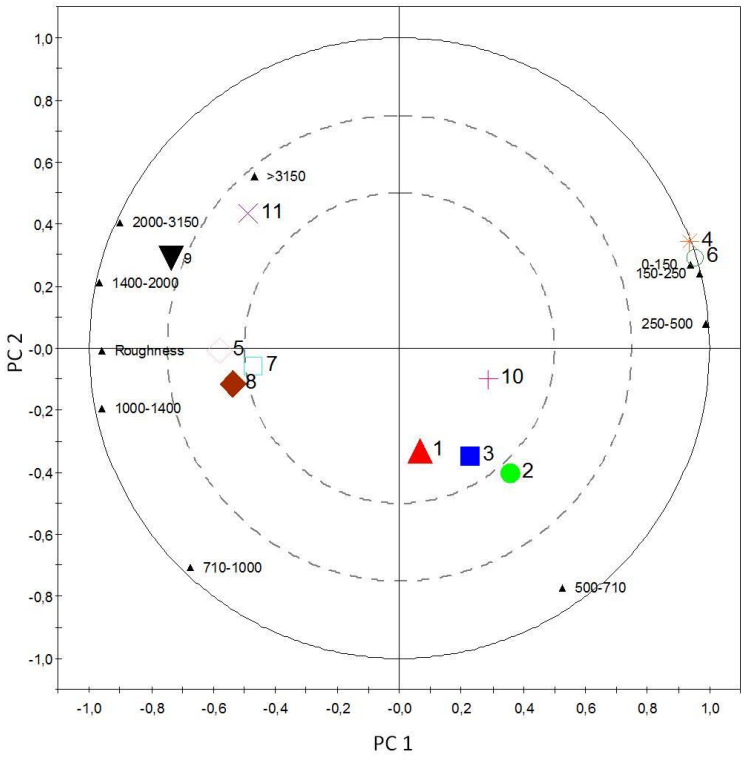

Figure 11.8. Flashsizer 3D-data: roughness and sieve fractions: PC 1 (73.55 %) versus PC 2 (21.19 %) bi-plot.

Finally, Figure 11.8 shows that the lower and higher sieve fractions are negatively correlated, indicating that when the amount of fines (0-250 µm) decreases, the amount of oversized granules increases (> 1400 µm), and vice versa. This also suggests that increasing or decreasing the amount of fines and oversized granules does not affect the yield (150 µm < yield < 1400 µm). The distance of the variables to the origin of the loadings plot also conveys information. The further away from the plot origin a variable is situated, the stronger impact that specific variable has on the model. The bi-plot shows that all variables have similar distances to the plot origin, indicating that all variables have a similar impact on the model. To conclude, the first PC seems to explain the variability in fines and oversized granules, while the second PC reflects the yield. Experiments 9 and 11 resulted into granules having a large oversized fraction and a high roughness value. Experiments 5, 7 and 8 also result in more oversized granules, but have a larger yield fraction compared to experiments 9 and 11. Experiments 4 and 6 result in granules with a large fine fraction, while experiments 1, 2, 3 and 10 result in granules having the largest yield fraction. Experiments 4 and 6 also have the lowest roughness value. After tapping the granules of these runs they have the highest densities of all experiments. This indicates that fines can fill the cavities in between larger granules. This leads to a flatter surface at the side of the rectangular plastic flask, which results in a smoother picture and hence a lower roughness value.

11.3.2. Partial Least Squares Modeling

This paragraph evaluates the possibility of using the complementary physical and chemical granule information (granule size distribution, shape, solid state) supplied by the at-line measurements for the prediction of critical granule properties, such as residual moisture content and flow properties. Therefore, three PLS models were developed and evaluated. The NIR and Raman spectra, as well as the imaging data (granule size distribution and roughness values) and the process settings of the DoE experiments were used as X-variables (Figure 11.9).

For the Raman and NIR data, the score values of the principal components of their PCA models (cfr. supra) were included in the X-matrix. Twenty Raman and NIR spectra were collected after each granulation run, resulting in 220 rows (i.e., 11 granulation runs x 20 spectra) for the X-matrix. From the imaging data, the per DoE experiment averaged granule

size distribution values and roughness values were used. The DoE process settings, being the temperature of the granulator barrel, the powder feed rate and the temperature of the drying air, completed the X-matrix.

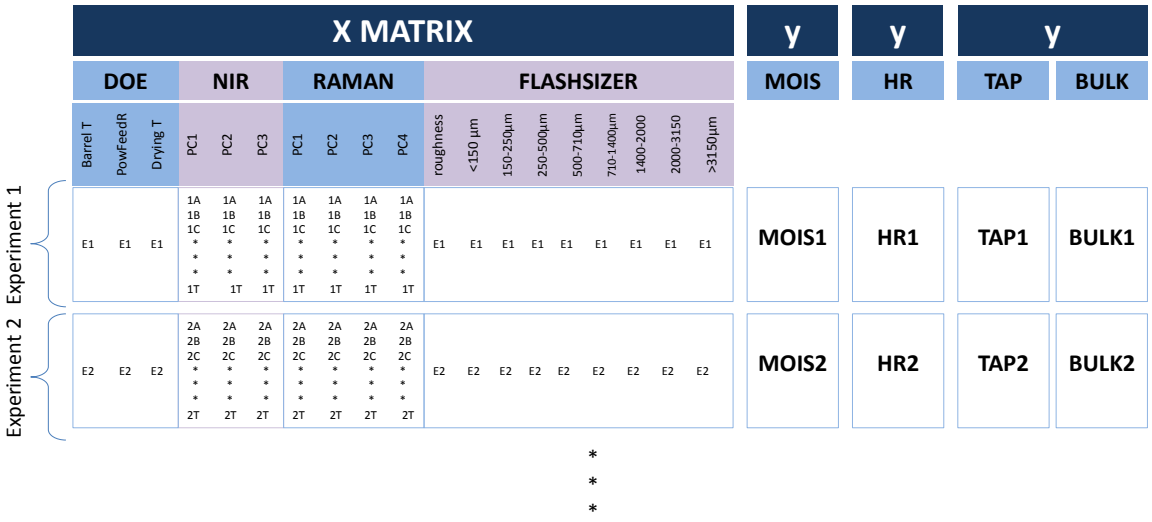

Figure 11.9. Data used for the development of the PLS models: X-matrix and y-variables.

PLS models for moisture content, flowability (Hausner ratio) and density were developed separately and evaluated based on their predictive performance after cross-validation. Cross-validation was done as follows: (1) $1/11^{th}$ (= 1 DoE experiment) of the data was kept out of the model development; (2) the experiment which was kept out of the model development was then predicted by the model: (3) the predictions of the kept out data were compared with the actual values, hence the Root Mean Square Error of Cross Validation (RMSECV) was calculated. This procedure was repeated for the eleven experiments.

The model for moisture content resulted in 2 PLS components, explaining 95.3 % of the variation (R^2). The model resulted in a RMSECV of 0.64 %. The loadings line plot of the first PLS component (Figure 11.10) suggests that the score values of the second PC of the NIR PCA model are positively correlated to the residual moisture content, while the score values of the first and second principal component of the Raman PCA model together with the temperature of the drying air are negatively correlated to the residual moisture content.

The influential effect of the score values from the second principal component of the NIR PCA model can simply be explained by the fact that this 2^{nd} PC differentiates between

theophylline spectra with and without hydrate-water. Indeed, the granules containing theophylline monohydrate have higher residual moisture contents. The importance of the score values of the first and second principal component of the Raman PCA model can be explained using Table 11.2. These two Raman PCA model principal components differentiate between granules containing theophylline monohydrate and granules without theophylline monohydrate. Hence, one can say that the higher the amount of theophylline monohydrate in the granules, the higher the residual moisture content will be. The negative loadings value for the drying temperature for the first PLS component shows that a high temperature of the drying air will result in a lower residual moisture content of the end product. The loadings of the first PLS component show that the DoE-parameters and the spectral data have the highest correlation with the moisture content (y), while the particle size and shape information have the lowest correlation with the moisture content (y). A new model was built, only taking these former parameters into account and excluding the imaging data. This resulted in a model with 1 PLS component and an RMSECV of 0.44%. A third model with the temperature of the drying air, the second PC of the NIR PCA model and the first and second PC of the Raman PCA model resulted in a model with 1 PLS component and an RMSECV of 0.29%.

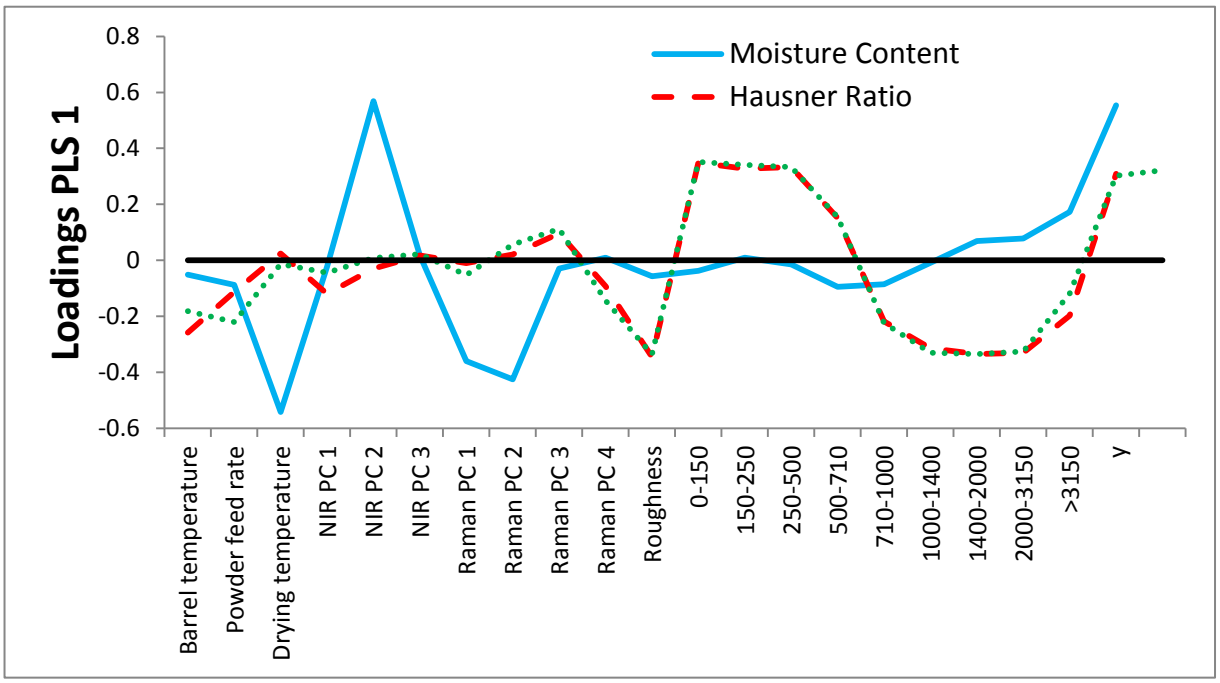

Figure 11.10. Loadings plot of the first PLS component of the three PLS models.

A second PLS model was developed in order to predict the density of the granules (y), taking both bulk and tapped density into account. The model, consisting of 1 PLS component, had an R^2 of 79.2%. The RMSECV was calculated to be 0.0127 g/ml for the bulk density and 0.0190 g/ml for the tapped density. The loadings line plot of the first PLS component (Figure 11.10) shows correlation between particle size distribution and bulk and tapped density. A positive correlation of the fines and smaller granules (<710 µm) and a negative correlation of the larger particles confirm that small particles can be more easily packed than large particles. Furthermore, the roughness value is negatively correlated with the density, since granulation experiments resulting in larger granules have high roughness values, which is resulted from the less densely packed powder bed surfaces (cfr. supra). The negative correlation of both barrel temperature and powder feed rate with the density parameters can be explained by the fact that larger granules are obtained when high barrel temperatures and high powder feed rates are applied [6]. A second model with only the DoE parameters and the imaging data in the X-matrix was built and resulted in an RMSECV of 0.0112 g/ml for the bulk density and 0.0165 g/ml for tapped density.

A last PLS model was developed for Hausner ratio (y), resulting in one PLS component, which explained 78.3% of the variation. This model resulted in an RMSECV of 0.0140. According to the loadings line plot of the first PLS component (Figure 11.10), correlation between the FlashSizer data and the Hausner ratio can be seen. The fines and small particles (< 710 µm) have a clear positive correlation with the Hausner ratio. The higher the Hausner ratio is the poorer granules will flow. Indeed, fines will decrease the flowability of the granules. On the other hand, larger granule sizes (710 µm and more) are negatively correlated to the Hausner ratio, as larger granules have a better flowability [3]. The roughness value is negatively correlated with the Hausner ratio as well. It was stated earlier (PSD and Roughness section) that granulation experiments leading to granules with a low roughness value contain more fines, which indeed results in a poorer flowability and a higher Hausner ratio. Finally, the barrel temperature, and to a lesser extent the powder feed rate have a negative influence on the Hausner ratio since a high barrel temperature and a high powder feed rate result in larger granules (i.e., a lower Hausner ratio). The model, built with the DoE parameters and imaging data only resulted in an RMSECV of 0.0130.

11.4. CONCLUSION

This study proves the utility of three PAT tools for the at-line analysis of continuously produced granules. Data were recorded with both a Raman and an NIR spectrometer next to a photometric imaging technique. The residual moisture content was mostly correlated with the NIR spectroscopic data, whereas the imaging data had the highest predictive capability for the flowability of the granules. Hence, the information offered by the spectrometers and the photometric imaging technique is complementary.

11.5. REFERENCES

[1] C. Vervaet, J.P. Remon, Continuous granulation in the pharmaceutical industry, Chemical Engineering Science, 60 (2005) 3949-3957.

[2] F. Roche, Continuous Processing In Secondary Manufacturing, in: Continuous OSD Production Seminar, Wommelgem, Belgium, 2011.

[3] H.G. Kristensen, T. Schaefer, GRANULATION - A REVIEW OF PHARMACEUTICAL WET-GRANULATION, Drug Dev. Ind. Pharm., 13 (1987) 803-872.

[4] T.O. Althaus, E.J. Windhab, Characterization of wet powder flowability by shear cell measurements and compaction curves, Powder Technology, 215–216 (2012) 59-65.

[5] FDA-Adminstration, Guidance for Industry - PAT - A Framework for Innovative Pharmaceutical Development, Manufacturing and Quality Assurance, in, 2004.

[6] M. Fonteyne, J. Vercruysse, D.C. Díaz, D. Gildemyn, C. Vervaet, J.P. Remon, T.D. Beer, Real-time assessment of critical quality attributes of a continuous granulation process, Pharmaceutical Development and Technology, *early online,* DOI: 10.3109/10837450.2011.627869.

[7] A. Burggraeve, T. Van Den Kerkhof, M. Hellings, J.P. Remon, C. Vervaet, T. De Beer, Evaluation of in-line spatial filter velocimetry as PAT monitoring tool for particle growth during fluid bed granulation, European Journal of Pharmaceutics and Biopharmaceutics, 76 (2010) 138-146.

[8] J. Huang, G. Kaul, J. Utz, P. Hernandez, V. Wong, D. Bradley, A. Nagi, D. O'Grady, A PAT Approach to Improve Process Understanding of High Shear Wet Granulation Through In-Line Particle Measurement Using FBRM C35, J. Pharm. Sci., 99 (2010) 3205-3212.

[9] C.V. Liew, L.K. Wang, P.W.S. Heng, Development of a Visiometric Process Analyzer for Real-Time Monitoring of Bottom Spray Fluid-Bed Coating, J. Pharm. Sci., 99 (2010) 346-356.

[10] K. Patchigolla, D. Wilkinson, Crystal Shape Characterisation of Dry Samples using Microscopic and Dynamic Image Analysis, Part. Part. Syst. Charact., 26 (2009) 171-178.

[11] T. Naervanen, K. Seppaelae, O. Antikainen, J. Yliruusi, A new rapid on-line imaging method to determine particle size distribution of granules, AAPS PharmsciTech, 9 (2008) 282-287.

[12] W. Yu, B.C. Hancock, Evaluation of dynamic image analysis for characterizing pharmaceutical excipient particles, International Journal of Pharmaceutics, 361 (2008) 150-157.

[13] W.L. Yu, K. Muteki, L. Zhang, G. Kim, Prediction of Bulk Powder Flow Performance Using Comprehensive Particle Size and Particle Shape Distributions, J. Pharm. Sci., 100 (2011) 284-293.

[14] N. Sandler, D. Wilson, Prediction of Granule Packing and Flow Behavior Based on Particle Size and Shape Analysis, J. Pharm. Sci., 99 (2010) 958-968.

[15] N. Sandler, Photometric imaging in particle size measurement and surface visualization, International Journal of Pharmaceutics, 417 (2011) 227-234.

[16] I. Soppela, S. Airaksinen, J. Hatara, H. Räikkönen, O. Antikainen, J. Yliruusi, N. Sandler, Rapid Particle Size Measurement Using 3D Surface Imaging, AAPS PharmsciTech, (2011) 1-9.

[17] A. Hartung, M. Knoell, U. Schmidt, P. Langguth, Role of continuous moisture profile monitoring by inline NIR spectroscopy during fluid bed granulation of an Enalapril formulation, Drug Dev. Ind. Pharm., 37 (2011) 274-280.

[18] A. Peinado, J. Hammond, A. Scott, Development, validation and transfer of a Near Infrared method to determine in-line the end point of a fluidised drying process for commercial production batches of an approved oral solid dose pharmaceutical product, Journal of Pharmaceutical and Biomedical Analysis, 54 (2011) 13-20.

[19] F.J.S. Nieuwmeyer, M. Damen, A. Gerich, F. Rusmini, K. van der Voort, H. Vromans, Granule characterization during fluid bed drying by development of a near infrared method to determine water content and median granule size, Pharmaceutical Research, 24 (2007) 1854-1861.

[20] L. Chablani, T.M. K, M. Amit, R. Patrick, S.W. C, Inline Real-Time Near-Infrared Granule Moisture Measurements of a Continuous Granulation-Drying-Milling Process, AAPS PharmsciTech, 12 (2011) 1050-1055.

[21] M.C. Sarraguca, A.V. Cruz, S.O. Soares, H.R. Amaral, P.C. Costa, J.A. Lopes, Determination of flow properties of pharmaceutical powders by near infrared spectroscopy, Journal of Pharmaceutical and Biomedical Analysis, 52 (2010) 484-492.

[22] M. Otsuka, Y. Mouri, Y. Matsuda, Chemometric Evaluation of Pharmaceutical Properties of Antipyrine Granules by Near-Infrared Spectroscopy, AAPS PharmsciTech, 4 (2003) 1-7.

[23] T. De Beer, A. Burggraeve, M. Fonteyne, L. Saerens, J.P. Remon, C. Vervaet, Near infrared and Raman spectroscopy for the in-process monitoring of pharmaceutical production processes, International Journal of Pharmaceutics, 417 (2011) 32-47.

[24] N.V. Phadnis, R. Suryanarayanan, Polymorphism in anhydrous theophylline - Implications on the dissolution rate of theophylline tablets, J. Pharm. Sci., 86 (1997) 1256-1263.

[25] S. Airaksinen, M. Karjalainen, E. Rasanen, J. Rantanen, J. Yliruusi, Comparison of the effects of two drying methods on polymorphism of theophylline, International Journal of Pharmaceutics, 276 (2004) 129-141.

[26] L. Eriksson, E. Johansson, N. Kettaneh-Wold, J. Trygg, C. Wikström, S. Wold, Multi- and Megavariate Data Analysis Part I: Basic Principles and Applications, Umetrics, Umea, 2006.

[27] H. Wikstrom, P.J. Marsac, L.S. Taylor, In-line monitoring of hydrate formation during wet granulation using Raman spectroscopy, J. Pharm. Sci., 94 (2005) 209-219.

[28] A. Dukic-Ott, T. De Beer, J.P. Remon, W. Baeyens, P. Foreman, C. Vervaet, In-vitro and in-vivo evaluation of enteric-coated starch-based pellets prepared via extrusion/spheronisation, European Journal of Pharmaceutics and Biopharmaceutics, 70 (2008) 302-312.

[29] E. Rasanen, J. Rantanen, A. Jorgensen, M. Karjalainen, T. Paakkari, J. Yliruusi, Novel identification of pseudopolymorphic changes of theophylline during wet granulation using near infrared spectroscopy, J. Pharm. Sci., 90 (2001) 389-396.

[30] G.X. Zhou, Z. Ge, J. Dorwart, B. Izzo, J. Kukura, G. Bicker, J. Wyvratt, Determination and differentiation of surface and bound water in drug substances by near infrared spectroscopy, J. Pharm. Sci., 92 (2003) 1058-1065.

[31] P. Luukkonen, J. Rantanen, K. Makela, E. Rasanen, J. Tenhunen, J. Yliruusi, Characterization of wet massing behavior of silicified microcrystalline cellulose and alpha-lactose monohydrate using near-infrared spectroscopy, Pharmaceutical Development and Technology, 6 (2001) 1-9.

CHAPTER 12

BLEND UNIFORMITY EVALUATION DURING CONTINUOUS MIXING IN A TWIN SCREW GRANULATOR BY IN-LINE NIR USING A MOVING F-TEST

"If a cluttered desk is a sign of a cluttered mind,

of what, then,

is an empty desk a sign?"

Albert Einstein (1879-1955)

ABSTRACT

This study focuses on the twin screw granulator of a continuous from-powder-to-tablet production line, ConsiGma™ 25 (GEA Pharma Systems nv., Wommelgem, Belgium). Whereas powder dosing into the granulation unit is possible from a container of preblended material, a truly continuous process uses several feeders (each one dosing an individual ingredient) and relies on a continuous blending step prior to granulation.

The aim of the current study was to investigate the in-line blending capacity of the twin screw granulator of the ConsiGma™ 25 unit. The feasibility of in-line NIR (SentroPAT, Sentronic GmbH, Dresden, Germany) spectroscopy for evaluating the blend uniformity of powders after the granulator was tested.

Anhydrous theophylline was used as a tracer molecule and was blended with lactose monohydrate. Theophylline and lactose were both fed from a different feeder into the twin screw granulator barrel. Both homogeneous mixtures and mixing experiments with induced error were investigated. The screws consisted of conveying elements only. The in-line spectroscopic analyses showed that the twin screw granulator is a useful tool for in-line blending in different conditions.

The capability of NIR spectroscopy for in-line blend homogeneity detection was evaluated by means of the moving F-test method and this showed to be valuable for replacing the time-consuming off-line UV-VIS spectrophotometry measurements.

The combination of a twin screw granulator equipped with an in-line spectrometer can be used for continuous mixing and evaluating blend homogeneity. Furthermore, the results of this study suggest, that the twin screw granulator might be capable of blending and granulating simultaneously, hence avoiding the need of a continuous blending step prior to granulation.

CHAPTER 12

BLEND UNIFORMITY EVALUATION DURING CONTINUOUS MIXING IN A TWIN SCREW GRANULATOR BY IN-LINE NIR USING A MOVING F-TEST

12.1. INTRODUCTION

By launching its Process Analytical Technology initiative [1], the Food and Drug Administration (FDA) strengthened the need for non-invasive and non-destructive analytical measurement tools for in-line monitoring of critical quality attributes during pharmaceutical manufacturing. Near infrared spectroscopy has clearly proven its usefulness within the pharmaceutical industry [2-8]. For instance, NIR spectroscopy has been researched extensively for the monitoring of pharmaceutical blending. Blending is a common batch unit operation step during the manufacturing of solid dosage forms, i.e. prior to capsule filling, granulation or tableting. Homogeneity of a powder blend is essential to guarantee the correct amounts of drug substances and excipients in every dosage unit. A large number of process input variables such as physical properties of drug substances and excipients, relative humidity, batch size, mixer type and possible interactions between these variables can be considered as critical for a blending process. The use of an in-line NIR blend control application is an alternative approach; since instead of controlling the input parameters, the NIR method can control the blend quality itself. Nowadays, it is also possible to blend in a continuous manner [9].

When monitoring a blending process by means of NIR spectroscopy, two different approaches can be used. The first set of methods uses a training set of spectra taken from homogeneous mixture(s). By comparing each new measurement with the reference spectra

or training set via dissimilarities or Principal Component Analysis (PCA) [10] it is evaluated whether homogeneity is reached. Partial Least Squares (PLS)-regression is the most applied technique for the development of a quantitative NIR method to monitor pharmaceutical blending [11-45], but also Classical Least Squares (CLS)-regression [46], Multivariate Curve Resolution (MCR) [47], Principal Component Regression (PCR) [30] and the net analyte signal (NAS) [48] have been used for this purpose.

The second approach is based on the evaluation of changes in the consecutively collected NIR spectra during blending: the linear superposition method [30] and a qualitative model based on NAS-values [48] are used for this purpose. Furthermore, the bootstrap error-adjusted single-sample technique (BEST) [49] and Principal Component Modified BEST [50], and another pattern recognition algorithm, Soft Independent Modeling of Class Analogies (SIMCA) [50] have been presented. Additionally, examples of traditional Chi-square analysis [49], SIMPLISIMA [51] and additive and iterative mixing models [52] in combination with NIR spectroscopy have been published. In 1998, the group of P. Hailey presented the moving block standard deviation approach applied on NIR spectra collected during blending [53-55]. This is a model-free approach that calculates the variability in the NIR spectra during time, in order to detect the end point of the blending cycle. Their approach has been adopted by several other researchers for NIR in blending [25, 29, 30, 56-59]. For these methods, it is assumed that, once the mixture is homogeneous, the spectra will not change anymore.

Plugge and van der Vlies already demonstrated the usefulness of the F-test for blend homogeneity determination [60] and Flåten et al. combined the moving block strategy with the F-test [61, 62].

The main **aim** of this study is to present a new statistical method, based on the moving F-test and without the need for an external calibration model, for the evaluation and control of blend uniformity using NIR spectroscopy during *continuous* mixing via a twin screw granulator (ConsiGma™ 25). The method development differs from conventional batch blending. Furthermore, both the α- and β-error were controlled. The rationale for evaluating the continuous mixing of powders in a twin screw granulator aligns with our future research

goals to examine whether continuous powder mixing and continuous wet granulation can be performed simultaneously using the same continuous unit operation equipment.

12.2. MATERIALS AND METHODS

12.2.1. Materials

A binary blend was evaluated, using anhydrous theophylline as model Active Pharmaceutical Ingredient (API) (Farma-Quimica sur SL, Malaga, Spain) and lactose monohydrate 200M (Caldic, Hemiksem, Belgium) as filler.

12.2.2. Batch blending

To develop the moving F-test method, some theophylline/lactose mixtures had to be blended batch wise (see results section). This was done using a tumbler mixer (20L Bioengineering, Inversina, Wald, Switzerland). Two thirds of the bin were filled (i.e. 6.5 kg) with the envisaged amounts of theophylline and lactose and the powders were mixed during ten minutes, with a speed of 25 rpm.

12.2.3. Continuous mixing using a twin screw granulator

The continuous mixing was performed using the twin screw granulator which is part of the ConsiGma™ 25 system (GEA Pharma Systems nv., Collette™, Wommelgem, Belgium). The screws were equipped with conveying elements only and two feeders were used, each feeding one component in the granulator. Theophylline was added via the first feeder (LWF D5, K-Tron AG, Niederlenz, Switzerland), whereas lactose was added 13.5 cm further in the barrel by a second feeder (K-CL-KT20, K-Tron Soder, K-Tron AG, Niederlenz, Switzerland) (Figure 12.1). Under the outlet of the granulator, an aluminium slide was mounted at an angle of 45°. The powder could flow freely on this slide. The flat-faced probe-head of an NIR spectrometer was mounted parallel to the slide with a distance of approx. 5 mm to the slide (Figure 12.2).

The feed rate, weight loss and remaining weight of the theophylline feeder were continuously logged, but no logged data could be collected from the stand-alone lactose feeder. Two continuous blending experiments were conducted. Experiment 1 was conducted with a target concentration of 30% theophylline in lactose. The total powder feed rate was 25 kg/h and the applied screw speed was 600 rpm. During Experiment 2 process disturbances were induced on purpose. The total powder feed rate was again 25 kg/h at all

times and the applied screw speed was 900 rpm. At the beginning of this experiment the targeted theophylline concentration was 25%. The theophylline feeder fed with a speed of 6.25 kg/h while the other feeder added 18.75 kg/h of lactose. During this experiment, the theophylline feeder was switched of three times: during ten seconds after two minutes, during twenty seconds after four minutes and during thirty seconds after six minutes. After eight minutes the theophylline feeder was set to 3.75 kg/h, resulting in a theophylline concentration of 15% in the powder blend. After eleven minutes the theophylline feed rate was decreased again to 1.25 kg/h, resulting in a theophylline concentration of 5% in the powder blend.

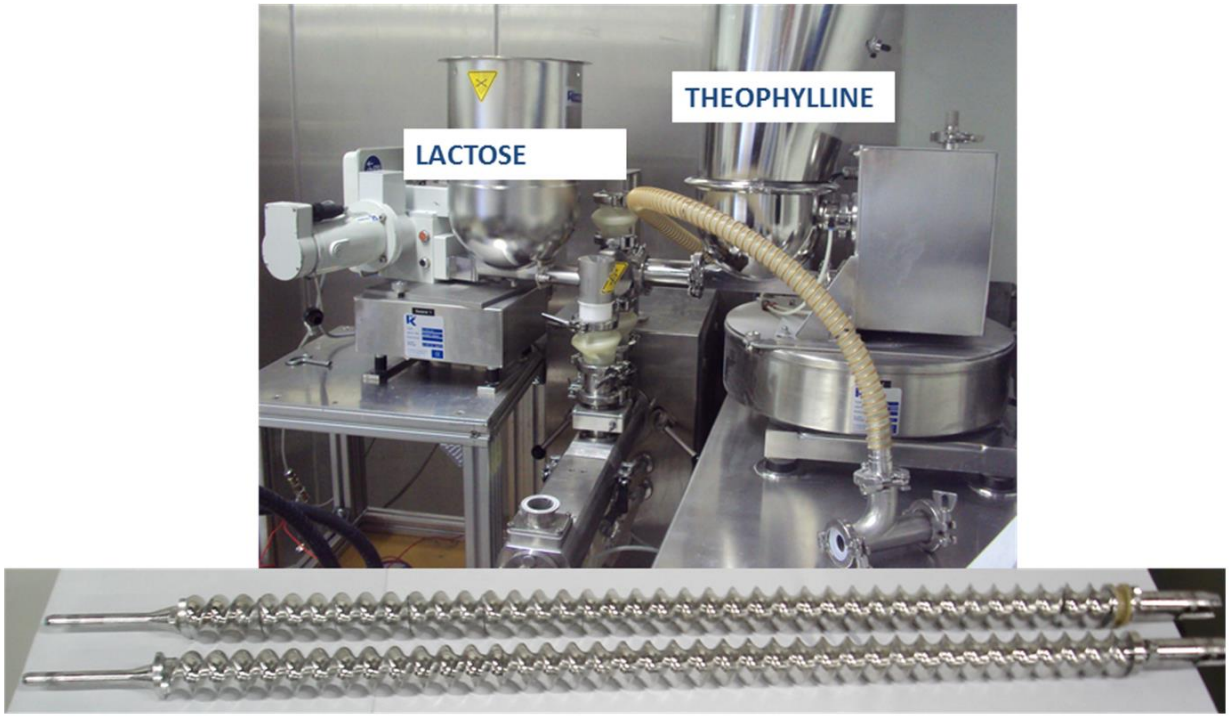

Figure 12.1. Continuous mixing using a twin screw granulator: set up and co-rotating screws (below).

12.2.4. NIR spectroscopy

For the NIR measurements, a SentroPAT FO system equipped with a Sentroprobe DR LS (Sentronic, Dresden, Germany) was used with an optical resolution of 12 nm and a pixel dispersion of 4.3 nm. Spectra were collected in the spectral region from 1150 to 2200 nm. An integration time of 4 ms was used, and each spectrum was the result of the average of ten scans. Furthermore, a spectral outlier algorithm was applied. The outlier detection was

executed on the wavelength 1300 nm, which represented baseline information. This outlier algorithm was calculated based on the ten spectra, used for averaging. Spectra were rejected if they occurred to be above a maximum allowed absorbance value or deviated to far from the lowest value in the set of ten spectra. Then, the average spectrum of the remaining spectra was calculated and presented as one spectrum. The collection of spectra starts automatically from the moment powder passes in front of the probe head. Due to processing time, the collection of one spectrum took approximately 1.5 s.

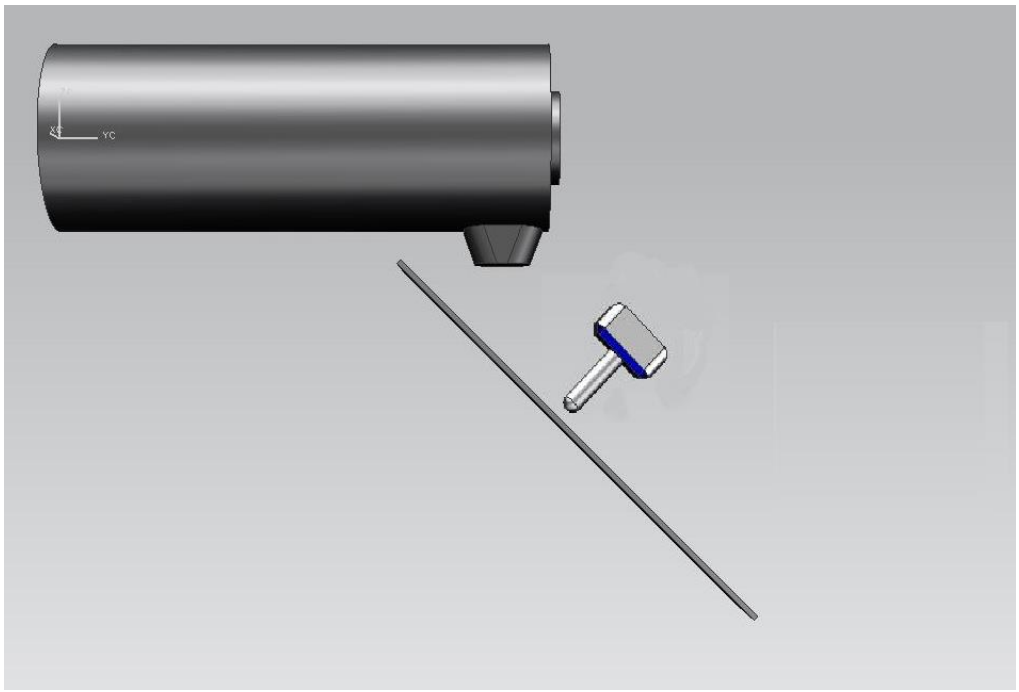

Figure 12.2. In-line NIR measurement set-up: granulator barrel, aluminium slide and SentroPAT FO.

12.2.5. Data analysis

Spectra were mean-centered and Standard Normal Variate (SNV)-corrected with a multivariate data analysis software package (Simca P+ 12.0, Umetrics AB, Umeå, Sweden). All moving F-test calculations for this study were done via the Matlab software, version R2013a (The MathWorks Inc., Natick, Massachusetts).

12.2.6. Moving F-test method

The moving F-test calculations itself will be elaborated in the results section. The theoretical background of this statistical method is briefly summarized here. The detection of blend uniformity via NIR by means of the moving F-test is a qualitative approach and does not need an external calibration model. This means that no actual value of the concentration of the API in the blend will be obtained. This method evaluates the homoscedasticity of consecutive spectra and hence assesses blend uniformity based on all ingredients. The in-line consecutively collected spectra are gathered as blocks of n spectra, and the spectral variance of these blocks is compared by means of the F-test (Figure 12.3). Once the variance is equal between two compared blocks, the blend can be considered uniform (if the sensitivity is sufficient with respect to relevant variations in concentrations – see results section).

A two-sided F-test should be applied, with:
H_0= variance of the two blocks of spectra is equal
H_1= variance of the two blocks of spectra is not equal

The α-error of a statistical test is the chance that the H_0 is rejected when it is true, or in this case when a uniform blend is not classified as uniform. The β-error on the other hand, is the chance that a false H_0 will not be detected, or for this study when a non-uniform blend is classified as uniform. Once the F-value of two blocks of spectra is calculated (Equation 12.7 in results section), it should be compared to a critical F value (F_{crit}). When the F value is below the F_{crit}, the H_0 is valid at a certain significance level, when the F value exceeds the F_{crit}, H_1 is valid at a certain significance level. F_{crit} is derived from the F-distribution tables and dependent on the chosen α-error and the block size. The β-error is dependent on the block size and sensitivity. How the appropriate block size is calculated, is explained in the results section. The aim of the moving F-test presented in this study is to have the α- and β-error under control. Therefore, the appropriate block size needs to be determined. Figure 12.4 shows how all the above described moving F-test statistical parameters and the sensitivity of the test are linked to each other.

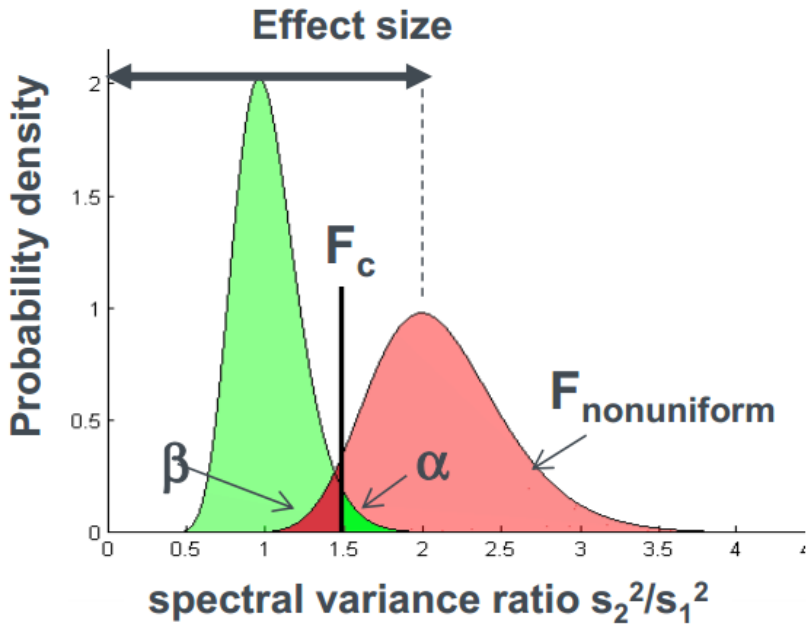

Figure 12.3. Moving F-test displayed.

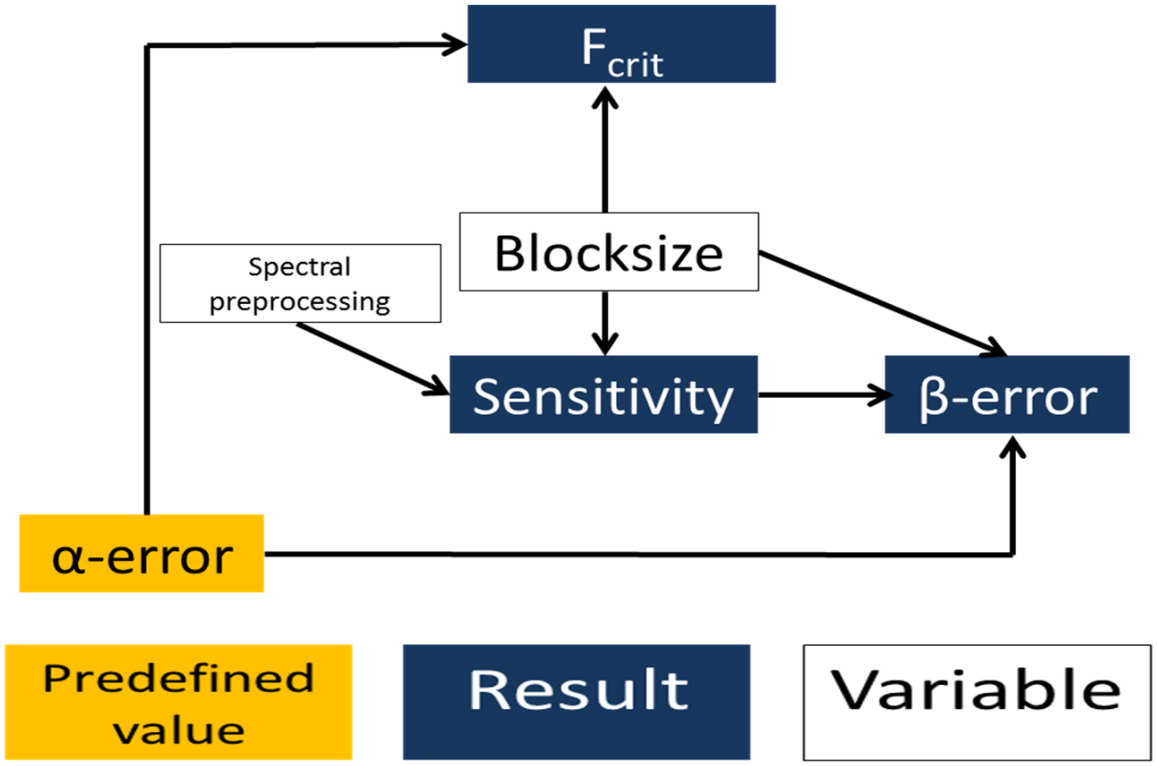

Figure 12.4. Moving F-test method: connection of the statistical terms.

12.3. RESULTS

12.3.1. Calculation of the minimum block size

The moving F-test method evaluates whether the variance between two blocks of spectra can be considered equal or not. In this paper, the aim was to use the moving F-test for blend uniformity evaluation during continuous mixing using a twin screw granulator at a throughput of 25 kg/h. Therefore the evaluated block size might not be too large. In this section the minimum required block size, B_{min} (i.e. amount of spectra in one block) will be calculated, ensuring an α-error of 5% and a β-error of maximum 5%. To start these calculations, an arbitrary block size needs to be chosen. In this study the arbitrary chosen block size (B_{arb}) was 30 spectra.

12.3.1.1. Calculation of the noise induced spectral variance (s^2_{noise})

The noise induced spectral variance, is the variance in the spectra which is not due to real differences (i.e. API concentration, humidity, impurities) in the mixtures, but due to noise spectral variation only. To calculate the noise induced spectral variance, a pre-blended mixture (prepared using the batch tumbler blender) consisting of 30% (w/w) of theophylline in lactose was fed into the twin screw granulator and NIR spectra were collected in-line on the aluminum slide (Figure 12.2). It was assumed that the pre-blend was homogeneous and remained homogeneous in the twin screw granulator. A total of 245 spectra was collected at 1051 different wavelengths (1150 to 2200 nm) and they were mean-centered and SNV-corrected (Figure 12.5). This resulted in a matrix of n spectra and k variables (wavelengths), [n x k] = [245 x 1051]. To start with, the spectral variance of the first thirty collected spectra was calculated, and the variance between these thirty spectra is calculated at each wavelength. Afterwards, these 1051 variances were summed. This was then repeated for the block consisting of spectra 2 till 31, spectra 3 till 32, spectra *i* till *i* + (B_{arb}-1) and spectra 216 till 245. A [1 x n] matrix is obtained, containing the different variances. Obviously, the first 29 values in the matrix, will be zero. Finally, the average of these variances was calculated, excluding the first 29 0-values, resulting in the noise induced spectral variance, s^2_{noise}, being 0.1169.

Equation 12.1.

$$s^2_{noise} = \frac{1}{B_{arb}-1} \sum_{j=1}^{k} \sum_{i=1}^{B_{arb}} \left(s^{noise}_{i,j} - \left(\frac{1}{M} \sum_{i=1}^{M} s^{noise}_{i,j}\right)\right)^2$$

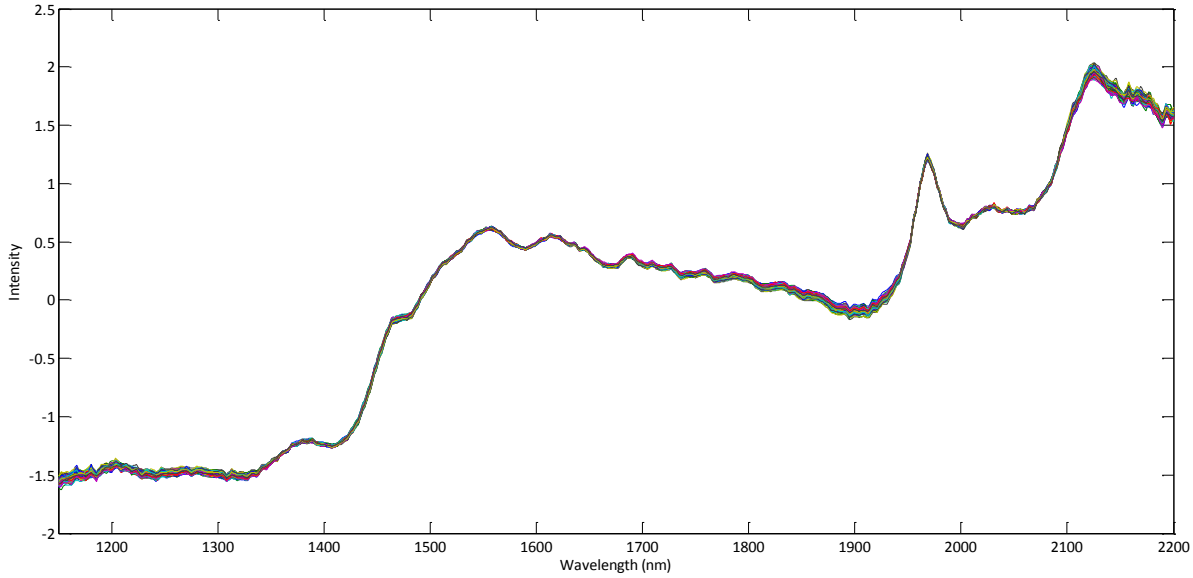

Figure 12.5. NIR Spectra of a pre-blended mixture of 30% theophylline in lactose. The 245 spectra are mean-centered and SNV-corrected.

12.3.1.2. Calculation of the API induced spectral variance (s^2_{API}) and the F-value

Spectral variance can evidently also be caused by changes in the composition of the blend. This variance is defined as s^2_{API}. In order to compute s^2_{API}, two other pre-blends, one containing 27% (w/w) and the other containing 33% (w/w) theophylline (i.e. 30% w/w +/- 10%), were produced using the batch blender (see materials and methods) and fed into the twin screw granulator. NIR spectra were again collected on the slide behind the granulator. From each blend, more than 500 spectra were collected (1150-2200 nm), SNV-corrected and then averaged, resulting in two further called "noise-free" spectra (Figure 12.6). The variance between these two averaged (noise-free) spectra is then only due to the composition of the mixture since the noise is erased by averaging the large number of spectra. Since a B_{arb} of 30 was chosen, thirty different blocks containing the two noise-free spectra can be constructed.

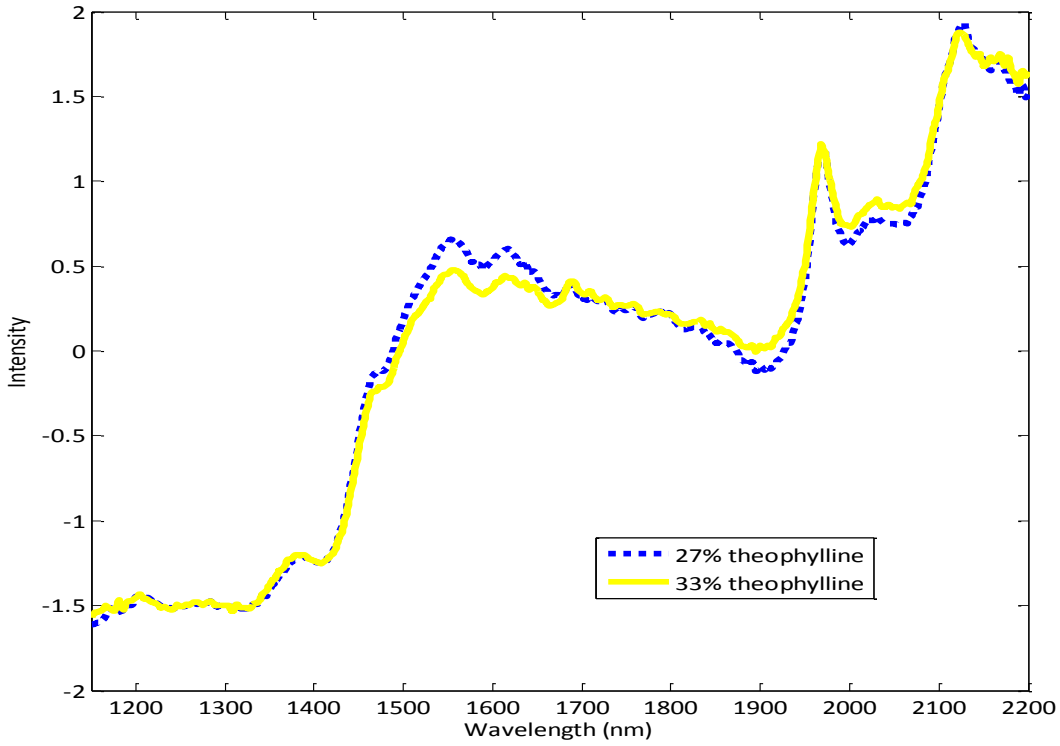

Figure 12.6. NIR 'noise-free' spectra after averaging the mean-centered, SNV-corrected spectra collected of pre-blends containing 27% and 33% of theophylline.

The first block consists of one time the 27% averaged spectrum and 29 times the 33% averaged spectrum, the second block consists of two times the 27% spectrum and 28 times the 33% spectrum and so on, till the 30th block which consists of 27% spectra only (Figure 12.7).

Figure 12.7. For a B_{arb} of 30, thirty different blocks of the two noise free spectra can be constructed. Blue lines = spectra of 27% theophylline in lactose and yellow lines = spectra of 33% theophylline in lactose.

For each of these blocks, the residual standard deviation (RSD) is calculated as follows:

$$\text{concentration} = \frac{(n_1\, c_1 + \, n_2\, c_2)}{n_1 + n_2}$$

$$RSD^2 = \frac{n_1\,[(n_1 + \, n_2)^*\, c_1\text{-}n_1\, c_1\text{-}n_2 c_2]^2 + \, n_2\,[(n_1 + n_2)^* c_2\text{-}\, n_1\, c_1\text{-}n_2 c_2]^2}{(n_1 + n_2\text{-}1)(n_1 + \, n_2)^2}$$

Equation 12.2.

$$RSD = \sqrt{\frac{(n_1 B_{arb}\text{-}n_1^2)}{B_{arb}(B_{arb}\text{-}1)}(c_1\text{-}c_2)^2}$$

With:

c_1 and c_2 the two evaluated noise-free concentrations, being 27% and 33% respectively

n_1 the number of 27% (c_1) spectra in the considered block

A [1 x B_{arb}]; [1 x 30]-matrix is obtained. Hence, 30 RSD values can be calculated (one for each block, in Figure 12.8 and Table 12.1). Evidently, the RSD of block 30 amounts zero, whereas the RSD values for block 1 and 29 for example are the same.

Secondly, the API induced spectral variance (s^2_{API}) is calculated for each block, resulting in 30 s^2_{API} values. This variance is only induced by composition differences in the block. It is calculated at each wavelength and then summed to result in the s^2_{API} :

Equation 12.3.

$$s^2_{API} = \frac{(n_1 B_{arb}\text{-}n_1^2)}{B_{arb}(B_{arb}\text{-}1)} \sum_{j=1}^{k} (s_{1,j}\text{-}s_{2,j})^2$$

With

$s_{1,j}$ being the j^{th} wavelength of the noise-free spectrum at c_1

$S_{2,j}$ being the j^{th} wavelength of the noise-free spectrum at c_2

k being the total number of wavelengths in the noise-free spectra.

Table 12.1. s^2_{API}, F_{API} and RSD, calculated for the thirty blocks.

number of spectra of 27% theophylline in each block	s^2_{API}	F_{API}	RSD
1	0.23	2.99	1.10
2	0.45	4.83	1.52
3	0.65	6.55	1.83
4	0.83	8.12	2.07
5	1.00	9.56	2.27
6	1.15	10.86	2.44
7	1.29	12.02	2.58
8	1.41	13.05	2.70
9	1.51	13.94	2.80
10	1.60	14.69	2.88
11	1.67	15.31	2.94
12	1.73	15.79	2.99
13	1.77	16.13	3.02
14	1.79	16.33	3.04
15	1.80	16.40	3.05
16	1.79	16.33	3.04
17	1.77	16.13	3.02
18	1.73	15.79	2.99
19	1.67	15.31	2.94
20	1.60	14.69	2.88
21	1.51	13.94	2.80
22	1.41	13.05	2.70
23	1.29	12.02	2.58
24	1.15	10.86	2.44
25	1.00	9.56	2.27
26	0.83	8.12	2.07
27	0.65	6.55	1.83
28	0.45	4.83	1.52
29	0.23	2.99	1.10
30	0	1	0

Again, the s^2_{API} is the same for block 1 and block 29, etc. and is zero for block 30. Furthermore, from Equations 12.2 and 12.3 it can be derived that the ratio between the

residual standard deviation and the spectral variance s^2_{API} is independent of the block size, since the proportionality of RSD and s^2_{API} is described by:

Equation 12.4.

$$\frac{s^2_{API}}{RSD^2} = \frac{\sum_{j=1}^{k}(s_{1,j} - s_{2,j})^2}{(c_1 - c_2)^2}$$

From the s^2_{noise} and the s^2_{API}, the F_{API}-value is calculated as follows:

Equation 12.5.

$$F_{API} = 1 + \frac{(B_{arb}-1)\ \sum_{j=1}^{k}(s_{1,j} - s_{2,j})^2}{\sum_{j=1}^{k}\sum_{i=1}^{B_{arb}}\left(s_{i,j}^{noise} - s_j^{noise}\right)^2 * (c_1 - c_2)^2} * RSD^2 = \frac{s^2_{noise} + s^2_{API}}{s^2_{noise}} = 1 + \left(\frac{s^2_{API}}{s^2_{noise}}\right)$$

This F_{API} value, which is the ratio of total spectral variance ($s^2_{API} + s^2_{noise}$) and noise spectral variance, needs to be determined in order to calculate the sensitivity (see next step). Since 1 s^2_{noise} value was obtained in step 1 and 30 s^2_{API} values are obtained from step 2, 30 F_{API} values are obtained (Table 12.1).

12.3.1.3. The sensitivity curve

Using Equation 12.5 and Table 12.1, a sensitivity curve, showing the relationship between RSD and F_{API} for the 30 different blocks, can be calculated for B_{arb} (Figure 12.8, blue line). For explicatory reasons, four of the thirty blocks are indicated in the graph to show their respective RSD versus F_{API} relationship. For each block, the obtained F_{API} needs to be compared with a critical F-value (F_{crit}) at a chosen significance level. The chosen significance level in this study is 0.95 (α-error 5%). The F_{crit} value derived from the F-distribution tables is 2.10 and is indicated by the red line in Figure 12.8. When F_{API} exceeds the F_{crit}, the s^2_{API} can be considered significantly different from the s^2_{noise}. In the presented case, one different spectrum in a block of 30 (e.g. 1 27% spectrum and 29 33% spectra) will already cause API induced variance, which is significantly different from noise induced spectral variance. The intersection of the sensitivity curve with the F_{crit} indicates how many spectra of a different concentration are needed within B_{arb}, to result in a variance of that block which is significantly different from the s^2_{noise} with an α-error of 5%. The intersection of the sensitivity

curve with the F_{crit} (RSD at F_{crit}), calculated for a block size of 30 is 0.8158. The $F_{\beta=5\%}$ is 3.91 (Figure 12.8, green line).

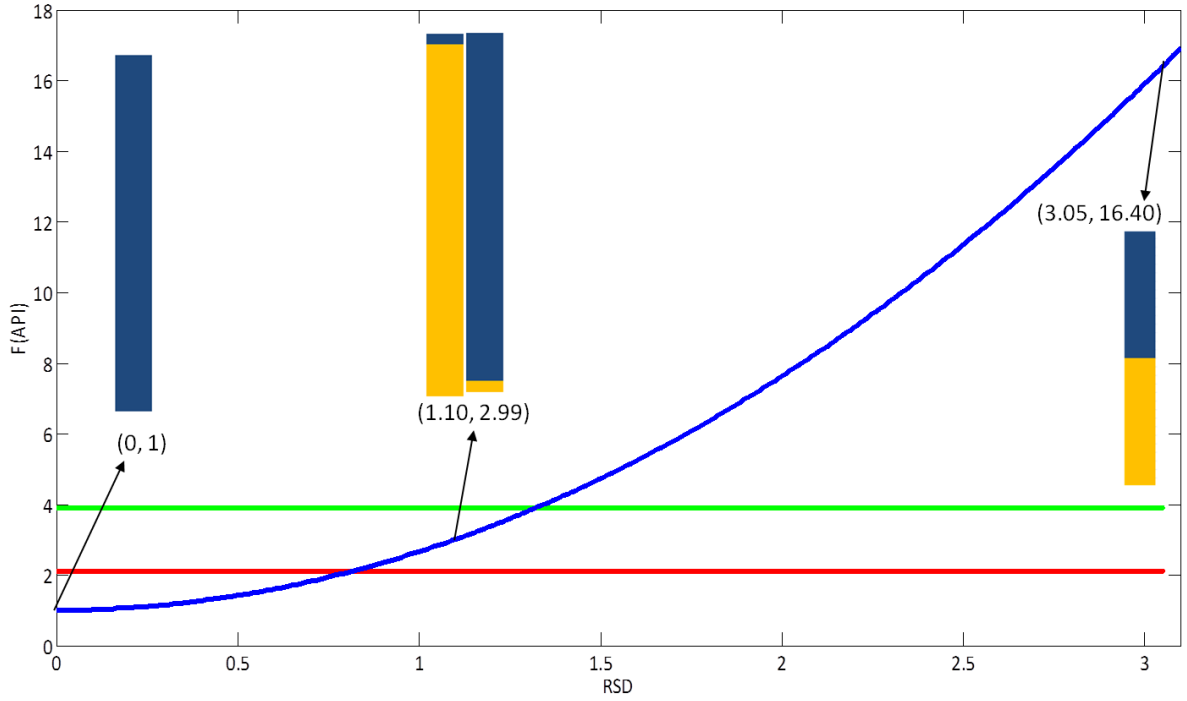

Figure 12.8. NIR data, considering a B_{arb} of 30: Sensitivity curve (blue line) and the critical F-value (F_{crit}) indicated in red and the F_{β} indicated in green.

12.3.1.4. Determination of the minimum block size (B_{min})

The above mentioned procedure (performed for a block size of 30 spectra) was repeated for block sizes consisting of 2 up till 50 spectra. Hence, a total of 49 sensitivity curve plots as in Figure 12.8 could be calculated. In each of these plots, the intersection between the sensitivity curve and F_{crit} was determined, resulting in 49 intersection values which are plotted in Figure 12.9 (full red line). The RSD at F_{crit} clearly decreases with increasing block size, because a larger block size determines true variance more accurately, and thus requires a variance ratio closer to 1 to classify variances as equal for the same α-error. The NIR blend uniformity method must be sensitive enough to assure blend uniformity according to the current draft guidance, compliant with a <5% SD level for the API based on 10 samples with a weight of approximately 1-3 dosage units. Equivalent to performance criteria of the

harmonized unit-dose uniformity test, the chance that a blend with a true RSD of 8.2% is accepted as uniform must be less than 5%. Hence the RSD at $F_{\beta=5\%}$, i.e. the F-value where β=5%, should not exceed 8.2%. Because of this, the maximum allowed RSD at F_{crit} should be calculated which is possible using Equation 12.6. These maximum allowed RSDs at each of F_{crit} of the 49 studied block sizes is shown in Figure 12.9 as the blue dashed line.

Equation 12.6.

$$RSD^{max}_{\alpha,\beta=5\%,n}(F_{crit}) = \sqrt{\frac{F_{crit}(\alpha,n,B)-1}{F_{\beta=5\%}(\alpha,n,B)-1}} * 8.2\%$$

Figure 12.9 hence clearly shows that a minimum block size of five (B_{crit}) is required to make sure that F_{crit} is below the maximum allowed RSD. This is the first minimum block size were the RSD at F_{crit} is below the maximum allowed RSD (β=5%). Applying a block size smaller than five would not guarantee that the chance that a blend with a true RSD of 8.2% is accepted as uniform is less than 5%. A small block size of spectra implies that the method is usable in a continuous production environment. It will only take 7.5s to fill one block of spectra that will be compared.

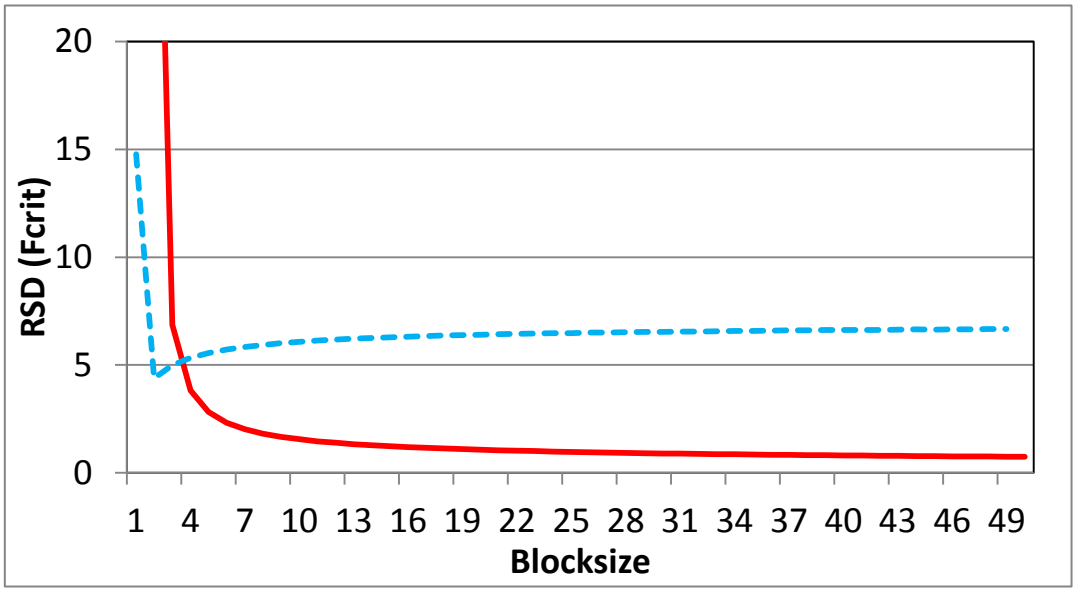

Figure 12.9. The intersections between the sensitivity curve and F_{crit} (full red line) and the maximum RSD allowed for Fcrit, based on a β-error of max 5% (dashed blue line).

12.3.2. Evaluation of the blending experiments

12.3.2.1. Experiment 1: a well mixed blend

The 266 spectra of experiment 1 were SNV-corrected prior to the moving F-test calculations. To start with, the F_{crit} value is calculated for a B_{crit} of five. The F_{crit}-value derived from the F-distribution tables is 9.6045. The collected spectra are divided in blocks: the first block consists of spectra 1 till 5, the second block of spectra 2 till 6, the n^{th} block of spectra *n* till *n* +(B_{crit}-1), the last block of spectra 262 till 266. The spectral variance is calculated for each block of five spectra. Next, the spectral variance of two consecutive blocks is used to calculate the F-value as follows:

Equation 12.7.

$$F = \frac{S_{p,max}}{S_{p,min}}$$

With:

$s_{p,max}$: the highest spectral variance and

$s_{p,min}$: the lowest spectral variance of the two consecutive blocks

The F-values of each pair of consecutive blocks of spectra are then plotted and compared to the F_{crit} (Figure 12.10). The F-value never exceeds F_{crit}, which means that the variance between all compared two blocks is due to noise only. Therefore, it can be concluded that the blend after the twin screw granulator is homogenous.

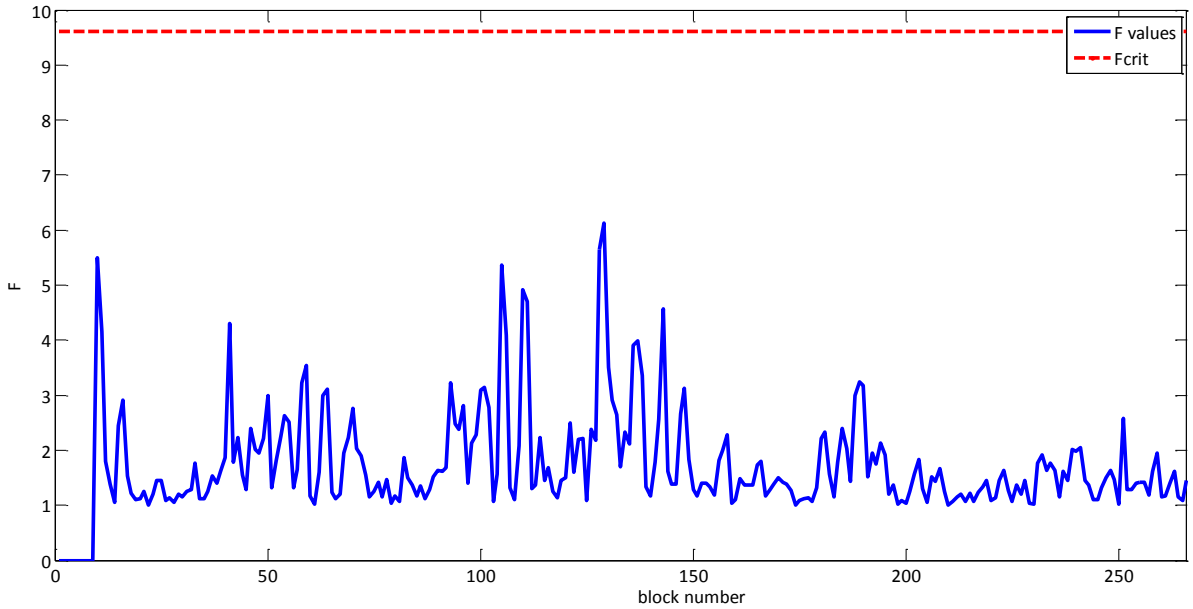

Figure 12.10. Experiment 1: The F-values of consecutive blocks of spectra (full blue line) plotted against the critical F-value (red dashed line).

12.3.2.2. Experiment 2: a disturbed mixing experiment

A disturbed mixing experiment using the twin screw granulator was monitored as well. The target theophylline concentration was initially 25%. Again, the F-test values of each pair of consecutive blocks of spectra are plotted and compared to the F_{crit} (Figure 12.11). During this mixing experiment, the F-value clearly exceeds the F_{crit} at certain time points. In the next section, these instabilities are discussed. From Figure 12.11, three major peaks can be distinguished, namely after approximately 2:20, 4:20 and 6:20 minutes. These disturbances can be easily explained by the induced errors in the feeder. After two, four and six minutes, the theophylline feeder was switched off for 10, 20 and 30 seconds respectively, as can be derived from Figure 12.12. This means, that after switching off the theophylline feeder it takes about 20 seconds for the F-test method to detect that the spectral variance of two consecutive blocks of spectra is not only due to noise.

These 20 seconds do not have a functional meaning but are the result of the emptying of the feeder, the residence time in the barrel, the movement of the powder on the slide, the time

needed to collect two blocks of spectra, and the fact that the spectrometer starts collecting automatically (so the timestamps of the feeder and the spectrometer are not synchronized).

When zooming in on the F-value versus block number graph (Figure 12.12), more time points where the F-value exceeds F_{crit} can be determined (indicated with green arrows). At time point a, the powder feeding plot explains that a feeding disturbance occurred after 52 seconds, hence the first peak where the F-value exceeds the F_{crit} is due to the fact that the theophylline feeder feeds first temporary at 6.585 kg/h and then drops down to 5.88 kg/h instead of 6.25 kg/h. At 3:02 (time point b), a drop in the theophylline feeding to 6.055 kg/h can be notified. Furthermore, the orange arrows indicate the timepoints were the F-value exceeds the F_{crit} due to an induced drop in the theophylline feeding.

The latter proves that the moving F-test method applied on NIR-spectra is not only able to detect the (obvious) induced disturbances, but also natural disturbances in the powder feeding are identified. It is important to stress here that the full overview is not available, since the feeder, which was feeding lactose, could not be logged. Nevertheless, the concept is proven.

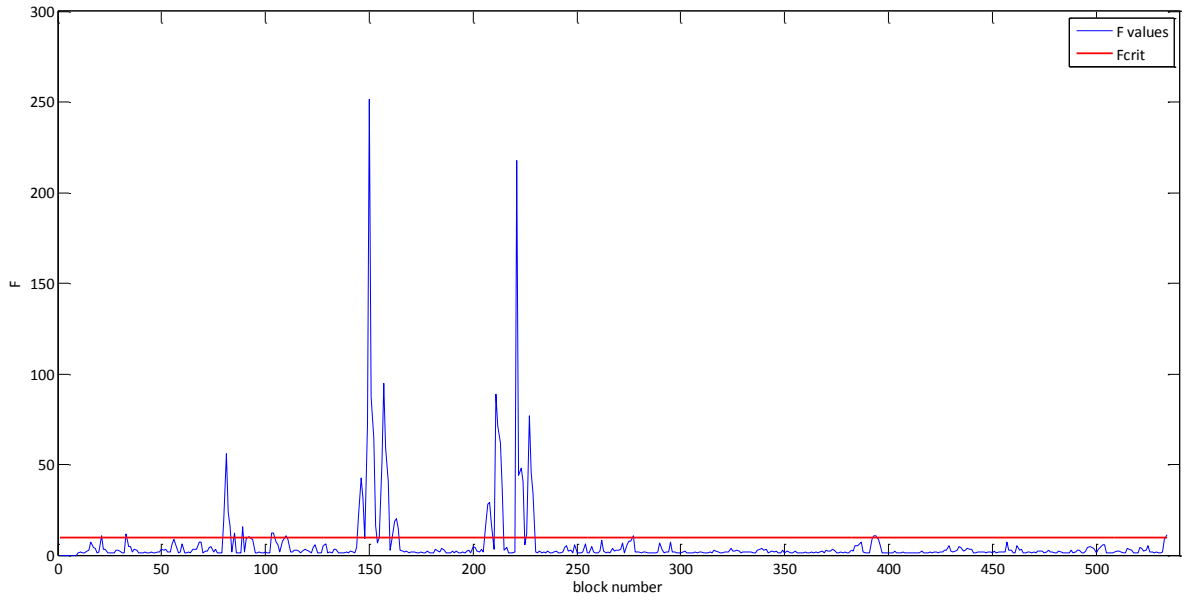

Figure 12.11. Experiment 2: The F-values of consecutive blocks of spectra (blue line) plotted against the critical F-value (red line).

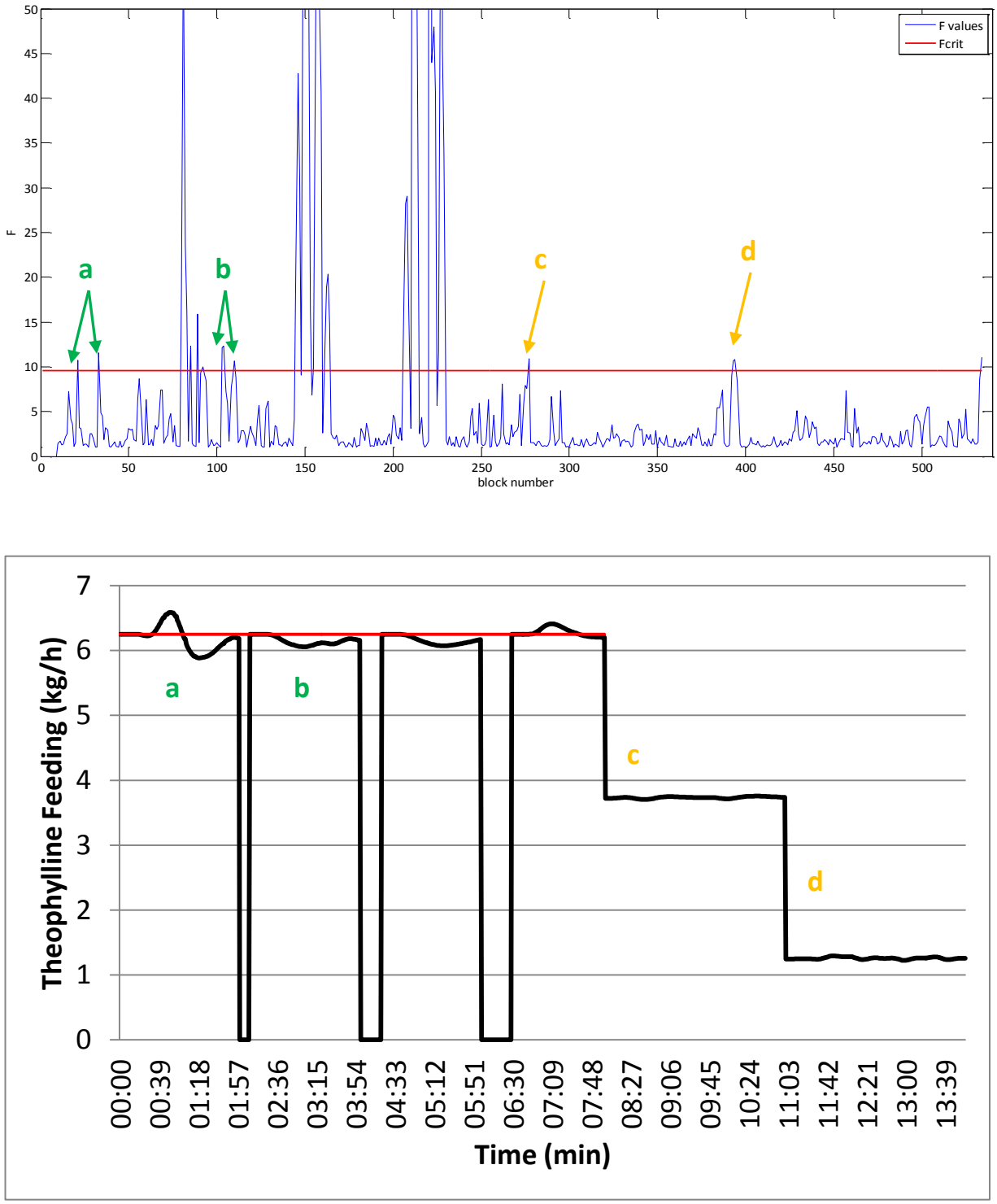

Figure 12.12. Experiment 2: The F-values of consecutive blocks of spectra (blue line) plotted against the critical F-value (red line), zoomed. Below: logging of the theophylline feeder.

12.4. DISCUSSION

Monitoring the blend homogeneity by means of the moving F-test has a lot of advantages. There is no need to construct an extensive calibration model, which is often labour-intensive and requires a lot of material. Furthermore, the method does not require maintenance. It can be transferred easily from one blender to another or can be applied with different parameter settings (i.e. powder feed rate, screw speed, …)

In this section, some important points of interest will be discussed. The monitoring of a continuous blending process differs a lot from the monitoring of a batch blending process. At the start of a batch blending process, the difference in spectral variance of two blocks will be at its maximum. This difference in spectral variance will decrease during time till the moment there is no significant difference anymore between two blocks. This time point is then considered as the end point of the blending cycle. The evaluation of blend homogeneity during continuous blending does not aim to detect an end point, but needs to make a continuous real-time decision between pass and fail. Therefore it is important to use a small amount of spectra in a block.

Firstly, it is important to invest in a good and reproducible set-up. To start with, a good set-up implies that no fouling of the probe occurs during processing. Furthermore, one should make sure that no extra variation can occur in the spectra, other than s^2_{noise} which was calculated during the calibration. New causes of variation might be: a slightly changed set-up, a change in ambient conditions, … When more accidental variation occurs during the experiments, the blend will be incorrectly determined as not homogeneous.

Secondly, the amount of spectra in a block should be well considered. A small block size is of course preferred because it makes rapid decision taking possible. Nevertheless, a fast, yet consistent change in API concentration might not be detected when the block size is too small. This is specifically important when back-mixing occurs during the blending process. Therefore, after the B_{crit} is determined statistically, it should be re-evaluated. Herewith, it is important to take into account that a larger block size implies a larger β-error and hence a lower Power of the method.

Thirdly, this method has been developed for a binary mixture. The spectra were only SNV-corrected over the whole spectral range, no further preprocessing was performed. Of course, pharmaceutical blends consist of more than two ingredients. Therefore, it might be necessary to evaluate specific spectral regions and different preprocessing techniques when monitoring a multi-component blend. This does not change anything to the method. The above described procedure can just be followed using the preprocessed spectra.

Furthermore, to use this method in an industrial environment, the use of a good software solution is beneficial. All process parameters should be logged. Then, a software package, which gathers and *synchronizes* the information from both feeders and the spectrometer, will provide a clear overview and make real-time decision taking possible. Therefore, it is also important to calculate the exact feeding and residence time in the barrel.

12.5. CONCLUSION

The moving F-test method can be applied on NIR-spectra and is a powerful tool to monitor blend uniformity in a continuous blender. In this chapter, the development of the method has been elaborated and by calculating an adequate block size, the α- and β-error were controlled. Furthermore, challenges regarding the implementation of this method have been discussed.

12.6. REFERENCES

[1] FDA-Adminstration, Guidance for Industry - PAT - A Framework for Innovative Pharmaceutical Development, Manufacturing, and Quality Assurance, in, 2004.

[2] M. Blanco, J. Coello, H. Iturriaga, S. Maspoch, C. de la Pezuela, Near-infrared spectroscopy in the pharmaceutical industry, Analyst, 123 (1998) 135R-150R.

[3] G. Reich, Near-infrared spectroscopy and imaging: Basic principles and pharmaceutical applications, Advanced Drug Delivery Reviews, 57 (2005) 1109-1143.

[4] J. Luypaert, D.L. Massart, Y.V. Heyden, Near-infrared spectroscopy applications in pharmaceutical analysis, Talanta, 72 (2007) 865-883.

[5] T. De Beer, A. Burggraeve, M. Fonteyne, L. Saerens, J.P. Remon, C. Vervaet, Near infrared and Raman spectroscopy for the in-process monitoring of pharmaceutical production processes, International Journal of Pharmaceutics, 417 (2011) 32-47.

[6] B.F. Macdonald, K.A. Prebble, SOME APPLICATIONS OF NEAR-INFRARED REFLECTANCE ANALYSIS IN THE PHARMACEUTICAL-INDUSTRY, Journal of Pharmaceutical and Biomedical Analysis, 11 (1993) 1077-1085.

[7] M. Jamrogiewicz, Application of the near-infrared spectroscopy in the pharmaceutical technology, Journal of Pharmaceutical and Biomedical Analysis, 66 (2012) 1-10.

[8] Y. Roggo, P. Chalus, L. Maurer, C. Lema-Martinez, A. Edmond, N. Jent, A review of near infrared spectroscopy and chemometrics in pharmaceutical technologies, Journal of Pharmaceutical and Biomedical Analysis, 44 (2007) 683-700.

[9] L. Pernenkil, C.L. Cooney, A review on the continuous blending of powders, Chemical Engineering Science, 61 (2006) 720-742.

[10] A.S. El-Hagrasy, F. D'Amico, J.K. Drennen, A Process Analytical Technology approach to near-infrared process control of pharmaceutical powder blending. Part I: D-optimal design for characterization of powder mixing and preliminary spectral data evaluation, J. Pharm. Sci., 95 (2006) 392-406.

[11] O. Berntsson, L.G. Danielsson, M.O. Johansson, S. Folestad, Quantitative determination of content in binary powder mixtures using diffuse reflectance near infrared spectrometry and multivariate analysis, Analytica Chimica Acta, 419 (2000) 45-54.

[12] O. Berntsson, L.G. Danielsson, B. Lagerholm, S. Folestad, Quantitative in-line monitoring of powder blending by near infrared reflection spectroscopy, Powder Technology, 123 (2002) 185-193.

[13] M. Popo, S. Romero-Torres, C. Conde, R.J. Romanach, Blend uniformity analysis using stream sampling and near infrared spectroscopy, AAPS PharmsciTech, 3 (2002) art 24.

[14] N.H. Duong, P. Arratia, F. Muzzio, A. Lange, J. Timmermans, S. Reynolds, A homogeneity study using NIR spectroscopy: Tracking magnesium stearate in Bohle bin-blender, Drug Dev. Ind. Pharm., 29 (2003) 679-687.

[15] International Conference on Harmonisation of Technical Requirements of Registration of Pharmaceuticals for Human Use. Quality Risk Management Q9, in, 2005.

[16] W.Y. Li, G.D. Worosila, Quantitation of active pharmaceutical ingredients and excipients in powder blends using designed multivariate calibration models by near-infrared spectroscopy, International Journal of Pharmaceutics, 295 (2005) 213-219.

[17] C. Bodson, W. Dewe, P. Hubert, L. Delattre, Comparison of FT-NIR transmission and UV-vis spectrophotometry to follow the mixing kinetics and to assay low-dose tablets containing riboflavin, Journal of Pharmaceutical and Biomedical Analysis, 41 (2006) 783-790.

[18] P.E. Arratia, N.H. Duong, F.J. Muzzio, P. Godbole, A. Lange, S. Reynolds, Characterizing mixing and lubrication in the Bohle Bin blender, Powder Technology, 161 (2006) 202-208.

[19] A.S. El Hagrasy, S.-Y. Chang, S. Kiang, Evaluation of risk and benefit in the implementation of near-infrared spectroscopy for monitoring of lubricant mixing, Pharmaceutical Development and Technology, 11 (2006) 303-312.

[20] A.S. El-Hagrasy, J.K. Drennen, A Process Analytical Technology approach to near-infrared process control of pharmaceutical powder blending. Part III: Quantitative near-infrared calibration for prediction of blend homogeneity and characterization of powder mixing kinetics, J. Pharm. Sci., 95 (2006) 422-434.

[21] S. Virtanen, O. Antikainen, J. Yliruusi, Uniformity of poorly miscible powders determined by near infrared spectroscopy, International Journal of Pharmaceutics, 345 (2007) 108-115.

[22] C. Benedetti, N. Abatzoglou, J.S. Simard, L. McDermott, G. Leonarda, L. Cartilier, Cohesive, multicomponent, dense powder flow characterization by NIR, International Journal of Pharmaceutics, 336 (2007) 292-301.

[23] L.J. Bellamy, A. Nordon, D. Littlejohn, Real-time monitoring of powder mixing in a convective blender using non-invasive reflectance NIR spectrometry, Analyst, 133 (2008) 58-64.

[24] H. Ma, C.A. Anderson, Characterization of pharmaceutical powder blends by NIR chemical imaging, J. Pharm. Sci., 97 (2008) 3305-3320.

[25] Z. Shi, R.P. Cogdill, S.M. Short, C.A. Anderson, Process characterization of powder blending by near-infrared spectroscopy: Blend end-points and beyond, Journal of Pharmaceutical and Biomedical Analysis, 47 (2008) 738-745.

[26] H. Wu, M. Tawakkul, M. White, M.A. Khan, Quality-by-Design (QbD): An integrated multivariate approach for the component quantification in powder blends, International Journal of Pharmaceutics, 372 (2009) 39-48.

[27] H. Zhang, Z. Jiang, J.Y. Pi, H.K. Xu, R. Du, On-Line Monitoring of Pharmaceutical Production Processes Using Hidden Markov Model, J. Pharm. Sci., 98 (2009) 1487-1498.

[28] Y. Sulub, B. Wabuyele, P. Gargiulo, J. Pazdan, J. Cheney, J. Berry, A. Gupta, R. Shah, H. Wu, M. Khan, Real-time on-line blend uniformity monitoring using near-infrared reflectance spectrometry: A noninvasive off-line calibration approach, Journal of Pharmaceutical and Biomedical Analysis, 49 (2009) 48-54.

[29] I. Storme-Paris, I. Clarot, S. Esposito, J.C. Chaumeil, A. Nicolas, F. Brion, A. Rieutord, P. Chaminade, Near InfraRed Spectroscopy homogeneity evaluation of complex powder blends in a small-scale pharmaceutical preformulation process, a real-life application, European Journal of Pharmaceutics and Biopharmaceutics, 72 (2009) 189-198.

[30] H. Wu, M.A. Khan, Quality-By-Design (QbD): An Integrated Approach for Evaluation of Powder Blending Process Kinetics and Determination of Powder Blending End-point, J. Pharm. Sci., 98 (2009) 2784-2798.

[31] A.U. Vanarase, M. Alcala, J.I.J. Rozo, F.J. Muzzio, R.J. Romanach, Real-time monitoring of drug concentration in a continuous powder mixing process using NIR spectroscopy, Chemical Engineering Science, 65 (2010) 5728-5733.

[32] A.D. Karande, C.V. Liew, P.W.S. Heng, Calibration sampling paradox in near infrared spectroscopy: A case study of multi-component powder blend, International Journal of Pharmaceutics, 395 (2010) 91-97.

[33] C.V. Liew, A.D. Karande, P.W.S. Heng, In-line quantification of drug and excipients in cohesive powder blends by near infrared spectroscopy, International Journal of Pharmaceutics, 386 (2010) 138-148.

[34] B.M. Zacour, B. Igne, J.K. Drennen, III, C.A. Anderson, Efficient Near-Infrared Spectroscopic Calibration Methods for Pharmaceutical Blend Monitoring, Journal of Pharmaceutical Innovation, 6 (2011) 10-23.

[35] Y. Sulub, M. Konigsberger, J. Cheney, Blend uniformity end-point determination using near-infrared spectroscopy and multivariate calibration, Journal of Pharmaceutical and Biomedical Analysis, 55 (2011) 429-434.

[36] D.M. Koller, A. Posch, G. Hoerl, C. Voura, S. Radl, N. Urbanetz, S.D. Fraser, W. Tritthart, F. Reiter, M. Schlingmann, J.G. Khinast, Continuous quantitative monitoring of powder mixing dynamics by near-infrared spectroscopy, Powder Technology, 205 (2011) 87-96.

[37] A. Porfire, L. Rus, A.L. Vonica, I. Tomuta, High-throughput NIR-chemometric methods for determination of drug content and pharmaceutical properties of indapamide powder blends for tabletting, Journal of Pharmaceutical and Biomedical Analysis, 70 (2012) 301-309.

[38] O. Scheibelhofer, D.M. Koller, P. Kerschhaggle, J.G. Khinast, Continuous powder flow monitoring via near-infrared hyperspectral imaging, in: 2012 IEEE International Graz, Austria, 2012, pp. 748-753.

[39] M. Jamrogiewicz, K. Cal, M. Gruszecka, A. Ciesielski, DETERMINATION OF API CONTENT IN A PILOT-SCALE BLENDING BY NEAR-INFRARED SPECTROSCOPY AS A FIRST STEP METHOD TO PROCESS LINE IMPLEMENTATION, Acta Poloniae Pharmaceutica, 70 (2013) 419-429.

[40] Y. Gao, F. Boukouvala, W. Engisch, W. Meng, F.J. Muzzio, M.G. Ierapetritou, Improving Continuous Powder Blending Performance Using Projection to Latent Structures Regression, Journal of Pharmaceutical Innovation, 8 (2013) 99-110.

[41] O. Scheibelhofer, N. Balak, P.R. Wahl, D.M. Koller, B.J. Glasser, J.G. Khinast, Monitoring Blending of Pharmaceutical Powders with Multipoint NIR Spectroscopy, Aaps Pharmscitech, 14 (2013) 234-244.

[42] A.U. Vanarase, M. Jarvinen, J. Paaso, F.J. Muzzio, Development of a methodology to estimate error in the on-line measurements of blend uniformity in a continuous powder mixing process, Powder Technology, 241 (2013) 263-271.

[43] L. Martinez, A. Peinado, L. Liesum, In-line quantification of two active ingredients in a batch blending process by near-infrared spectroscopy: Influence of physical presentation of the sample, International Journal of Pharmaceutics, 451 (2013) 67-75.

[44] L. Martinez, A. Peinado, L. Liesum, G. Betz, Use of near-infrared spectroscopy to quantify drug content on a continuous blending process: Influence of mass flow and rotation speed variations, European Journal of Pharmaceutics and Biopharmaceutics, 84 (2013) 606-615.

[45] B. Igne, S. Talwar, J.K. Drennen, III, C.A. Anderson, Online Monitoring of Pharmaceutical Materials Using Multiple NIR Sensors-Part II: Blend End-point Determination, Journal of Pharmaceutical Innovation, 8 (2013) 45-55.

[46] B. Igne, B.M. Zacour, Z. Shi, S. Talwar, C.A. Anderson, J.K. Drennen, III, Online Monitoring of Pharmaceutical Materials Using Multiple NIR Sensors-Part I: Blend Homogeneity, Journal of Pharmaceutical Innovation, 6 (2011) 47-59.

[47] J. Jaumot, B. Igne, C.A. Anderson, J.K. Drennen, A. de Juan, Blending process modeling and control by multivariate curve resolution, Talanta, 117 (2013) 492-504.

[48] E.T.S. Skibsted, H.F.M. Boelens, J.A. Westerhuis, D.T. Witte, A.K. Smilde, Simple assessment of homogeneity in pharmaceutical mixing processes using a near-infrared reflectance probe and control charts, Journal of Pharmaceutical and Biomedical Analysis, 41 (2006) 26-35.

[49] D.J. Wargo, J.K. Drennen, Near-infrared spectroscopic characterization of pharmaceutical powder blends, Journal of Pharmaceutical and Biomedical Analysis, 14 (1996) 1415-1423.

[50] A.S. El-Hagrasy, M. Delgado-Lopez, J.K. Drennen, A Process Analytical Technology approach to near-infrared process control of pharmaceutical powder blending: Part II: Qualitative near-infrared models for prediction of blend homogeneity, J. Pharm. Sci., 95 (2006) 407-421.

[51] F.C. Sanchez, J. Toft, B. Vandenbogaert, D.L. Massart, S.S. Dive, P. Hailey, MONITORING POWDER BLENDING BY NIR SPECTROSCOPY, Fresenius Journal of Analytical Chemistry, 352 (1995) 771-778.

[52] C. Ufret, K. Morris, Modeling of powder blending using on-line near-infrared measurements, Drug Dev. Ind. Pharm., 27 (2001) 719-729.

[53] P.A. Hailey, P. Doherty, P. Tapsell, T. Oliver, P.K. Aldridge, Automated system for the on-line monitoring of powder blending processes using near-infrared spectroscopy .1. System development and control, Journal of Pharmaceutical and Biomedical Analysis, 14 (1996) 551-559.

[54] S.S. Sekulic, J. Wakeman, P. Doherty, P.A. Hailey, Automated system for the on-line monitoring of powder blending processes using near-infrared spectroscopy - Part II. Qualitative approaches to blend evaluation, Journal of Pharmaceutical and Biomedical Analysis, 17 (1998) 1285-1309.

[55] S.S. Sekulic, H.W. Ward, D.R. Brannegan, E.D. Stanley, C.L. Evans, S.T. Sciavolino, P.A. Hailey, P.K. Aldridge, On-line monitoring of powder blend homogeneity by near-infrared spectroscopy, Analytical Chemistry, 68 (1996) 509-513.

[56] A.S. El-Hagrasy, H.R. Morris, F. D'Amico, R.A. Lodder, J.K. Drennen, Near-infrared spectroscopy and imaging for the monitoring of powder blend homogeneity, J. Pharm. Sci., 90 (2001) 1298-1307.

[57] J.J. Moes, M.M. Ruijken, E. Gout, H.W. Frijlink, M.I. Ugwoke, Application of process analytical technology in tablet process development using NIR spectroscopy: Blend uniformity, content uniformity and coating thickness measurements, International Journal of Pharmaceutics, 357 (2008) 108-118.

[58] W. Momose, K. Imai, S. Yokota, E. Yonemochi, K. Terada, Process analytical technology applied for end-point detection of pharmaceutical blending by combining two calibration-free methods: Simultaneously monitoring specific near-infrared peak intensity and moving block standard deviation, Powder Technology, 210 (2011) 122-131.

[59] T. Puchert, C.V. Holzhauer, J.C. Menezes, D. Lochmann, G. Reich, A new PAT/QbD approach for the determination of blend homogeneity: Combination of on-line NIRS analysis with PC Scores Distance Analysis (PC-SDA), European Journal of Pharmaceutics and Biopharmaceutics, 78 (2011) 173-182.

[60] W. Plugge, C. vanderVlies, Near-infrared spectroscopy as a tool to improve quality, Journal of Pharmaceutical and Biomedical Analysis, 14 (1996) 891-898.

[61] G.R. Flaten, R. Belchamber, M. Collins, A.D. Walmsley, Caterpillar - an adaptive algorithm for detecting process changes from acoustic emission signals, Analytica Chimica Acta, 544 (2005) 280-291.

[62] G.R. Flaten, A.P. Ferreira, L. Bellamy, P. Frake, PAT within the QbD Framework: Real-Time End Point Detection for Powder Blends in a Compliant Environment, Journal of Pharmaceutical Innovation, 7 (2012) 38-45.

SUMMARY AND GENERAL CONCLUSIONS

“It always seems impossible, until it's done.”

Nelson Mandela (1918-2013)

SUMMARY AND GENERAL CONCLUSIONS

Continuous processing is well established in the chemical, cosmetics and food industry, whilst it is still in its infancy in the pharmaceutical industry. However, there exists the intention to shift pharmaceutical manufacturing from traditional batch production towards continuous production. Continuous pharmaceutical manufacturing has several advantages, but with its implementation one major question rises as well: “How to assure the quality of both the in-process materials and the end product?". Indeed, the quality of pharmaceutical products obtained via traditional batch-wise processes is generally assessed via sampling and time-consuming off-line analyses in analytical laboratories. These quality evaluation methods would annul the advantages of continuous processing. It is clear that real-time quality assessment and control by means of Process Analytical Technology (PAT) tools is indispensable for continuous production. In this dissertation, the strengths and weaknesses of several complementary PAT tools, implemented in a continuous wet granulation process, which is part of a fully continuous from powder-to-tablet production line, were evaluated. Furthermore, the influence of raw material variability upon processability, intermediates and end products was investigated. Process understanding is gained and the presented approach fits in the Quality by Design (QbD) framework as it is presented by the Food and Drug Administration (FDA) and International Conference on Harmonisation (ICH).

In **Chapter 1** the advantages and challenges regarding continuous pharmaceutical manufacturing are briefly discussed. **Chapter 2** extensively describes the commercially available continuous production line (ConsiGma™ 25), which is used in this research work.

In **Chapter 3**, an overview of different applications of PAT tools applied in continuous pharmaceutical processes is provided. Overall, it can be stated that few research has been performed on the implementation of PAT in continuous production lines. Several authors came across similar challenges, for example the importance of similar environmental conditions for the development of calibration models (data-driven models) and the real test environment. Furthermore, interfacing and fouling of the probes were much reported issues.

The first experimental part of this research thesis focused on the effects of the use of variating raw materials upon critical quality attributes of pharmaceutical products. Furthermore, the influence of raw materials variability on their processability was investigated. In **Chapter 4**, seven different grades of anhydrous theophylline were evaluated. Premixes with 30% of theophylline, 67.5% of lactose monohydrate and 2.5% of PVP were granulated, using constant process parameters. The seven grades differed in particle size and this difference also manifested in the granule size distribution. Granules prepared from theophylline with smaller particle sizes, resulted in more fine granules. The obtained granules were tableted and the differences in granule size distribution had also an influence on both the tablet properties and the compression process. Tablets produced from granules consisting of more fines, resulted in stronger tablets. Furthermore, process difficulties occurred during the tableting of granules produced from the smallest grade of theophylline, since remaining ungranulated pure theophylline powder blocked the lower punches of the tablet press. The characteristics of the used powders, obtained granules and tablets as well as the process parameters were analyzed by means of principal component analysis. The results of this study showed that differences in raw material properties both affect their processability and several critical quality attributes of the resulting granules and tablets.

The differences in theophylline properties were specified by the supplier. In **Chapter 5**, six different samples of raw materials (MCC) were studied. These samples showed variation in processability, but no information regarding MCC variability was provided by the supplier. The different MCC samples did not differ regarding any pharmacopeial specifications. A model formulation of 60% of lactose, 10% of starch and 30% of MCC was granulated six times using the twin screw granulator, one time with each sample. The process parameters were kept constant. Two sets of process parameters were evaluated, characterized by a longer or shorter interaction time between powder and granulation liquid. With both sets of parameters a clear difference in obtained granule size distribution between the six different MCC samples was obtained. The cause of this different size distribution was found to be a different water binding capacity of the six MCC samples. When the water binding capacity of a batch was high, a large amount of granulation liquid was absorbed by the MCC powder, and thus no longer available for granulation, hence resulting in more fine granules. The

differences in water binding capacity were related to different degrees of MCC crystallinity. The higher the degree of crystallinity, the lower the amount of water that is absorbed per gram MCC. Next, an experimental design was performed to compare the effect of water binding capacity and other process parameters on the granule size distribution. Water binding capacity showed to have a significant influence on the granule size distribution, as well as powder feed rate, screw configuration and liquid addition. This experimental design was then used to calculate the necessary process parameters for a preset granule size distribution. The model was successful for this purpose and hence able to correct for the studied MCC raw material variability. Finally, it was investigated whether the MCC variability in water binding capacity still had an effect on the granule size distribution if a binder was added to the formulation. Indeed, a higher water binding capacity still resulted in more granules <500 µm.

The second part of this research evaluated the use of different PAT tools for the in-process evaluation of processed materials as well as end product properties.

In **Chapter 4 and 5**, as well as in most other published studies regarding twin screw granulation, a bimodal granule size distribution is obtained. In **Chapter 6**, Coherent anti-Stokes Raman scattering microscopy was applied for the visualization of binder (PVP) within a granule. The hypothesis was that an inhomogenous spread of binder, caused by the short residence time in the granulator barrel, could be the reason for this bimodal distribution. A feasibility study was performed, which proved that CARS is a suitable technique for the detection of PVP within the granules. Nevertheless, no PVP-riche zones could be detected in the granules, hence suggesting a homogeneous spread of binder. Hence, the cause of the typical bimodal distribution is not inadequate binder mixing in the granulator.

Chapter 7 focused on the monitoring of theophylline containing *wet* granules, as they leave the granulator barrel. Both NIR and Raman spectroscopy were used in a static way, whereas a spatial filter velocimetry technique was used dynamically in order to measure the granule size in real-time. An experimental design was performed to evaluate which process parameters (powder feed rate, granulation liquid addition, screw speed and temperature of the granulator barrel) had an influence on the granule size distribution and solid state of the

API. The temperature of the granulator barrel and the powder feed rate had a significant effect on the granule size. Furthermore, the conversion from anhydrous theophylline to theophylline monohydrate during twin screw granulation was monitored, and showed to be influenced by the temperature of the granulator barrel, the added amount of granulation liquid, and to a lesser extent also the powder feed rate. Lower addition of granulation liquid, higher barrel temperatures and a higher powder feed rate were the parameters in favor for small amounts of anhydrous theophylline. The results obtained by Raman spectroscopy were confirmed by NIR spectroscopy. Therefore, both Raman and NIR spectroscopy in combination with experimental design showed to be valuable tools to investigate and better understand solid state transformations in wet granules. Even small amounts of a non-expected polymorph could be detected.

Chapter 8 discusses different approaches for end point detection of drying in the six-segmented fluid bed dryer of the ConsiGma™ 25. Classical approaches such as the monitoring of the outlet air humidity and product temperature are compared to mass balance models and monitoring methods via PAT tools (in-line Raman and NIR spectroscopy). An NIR based PLS model was constructed for the in-line monitoring of the granules' moisture content in the dryer. The in-line obtained moisture values were evaluated and the end point of drying was determined. Both the NIR prediction model and the mass balance model indicated the drying process end point sooner than the two classical, indirect methods. Furthermore, NIR and Raman spectroscopy were capable of monitoring the dehydration of the API (theophylline monohydrate converted to anhydrous theophylline). The time points of solid state conversion derived from the Raman and NIR spectra were comparable with the drying process end points calculated using the NIR-based PLS model. The PAT-based method showed to be the most suited for use in a production set-up. In **Chapter 9**, an NIR based PLS model for the water quantification during drying was thoroughly validated by means of accuracy profiles.

In **Chapter 10**, 19 different granulation experiments were performed with changing temperature of the granulator barrel, powder feed rate, temperature of the drying air and air flow of the drying air. Lactose – anhydrous theophylline – PVP (67.5, 30, 2.5 %) was used as model formulation. The granules were separated after drying in three fractions: fines (<

150 µm), yield (151-1400 µm) and oversized granules (> 1400 µm). Then, the moisture content of the total granule load as well as from each fraction was determined. Furthermore, Raman spectra were collected, again from the total granule load as well as from the different fractions. These experiments showed that the overall determined moisture content and the solid state information derived from the total granule load differed from moisture content and solid state of the different size fractions. Fines tend to dry faster and will contain theophylline anhydrate, whereas the oversized granules will consist of theophylline monohydrate or metastable theophylline.

In **Chapter 11** three complementary PAT tools were used to monitor dry granules: Raman and NIR spectroscopy and a photometric imaging technique. In this chapter it was investigated if Raman spectra, NIR spectra, granule size and roughness information together with the used process parameters could be used to predict the bulk and tapped density as well as flowability and moisture content of the granules. In this case, PAT tools could replace the time consuming off-line analysis, such as Karl Fischer moisture determination and tapped density experiments. Three PLS models were constructed, one to predict the moisture content, one for Hausner Ratio and one for the prediction of both bulk and tapped density. These models proved their utility for the at-line analysis of continuously produced granules. The residual moisture content was mostly correlated with the spectroscopic data, whereas the imaging data had the highest predictive capability for the flowability of the granules.

Chapter 12 evaluates the use of NIR spectroscopy for homogeneity measurements after a continuous blender. The moving F-test is used for this purpose and elaborated in this chapter. The method is developed in such way that both the α- and β- error are under control. Once developed, the method was used to monitor continuous blending experiments in-line. The first experiment resulted in a homogenous blend, and was evaluated as such with the moving F-test method. A second experiment was conducted and this time error were induced during the process. The method was capable of detecting both this induced errors as well as natural disturbances in the feeder.

FUTURE PERSPECTIVES

"It is said that the present is pregnant with the future."

Voltaire (1694-1778)

FUTURE PERSPECTIVES

This thesis evaluated both complementary PAT tools for the monitoring of a continuous pharmaceutical process and the influence of different raw materials upon processability and end products. Hence an improved process understanding was gained. As is also stated in **Chapter 3**, limited studies on the implementation of PAT tools in continuous pharmaceutical manufacturing processes (i.e. continuous wet granulation) have been performed. Moreover researchers have worked on different continuous processes, but they came across similar challenges.

1. It is important that the measurement conditions when collecting data to develop data-driven models and the conditions during in-process data collection are similar.

2. There is a need for adequate interfacing of the PAT tools. An interfacing device should make sure that the probe does not interfere with the process or the product stream. Chutes for example are usable in an R&D environment but should be switched to contained devices in a production setting. Once a PAT tool shows to be useful for implementation in a production environment, an adequate interfacing device should be developed.

3. Since pharmaceutical processing deals mainly with powders, fouling of probes is a much-reported problem when implementing PAT probes. The first solutions are now on the market (for example, the FBRM® probe with scraper, Parsum® with air purge and Lighthouse Probe™ with window wash). Manufacturers would improve the usability of their products significantly when providing a solution against probe fouling. Another option to prevent fouling is the use of probes which have a large focus distance (for example, the Raman Phat probe).

4. This thesis overviewed and evaluated several PAT techniques. From **Chapter 3**, it was clear that, currently, NIR spectroscopy is the most used PAT tool. Nevertheless, researchers should question which tool is the most appropriate for the monitoring of a certain critical quality attribute. Often, NIR spectroscopy is used because it is the most readily available technique, but other techniques might be superior.

5. With the enhanced knowledge on critical quality attributes and critical process parameters, the *"design space"* should be developed. The design space is a multidimensional combination and interaction of input variables (i.e., material attributes) and process parameters, within which acceptable product quality is obtained. Working within the design space is not considered as a change. Continuous control of the design space using suitable PAT tools is essential for continuous production.

6. When aiming real-time-release, the process should not only be monitored, but steering the process (i.e., process control) is as important to stay within its design space. To our knowledge, no research has been presented which uses the information about the processed material derived from PAT tools for feedback and feedforward control of pharmaceutical processes. Therefore, as a next step, the process knowledge gathered in this work should be used to develop and implement an adequate process control strategy (Figure). Once a closed control loop is developed, small disturbances in the process environment (i.e. changes in raw material as stated in **Chapter 4 and 5**, changes in temperature, etc.) will be countered by the controller. The basis of control is to calculate a new input for the process, based on the deviation from the setpoint, and subsequently feed the input to the process so that the output of the process keeps on following a predefined setpoint regardless of disturbances acting on the process. In this way, the process will always run within its design space, hence assuring the quality of the end product at all times.

Research regarding the design space and process control of the ConsiGma™ 25 is currently conducted in our research group.

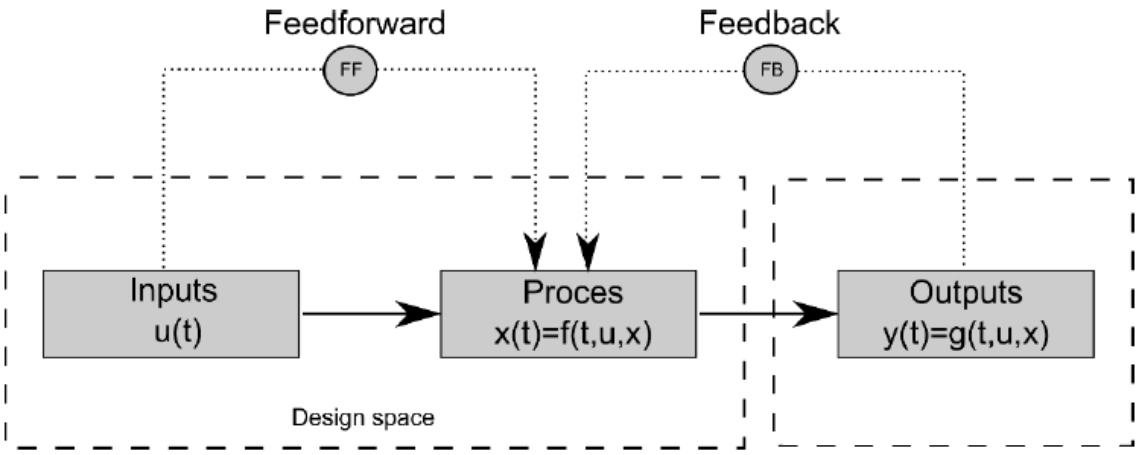

Figure. Closed-loop control with feedforward and feedback loops.

SAMENVATTING EN ALGEMEEN BESLUIT

"Rien ne calme comme une décision prise."

Charles-Maurice de Talleyrand (1754-1838)

SAMENVATTING EN ALGEMEEN BESLUIT

Continue productie is goed ingeburgerd in de chemische, voedsel- en cosmetica-industrie. In de farmaceutische industrie staat continu produceren nog in zijn kinderschoenen. Door recente ontwikkelingen, stijgt nu ook de interesse van de farmaceutische industrie om over te schakelen van batch- naar continue processen. Continue productie heeft namelijk veel voordelen. Tegelijk met de implementatie van continue lijnen rijst ook een prangende vraag: "Hoe kan de kwaliteit van zowel de intermediaire als de eindproducten gegarandeerd worden?". Batchprocessen werden namelijk altijd gecontroleerd door staalname gevolgd door klassieke off-line laboratorium testen. Staalname is moeilijk te verwezenlijken in een continue lijn, tevens zouden tijdrovende off-line analyses de voordelen van continu produceren teniet doen. Daarom moeten continue processen *in real-time* gecontroleerd worden door middel van proces analytische technieken. Dit werk focust op de sterktes en zwaktes van verschillende complementaire proces analytische technieken, die geïmplementeerd werden in een continue van-poeder-tot-tablet productielijn. Daarnaast werd de invloed van verschillen in startmateriaal, op zowel het proces zelf als het eindproduct, onderzocht. Dit leidde tot nieuwe proceskennis, zoals ook wordt vooropgesteld door de Quality by Design (QbD) richtlijnen van de Food and Drug Administration (FDA) en de International Conference on Harmonisation (ICH).

In **Hoofdstuk 1** worden de voordelen en uitdagingen betreffende continue productie kort besproken. **Hoofdstuk 2** geeft daarbij aansluitend een uitgebreide beschrijving van de commercieel beschikbare continue productielijn (ConsiGma™ 25), die bestudeerd werd in deze thesis.

Hoofdstuk 3 geeft een overzicht van verschillende reeds gepubliceerde PAT toepassingen in continue farmaceutische productie. Tot op heden is er slechts weinig onderzoek verricht naar PAT in continue lijnen. Uit de bestaande literatuur blijkt verder dat verschillende auteurs dezelfde problemen ondervonden tijdens hun onderzoek. Het belang van gelijkaardige condities tijdens calibratie experimenten en de echte procescondities en

problemen met implementatie en vuil worden van de probes, zijn de meest frequent gerapporteerde problemen.

Het eerste experimentele deel van deze onderzoeksthesis focust op het gebruik van verschillende startmaterialen en hun effect op de eigenschappen van intermediaire en eindproducten, alsook op hun proceseerbaarheid. In **Hoofdstuk 4** werd gebruik gemaakt van zeven verschillende soorten theofylline anhydraat, die verschilden in deeltjesgrootte distributie. Mengsels van 30% theofylline, 67.5% lactose en 2.5% polyvinylpyrrolidone werden achtereenvolgens gegranuleerd, gedroogd in de oven en getabletteerd. De procesparameters werden steeds constant gehouden. De verschillende deeltjesgrootte distributie van de poeders manifesteerde zich ook in de granulaatgrootte distributie. Granulaten geproduceerd uit kleinere theofylline poeders werden gekenmerkt door een grotere hoeveelheid fijne granulaten (< 150 µm). Wanneer de granulaten getabletteerd werden, was de invloed van de verschillende granulaatgroottes ook zichtbaar: tabletten aangemaakt uit granulaat met een grotere fractie fijne granulaten, resulteerden in sterkere tabletten. Tijdens het tabletteren van de granulaten, aangemaakt met de twee fijnste soorten theofylline, traden moeilijkheden op. Kleine hoeveelheden puur theofylline poeder (met kleine deeltjesgrootte) blokkeerden de onderste stempels van de tabletpers. De eigenschappen van de poeders, granulaten, tabletten alsook hun proceseerbaarheid werden geanalyseerd door middel van principale component analyse. De resultaten van deze studie toonden aan dat verschillen in startmaterialen zowel de proceseerbaarheid als verschillende kritische kwaliteitseigenschappen van de granulaten en tabletten beïnvloeden.

De verschillende eigenschappen van de theofylline poeders werden meegedeeld door de leverancier. In **Hoofdstuk 5** daarentegen worden zes verschillende stalen micro kristallijne cellulose (MCC) bestudeerd, die variatie vertoonden tijdens productie. Er werd in dit geval echter geen verschil meegedeeld door de producent. De zes verschillende stalen vertoonden geen verschillen volgens de richtlijnen van de farmacopee. Een modelformulatie van 60% lactose, 10% zetmeel en 30% MCC werd telkens zes keer gegranuleerd, een keer met elk staal, met dezelfde procescondities. Twee sets van parameters werden geëvalueerd, een set was gekenmerkt door een lange interactietijd tussen poeder en granulatievloeistof, de andere door een korte interactietijd. Met beide instellingen werd een duidelijk verschil

waargenomen in de granulaatgrootte distributie tussen de zes stalen. De oorzaak van die verschillende granulaatgrootte distributie was te vinden in een verschil in waterbindingscapaciteit. Wanneer de waterbindingscapaciteit van een staal hoogt ligt, zal een grote hoeveelheid granulatievloeistof worden opgenomen door het MCC poeder en zodoende niet meer beschikbaar zijn voor granulatie. Dit resulteert dan in een grotere fractie fijne granulaten. Het verschil in waterbindingscapaciteit is toe te schrijven aan een verschillende graad van kristalliniteit tussen de loten. Wanneer een groter percentage van een poeder in kristallijne toestand is, kan er minder water geabsorbeerd worden per gram MCC. Er werd een experimenteel design uitgevoerd om de effecten van waterbindingscapaciteit en variatie in procesparameters op granulaatgrootte distributie te vergelijken. De waterbindingscapaciteit, voedingssnelheid van het poeder, de schroefconfiguratie en de hoeveelheid toegevoegde granulatievloeistof hadden een significante invloed op de granulaatgrootte distributie. Dit experimenteel design werd dan succesvol gebruikt om de optimale procesparameters te berekenen voor het bekomen van een vooraf bepaalde granulaatgrootte distributie. Vervolgens werd onderzocht of MCC variatie in waterbindingscapaciteit nog steeds een significant effect op de granulaatgrootte heeft, wanneer een binder wordt toegevoegd aan de formulatie. Dit was het geval, gezien een hogere waterbindingscapaciteit resulteerde in grotere hoeveelheden granulaten kleiner dan 500 µm.

Het tweede deel van dit onderzoek evalueert het gebruik van verschillende PAT technieken om zowel intermediaire als eindproducten te monitoren.

Zowel in **Hoofdstuk 4** als **5**, werd duidelijk een bimodale granulaatgrootte distributie waargenomen. In **Hoofdstuk 6** werd Coherent anti-Stokes Raman scattering (CARS) microscopy gebruikt om de binder (PVP) in de granulaten te visualiseren. De gestelde hypothese was dat een slechte verdeling van PVP in de granulaten, veroorzaakt door de korte residentietijd in de granulator, de oorzaak was voor de bimodale granulaatgrootte distributie. Daarom werd eerst een haalbaarheidsstudie uitgevoerd, waaruit bleek dat CARS een geschikte techniek was voor de detectie van PVP in de dwarsdoorsnede van granulaten. Wanneer de granulaten geanalyseerd werden konden geen zones met een verhoogde PVP-

concentratie worden waargenomen. Een slechte verspreiding van PVP in de granulaten is dus niet de oorzaak van de bimodale granulaatgrootte distributie.

In **Hoofdstuk 7** werden opnieuw granulaten geproduceerd bestaande uit theofylline anhydraat (30%), lactose (67.5%) en PVP (2.5%). Deze granulaten werden nat geanalyseerd, bij het verlaten van de granulator. NIR en Raman spectra werden statisch opgenomen, met behulp van een cuvet. De deeltjesgrootte werd dynamisch gemeten aan de hand van een *Spatial Filter Velocimetry* (SFV) probe. Er werd opnieuw een experimenteel design uitgevoerd om na te gaan of procesparameters (voedingssnelheid van het poeder, schroefsnelheid, toegevoegde hoeveelheid granulatievloeistof en temperatuur van de granulator) een invloed hebben op de granulaatgrootte distributie en hydratatietoestand van theofylline. De temperatuur van de granulator en de voedingssnelheid van het poeder hadden een significante invloed op de granulaatgrootte. De conversie van theofylline anhydraat naar theofylline monohydraat werd ook geëvalueerd en werd beïnvloed door de temperatuur van de granulator, de hoeveelheid granulatievloeistof toegevoegd en in mindere mate door de voedingssnelheid van het poeder. Minder granulatievloeistof toegevoegd, hogere temperaturen van de granulator en hogere voedingssnelheid van het poeder leidden tot kleine hoeveelheden overgebleven theofylline anhydraat. De resultaten, bekomen via Raman spectroscopie, werden bevestigd door NIR spectroscopie. Zodoende bewezen Raman en NIR spectroscopie in combinatie met experimenteel design waardevolle technieken te zijn om proceskennis op te doen over de hydratatietoestand van het API in natte granulaten.

In **Hoofdstuk 8** worden verschillende methoden voor het bepalen van het eindpunt van een wervelbeddroogproces met elkaar vergeleken. Klassieke methoden zijn bijvoorbeeld het monitoren van de vochtigheid van de drooglucht, wanneer deze de droger verlaat en de temperatuur van het product tijdens drogen. Deze werden vergeleken met in-line analyse via PAT technieken (Raman en NIR spectroscopie) en een massabalans model. Een PLS model, gebaseerd op NIR spectra werd opgesteld voor het in-line monitoren van het vochtgehalte van granulaten tijdens drogen. Aan de hand van het model werden de in-line gecollecteerde spectra omgezet tot vochtgehaltes. De evolutie van het resterende vocht werd uitgezet en het eindpunt van de droogcyclus werd bepaald. Zowel het NIR-PLS model

als het massa balans model duidden het eindpunt van drogen veel sneller aan dan de twee klassieke, indirecte methoden. Daarenboven, geven NIR en Raman spectroscopie, in tegenstelling tot de andere technieken, ook informatie over de chemische toestand van het API. In het hier beschreven geval kon de dehydratatie van theofylline monohydraat, over metastabiel theofylline naar theofylline anhydraat in real-time gevolgd worden. Het tijdstip waarop theofylline dehydrateert, gedetecteerd werd, kwam overeen met het eindpunt van de droogcyclus zoals berekend met het NIR-PLS model. Het gebruik van PAT technieken was dan ook de geprefereerde methode voor eindpunt detectie van een wervelbeddroogproces in een productie-omgeving. In **Hoofdstuk 9** werd een NIR-PLS model voor de voorspelling van vochtgehalte gevalideerd aan de hand van accuraatheidsprofielen.

In **Hoofdstuk 10** werden 19 experimenten uitgevoerd aan de hand van een experimenteel design, met 4 factoren (temperatuur van de granulator, voedingssnelheid van het poeder, temperatuur van de drooglucht en debiet van de drooglucht). Lactose – theofylline – PVP (67.5 – 30 – 2.5 %) werd gebruikt als modelformulatie. Na drogen werd een deel van de granulaten opgesplitst in drie fracties: de fijne granulaten (<150 µm), de opbrengst (150 – 1400 µm) en de grote granulaten (> 1400 µm). Het vochtgehalte van de totale fractie alsook van de drie deelfracties werd bepaald met Karl Fischer titratie. Er werden ook Raman spectra opgenomen van de totale fractie en de drie deelfracties. Uit deze experimenten bleek dat het vochtgehalte bepaald op de totale fractie en de hydratatietoestand bepaald op de totale fractie verschilde van het vochtgehalte en hydratatietoestand van de deelfracties. Fijne granulaten droogden sneller en bevatten theofylline anhydraat, terwijl de grote granulaten een hoger vochtgehalte hadden en theofylline monohydraat of metastabiel theofylline bevatten.

Drie complementaire PAT technieken werden in **Hoofdstuk 11** gebruikt voor het monitoren van droge granulaten. Er werd gebruik gemaakt van zowel Raman als NIR spectroscopie, als van een fotometrische beeldvormingstechniek. In dit hoofdstuk werd geëvalueerd of informatie verzameld uit Raman spectra, NIR spectra samen met granulaatgrootte distributie en een reflectieparameter kon gebruikt worden voor het voorspellen van stort- en schudvolume, vloeibaarheid en vochtgehalte van de granulaten. Indien dit mogelijk zou zijn, kunnen PAT technieken de tijdrovende off-line laboratoriumtesten, zoals Karl Fischer titratie

of densiteitsmetingen, vervangen. Er werden drie PLS modellen opgesteld, een om vochtgehalte te voorspellen, een voor Hausner ratio en een voor stort- en schudvolume. Deze modellen bewezen hun bruikbaarheid voor de at-line analyse van continu geproduceerde granulaten. Het vochtgehalte was eerder gecorreleerd met de NIR spectroscopische data, terwijl de beeldvormingsdata de vloeibaarheid van de granulaten konden voorspellen.

In **Hoofdstuk 12** wordt NIR spectroscopie gebruikt voor het monitoren van een continu mengproces. De gebruikte statistische methode, de moving F-test, werd uitgebreid besproken. Eerst werd het minimaal aantal spectra per blok nodig om de α- en β- error te controleren bepaald. Daarna werd de methode toegepast op twee mengexperimenten, uitgevoerd met de continue granulator van het ConsiGma™ systeem. Het eerste experiment leverde een homogeen mengsel op en dit werd ook zo aangeduid door de methode. Tijdens een tweede experiment werden fouten geïntroduceerd in het proces. Niet alleen deze geïnduceerde fouten, maar ook natuurlijke fluctuaties in de poedertoevoer werden gedetecteerd door de Moving F-test methode.

CURRICULUM VITAE

PERSONAL INFORMATION

Surname:	FONTEYNE
First name:	Margot E.J.L.
Birth place:	Ghent, Belgium
Nationality:	Belgian
Email:	Margot.Fonteyne@Ugent.be

LANGUAGE SKILLS

Native language:	Dutch
Fluent in:	French and English

EDUCATION

2010 – present:	PhD candidate in Pharmaceutical Process Analytical Technology Ghent University
2013 – present:	Bachelor in Educational Sciences, free student, Ghent University
2010 – 2013:	Specific Teacher Training Program, CVO Brussels
2004 - 2009:	Pharmaceutical Sciences, Master in Drug Development Ghent University

RESEARCH EXPERIENCE

Apr 2014 – present:	Postdoctoral fellow Solid State Properties Analytics F. Hoffmann-La Roche Ltd, Basel, Switzerland
Jan 2010 – Mar 2014:	PhD research: Development and validation of process analytical methods for a continuous pharmaceutical manufacturing process of tablets based on wet granulation, supervised by Prof. T. De Beer

Oct 2011 – Mar 2012: Research visit: Understanding the solid state and physical characteristics of continuously produced wet granules, School of Pharmacy, Otago University, Dunedin, New Zealand, supervised by Prof. T. Rades

Feb -May 2008: Master thesis: Use of NIR-Spectroscopy for Characterization of freeze-dried mannitol-sucrose mixtures, Copenhagen University, Denmark, supervised by Prof. J. Rantanen

PUBLICATIONS IN PEER REVIEWED JOURNALS

1. **Fonteyne M.**, Gildemyn D., Peeters E., Mortier S., Vercruysse J., Gernaey K.V.,Vervaet C., Remon J.P., Nopens I., De Beer T. (2014) Moisture and drug solid state monitoring during a continuous drying process using empirical and mass balance models, European Journal of Pharmaceutics and Biopharmaceutics, doi:10.1016/j.ejpb.2014.02.015.
2. **Fonteyne M.**, Wickström H., Peeters E., Vercruysse J., Ehlers H., Peters B.H., Remon J.P., Vervaet C., Ketolainen J., Sandler N., Rantanen J., Naelapää K., De Beer T. (2014) Influence of raw material properties upon critical quality attributes of continuously produced granules and tablets, European Journal of Pharmaceutics and Biopharmaceutics, 87 (2), 252-63.
3. Vercruysse J., Córdoba Díaz D., Peeters E., **Fonteyne M.**, Delaet U., Van Assche I.,De Beer T., Remon JP., Vervaet C. (2014) Continuous twin screw granulation: influence of process variables on granule and tablet quality, European Journal of Pharmaceutics and Biopharmaceutics, 82 (1), 205-11.
4. **Fonteyne M.**, Fussell A.L., Vercruysse J., Vervaet C., Remon J.P., Strachan C., Rades T., De Beer T. (2014) Distribution of binder in granules produced by means of twin screw granulation, International Journal of Pharmaceutics, 462 (1-2), 8-10.
5. Vercruysse J., Toiviainen M., **Fonteyne M.**, Helkimo N., Ketolainen J., Juuti M., Delaet U., Van Assche I., Remon J.P., Vervaet C., De Beer T. (2014) Visualization and understanding of the granulation liquid mixing and distribution during continuous twin screw granulation using NIR chemical imaging, European Journal of Pharmaceutics and Biopharmaceutics, 86 (3), 383-92.

6. **Fonteyne M.**, Vercruysse J., Córdoba Díaz D., Gildemyn D., Vervaet C., Remon J.P., De Beer T. (2013) Real-time assessment of critical quality attributes of a continuous granulation process, Pharmaceutical Development and Technology, 18 (1), 85-97.
7. **Fonteyne M.**, Soares S., Vercruysse J., Peeters E., Burggraeve A., Vervaet C., Remon J.P., Sandler N., De Beer T. (2012) Prediction of quality attributes of continuously produced granules using complementary pat tools, European Journal of Pharmaceutics and Biopharmaceutics, 82 (2), 429-36.
8. Mortier S.T., De Beer T., Gernaey K.V., Vercruysse J., **Fonteyne M.**, Remon J.P, Vervaet C., Nopens I. (2012) Mechanistic modelling of the drying behaviour of single pharmaceutical granules, European Journal of Pharmaceutics and Biopharmaceutics, 80 (3), 682-9.
9. De Beer T., Burggraeve A., **Fonteyne M.**, Saerens L., Remon J.P., Vervaet C. (2011) Near infrared and Raman spectroscopy for the in-process monitoring of pharmaceutical production processes, International Journal of Pharmaceutics, 417 (1-2), 32-47.
10. Grohganz H., **Fonteyne M.**, Skibsted E., Falck T., Palmqvist B., Rantanen J. (2010) Classification of lyophilised mixtures using multivariate analysis of NIR spectra, European Journal of Pharmaceutics and Biopharmaceutics, 74 (2), 406-12.
11. Grohganz H., **Fonteyne M.**, Skibsted E., Falck T., Palmqvist B., Rantanen J. (2009) Role of excipients in the quantification of water in lyophilised mixtures using NIR spectroscopy, Journal of Pharmaceutical and Biomedical Analysis, 49 (4), 901-7.

PUBLICATIONS IN PROGRESS

12. **Fonteyne M.**, Vercruysse J., De Leersnyder F., Van Snick B., Vervaet C., Remon J.P., De Beer T. (2014) Process analytical techniques for the continuous manufacturing of solid dosage forms, Trends in Analytical Chemistry, *invitation*.
13. **Fonteyne M.**, Arruabarrena J., De Beer J., Hellings M., Van den Kerkhof T., Burggraeve A., Vervaet C., Remon J.P., De Beer T. (2014) NIR spectroscopic method for the in-line assessment during drying in a six-segmented fluid bed dryer of a continuous tablet production line: validation of quantifying abilities and

uncertainty assessment, Journal of Pharmaceutical and Biomedical Analysis, *reviewed (moderate revision)*.

14. Vercruysse J., **Fonteyne M.**, Kumar A., Delaet U., Van Assche I., Nopens I., De Beer T., Remon J.P., Vervaet C. (2014) Evaluation of powder blending with a twin screw granulator: an experimental approach, *submitted to International Journal of Pharmaceutics.*
15. **Fonteyne M.**, Correia A., De Plecker S., Vercruysse J., Isić I., Zhou Q., Vervaet C., Remon J.P., Onofre F., Bulone V., De Beer T. (2014) Impact of microcrystalline cellulose material attributes: a case study on continuous twin screw granulation, *in preparation.*
16. Peeters E., Silva A., Toiviainen M., Juuti M., Van Renterghem J., **Fonteyne M.**, Vercruysse J., Lopes J., De Beer T., Vervaet C., Remon J.P. (2014) Assessment of the properties of continuously produced tablets using transmission and backscattering Raman spectroscopy and transmission NIR spectroscopy, *in preparation.*
17. **Fonteyne M.**, Vercruysse J., De Leersnyder F., Remon J.P., Vervaet C., Oostra W., Gerich A., Besseling R., De Beer T. (2014) Blend uniformity evaluation during continuous mixing in a twin screw granulator by means of in-line NIR spectroscopy using a moving F-test, *in preparation.*

PRESENTATIONS AT CONFERENCES

Oral presentations

The evaluation of twin-screw granulation as a continuous blending tool.

Fonteyne M., Vercruysse J., Vervaet C., Remon J.P., De Beer T.

Sixth pan-European QbD and PAT Science conference, EuPAT 6, Porto, Portugal, 23-24 September 2013

Effect of raw material properties on quality attibutes of continuously produced granules.

Fonteyne M., Correia A., De Plecker S., Vercruysse J., Vervaet C., Remon J.P., De Beer T.

7th PSSRC Annual Symposium, Lille, France, 4-6 July 2013

Influence of raw material properties upon critical quality attributes of continuously produced granules and tablets.
Fonteyne M., Vercruysse J., Peeters E., Remon J.P., Vervaet C., Sandler N., Naelapää K., De Beer T.
6th International Granulation Workshop, Sheffield, UK, 26-28 June 2013

Influence of raw material properties upon critical quality attributes of continuously produced granules and tablets.
Fonteyne M., Vercruysse J., Peeters E., Remon J.P., Vervaet C., Sandler N., Naelapää K., De Beer T.
PARTEC 2013, Nuremberg, Germany, 23-25 April 2013

Prédiction de caractéristiques relatives à la qualité de granules lors de leur production continue grâce à l'utilisation d'outils PAT.
Fonteyne M.
Umetrics – Sigma Plus, Journée technique, Paris, France, 15 November 2012, invited speaker

Prediction of quality attributes of continuously produced granules using complementary PAT tools.
Fonteyne M.
ConsiGma™ Seminar GEA PS-Idifarma, Pamplona, Spain, 25-26 October 2012, invited speaker

Influence of raw material properties upon critical quality attributes of continuously produced granules and tablets.
Fonteyne M., Vercruysse J., Peeters E., Remon J.P., Vervaet C., Sandler N., Naelapää K., De Beer T.
6th PSSRC Annual Symposium, Lisbon, Portugal, 26-28 August 2012

Understanding of the binder distribution in continuously produced granules.
Fonteyne M., Vercruysse J., Remon J.P., Vervaet C., De Beer T., Rades T.
6th PSSRC Annual Symposium, Lisbon, Portugal, 26-28 August 2012

Evaluation and prediction of critical quality attributes during a continuous granulation and drying process.
Fonteyne M., Gildemyn D., Vercruysse J., Córdoba Díaz D., Vervaet C., Remon JP., De Beer T.
14th Conference on Formulation and Delivery of Bioactives, Dunedin, New Zealand, 16-17 February 2012

Implementing PAT tools in a continuous pharmaceutical granulation process for the in-line monitoring of critical process and product quality attributes.
Fonteyne M., Vercruysse J., Córdoba Díaz D., Vervaet C., Remon J.P., De Beer T.
5th International Granulation Workshop, Lausanne, Switzerland, 20-22 June 2011

In-line monitoring of a continuous granulation and drying process.
Fonteyne M., Gildemyn D., Vercruysse J., Córdoba Díaz D., Vervaet C., Remon JP., De Beer T.
15th Forum of Pharmaceutical Sciences, Spa, Belgium, 12-13 May 2011

Poster presentations

The evaluation of twin-screw granulation as a continuous blending tool by means of the moving F-test.
Fonteyne M., Vercruysse J., Remon J.P., Vervaet C., De Beer T.
EuroPACT, Barcelona, Spain, 6-9 May 2014

A thorough validation of a lighthouse probe for the in-line NIR based granule moisture assessment in the drying unit of a continuous pharmaceutical tableting process.
Fonteyne M., Arruabarrena J., Vercruysse J., Vervaet C., Remon J.P., De Beer T.
EuPAT 6, Porto, Portugal, 23-24 September 2013

Comparison of two different fiber optic probes for the in-line NIR based granule moisture assessment in the drying unit of a continuous pharmaceutical tableting process.
Fonteyne M., Arruabarrena J., Vercruysse J., Vervaet C., Remon J.P., De Beer T.
6th International Granulation Workshop, Sheffield, UK, 26-28 June 2013

Effect of raw material properties on quality attributes of continuously produced granules.
Fonteyne M., De Plecker S., Vercruysse J., Vervaet C., Remon J.P., De Beer T.
Knowledge for Growth, Ghent, Belgium, 30 May 2013

Prediction of quality attributes of continuously produced granules using complementary PAT tools.
Fonteyne M., Soares S., Vercruysse J., Vervaet C., Remon J.P., Sandler N., De Beer T.
EuPAT 5, Ghent, Belgium, 8-10 May 2012

In-line monitoring of a continuous pharmaceutical granulation and drying process.
Fonteyne M., Vercruysse J., Córdoba Díaz D., Vervaet C., Remon J.P., De Beer T.
Laser and Applications Research Theme (LART), Dunedin, New Zealand, 18 November 2011

In-line monitoring of a continuous pharmaceutical granulation and drying process.
Fonteyne M., Vercruysse J., Córdoba Díaz D., Vervaet C., Remon J.P., De Beer T.
5th International Granulation Workshop, Lausanne, Switzerland, 20-22 June 2011

In-line monitoring of a continuous pharmaceutical granulation and drying process.
Fonteyne M., Vercruysse J., Córdoba Díaz D., Vervaet C., Remon J.P., De Beer T.
EuroPACT, Glasgow, UK, 26-29 April 2011

AWARD

2nd Prize Best Poster Award 'Innovative Application of the Chemical Sciences to Granulation Technology'
5th International Granulation Workshop, Lausanne, Switzerland, 20-22 June 2011

ATTENDED CONFERENCES, COURSES AND WORKSHOPS

Course: Particle size monitoring using various techniques, 6 May 2014, Barcelona, Spain

Course: Introduction to Multivariate Statistical Process Control, 6 May 2014, Barcelona, Spain

Course: Speedreading, 16 December 2013, Ghent Belgium

Course: Efficient Product Characterization and Processing of Pharmaceuticals Particulate Solids, 21-31 May 2013, Magdeburg, Germany

Conference: Advances in Chemometrics, Belgian Chemometrics Society, 8 June 2012, Ghent, Belgium

Workshop: EuPAT 5 Pre-conference workshop, Continuous Processing for Tablet Manufacturing, 8 May 2012, Ghent, Belgium

Workshop: Polymers in Drug Delivery, New Zealand and Australian Chapters of the Controlled Release Society, 15 February 2012, Dunedin, New Zealand

Course: CPACT Introduction to Process Control for Chemists and Pharmacists & Formulation Scientists course, 27-29 June 2011, Cheshire, UK

Workshop: The continuous OSD Production Seminar, 7-8 June 2011, Wommelgem, Belgium

Course: Design of Experiments, 26 April 2011, Glasgow, UK

Course: Multivariate Curve Resolution, 26 April 2011, Glasgow, UK

Conference: Fourth pan-European PAT Science Conference: Taking PAT to the next level, 5-6 May, Kuopio, Finland

Workshop: Basisassistententraining, March 2010, Ghent, Belgium

Course: Presentation skills, March 2010, VUB, Brussels, Belgium